Thermal Desorption of Helium Films: Theory and Experiment

Thesis by

Michael B. Weimer

In Partial Fulfillment of the Requirements

for the Degree of

Doctor of Philosophy

California Institute of Technology

Pasadena, California

1986

(Submitted March 26, 1986)

I wish to dedicate this thesis

to my dear and respected parents,

to my loving sister,

and to the cherished memory of my late uncle, Leo.

The wonderful thing about time

is that it keeps everything from happening all at once.

Acknowledgements

The successful completion of this work owes much to the assistance extended me by many generous people. It is a pleasure to have this opportunity to acknowledge their contributions and to express my gratitude to them.

To my thesis advisor, Professor David Goodstein, I extend my sincere appreciation for his support and guidance throughout this project, for sharing freely of his physical intuition, and for showing me, through his example, the value of clearly, simply, and effectively communicating scientific ideas.

During the course of my research, the intellectual environment of our laboratory has been enriched by the presence of several visiting faculty members. I owe a special debt of gratitude to Professor Robert Housley, of the Rockwell Science Center, whose insight, thoughtful criticism, and willingness to help at every turn have left their mark on many aspects of this thesis. I have also benefited from my association with Professor Milton Cole, of the Pennsylvania State University, whose contagious enthusiasm for physics made him a joy to work with as well as to learn from.

My development as an experimental physicist has been furthered by the unique resource offered by the people of the Caltech Low Temperature Physics Group. In particular, I wish to thank Dr.'s John Dick, Jean Delayen, and Don Strayer for innumerable discussions and useful suggestions, Professor Jim Mercereau for his encouragement and interest, and especially Edward Boud whose invaluable technical assistance and steady, experienced calm saw me through many seemingly insurmountable experimental hurdles, and to whom I could always turn to for advice. I am also indebted to fellow and former low-temperature physics students Michael Pettersen, Mark Lysek, Roya Maboudian, and Brad Axan, each of whom has materially contributed to the progress of my work. Special thanks are also due Jennifer Gertson for her cheerful and efficient assistance in the monumental task of typing and assembling this manuscript.

I have profited from, and wish to acknowledge, conversations with Professors Noel Corngold, Joel Franklin, Steven Frautschi, and Phillip Saffman, who have all been generous with their time.

I would like to thank the California Institute of Technology for its academic and financial support over the many years of my graduate studies. The financial assistance of the Office of Naval Research in carrying out this work is also gratefully acknowledged.

In reflecting on my formative years as an undergraduate physics student at the Massachusetts Institute of Technology, I look back, with particular regard, to my bachelor's thesis advisor, Professor Min Chen, who first introduced me to the excitement of experimental research. His kindness and concern for my growth as a scientist will always be warmly remembered.

It is with genuine pleasure that I mention those friends whose encouragement, along with that of my family, has meant so much to me during these years. To Sarbmeet Kanwal, dear friend and kindred spirit with whom I felt privileged to share both the triumphs and occasional reverses of our graduate careers, I can hardly begin to express my thanks. I feel a similar sense of gratitude towards David Pepper whose boundless generosity and caring advice have been much more like that of an older brother than simply a valued friend. Murray Daw, Paul Linsay, Norm and Ann Bobroff, have all remained close long after their own passage through the portals of Caltech, and I feel my life enriched by their continued friendship. Likewise thoughts extend to Rajan Gupta, David and Deborah Kelly, Gayle Sugiyama, Jeffrey White, and Daphne Wilcox, whose companionship and good cheer also sustained me.

Finally, my deepest sense of appreciation goes to my family whose love, patient support, and constant faith in me have been an ever–present source of renewal. Words alone cannot begin to touch the extent of my gratitude.

Abstract

The desorption kinetics of helium films is explored in the context of a phenomenological model wherein the film is assumed to have the thermodynamic properties of bulk liquid and the vapor is described by simple kinetic theory. When supplemented by the condition that desorption proceed at the maximum rate permitted by detailed balance, equations for energy and mass conservation completely determine the dynamics of the system.

The model is applied to the specific problem of characterizing the time response of an adsorbed film when the equilibrium between it and the ambient vapor is perturbed by a sudden change in substrate temperature and the system subsequently evolves toward a new steady state. Analysis reveals that for infinitesimal perturbations from equilibrium the equations of motion are linear and result in exponential solutions for the time dependence of the desorption flux. For finite temperature elevations and realistic adsorption isotherms, however, the equations of motion are highly nonlinear. In either case, isothermal desorption at the temperature of the substrate is shown to be a general feature of the solutions under usual experimental conditions and this considerably simplifies interpretation of the nonlinear problem. Under these circumstances one can identify a continuous succession of coverage–dependent relaxation time scales which are given in terms of instantaneous properties of the adsorption system. These time scales are distinct from, and in general unrelated to, the coverage–dependent mean lifetime of an atom on the surface. To characterize the overall time scale of the nonlinear evolution towards steady state, a global measure is defined in terms of both instantaneous and steady–state properties and used to summarize experimental data.

A direct method for measuring the relaxation time of monolayer helium films flash desorbed from evaporated metal–film substrates is described and used to test the model. The technique is based on a rapid heating scheme made possible by the unique properties of ballistic phonon propagation in single

crystals at low temperature. Global time constants extracted from the data in the near–equilibrium regime agree well with the predictions of the model. When these results are combined with earlier data at higher substrate temperatures and different ambient conditions, the picture is consistent with scaling properties implied by the theory. It is shown how the particular dependence on initial conditions of the exponent in a Frenkel–Arrhenius parameterization of the global time constant may be traced to the curvature of the equilibrium adsorption isotherm. This curvature is substantiated by the behavior of the instantaneous relaxation time scales, the time–of–flight spectrum of the desorbing flux, and the kinetics of readsorption.

Contents

Introduction

This thesis is concerned with what happens when the equilibrium between an adsorbed film and the vapor above it is disturbed by a change in the temperature of the substrate on which the film rests. We will be particularly interested in the time scales that characterize the resulting changes in macroscopically observable quantities such as the temperature of the adsorbate and the net evaporation rate of particles from the condensed state into the gaseous one. This evaporation process is termed desorption, as distinguished from the reverse process of adsorption, and our focus is on the kinetic aspects of this phenomenon.

The study of dynamic processes typically poses the most formidable challenges to one's understanding of the physical principles governing the phenomena of interest but it also offers the potential of insights not available by other means. For example, chemisorption, like gas–phase chemical reactions, is often an activated process and kinetic studies allow one to learn both about the strength of the atom–surface interaction, and hence the specific nature of the bonding, as well as about the properties of the transition state, or so–called activated complex, through the temperature dependence of desorption rates [Tompkins]. In molecular systems, information on the concentration dependence of rates provides clues as to whether or not a compound structure fragments, or dissociates, into smaller structures upon adsorption and, conversely, how many of these smaller units must come together on the surface before the reverse process of desorption can take place. In the simplest instance of atomic adsorption, where, by definition, dissociation cannot occur, particles are usually regarded as interacting with the surface independently of each other (with the exception of site exclusion) and so lead to what are termed first–order kinetics: linear equations of motion resulting in an exponential dependence of the surface concentration on time.

By way of contrast, in physisorbed systems, where the attraction between adsorbate and substrate results from the mutual van der Waals forces between them so that condensation proceeds without chemical transformation or chemical bond formation, activation energies do not differ appreciably from the simple heat of adsorption. Physisorption is not, fundamentally, an activated process with a potential barrier whose height is of distinctly kinetic significance; rather, this barrier is of only thermodynamic, or more properly thermostatic, significance.

The barrier to surface migration in physisorption is typically much less than the surface binding energy but in chemisorption these two quantities are of comparable magnitude. Also, chemisorption usually saturates at monolayer completion whereas physisorption systems can form multilayer films. Because of both the collisions that result from this enhanced mobility, and because of the interactions arising from multilayer growth, physisorbed systems show important signs of *collective* behavior. Therefore, except at very low coverage, one cannot arbitrarily ignore adatom–adatom interactions in favor of adatom–surface forces alone. As a result of these additional interactions, the environment in which particles remaining on the surface find themselves, as others desorb, changes continually with time. Consequently, for all but infinitesimal disturbances from equilibrium, the time evolution of the evaporation process is governed by nonlinear equations. This leads to nonexponential time dependences and confronts one with the difficult problem of finding one or more suitable time scales to characterize the situation.

Chemisorption studies are often conducted using a method called Temperature Programmed Desorption [Menzel (1975), Gomer (1975)]. In this technique, the temperature of the substrate is slowly raised in a controlled manner and the gas evolved is pumped away so that readsorption does not occur concurrently with the desorption being analyzed. The situation addressed here, on the other hand, is the response of an adsorbed film to a sudden jump in substrate

temperature in the presence of an ambient gas, and the resulting change of surface coverage with time as the system moves toward a new dynamic steady state. This rapid flash desorption is made possible by novel techniques based on the ballistic propagation of phonons in pure single crystals at low temperature.

We will see that both the particular boundary conditions of the experiments (i.e., the presence of the ambient gas) and the nonlinear properties of the adsorption system interact in a complicated way to produce unusual results in a Frenkel–Arrhenius parameterization of the rate data. These factors do not seem to have been appreciated in previous work on this subject, and it is our view that concentrating only on this parameterization, as is often done, buries many crucial details about the film's dynamics in a formalism that is insufficiently flexible, subtle, or precise, to summarize the true complexity of the situation.

The experiments we describe are somewhat primitive in the sense that they concentrate on measuring average properties of the desorption from ill–defined and uncharacterized surfaces. Ideally, we would prefer to have a situation more akin to spectroscopy where we could control the quantum numbers of the various elementary excitations used to probe the system and similarly measure the momentum and energy of atoms coming off of the surface in every possible direction. In addition, it would be important to be able to correlate these results with the condition of the surface by having a substrate whose properties are well established. Unfortunately, this is all beyond our technical grasp. As a result, we are forced into simplifying our discussion by introducing concepts such as continuous media, temperatures, total rates, etc., and in so doing we will take a step backward in the level and detail of our understanding. Nevertheless, just putting into focus the important issues affecting a macroscopic measurement turns out to be a challenging proposition.

Thus, while in the end we will be able to give a satisfactory account of the data summarizing the gross time dependence of the relaxation to a new steady state, and even have some intuitive pictures with which to interpret the

possibilities under differing circumstances, we will really come no closer to understanding anything fundamental about the gas–surface interaction or the changes of phase which characterize the transformation from gaseous to adsorbed state. These latter problems are of almost universal significance and play an important role in such diverse phenomena as the microphysics of aerosols [Brock (1980)], the production of high vacuum [Maissel and Glang; Roth], sound reflection from the surface of liquids where evaporation takes place [Robnik, Kuscer and Lang (1978)], the temperature and viscous slip of gases flowing past surfaces on which films may have condensed [Goodman and Wachman], the drag and lift on bodies moving through rarefied atmospheres under free–molecular flow conditions [Goodman and Wachman], and the general questions of sticking and thermal accommodation on clean and dirty surfaces. These issues have even become of overwhelming practical significance in recent attempts to observe a new state of matter – the Bose condensation of spin–aligned hydrogen at millikelvin temperatures – as experimenters find themselves limited in their ability to cool an atomic hydrogen gas by the inefficiency of energy exchange between this gas and the helium–film covered walls of their apparatus [Statt (1985), Goldman (1986)].

This thesis is organized as follows. In Chapter 1 we review the concept of detailed balance as applied to the gas–surface scattering problem and show how the elementary processes of adsorption and desorption may be related to one another under suitable circumstances. We also discuss a particular equilibrium model of physisorption leading to an equation of state that we will make extensive use of later.

In Chapter 2 we describe a simple model of helium desorption kinetics based on the ideas developed in Chapter 1. The film is treated as a slab of bulk liquid in the external field of the substrate and exchange with the vapor is treated via simple kinetic theory and detailed balance resulting in the well–known Hertz–Knudsen–Langmuir expression for the desorption flux. The dynamics are made

specific by adopting the desorption analog of a perfect black–body for the scattering properties of the film. Coupled equations for energy and mass conservation then determine the time evolution of the perturbed system. Solutions for the linearized near–equilibrium case are presented and discussed.

In Chapter 3 we develop the mathematical structure of the model extending the analysis to the more difficult finite temperature–jump domain of the experiments. Isothermal desorption is shown to be a general feature, within the assumptions of the model, under all realistic experimental conditions. This considerably simplifies the analysis and permits a simple geometrical interpretation of the resulting desorption dynamics in terms of properties of the equilibrium adsorption isotherm. Realistic isotherms lead to a nonexponential time dependence for the desorption flux and various cases are discussed. Several different classes of time constants can be distinguished in the nonlinear case and the significance of these relaxation times, as distinct from the mean dwell time or desorption lifetime, is made clear.

In Chapter 4 we review the experimental techniques with particular attention to the circumstances necessary for a proper evaluation of the data. Considerable emphasis is placed on the methodology of signal analysis. New experimental results are presented which push the data closer to the near–equilibrium regime and thereby eliminate the possibility of artifacts which may have affected earlier observations. The experimental results agree well with the model predictions, and when combined with earlier data expressed in terms of appropriate dimensionless variables, confirm certain scaling properties of the theory. In addition, the characteristics of a Frenkel–Arrhenius parameterization of the relaxation rate data can be traced to the nonlinear dynamics arising from the particular curvature of the underlying equilibrium adsorption isotherm. Other results sensitive to the very same factors, such as variations in the shape of the time–of–flight spectrum of desorbing atoms in response to changes in the frequency of temperature perturbation, substantiate this curvature.

Finally, we conclude with a brief summary recapitulating the strengths and weaknesses of our point of view and comment on the prospects for more incisive measurements.

References

Brock, J. R., in *Aerosol Microphysics I: Particle Interaction,* W. H. Marlow, ed., Vol. 16 of Topics in Current Physics (Springer–Verlag, Berlin, 1980).

Goldman, V. V., Phys. Rev. Lett. **56,** 612 (1986).

Gomer, R., in *Solid State Physics,* H. Ehrenreich, F. Seitz and D. Turnbull, eds., Vol. 30 (Academic Press, New York, 1975).

Goodman, F. O. and Wachman, H. Y., *Dynamics of Gas-Surface Scattering* (Academic Press, New York, 1978).

Maissel, L. I. and Glang, R., *Handbook of Thin Film Technology* (McGraw–Hill, New York, 1970).

Menzel, D., in *Interactions on Metal Surfaces,* R. Gomer, ed. (Springer–Verlag, Berlin, 1975).

Robnik, M. Kuscer, I. and Lang, H., Int. J. Heat Mass Transfer **22,** 461 (1978).

Roth, A., *Vacuum Technology,* 2nd edition (North–Holland, Amsterdam, 1982).

Statt, B. W., Phys. Rev. B **32,** 7160 (1985).

Tompkins, F. C. *Chemisorption of Gases on Metals* (Academic Press, New York, 1978).

Chapter 1
Fundamentals

1. Detailed Balance

In order to fully appreciate what follows in this and subsequent chapters, we begin with a review of the concept of detailed balance. To keep our discussion as simple as possible, we confine our attention to a consideration of monatomic particles without internal degrees of freedom. The quantum states of these particles are completely determined by specifying the three components of momentum corresponding to translational motion, and this description faithfully represents the physical situation we are primarily interested in, which is the dynamics of low energy ^{4}He atoms interacting with a surface. Generalizations to systems with spin and to polyatomic gases may be found in the cited literature.

1.1 Collisions Between Atoms

Let us focus on the collisions which occur between the atoms of a dilute monatomic gas in thermal equilibrium. It is often the case that these collisions must be treated quantum mechanically. Then the number of transitions per unit time in which an atom with momentum $\mathbf{p}_1$ and another with momentum $\mathbf{p}_2$ scatter to states $\mathbf{p}_1'$ and $\mathbf{p}_2'$, within ranges d^3p_1' and d^3p_2' respectively, is given by

$$\frac{2\pi}{\hbar}\frac{d^3p_1'}{(2\pi\hbar)^3}\frac{d^3p_2'}{(2\pi\hbar)^3}\,|\langle\mathbf{p}_1'\mathbf{p}_2'|\hat{T}|\mathbf{p}_1\mathbf{p}_2\rangle|^2\,\delta\left(\frac{p_1^2}{2m}+\frac{p_2^2}{2m}-\frac{p_1'^2}{2m}-\frac{p_2'^2}{2m}\right) \qquad (1.1)$$

$$\times\; f_o(\mathbf{p}_1)\,f_o(\mathbf{p}_2)\,d^3p_1d^3p_2.$$

The quantities $f_o(\mathbf{p}_1)d^3p_1$ and $f_o(\mathbf{p}_2)d^3p_2$ represent the number of particles per unit volume with initial momenta $\mathbf{p}_1$ and $\mathbf{p}_2$ in thermal equilibrium, as given by the appropriately normalized Maxwell–Boltzmann distribution.

The matrix elements appearing in (1.1) are those of the exact transition

operator (or T–matrix, [Schiff]) in a plane wave basis. These matrix elements may be calculated, in principle, to any desired order in perturbation theory once the interaction between atoms is specified. For a pairwise potential depending only on relative separation, the transition rate is proportional to $\delta^3(\mathbf{p}_1'+\mathbf{p}_2'-\mathbf{p}_1-\mathbf{p}_2)$, which enforces momentum conservation, and also proportional to the total volume. Dividing through by this volume we obtain a result independent of the size of our system.

The number of transitions per unit time and volume obtained from (1.1) may be written more compactly [Lifshitz & Pitaevskii, *PK*] as,

$$w(\mathbf{p}_1'\mathbf{p}_2' ; \mathbf{p}_1\mathbf{p}_2)\, f_o(\mathbf{p}_1)\, f_o(\mathbf{p}_2)\; d^3p_1 d^3p_2 d^3p_1' d^3p_2' \,. \tag{1.2}$$

Because the laws governing the collisions of atoms are known to be time–reversal invariant, the T–matrix, and hence w, must be unchanged under an exchange of initial and final states and a reversal of the sign of all momenta. That is, since

$$|\langle \mathbf{p}_1'\mathbf{p}_2' |\hat{T}| \mathbf{p}_1\mathbf{p}_2\rangle| \;=\; |\langle -\mathbf{p}_1-\mathbf{p}_2 |\hat{T}| -\mathbf{p}_1'-\mathbf{p}_2'\rangle| \tag{1.3a}$$

it follows that

$$w(\mathbf{p}_1'\mathbf{p}_2' ; \mathbf{p}_1\mathbf{p}_2) = w(-\mathbf{p}_1-\mathbf{p}_2;-\mathbf{p}_1'-\mathbf{p}_2') \,. \tag{1.3b}$$

As a consequence, the collision rate $\mathbf{p}_1\mathbf{p}_2 \rightarrow \mathbf{p}_1'\mathbf{p}_2'$ is equal, in equilibrium, to the rate $-\mathbf{p}_1'-\mathbf{p}_2' \rightarrow -\mathbf{p}_1-\mathbf{p}_2$. Specifically,

$$w(-\mathbf{p}_1-\mathbf{p}_2;-\mathbf{p}_1'-\mathbf{p}_2')f_o(-\mathbf{p}_1')f_o(-\mathbf{p}_2')d^3p_1' d^3p_2' d^3p_1 d^3p_2 = \tag{1.4}$$

$$w(\mathbf{p}_1'\mathbf{p}_2' ; \mathbf{p}_1\mathbf{p}_2)f_o(\mathbf{p}_1)f_o(\mathbf{p}_2)d^3p_1 d^3p_2 d^3p_1' d^3p_2' \,.$$

This is the statement of detailed balance. It holds because the product of equilibrium distribution functions on both sides of (1.4) is proportional to $e^{-(\varepsilon_1+\varepsilon_2)/kT}$ which depends only on the total energy of the particles. This quantity does not change sign under time reversal and is strictly conserved in the collision.

The interaction between atoms in a homogeneous gas exhibits another symmetry property, namely, invariance under inversion of the coordinate axes – or parity – according to which all momenta are reversed without interchanging initial and final states. The combined effect of time reversal and parity invariance,

$$w(\mathbf{p}_1'\mathbf{p}_2' ; \mathbf{p}_1\mathbf{p}_2) = w(\mathbf{p}_1\mathbf{p}_2 ; \mathbf{p}_1'\mathbf{p}_2') , \tag{1.5}$$

guarantees the equality of rates for a process and its inverse. The relationship between direct, time–reversed, and inverse processes is illustrated in Fig. 1.1a. A distinction between (1.4) and (1.5) is often made in the literature where the first of these is sometimes referred to as reciprocity instead of detailed balance. We will always mean (1.4) when using the latter term.

It is interesting to note that the justification of detailed balance given in many elementary treatments is misleading. To lowest order, the transition operator is the perturbation Hamiltonian, $\hat{H}'$, and (1.1) reduces to Fermi's Golden Rule. Equation (1.5) follows, it is argued, because the Hamiltonian is hermitian. The symmetry implied by the hermiticity of $\hat{H}'$ fails to hold in second and higher orders, however [Landau and Lifshitz, *QM*], leaving one with the impression that detailed balance is a statement only about first–order perturbation theory. Concentrating instead on the symmetry of the T–matrix under time reversal, we see that, in fact, it is more general than this.

1.2 Collisions with a Surface

We now consider the consequences of time–reversal invariance for gas atoms scattering from a wall. The time–independent distribution function, f_+, describing the scattered atoms may be expressed in terms of the incident distribution function, f_-, by the equation

$$\frac{|\mathbf{p}'\cdot\mathbf{n}|}{m} f_+(\mathbf{p}') = \int_{\mathbf{p}\cdot\mathbf{n}<0} d^3p \frac{|\mathbf{p}\cdot\mathbf{n}|}{m} f_-(\mathbf{p})\, P(\mathbf{p}\to\mathbf{p}') \qquad \mathbf{p}'\cdot\mathbf{n}>0 \tag{1.6}$$

Figure 1.1. Direct, time–reversed and inverse scattering processes illustrated for (a) binary collisions in a homogeneous gas and (b) collisions between gas atoms and a surface. T, P and TP represent the effects of time reversal, parity, and their combined product, respectively.

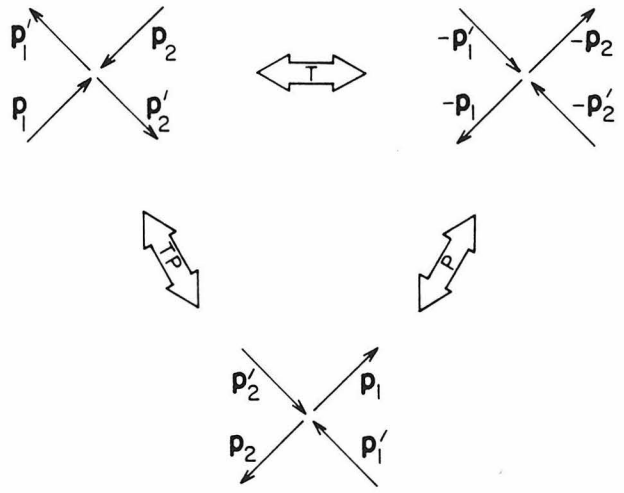

(a)

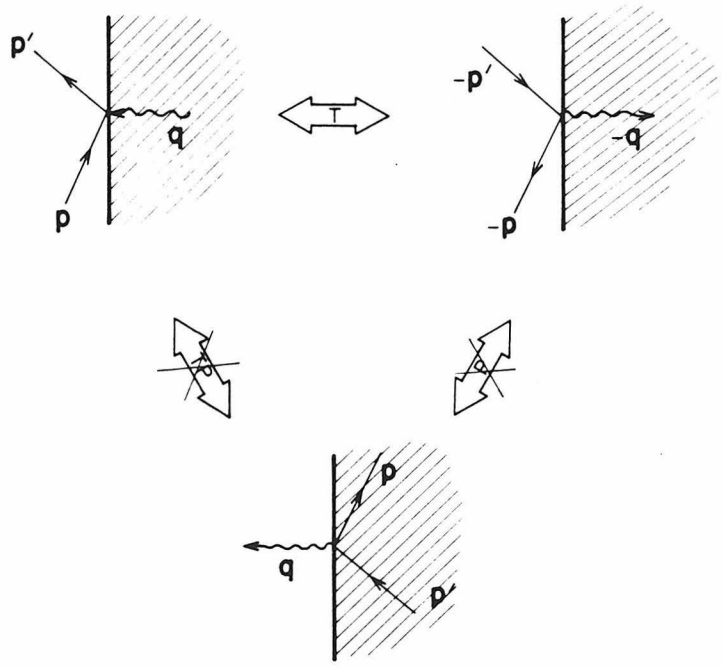

(b)

where $\mathbf{n}$ is a unit vector in the outward direction normal to the wall. Equation (1.6) relates the number of particles per momentum interval per unit area per second leaving the surface to the total flux approaching the surface and serves as a boundary condition on the Boltzmann equation describing transport processes in the gas.

The scattering kernel, $P(\mathbf{p}\rightarrow\mathbf{p}')$, represents the conditional probability density that a particle incident with momentum $\mathbf{p}$ is scattered into $\mathbf{p}'$ within d^3p'. If all atoms are reflected by the surface (for example, if there is no adsorption) then $P(\mathbf{p}\rightarrow\mathbf{p}')$ satisfies a normalization condition,

$$\int_{\mathbf{p}'\cdot\mathbf{n}>0} d^3p'\, P(\mathbf{p}\rightarrow\mathbf{p}') = 1\ . \tag{1.7}$$

Whatever the incident distribution or scattering law, the kernel must display the following symmetry [Wenaas (1971), Kuscer (1971)]

$$\frac{|-\mathbf{p}'\cdot\mathbf{n}|}{m} f_o(-\mathbf{p}')P(-\mathbf{p}'\rightarrow-\mathbf{p}) = \frac{|\mathbf{p}\cdot\mathbf{n}|}{m} f_o(\mathbf{p})P(\mathbf{p}\rightarrow\mathbf{p}') \tag{1.8}$$

where $f_o(\mathbf{p})$ is the equilibrium distribution function for a gas at the temperature of the wall. This relation is the expression of detailed balance for the case of gas–surface scattering, and it replaces (1.4).

Before proceeding with a demonstration of (1.8), it is worthwhile to make several comments. Scattering from a surface makes clear the need to distinguish between time–reversed and inverse processes. Referring to Fig. 1.1b, we see that while $\mathbf{p}\rightarrow\mathbf{p}'$ and its time reverse $-\mathbf{p}'\rightarrow-\mathbf{p}$ are clearly defined, the inverse, $\mathbf{p}'\rightarrow\mathbf{p}$, cannot occur. It corresponds to a physically realizable situation only if we simultaneously reflect the coordinates of the wall.

Inelastic processes give us special insight into the relationship between scattering probabilities implied by detailed balance. For a gas in equilibrium with the wall, (1.8) expresses the equality of rates between scattering and its time–reverse since the products $|\mathbf{p}\cdot\mathbf{n}|f_o(\mathbf{p})$ and $|\mathbf{p}'\cdot\mathbf{n}|f_o(-\mathbf{p}')$ are just the

respective incident fluxes. In thermal equilibrium, the flux of low energy atoms toward the surface must be exponentially greater than the flux of high energy atoms. The equality of scattering rates therefore implies a compensating relationship for the scattering probabilities. This difference in scattering probabilities stems from the fact that there are an exponentially greater number of states available to the wall if it absorbs energy rather than losing it, i.e., the wall acts as a heat bath.

As a consequence of the detailed–balance relation, a gas in equilibrium with a surface maintains an equilibrium distribution of energies. That is, if we consider (1.6) for the special case $f_- = f_o$, then (1.8) and the normalization condition (1.7) lead us to conclude

$$\frac{|\mathbf{p}' \cdot \mathbf{n}|}{m} f_+(\mathbf{p}') = \frac{|-\mathbf{p}' \cdot \mathbf{n}|}{m} f_o(-\mathbf{p}') \,. \tag{1.9}$$

Of course, since each atom reverses its direction upon striking the wall, a net momentum is imparted to the gas, and a complimentary wall is necessary to maintain zero drift velocity.

If we imagine a reference plane drawn within a mean free path of the surface, Eq. (1.9) states that the number of atoms crossing this plane per unit area per second is identical to the number crossing in the opposite direction for each velocity and angle of incidence. This implies that the surface may be replaced by a half–space of ideal gas at the same temperature for the purpose of calculating the equilibrium particle flux. Obviously, this construction is not valid for an arbitrary incident distribution such as a molecular beam, or for that matter, a gas in equilibrium at a temperature different from that of the wall. In such instances we obtain instead

$$\frac{|\mathbf{p}' \cdot \mathbf{n}|}{m} f_+(\mathbf{p}') = \frac{|-\mathbf{p}' \cdot \mathbf{n}|}{m} f_o(-\mathbf{p}') \int_{\mathbf{p} \cdot \mathbf{n} < 0} d^3p \, \frac{f_-(\mathbf{p})}{f_o(\mathbf{p}')} \, P(-\mathbf{p}' \to -\mathbf{p}) \tag{1.10}$$

and only if the scattering law follows the special form

$$P(\mathbf{p}' \to \mathbf{p}) = \frac{|\mathbf{p} \cdot \mathbf{n}| f_o(\mathbf{p})}{\int_{\mathbf{p} \cdot \mathbf{n} > 0} d^3p \; |\mathbf{p} \cdot \mathbf{n}| f_o(\mathbf{p})} \tag{1.11}$$

do we recover (1.9), apart from a normalization factor dependent on the incident flux. The kernel of (1.11) is said to represent complete accommodation with the surface [Kuscer (1974)], whereby atoms are scattered without regard to their initial momentum into a distribution characteristic of an effusive source at the temperature of the wall.

On the basis of (1.9) it was predicted [Wenaas (1971)] that the total scattered intensity as a function of angle must vary, in equilibrium, as cosΘ. Early molecular beam experiments on the scattering of He and H_2 off of freshly cleaved LiF (001) surfaces showed marked angular structure, due mainly to diffraction. The complex nature of these scattering spectra led Palmer and O'Keefe to question whether the particular superposition of distributions due to an equilibrium source would add up, in just the right way necessary, to produce a simple cosine dependence of the total flux. They designed an experiment to measure the angular dependent scattering from the cleavage plane of LiF of an isotropic gas source of He, H_2 or Ar in equilibrium with the surface [Palmer and O'Keefe (1970)]. Their results, sensitive to deviations at the percent level, demonstrated conclusively that the total flux leaving the surface did, in fact, follow a cosine law.

The demonstration of (1.8) follows in a general way from time–reversal symmetry and the assumption of thermal equilibrium for the wall. We must now say something about the microscopic states of the wall. The only crucial assumption is that these states are distributed canonically, but for convenience in labeling them we will assume that the elementary excitations of the solid are phonons and that atoms inelastically scattered from the surface absorb, emit and scatter from these phonons (Fig. 1.1b). Then for a gas in thermal equilibrium with the wall, the number of transitions per unit time taking atoms from $\mathbf{p}$ to $\mathbf{p}'$

is given by

$$\frac{2\pi}{\hbar} \sum_{\{n'_{\mathbf{q}}\}} \sum_{n_{\mathbf{p}'}} \sum_{n_{\mathbf{p}}} \sum_{\{n_{\mathbf{q}}\}} |\langle n_{\mathbf{p}'}+1\ n_{\mathbf{p}}-1\ \{n'_{\mathbf{q}}\}|\hat{T}|n_{\mathbf{p}'}\ n_{\mathbf{p}}\ \{n_{\mathbf{q}}\}\rangle|^2 \qquad (1.12a)$$

$$\times\ P(n_{\mathbf{p}})\,P(n_{\mathbf{p}'})\,P(\{n_{\mathbf{q}}\})\,\delta\left(\frac{p'^2}{2m} + E\{n'_{\mathbf{q}}\} - \frac{p^2}{2m} - E\{n_{\mathbf{q}}\}\right) \quad .$$

The state vectors are labeled according to the occupation number representation so that $\{n_{\mathbf{q}}\}$, for example, represents the entire set of occupation numbers for all phonon modes prior to scattering.

We follow the usual procedure of averaging over initial and summing over final states in (1.12a). The probability that there are initially $n_{\mathbf{p}}$ atoms with momentum $\mathbf{p}$ and $n_{\mathbf{p}'}$ atoms with momentum $\mathbf{p}'$, in the gas, is given by $P(n_{\mathbf{p}})P(n_{\mathbf{p}'})$. The sums over these occupation numbers are restricted, if need be, depending upon the statistics of the particles. The collective excitations of the solid are regarded as quasi–particles obeying Bose statistics with vanishing chemical potential, and $P(\{n_{\mathbf{q}}\})$ is the probability for a particular set of phonon occupation numbers.

The transition rate (1.12a) may also be written directly in terms of the time–independent scattering probability and incident flux as

$$A\ \frac{|\mathbf{p}\cdot\mathbf{n}|}{m}\ f_o(\mathbf{p})\,P(\mathbf{p}\rightarrow\mathbf{p}')\,d^3p\,d^3p' \qquad (1.12b)$$

where A is the area of the wall. The transition rate for the time–reversed process is given by

$$\frac{2\pi}{\hbar} \sum_{\{n_{-\mathbf{q}}\}} \sum_{n_{-\mathbf{p}}} \sum_{n_{-\mathbf{p}'}} \sum_{\{n'_{-\mathbf{q}}\}} |\langle n_{-\mathbf{p}'}\ n_{-\mathbf{p}}\ \{n_{-\mathbf{q}}\}|\hat{T}|n_{-\mathbf{p}'}+1\ n_{-\mathbf{p}}-1\ \{n'_{-\mathbf{q}}\}\rangle|^2 \qquad (1.13a)$$

$$\times\ P(n_{-\mathbf{p}'}+1)\,P(n_{-\mathbf{p}}-1)\,P(\{n'_{-\mathbf{q}}\})\,\delta\left(\frac{p^2}{2m} + E\{n_{-\mathbf{q}}\} - \frac{p'^2}{2m} - E\{n'_{-\mathbf{q}}\}\right)$$

which is equal to

$$A\frac{|-\mathbf{p}'\cdot\mathbf{n}|}{m} f_o(-\mathbf{p}')\,P(-\mathbf{p}'\to-\mathbf{p})\,d^3p'd^3p\,. \tag{1.13b}$$

Comparing (1.12b) and (1.13b), we see that (1.8) rests on showing the equivalence of (1.12a) to (1.13a). The Gibbs distribution applied to a system with a variable number of particles [Landau and Lifshitz, $SP1$] gives for the probability of any particular configuration, $\{n_{\mathbf{q}}\}$, the relation $P(\{n_{\mathbf{q}}\}) \sim e^{-E\{n_{\mathbf{q}}\}/kT}$ so that

$$P(n_{-\mathbf{p}'}+1)\,P(n_{-\mathbf{p}}-1)\,P(\{n'_{-\mathbf{q}}\}) = P(n_{-\mathbf{p}'})\,P(n_{-\mathbf{p}})\,P(\{n_{-\mathbf{q}}\}) \tag{1.14}$$

$$\times\; e^{(\frac{p^2}{2m}-\frac{p'^2}{2m}+E\{n_{-\mathbf{q}}\}-E\{n'_{-\mathbf{q}}\})/kT}\,.$$

Because of the energy conserving δ–function, the exponential term can be set equal to one. Time–reversal invariance of the T–matrix then yields the desired result.

The precise meaning of $f_o(\mathbf{p})$ requires some explanation. As noted previously, it represents the mean number of atoms in state $\mathbf{p}$ within d^3p, per unit volume. If the gas is in the classical limit, this is just the Maxwell–Boltzmann distribution. On the other hand, if the gas is in the extreme quantum limit, then we must use

$$f_o(\mathbf{p}) = \frac{<n_{\mathbf{p}}>}{(2\pi\hbar)^3} = \frac{1}{(2\pi\hbar)^3}\,\frac{1}{e^{(p^2/2m-\mu)/kT}\pm1} \tag{1.15}$$

where $<n_{\mathbf{p}}>$ is the usual Bose or Fermi distribution function.

The case of Bose statistics for the atoms is particularly easy to follow. For the direct process the only term in the transition operator producing a nonzero matrix element involves the pair of atom creation and annihilation operators $a^{\dagger}_{\mathbf{p}'}\,a_{\mathbf{p}}\,d^3p'd^3p$ while for the reverse process it is the pair $a^{\pm}_{-\mathbf{p}}\,a_{-\mathbf{p}'}\,d^3p'd^3p$ which contributes. The rate depends on $<n_{\mathbf{p}}>$ in (1.12) and on $<n_{-\mathbf{p}'}>$ in (1.13) because the squared matrix elements are proportional to $n_{\mathbf{p}}$ and $n_{-\mathbf{p}'}$ respectively. Summation over the initial occupation probabilities then yields the mean values. If

we consider the scattering of ^{4}He atoms by a surface at temperatures much less than the Debye temperature of the solid, the phonon system is in the quantum limit. By maintaining a sufficiently low pressure, however, it is possible to keep the gas essentially classical; this reflects the actual situation in the experiments to be described later. The detailed–balance argument applies irrespective of whether we are concerned with the interaction between a quantum solid and a classical gas or a quantum solid and a quantum gas, so long as we use the correct form of $f_o(\mathbf{p})$.

1.3 Evaporation from a Liquid

A liquid in equilibrium at a given temperature has a gas at saturated vapor pressure above it. The atoms of this gas approaching the surface of the liquid may either scatter or condense. In the absence of any gas, there would still be a flux of atoms leaving the liquid surface due to evaporation. Accordingly, the boundary condition (1.6) must be modified [Lang and Kuscer (1974)] to

$$\frac{|\mathbf{p}'\cdot\mathbf{n}|}{m} f_+(\mathbf{p}') = \frac{|\mathbf{p}'\cdot\mathbf{n}|}{m} f_e(\mathbf{p}') + \int_{\mathbf{p}\cdot\mathbf{n}<0} d^3p \, \frac{|\mathbf{p}\cdot\mathbf{n}|}{m} f_-(\mathbf{p})\, P(\mathbf{p}\to\mathbf{p}') \qquad (1.16)$$

where $f_e(\mathbf{p})$ is the distribution function of evaporated atoms.

The scattering kernel need no longer be normalized and

$$\int_{\mathbf{p}'\cdot\mathbf{n}>0} d^3p' \, P(\mathbf{p}\to\mathbf{p}') = s(\mathbf{p}) \qquad (1.17)$$

represents the total scattering probability. As long as the liquid remains in internal equilibrium, the detailed–balance relation (1.8) for the kernel $P(\mathbf{p}\to\mathbf{p}')$ still applies. We note that, because of the isotropy of a liquid surface, time–reversed states may be related to reflected states (where the component of momentum normal to the surface has been reversed but the parallel component remains unchanged) by rotation of 180° about the surface normal. This additional symmetry is not true for all crystalline surfaces.

We define the sticking, or condensation, probability $\sigma(\mathbf{p})$ by

$$\sigma(\mathbf{p}) = 1 - s(\mathbf{p}) . \tag{1.18}$$

Naturally, $\sigma(\mathbf{p})$ represents a sum, similar to (1.17), over the transition probabilities to every distinct bound state of the liquid. Using the same principles of microscopic reversibility and internal equilibrium as before we conclude

$$\frac{|\mathbf{p}\cdot\mathbf{n}|}{m} f_e(\mathbf{p}) = \frac{|-\mathbf{p}\cdot\mathbf{n}|}{m} f_o(-\mathbf{p})\sigma(-\mathbf{p}) . \tag{1.19}$$

This statement is entirely analogous to Kirchoff's laws for the emission of light from a body, and σ plays the same role as the wave–vector dependent absorption coefficient. The cases $\sigma = 1$ or $\sigma = const$ correspond, in terms of the analogy with light, to black or gray bodies.

It is evident from (1.19) that evaporated atoms follow an equilibrium distribution at the temperature of the liquid only if $\sigma(\mathbf{p})$ is independent of momentum. In particular, the expectation that the flux of these atoms obeys well–known laws [Comsa (1977), (1981)], varying with angle as cosΘ (Knudsen law) and with velocity as $v^3 e^{-mv^2/2kT}$ (Maxwell law), is satisfied only if the sticking probability is independent either of incident angle, or incident speed.

Integrating (1.19) gives the total number evaporated per unit area per unit time,

$$J_e = \int_{\mathbf{p}\cdot\mathbf{n}>0} d^3p \, \frac{|\mathbf{p}\cdot\mathbf{n}|}{m} f_o(\mathbf{p})\sigma(\mathbf{p}) \tag{1.20}$$

while the number condensing is

$$J_c = \int_{\mathbf{p}\cdot\mathbf{n}<0} d^3p \, \frac{|\mathbf{p}\cdot\mathbf{n}|}{m} f_-(\mathbf{p})\sigma(\mathbf{p}) . \tag{1.21}$$

Net evaporation is due to the difference $J_e - J_c$. It is clear from (1.20) that the maximum evaporation rate occurs for $\sigma(\mathbf{p}) = 1$ and results in the same particle

flux, J_o, as that of the equilibrium gas. Relating the actual rate to its maximum possible value, $J_e = \sigma_e J_o$, defines an evaporation coefficient σ_e which is an average of the sticking probability over the equilibrium flux

$$\sigma_e = <\sigma(\mathbf{p})>_o \ . \tag{1.22}$$

By restricting this average to be over the magnitude of the momentum only, we are led naturally to the concept of an angle–dependent evaporation coefficient. The condensation coefficient σ_c can be similarly defined as the corresponding average over the incident distribution

$$\sigma_c = <\sigma(\mathbf{p})>_- \tag{1.23}$$

or, equivalently, as the ratio of condensing to total incident flux, $J_c = \sigma_c J_-$. The condensation and evaporation coefficients are equal if the incident distribution is the equilibrium one, $f_- = f_o$, but differ in general unless the scattering probability is independent of $\mathbf{p}$.

We will be concerned later on not only with the interchange of particles between liquid and vapor, but also with exchanges of energy. The mean energy carried away from a liquid, per evaporating atom, is given in terms of the free–particle energies, $\varepsilon(\mathbf{p})$, by

$$E_e = \frac{1}{J_e} \int_{\mathbf{p}\cdot\mathbf{n}>0} d^3p \ \varepsilon(\mathbf{p}) \ \frac{|\mathbf{p}\cdot\mathbf{n}|}{m} f_o(\mathbf{p})\sigma(\mathbf{p}) \ . \tag{1.24}$$

A similar expression involving J_c and f_- yields the mean energy, E_c, deposited per condensing atom. Furthermore, as in the case of reflection from a wall, energy may be transferred between gas and liquid by inelastic scattering without sticking. The net energy transfer, per particle, due to scattering is given by

$$E_s = \frac{1}{J_- - J_c} \int_{\mathbf{p}'\cdot\mathbf{n}<0} d^3p' \int_{\mathbf{p}\cdot\mathbf{n}>0} d^3p \ [\varepsilon(\mathbf{p}')-\varepsilon(\mathbf{p})] \ \frac{|\mathbf{p}\cdot\mathbf{n}|}{m} f_-(\mathbf{p}) \ P(\mathbf{p}\rightarrow\mathbf{p}') \ . \tag{1.25}$$

E_s vanishes in equilibrium – which may be explicitly demonstrated by means of

the detailed–balance relation (1.8) – as does the distinction between E_e and E_c. For any incident distribution other than the equilibrium one, (1.25) is nonzero unless scattering is absent or is entirely elastic.

As before, the mean energies introduced above may be expressed as averages of the sticking probability over equilibrium and incident fluxes,

$$E_e = \frac{1}{\sigma_e} <\varepsilon(\mathbf{p})\, \sigma(\mathbf{p})>_o = \frac{\alpha_e}{\sigma_e} E_o \tag{1.26}$$

and

$$E_c = \frac{1}{\sigma_c} <\varepsilon(\mathbf{p})\, \sigma(\mathbf{p})>_- = \frac{\alpha_c}{\sigma_c} E_- . \tag{1.27}$$

E_o is the mean energy per atom approaching the surface in equilibrium, $<\varepsilon(\mathbf{p})>_o$, and is equal to $2kT$. The net energy exchange due to scattering may also be written in terms of the mean incident energy E_- as $E_s = \alpha_s E_-$. In general then, if we wish to distinguish between condensation and scattering, three additional coefficients are necessary to describe the overall exchange of energy between a liquid and vapor which are not in equilibrium with each other.

1.4 Adsorption and Desorption

We have shown above how evaporation may be related to condensation using detailed balance once the momentum–dependent sticking probability is known. The scattering and sticking probabilities of a liquid are properties which depend only on its composition and temperature. They are unaffected by the occurrence of the phenomena they describe.

Virtually all of what has been said so far about evaporation and condensation applies directly to the related case of adsorption and desorption. There is in this instance, however, another complication whose nature is easy to appreciate. If only a few atoms bind to the substrate, so that the coverage is a fraction of a monolayer, the scattering and sticking probabilities will be essentially those of a

bare surface. On the other hand, if many layers condense, then the properties of the film start to look very much like those of a bulk liquid and we would expect the scattering and sticking probabilities to reflect this fact. Anywhere between these two extremes the film presents an intermediate case so that, for adsorption and desorption, the sticking probability will, in principle, depend on the degree of surface coverage.

The sticking probability can have a dramatic effect on even such gross quantities as the mean kinetic energy per desorbed particle, (1.26). Previous work by others had shown that desorption of H_2, HD and D_2 from a variety of metal surfaces was more or less strongly peaked in the normal direction. Comsa, *et al.* [Comsa, David and Rendulic (1977)] then studied the angular dependence of the mean kinetic energy per D_2 molecule desorbing from Ni. They found a variation between $2kT$ at glancing angles to $3.35kT$ in the direction of the surface normal as well as significantly elevated mean energies for H_2 and HD desorbing at $\Theta = 0°$.

Up to this point we have said nothing about how distribution functions change in time. The discussion has concentrated solely on the stationary properties of the scattering and sticking probabilities. A general nonequilibrium situation is usually described by a set of master equations relating the time-dependent occupation probabilities of all states to the time-dependent occupation of all other states to which they are connected by transition matrix elements. It is a feature of all experiments studying the dynamical properties of desorbing atoms that it is necessary to perform measurements under nonequilibrium conditions, otherwise it would not be possible to separately identify desorbing atoms from the totality of those leaving the surface due to other processes such as elastic or inelastic scattering, diffraction, etc. The question then arises, under what conditions are we justified in using the stationary sticking probability to relate desorption to adsorption in experiments?

The detailed–balance arguments we have put forward are valid, as long as the condensate (adsorbed film, liquid, or solid wall) remains in internal equilibrium even though the gas may be in any arbitrary state whatsoever. The occupation functions of the condensate states occurring in the master equation then have the special property that their relative number is governed by a canonical distribution at some temperature T, and the time merely reflects changes in the temperature parameter characterizing this distribution. We use the term "quasi–equilibrium" to express this idea.

A very beautiful confirmation of the applicability of the quasi–equilibrium idea to desorption is found in the experiments of Cardillo *et al.* who studied the dissociative adsorption of molecular hydrogen on copper [Cardillo, Balooch and Stickney (1975)]. Using molecular–beam techniques, they measured the momentum–dependent sticking probability for H_2 to dissociate and adsorb on a copper surface at a variety of energies and angles. From these data, they synthesized the expected results for an equilibrium incident distribution and using the detailed–balance equation (1.19), predicted the angular dependence of the total flux for associative desorption. They tested these predictions in a separate experiment where atomic hydrogen was allowed to permeate through the bulk of the crystal to the surface where it subsequently recombined into molecular hydrogen and desorbed into the surrounding vacuum. The agreement between predicted and measured angular–dependent total fluxes was excellent.

There is another subtlety which we have overlooked. It has been assumed that an atom either scatters promptly, or falls into a bound state of the condensate. This specifically neglects the possibility of scattering with a significant time delay, which would necessitate generalizing (1.6) to time–dependent kernels [Kuscer (1971), (1977)]. Phenomena of this kind are known to occur in the resonant scattering of He atoms from crystals and go by the name of selective adsorption (for a concise discussion see, for example, [Cole and Toigo (1981)]). A quasi–bound state, which is actually degenerate with the continuum, exists for

certain energies and angles of incidence where momentum of the atom perpendicular to the surface is transformed into momentum parallel to the surface by the addition of a crystal reciprocal lattice vector. The atom then spends a period of time on the surface where it may or may not interact with phonons before returning to a scattering state.

A particular choice for the scattering and sticking probabilities is the underlying dynamical assumption in our discussion of desorption in the following chapter. We suppose that a fraction α of the incident atoms stick without regard to their initial momentum while the remaining fraction, $1-\alpha$, elastically scatter. It is a unique consequence of this choice (called the Maxwell model) that the coefficients σ_e, σ_c, α_e and α_c introduced above are equal to each other and to the single parameter α, while α_s vanishes [Kuscer (1974)]. The analysis presumes that α is independent of temperature (which is always justified if we restrict our attention to a sufficiently narrow range) and also independent of coverage. In this last respect, we regard the film much as we would a liquid, and a consistent approach to physical adsorption based on this view is the subject of the next section. The idealizations we have just outlined are adopted so that we may make progress in simply describing the essential features which govern the time evolution and desorption of a heated film. As we shall see, even at this level, the task is still a challenging one, and later on we will be in a better position to assess the significance of modifications in our fundamental assumptions about the scattering and sticking probabilities.

2. Local Thermodynamics

One picture of physical adsorption treats a film, insofar as its thermodynamic properties are concerned, as a slice of the corresponding bulk material. This notion must be asymptotically correct in the limit of thick films, but it can only serve as a qualitative guide in the case of thin films. What distinguishes adsorption from ordinary condensation is that this slice finds itself in an

external field arising due to the difference between the van der Waals potential of the actual substrate and the half space of bulk material which has been displaced.

2.1 Thermodynamic Systems in External Fields

The condition of maximum entropy for a system of particles in a spatially varying external field subject to fixed volume and total energy requires that $T = const$ and

$$\mu_o(T,P) + V_{ext}(\mathbf{r}) = const \tag{1.28}$$

in equilibrium [ter Haar and Wergeland]. μ_o is the chemical potential of the homogeneous substance as a function of temperature and pressure, and $V_{ext}(\mathbf{r})$ is the potential energy at position $\mathbf{r}$ due to external forces. As a consequence of the uniformity of temperature, the equilibrium pressure must vary from point to point in such a way as to satisfy (1.28). Applying this to the case of an isothermal atmosphere in a gravitational field, for example, we recover the familiar barometric formula for pressure as a function of altitude.

The derivation of (1.28) rests on the assumption that it is possible to identify subsystems, localized around each position $\mathbf{r}$, whose volume is small enough that within any particular subsystem the external field may be regarded as constant. At the same time, it is necessary that these subsystems be so large that they may be treated thermodynamically. These considerations are the same ones motivating the Thomas–Fermi model of many electron atoms.

2.2 Frenkel–Halsey–Hill Isotherm

If we view an adsorbed film of thickness δ as a thin layer of bulk liquid atop a plane solid substrate (Fig. 1.2), then evaluation of (1.28) at the film–vapor interface gives

Figure 1.2. Bulk layer model of physisorption.

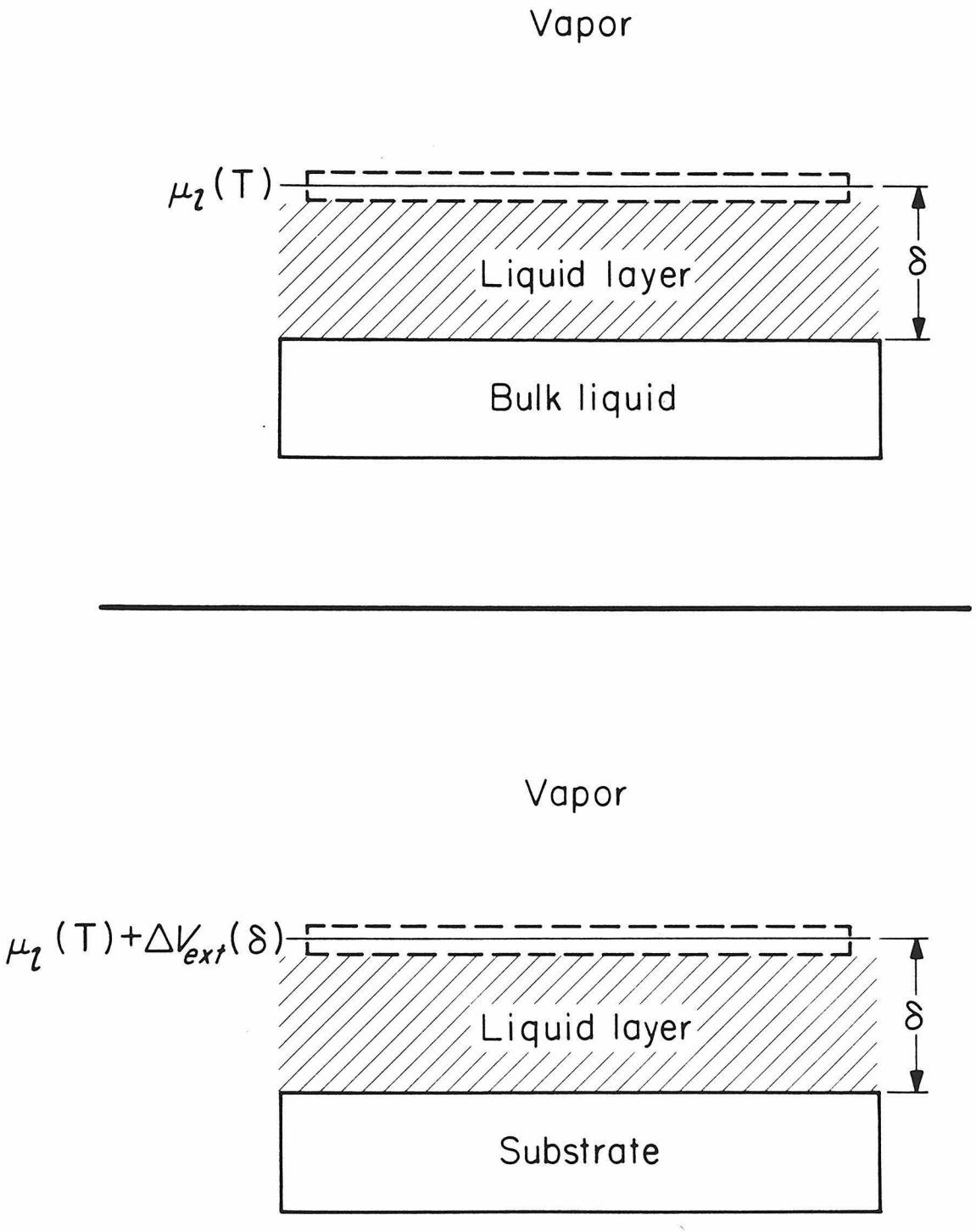

$$\mu_l(T) + \Delta V_{ext}(\delta) = \mu_f(T,\delta)\,. \tag{1.29}$$

The chemical potential of saturated vapor in equilibrium with bulk liquid, $\mu_l(T)$, replaces μ_o. It is a function of temperature only. $\Delta V_{ext}(\delta)$ is the change in potential energy caused by substituting substrate for bulk adsorbate below depth δ.

Far away from the substrate we can neglect ΔV_{ext}, which is of short range. Since (1.29) must be constant throughout the system, the vapor at infinity therefore satisfies

$$\mu_v(T,P) = \mu_f(T,\delta)\,. \tag{1.30}$$

Assuming this vapor is ideal with

$$\mu_v(T,P) = kT \ln\left[\frac{P}{kT}\left[\frac{2\pi\hbar^2}{mkT}\right]^{3/2}\right] \tag{1.31}$$

then (1.29) – (1.31) together show that

$$\ln(P/P_o) = \Delta V_{ext}(\delta)/kT\,. \tag{1.32}$$

P is the vapor pressure of the film and P_o the saturated vapor pressure of the bulk phase.

The van der Waals potential between two atoms varies as the inverse–sixth power of their separation. Integrating over a plane semi–infinite substrate one finds

$$V_{ext}(\delta) = \frac{-\gamma}{\delta^3} \tag{1.33}$$

for a film thin enough that retardation effects may be ignored [Dzyaloshinskii, Lifshitz and Pitaevskii (1961)]. A simple additivity argument then gives the difference between solid substrate and bulk liquid as

$$\Delta V_{ext}(\delta) = \frac{-\gamma+\gamma_{bulk}}{\delta^3}\,. \tag{1.34}$$

Because helium atoms attract each other so much more weakly than they attract any other substrate, γ_{He} is of the same magnitude as the theoretical uncertainty in γ [Sabisky and Anderson (1973)]. For this reason, the correction due to γ_{bulk} is usually ignored when dealing with helium films, so substituting (1.34) into (1.32) we obtain

$$P(T,\delta) = P_o(T)\, e^{-\gamma/\delta^3 kT} . \tag{1.35}$$

Equation (1.35) is known as the Frenkel–Halsey–Hill isotherm [Frenkel (1949), Halsey (1949), Hill (1949)]. It relates the vapor pressure at infinity to the film thickness (or surface coverage) and temperature, and is illustrated for the case of helium on sapphire in Fig. 1.3.

The equilibrium adsorption isotherm, along with the stationary sticking probability, contains all the information relevant to desorption if quasi-equilibrium is maintained because adsorption and desorption are then related via detailed balance. Thus, if desorption is due to the evolution of a film through a succession of equilibrium states with time, the expression (1.35) gives us the pressure, $P_f(T_f(t), \delta_f(t))$, of the equilibrium gas in terms of which the instantaneous particle and energy fluxes may be evaluated.

The chemical potential (1.29) leading to the isotherm (1.35) requires comment. First, it is a feature of the approximations inherent in its derivation that (1.29) splits into separate temperature dependent and film–thickness dependent parts. All of the interaction between particles in the condensate is lumped into $\mu_l(T)$ which reflects the three–dimensional liquid, and all of the interaction with the substrate appears in $\Delta V_{ext}(\delta)$. In general, the chemical potential $\mu_f(T,\delta)$ will not split so cleanly and will reflect, for thin films, interactions in the condensate which are essentially two–dimensional in character. Second, while the van der Waals force law (1.33) has been experimentally verified for films as thin as 3 layers [Sabisky and Anderson (1973)], it cannot hold all the way down to the substrate surface. If it did, the binding energy and chemical potential (1.29) would

Figure 1.3 Frenkel–Halsey–Hill Isotherm.

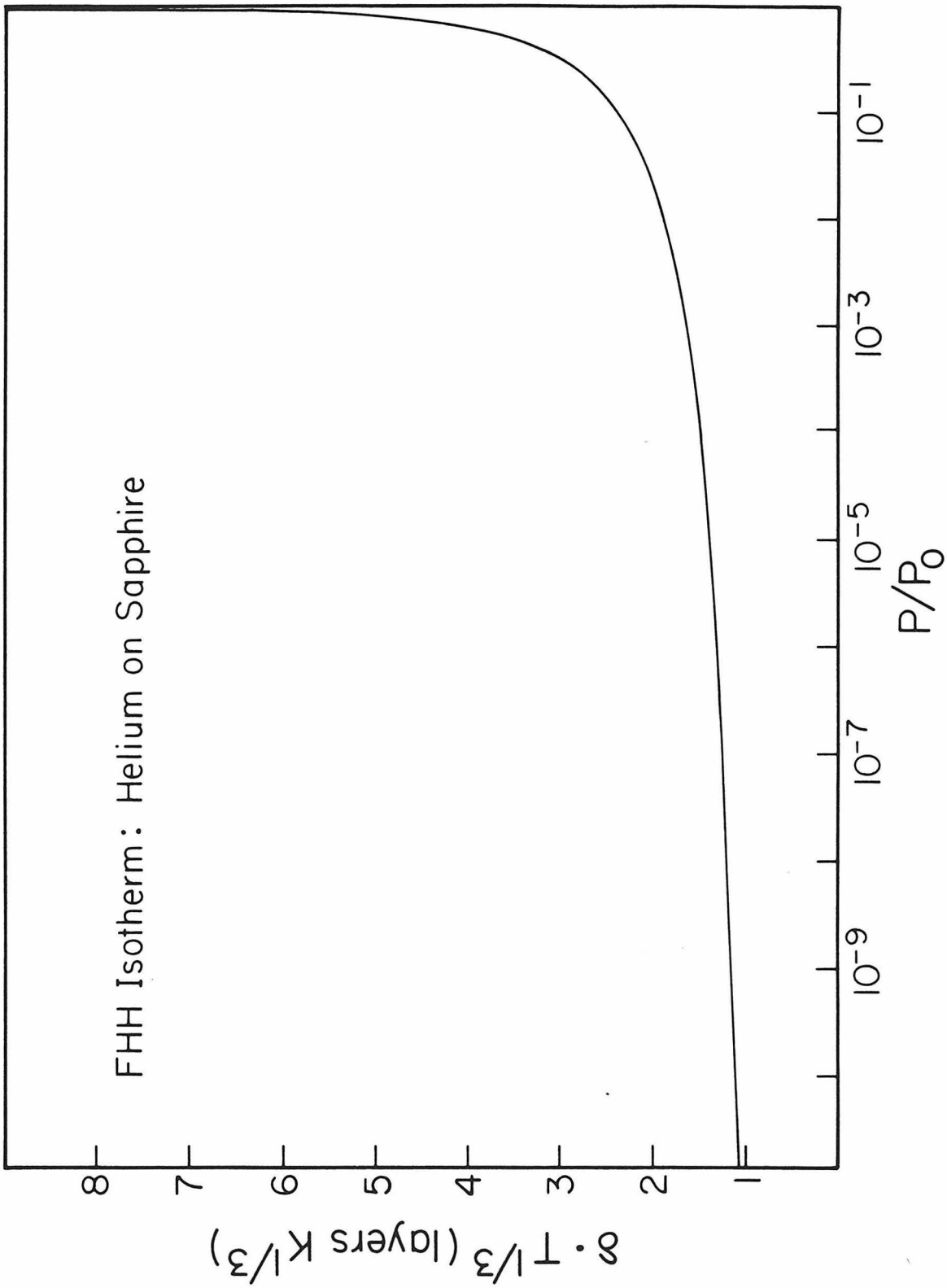

grow without bound. Atoms in the first layer experience not only the van der Waals attraction, but also the hard core repulsion of substrate atoms. A more realistic expression for the potential, including this short range repulsion, is the Lennard Jones 6–12 form. Integrating over a plane semi–infinite solid yields [Dash (1975)]

$$V(\delta) = 4\pi\varepsilon n_s[(\sigma^{12}/45\delta^9) - (\sigma^6/6\delta^3)] \tag{1.36}$$

where ε is the well depth, σ the hard–core diameter, and n_s the atomic density of the solid. Even this additional sophistication, though, represents a laterally averaged potential which neglects the effects of substrate periodicity. On a clean, well–ordered surface, this periodicity can significantly influence thermodynamic properties in the first layer (as one important example, we refer the reader to [Silva–Moreira, Codona and Goodstein (1980)] for a discussion of band–structure effects in the heat capacity of helium adsorbed on graphite).

While it is certainly not quantitatively correct to do so, we will nevertheless apply (1.29) and (1.35) to one– and two–layer helium films as a rough guide. Our justification in taking this approach is that they provide us with an analytic expression for the equation of state, and so we are able to develop a model of desorption whose consequences can be worked through explicitly. The results may then be compared directly with experiment and, armed with the insights provided by a theory whose physical foundation is so easily surveyed, we will hopefully be capable of generalizing beyond these limitations.

Finally, a remark concerning applicability of the quasi–equilibrium assumption is in order. We will always be concerned with departures from equilibrium caused by a sudden heating of the substrate on which the film rests. Presuming this substrate possesses a well–defined temperature and that the film can be viewed as a continuous medium, the relaxation time for a temperature jump to propagate through the film is of the order of l^2/χ. l is a dimension characteristic of the adsorbed layer, and χ its thermal diffusivity as given by the

ratio of thermal conductivity to specific heat per unit volume, $\kappa/\rho c_p$ [Landau and Lifshitz, *FM*]. The phenomena we seek to describe will be confined to times of 10^{-8} seconds or longer. Since the thermal relaxation time is utterly negligible on this scale, a helium film several layers thick may be regarded as having a uniform temperature at each instant if external conditions vary no more rapidly than this.

References

Cardillo, M. J., Balooch, M. and Stickney, R. E., Surf. Sci. **50** 263 (1975).

Cole, M. W. and Toigo, F. in *Interfacial Aspects of Phase Transformations*, Lectures at Ettore Majorana International School of Crystallography (1981).

Comsa, G. in *Proc. 7th Intern. Vac. Congr. & 3rd Intern. Conf. Solid Surfaces*, p. 1317 (Vienna, 1977).

Comsa, G. in *Dynamics of Gas Surface Interaction*, G. Benedek and V. Valbusa, eds., p. 117 (1981).

Comsa, G., David, R. and Rendulic, K. D., Phys. Rev. Lett. **38,** 775 (1977).

Dash, J. G., *Films on Solid Surfaces* (Academic Press, New York, 1975).

Dzyaloshinskii, I.E., Lifshitz, E. M. and Pitaevskii, L. P., Advan. Phys. **10,** 165 (1961).

Frenkel, J., *Kinetic Theory of Liquids* (Oxford University Press, London & New York, 1949).

Haar, D., ter and Wergeland, H. *Elements of Thermodynamics* (Addison Wesley, Reading, Mass., 1966).

Halsey, G. D., J. Chem. Phys. **17,** 520 (1949).

Hill, T. C., J. Chem. Phys. **17,** 590 (1949).

Kuscer, I., Surf. Sci. **25,** 225 (1971).

Kuscer, I. in *Rarefied Gas Dynamics*, 9th Symposium, p. E–1 (1974).

Kuscer, I. in *Fundamental Problems in Statistical Mechanics IV*, E. G. D. Cohen and W. Fiszdon, eds., p. 441 (1977).

Landau, L. D. and Lifshitz, E. M., *Fluid Mechanics* (Pergamon Press, New York, 1959).

Landau, L. D. and Lifshitz, E. M., *Quantum Mechanics (Non-relativistic Theory)*, 3rd edition (Pergamon Press, New York, 1979).

Landau, L. D. and Lifshitz, E. M., *Statistical Physics*, 3rd edition, Part 1 (Pergamon Press, New York, 1981).

Lang, H. and Kuscer, I. in *Rarefied Gas Dynamics*, 9th Symposium, p. F–12 (1974).

Lifshitz, E. M. and Pitaevskii, L. P., *Physical Kinetics* (Pergamon Press, New York, 1981).

Palmer, R. L. and O'Keefe, D. R., Appl. Phys. Lett. **16,** 529 (1970).

Sabisky, E. S. and Anderson, C. H., Phys. Rev. A **7,** 790 (1973).
Schiff, L. I., *Quantum Mechanics,* 3rd edition (McGraw–Hill, New York, 1968).
Silva–Moreira, A. F. Codona, J. and Goodstein, D., Phys. Lett. **76A,** 324 (1980).
Wenaas, E. P., J. Chem. Phys. **54,** 376 (1971).

Chapter 2
Continuum Model of Helium Desorption Kinetics

1. Introduction

A simple model of helium desorption kinetics based on the ideas developed in Chapter 1 is presented in the paper reproduced here.†

Overall, the point of view is easily summarized as follows. When a continuously heated film warms, its vapor pressure increases above that of the ambient gas and net desorption occurs. As desorption at the elevated temperature proceeds, the film thickness decreases, the binding energy of those atoms which remain at the film–gas interface increases, and as a consequence, the film vapor pressure begins to drop. Eventually, a steady state is achieved when the vapor pressure is low enough for the number of atoms per unit area per second, leaving the hot film to be exactly balanced by the number condensing from the cooler ambient gas. The task confronting one, then, is to characterize the time necessary to reach this steady state.

While the abstract speaks for itself, some guide to the article's content may be useful. The paper begins by introducing the experimental situation and then follows with a comprehensive (and, we hope, comprehensible) derivation of the basic relations governing the evolution of an adsorbed helium film subject to an instantaneous jump in substrate temperature. Energy and mass conservation result in coupled nonlinear ordinary differential equations describing the film temperature and thickness as a function of time. Solutions to the linearized equations are discussed and compared with experiment. A specific numerical integration of the nonlinear equations is also presented. Particular reference is made to the emergence of two very different time scales in the problem at low

† We apologize for the inevitable notational inconsistencies which develop from incorporating an already published manuscript into the body of this work. Subsequent references to the numbered figures and equations in this section will include a chapter designation so that, for example, Fig. 1 will be recalled hereafter as Fig. 2.1, Eq. (1) as (2.1), etc.

ambient pressures, representing rapid warming of the film and subsequent slow desorption. Finally, a connection is established between desorption and the long standing problem of heat transport across the solid–helium interface (Kapitza effect). In particular, it is shown that the results of phonon reflection experiments studying this phenomenon in thin films may be explained on the basis of desorption kinetics.

All of the principal insights obtained from the linearized theory are concisely summarized in [Weimer and Goodstein, Phys. Rev. Lett. **50,** 193 (1983)] which is not included here.

2. The Continuum Model

Surface Science 125 (1983) 227–252
North-Holland Publishing Company

A SIMPLE MODEL OF HELIUM DESORPTION KINETICS

David GOODSTEIN and Michael WEIMER
California Institute of Technology, Pasadena, California 91125, USA

Received 15 June 1982; accepted for publication 26 July 1982

Recent experiments studying helium desorption by heat pulse techniques are interpreted in terms of a model in which the film is assumed to have the thermodynamic properties of bulk liquid helium, and the vapor is described by kinetic theory. Equations for energy and mass conservation are sufficient to determine the behavior of the system. The most important parameter in the model turns out to be the interfacial thermal resistance between the film and vapor, R_f. This quantity varies over orders of magnitude, and is found to govern a number of the phenomena observed in the experiments. In addition to resolving some of the puzzles arising in desorption experiments, the model serves to clarify the relationship between this work and an earlier body of work concerning the Kapitza resistance in adsorbed films. Predictions of the model compare remarkably well to the results of both types of experiment.

1. Introduction

A series of recent experiments [1–5] studying the desorption of helium films on submicrosecond timescales have begun to give the problem of desorption kinetics a solid empirical foundation. Theories available for interpreting these results [6–11] have tended to be microscopic in orientation, taking as their starting points one or another model of the substrate phonon – adsorbed atom interaction. In this paper we adopt the opposite point of view, considering the accumulated experimental results in the context of a macroscopic continuum model. The model serves to identify which experimental results ought to be regarded as surprising or in need of theoretical clarification. Furthermore it provides an important conceptual link between recent desorption experiments and an earlier body of work concerning the anomalously large transport of heat across a solid/helium interface [12] – the Kapitza effect – and especially phonon reflection as a probe of that phenomenon [13–16].

The evolution of an adsorbed film with time is central to any understanding of desorption. Sinvani, Taborek and Goodstein [1] have recently reported an

* This work was supported in part by ONR Contract No. N0014-80-C-0447.

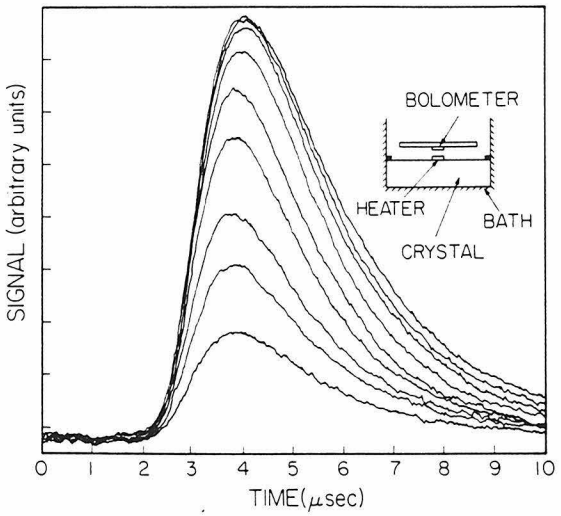

Fig. 1. Desorption time constant measurement of Sinvani et al. The sequence of curves illustrates, in ascending order, dependence of the bolometer signal on increasing heater pulse width at fixed power. The pulse widths are, respectively, 0.03, 0.06, 0.08, 0.15, 0.22, 0.5, 1, 1.5 and 2.5 μs. Inset shows experimental arrangement. Reprinted from ref. [1].

elegant technique for measuring the characteristic time needed by a heated helium film to reach steady state. The experiment is illustrated in fig. 1. An ohmic heater is thermally anchored to a phonon transparent crystal. Situated some distance above the heater is a superconducting transition bolometer. An adsorbed helium film covers the crystal and heater surfaces. When the heater is pulsed, atoms travel ballistically to the bolometer, where they are detected. For pulses of a given heater power (and hence a given steady state temperature of the adsorption substrate), the bolometer signal depends on the pulse width for short pulses, but becomes independent of it if the pulse is long enough for the film to reach steady state. Desorption time constants are extracted by measuring the exponential approach to saturation of the signal as a function of pulse width. The model we present in this paper gives a qualitative and a semi-quantitative understanding of the results of these experiments.

A typical phonon reflection experiment [16] is shown in fig. 2. When the heater is pulsed it injects a short burst of phonons into the crystal, a substantial fraction of which travel ballistically to the far surface where some will be reflected back to the bolometer. The bolometer signal with the reflecting surface in vacuum is compared to that with the surface under liquid helium to find the fraction of the incident phonons transmitted into the helium. The Khalatnikov theory [17] predicts that because of the large disparity in the

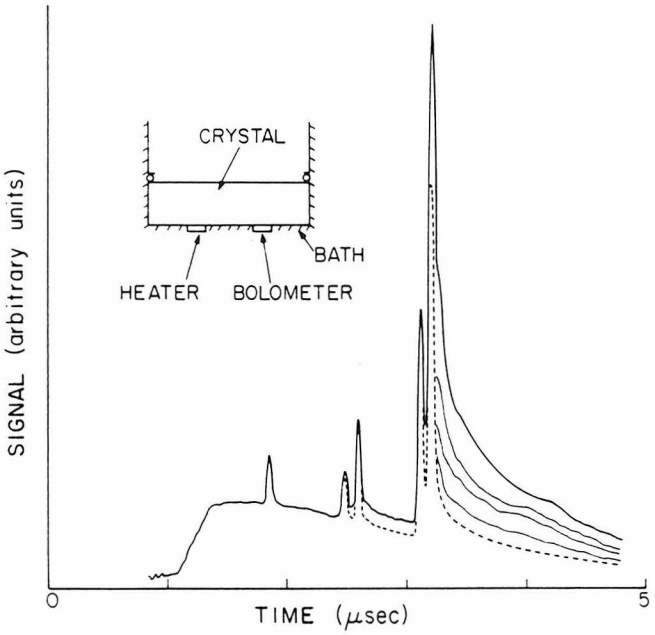

Fig. 2. Phonon reflection spectrum of Taborek and Goodstein. Heavy upper curve is for vacuum interface and dashed curve is for bulk He. Intermediate curves correspond to partial saturation P_g/P_0 of 6×10^{-5}, 3×10^{-4} and 3×10^{-3} respectively. Experimental arrangement shown in inset. Reprinted from ref. [16].

acoustic impedances of the two media this fraction should be undetectably small (~ 0.5%), but instead it is found that roughly half of the vacuum signal is lost to the helium.

It is natural to regard this result as a manifestation of the anomalous Kapitza conductance. As a means of studying the Kapitza effect, phonon reflection experiments afford a unique opportunity in that one can study the reflection signal from adsorbed films, observing the evolution from vacuum to bulk helium. It is found (see fig. 2) that the bolometer's response diminishes as the film thickness grows starting from zero, but that the change saturates, giving the bulk liquid signal when the film is only about 3 atomic layers thick. No further change in the spectrum is observed with increasing pressure up to bulk vapor pressure and beyond, into the pressurzed liquid, and even up to the solidification pressure of bulk helium [18].

This saturation of the signal, which we call the "three layer effect" was originally observed by Guo and Maris [13], by Long, Sherlock and Wyatt [14], and by Dietsche and Kinder [15]. Guo and Maris studied the dependence of the change in reflection on adsorption parameters within the first three layers

and concluded than it was correlated with film thickness and not strongly dependent on pressure or temperature – the implication being that the mechanism responsible for the anomalous heat transport becomes fully developed within about 10 Å (or three layers) of the interface. Dietsche and Kinder, working at lower temperatures, found instead that the change was dependent upon the pressure of the vapor in equilibrium with the adsorbed film. They attributed the evolution of the signal to the ratio of film–crystal to film–vapor interfacial resistances assuming the latter to be inversely proportional to the gas pressure. As we shall see, the thermal boundary resistance at the film–gas interface does indeed have this dependence.

Both of these explanations were, however, found to be untenable in the light of results obtained in what we call the power-sharing configuration. Experiments of this type, first reported by Ishiguro and Fjeldy [19], were applied to films by Taborek, Sinvani, Weimer and Goodstein [5]. The geometry is illustrated in the inset to fig. 3. From the point of view of the adsorbed helium the situation is identical to that of the time constant experiments of fig. 1. Instead of looking at the desorbed atoms, however, one concentrates on the phonons radiated back into the crystal. When a film is adsorbed on the heater, power is shared between the film and the crystal. The bolometer signal may then be compared to its value when the cell is evacuated. When the heater is

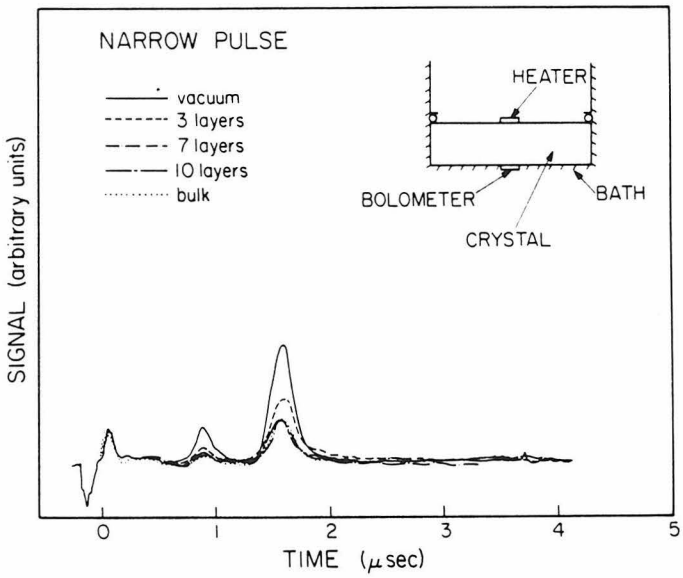

Fig. 3. Power sharing experimental configuration. Data are phonon signal as a function of helium film thickness at $T = 2$ K for heater pulse of 150 ns duration and power density 0.2 W/mm^2. Reprinted from ref. [5].

pulsed for durations comparable to those used in phonon reflection experiments in order to achieve time of flight resolution (typically ≤ 100 ns), a saturation effect at a few layers consistent with reflection spectra is obtained. When, however, the experiment is performed with long pulses (~ 10 μs) one finds (fig. 4) that the signal due to a multilayer film is more nearly like the vacuum result than like the bulk result.

This surprising observation implies that the three layer effect is a dynamic, time dependent phenomenon. Moreover, since the long heat pulse conditions are more nearly like the usual steady state measurements of the Kapitza effect and show no three layer saturation in thin films, this result casts doubt on the relevance of phonon reflection experiments to the study of the Kapitza resistance. Other authors have previously expressed doubts on this point [20].

As we shall see, one of the principal virtues of the macroscopic continuum description is that it gives an appealing account of both reflection and power sharing experiments in adsorbed films, and of the relation of these results to the Kapitza effect. The dynamics of desorption will be seen to play the central role. Previous attempts to connect these phenomena have focused on static or microscopic considerations.

In the next section of this paper, the macroscopic continuum model and some of its solutions are presented. The results of the model are compared to experiments in section 3, and the consequences are discussed in section 4. The

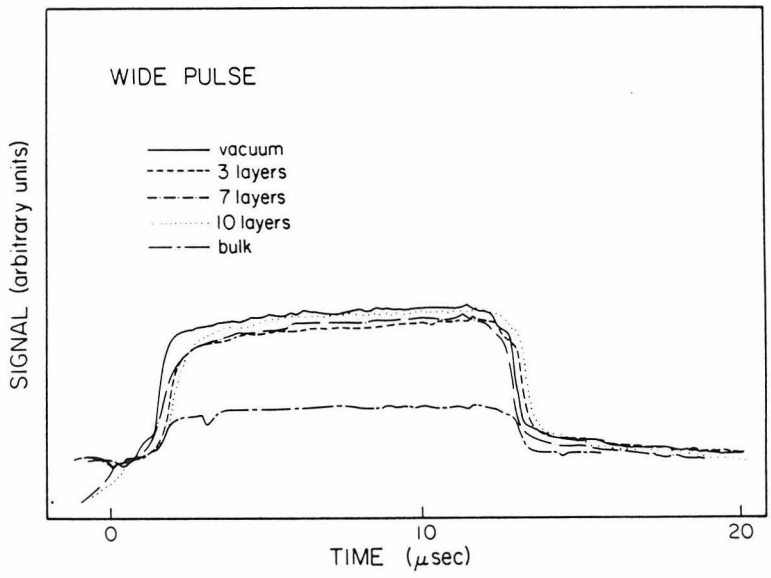

Fig. 4. Phonon signal in power sharing geometry for heater pulse of 12 μs. Other conditions identical to those in fig. 3. Reprinted from ref. [5].

quantitative estimates we have used in evaluating the model are described in the appendix.

2. The macroscopic continuum model

2.1. Basic equations

In all cases of interest to us here we are dealing with a problem whose geometry is essentially one-dimensional – an adsorbed film sandwiched between a semi-infinite gas and a substrate as sketched in fig. 5. Desorption proceeds when heat is injected into the film from the substrate, which may be either a metallic heater or crystal surface. The heated film evolves in time toward a steady state at an elevated temperature and reduced thickness. The object of the model is to predict that evolution based upon the simplest possible assumptions.

The basic strategy is to treat the adsorbed film, wherever possible, as a thin slab of bulk liquid, in instantaneous internal thermal equilibrium, and having known properties. For example, in equilibrium at temperature T_0 a film of thickness δ_0 is assumed to have chemical potential

$$\mu_{f_0} = \mu_l(T_0) - \gamma/\delta_0^3, \tag{1}$$

where $\mu_l(T_0)$ is the chemical potential of liquid ^{4}He at T_0 and γ/δ_0^3 is the attractive Van der Waals potential due to the substrate. It follows that the

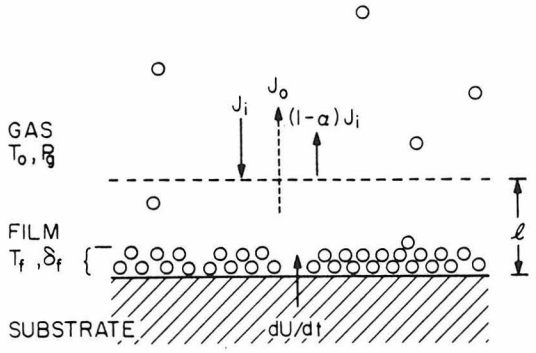

Fig. 5. Basic features of the model. Adsorbed film is treated as a thin slice of bulk liquid in equilibrium at instantaneous temperature T_f and thickness δ_f. Energy flux, dU/dt, enters the film from the substrate. Mass and kinetic energy leave the film crossing a reference boundary into the gas, which remains at ambient conditions T_0 and P_g. The fluxes J are calculated from simple kinetic theory treating the gas as ideal.

pressure in equilibrium with the film is

$$P_g = P_0(T_0)\, e^{-\gamma/\delta_0^3 k_B T_0}, \tag{2}$$

where $P_0(T_0)$ is the liquid vapor pressure at T_0.

The statement of conservation of energy for the film–gas system as a whole is simply

$$dU = dU_f + dU_g, \tag{3}$$

where U is the energy injected per unit area from the substrate, and subscripts f and g refer to film and gas respectively. Since the film itself is regarded as a subsystem internally in thermodynamic equilibrium at all times, we may write [21]

$$dU_f = T_f\, dS_f + \mu_f\, dN_f, \tag{4}$$

where S_f is the film entropy, and N_f is given by

$$N_f = n\delta_f. \tag{5}$$

Here n is the number density in the film, assumed constant and given by the bulk liquid density, and T_f and δ_f are the instantaneous film temperature and thickness. All extensive quantities are per unit area. Taking $S_f = S_f(T_f, N_f)$ one finds

$$dU_f = C_N\, dT_f + (\mu_f + T_f s_l) n\, d\delta_f, \tag{6}$$

where C_N is the isosteric heat capacity. In the spirit of the model, we have used s_l, the specific entropy of liquid helium in place of $(\partial S_f/\partial N_f)_{T_f}$.

The gas, treated as ideal throughout, is thought of as an infinite reservoir whose temperature, T_0, and pressure, P_g, are unaffected by the desorption taking place. Referring again to fig. 5 we assume the mean free path in the gas, λ, to be sufficiently large that we may imagine a plane a distance l above the substrate, subdividing the film and gas systems, such that $l \ll \lambda$, $\gamma/l^3 \ll k_B T_0$, and including a negligibly small number of gas atoms. These conditions are easily satisfied for most cases of interest with $l \sim 100$ Å. We thus envisage energy exchange between the subsystems as mediated by two independent streams of particles, one from the gas into the film and one from the film into the gas, unaffected by each other and unaffected by the Van der Waals potential exerted by the substrate. The flux of gas atoms crossing the plane from above is then given by

$$J_i = P_g/(2\pi m k_B T_0)^{1/2}. \tag{7}$$

These atoms carry energy per unit time

$$\dot{Q}_i = P_g(2k_B T_0/\pi m)^{1/2}, \tag{8}$$

where m is the mass of a ^{4}He atom.

Supposing that all of these atoms are either adsorbed, with constant probability α, or elastically reflected with probability $1 - \alpha$, the outgoing flux across the reference plane is given by

$$J_o + (1 - \alpha) J_i, \tag{9}$$

where J_o represents the number of particles evaporated from the film per unit time per unit area. J_o, obtained by considering the gas that would be in equilibrium with the film at temperature T_f and thickness δ_f, is

$$J_o = \alpha P_f / (2\pi m k_B T_f)^{1/2}, \tag{10}$$

with P_f given by

$$P_f = P_0(T_f)\, e^{-\gamma/\delta_f^3 k_B T_f}, \tag{11}$$

and where

$$\dot{Q}_o = \alpha P_f (2k_B T_f/\pi m)^{1/2} \tag{12}$$

is the corresponding energy flux. We simplify matters further by adopting the value $\alpha = 1$ independent of velocity because experiments indicate that to be very nearly correct for bulk liquid helium [22]. The net energy transported into the gas is then

$$dU_g = (\dot{Q}_o - \dot{Q}_i)\, dt. \tag{13}$$

Substituting eqs. (6), (8), (12), and (13) into the statement of energy conservation, eq. (3), yields

$$\frac{dU}{dt} = C_N \frac{dT_f}{dt} + (\mu_f + T_f s_l) n \frac{d\delta_f}{dt} + \left(\frac{2k_B}{\pi m}\right)^{1/2} \left(P_f T_f^{1/2} - P_g T_0^{1/2}\right). \tag{14}$$

Each term in (14) has an appealingly direct physical interpretation. The energy injected into the film–gas system (left hand side) is used up in warming the film (first term on the right), in latent heat when there is net desorption (second term) and in the excess kinetic energy of warm desorbing atoms over cool adsorbing atoms (third term).

Combining eqs. (5), (7), and (10), provides a second equation expressing the conservation of mass,

$$-n\, d\delta_f/dt = (2\pi m k_B)^{-1/2} \left(P_f T_f^{-1/2} - P_g T_0^{-1/2}\right). \tag{15}$$

The response of the film is governed by these two fundamental equations. C_N and μ_f depend on both T_f and δ_f, s_l is a function of T_f alone, and all quantities with subscript f may change with time. Noting that P_f may be eliminated by means of eq. (11) and using

$$\mu_f = \mu_l(T_f) - \gamma/\delta_f^3, \tag{16}$$

the problem can thereby be reduced to a pair of coupled, nonlinear differential

equations, (14) and (15), which yield the dynamical behavior of T_f and δ_f for any known heat flux, dU/dt.

2.2. The heat flux term

Let us now consider the specific experimental arrangement of figs. 1 and 3. The helium film is adsorbed on an ohmic heater which is itself a thin metallic film (typically $< 10^3$ Å) evaporated onto a crystal substrate. We assume that power dissipated in the heater at a rate W is radiated either into the film–gas system or into the crystal according to

$$W = \sigma_k\left(T_h^4 - T_f^4\right) + \sigma_c\left(T_h^4 - T_0^4\right), \tag{17}$$

where T_h is the heater temperature. We also assume that the crystal, like the gas, is an infinite reservoir whose temperature is always T_0. For small temperature differences this becomes

$$W = \frac{T_h - T_f}{R_k} + \frac{T_h - T_0}{R_c}, \tag{18}$$

where the coefficients σ_k and σ_c, effective Stefan–Boltzmann constants for phonon radiation, are related to the Kapitza resistances R_k and R_c via

$$R_{k,c}^{-1} = 4T^3\sigma_{k,c}. \tag{19}$$

R_c or σ_c which relates to the interface between the heater and the crystal may be dependably computed from acoustic mismatch theory [23]. In the spirit of the model, R_k, between heater and film, is taken as the measured Kapitza resistance between the heater material and liquid helium. We then have

$$dU/dt = \sigma_k\left(T_h^4 - T_f^4\right). \tag{20}$$

With W a known experimental quantity, T_h is a third dynamical variable along with T_f and δ_f, and (17) another equation supplementing (14) and (15). This allows through (20) the elimination of dU/dt from (14). We note eq. (17) assumes implicitly that the intrinsic time constant of the heater, $C_h R_k R_c (R_k + R_c)^{-1}$, typically of order 10 ns with C_h the metal film heat capacity, is much less than any other time in the problem.

Experiments in the phonon reflection geometry of fig. 2 are of an essentially different nature, requiring an alternate form for dU/dt. We imagine a phonon energy flux, $\dot{R}$ (energy/time · area) incident at the upper crystal surface. Taborek and Goodstein [16] have shown that a fraction of this flux, $(1 - \eta)\dot{R}$, is specularly reflected. We assume the remaining fraction, $\eta\dot{R}$, to be absorbed at the interface. The absorbed phonons heat the film to temperature T_f, causing energy to be radiated back into the crystal at a rate $\sigma_k(T_f^4 - T_0^4)$ so that

$$dU/dt = \eta\dot{R} - \sigma_k\left(T_f^4 - T_0^4\right). \tag{21a}$$

Since in experiments of this kind the energy flux is typically very much smaller than with the film adsorbed directly on the heater, a linear approximation seems likely to be justified. Under these circumstances we obtain

$$dU/dt = \eta\dot{R} - (T_f - T_0)/R_k \tag{21b}$$

to replace dU/dt in eq. (14).

2.3. The Kapitza resistance of the film–gas interface

If dU/dt is constant for a sufficiently long period all other time derivatives in (14) and (15) may be set to zero. Eliminating P_f between the two equations yields

$$dU/dt = (T_f - T_0)/R_f, \tag{22}$$

where R_f, given by

$$R_f = (\pi m/2k_B)^{1/2}\left(T_0^{1/2}/P_g\right), \tag{23}$$

is the Kapitza resistance of the film–gas interface. In steady state, energy transport between the film and gas is thus linear in the temperature difference. We should stress that the coefficient of proportionality, R_f^{-1}, depends only on the preexisting gas conditions T_0 and P_g. This result, unlike eq. (18) for example, is exact, provided that the gas is largely undisturbed, and valid even if $T_f - T_0$ is not small. The expression for R_f may be compared with previous work by restoring α, the sticking coefficient, to our equations and writing $P_g = (\rho_g/m)k_B T_0$. Then,

$$R_f = \left(m/2\alpha\rho_g k_B\right)(2\pi m/k_B T_0)^{1/2}, \tag{24}$$

which is identical to the result of a simple Knudsen gas model of evaporation from the bulk [24].

To appreciate the role played by R_f in the model let us begin by considering the situations illustrated in figs. 1 and 3. In most experiments of this kind, W is not sufficiently small to justify linearizing the dynamical equations. Nevertheless, some qualitative insight may be gained by doing so. Equating (22) and the linear approximation to (20) combined with (18) gives

$$T_f - T_0 = R_f R_c W/(R_c + R_k + R_f). \tag{25}$$

This equation expresses the fact that in steady state as much heat flows into the helium as the gas is capable of carrying away in the form of excess kinetic energy of evaporating over condensing atoms. The situation can be usefully represented by a simple circuit diagram, fig. 6a, in which heat flux appears as electric current, temperature as voltage, and thermal resistance as electrical resistance. The energy flow and temperature drops that result are a consequence of the current divider formed by the series combination of R_k and R_f,

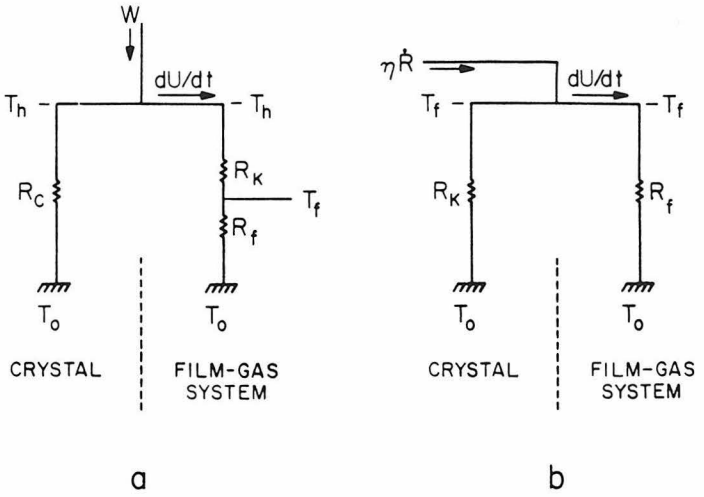

Fig. 6. Equivalent circuits for linearized equations in steady state. Heat fluxes, temperature differences and thermal boundary resistances are equivalent to currents, voltage drops and electrical resistances respectively. (a) Desorption (fig. 1) and power sharing (fig. 3) configurations. (b) Phonon reflection configuration (fig. 2). Consult text for details.

in parallel with R_c. Now R_f is inversely proportional to the gas pressure and may vary over many orders of magnitude as a function of initial film thickness and temperature. R_k and R_c vary little in comparison. For thin films at low temperatures, when $R_f \gg R_k$ or R_c, the flow of energy into the helium is effectively choked off. The film temperature approaches that of the heater with very little energy escaping into the gas. A similar circuit (fig. 6b) describes the steady state behavior in reflection experiments, with identical consequences for thin films. If we now consider the opposing limit of thicker films and higher temperatures, R_f may become small enough to short circuit R_k causing heat to flow freely from the substrate into the gas. The film temperature never gets above ambient and negligible energy is re-radiated back into the crystal. This is basically the explanation offered by Dietsche and Kinder [15] for the three-layer effect. Unfortunately, it does not give the three-layer effect quantitatively, and moreover is only applicable in steady state where there is no three-layer effect. We shall return to these points in section 3.

What we wish to emphasize here instead is that R_f is very important in determining the overall character of the film's behavior. This point, illustrated in the steady state above, applies equally well to the full dynamical equations as we shall see below.

2.4. The linearized problem

Defining

$$\chi = (\delta_f - \delta_0)/\delta_0, \tag{26}$$

$$\theta = (T_f - T_0)/T_0, \tag{27}$$

eq. (14) may be rewritten as

$$\frac{R_f}{T_0} Q = R_f C_N \frac{d\theta}{dt} + \theta + R_f G\left[(1+\theta)^4 - 1\right] + nk_B\delta_0 R_f \frac{d\chi}{dt}\left[\frac{-l(T_0(1+\theta))}{k_B T_0} + \tfrac{1}{2}(1+\theta) - \frac{1}{(1+\chi)^3}\ln\left(\frac{P_0(T_0)}{P_g}\right)\right], \tag{28}$$

where $Q = \sigma_k W/(\sigma_c + \sigma_k)$ and $G = \sigma_c\sigma_k T_0^3/(\sigma_c + \sigma_k)$ if dU/dt is of the form (20), or $Q = \eta\dot{R}$ and $G = \sigma_k T_0^3$ if dU/dt is of the form (21a). Eq. (15) becomes

$$2nk_B\delta_0 R_f \frac{d\chi}{dt} = 1 - \frac{1}{(1+\theta)^{1/2}} \frac{P_0(T_0(1+\theta))}{P_0(T_0)} \times \left[\left(\frac{2k_B}{\pi m T_0}\right)^{1/2} R_f P_0(T_0)\right]^{1 - 1/(1+\theta)(1+\chi)^3} \tag{29}$$

We have made use here of the fact that $\mu_l(T) = \mu_{sv}(T)$, the chemical potential of the saturated vapor in equilibrium with bulk liquid, where

$$\mu_{sv}(T) + Ts_l = \tfrac{5}{2}k_B T - l(T), \tag{30}$$

and l is the bulk latent heat of evaporation at temperature T,

$$l(T) = k_B T^2 \, d\ln[P_0(T)]/dT. \tag{31}$$

Eqs. (28) and (29) are convenient forms for numerical integration and other manipulations. They also display clearly the importance of R_f, which changes over orders of magnitude while all other coefficients change slowly.

For changes in δ_f and T_f small compared to their original values eqs. (28) and (29) may be linearized to leading order in χ and θ. Then,

$$J = \tau_b(d\theta/dt) - \tfrac{1}{2}\tau_a B(d\chi/dt) + D\theta \tag{32}$$

replaces the expression of energy balance eq. (14), and

$$-\tau_a(d\chi/dt) = A\chi + B\theta \tag{33}$$

replaces the expression of mass balance eq. (15), with coefficients

$$A = 3\ln(P_0/P_g), \quad B = l_0/k_B T_0 + \ln(P_0/P_g) - \tfrac{1}{2}, \tag{34a}$$

$$\tau_a = 2k_B n\delta_0 R_f, \quad \tau_b = C_N R_f, \tag{34b}$$

where $P_0 = P_0(T_0)$ and l_0 is given by eq. (31) evaluated at $T = T_0$. In those instances where the film is adsorbed directly on the heater,

$$J = \frac{R_f}{T_0}\frac{R_c}{R_k + R_c} W, \tag{35a}$$

$$D = 1 + \frac{R_f}{R_c + R_k}, \tag{35b}$$

whereas in the reflection geometry

$$J = (R_f/T_0)\eta\dot{R}, \tag{36a}$$

$$D = 1 + R_f/R_k. \tag{36b}$$

The film is initially undisturbed with

$$\chi(t=0) = \theta(t=0) = 0. \tag{37}$$

We are interested in understanding what happens when either a heater is pulsed or a steady phonon flux is suddenly incident at the crystal's surface. Mathematically, this corresponds to obtaining the solutions of the coupled system, eqs. (32) and (33) subject to (37), for a step in the driving function J. These solutions, conveniently found using Laplace transforms or more elementary techniques, are

$$\theta = \theta_{ss} f(t), \tag{38}$$

$$\chi = \chi_{ss} g(t), \tag{39}$$

with

$$f(t) = 1 - \theta_1 e^{-t/\tau_1} - \theta_2 e^{-t/\tau_2}, \tag{40}$$

$$g(t) = 1 - \chi_1 e^{-t/\tau_1} - \chi_2 e^{-t/\tau_2}, \tag{41}$$

where in steady state

$$\theta_{ss} = J/D, \tag{42}$$

$$\chi_{ss} = -BJ/AD. \tag{43}$$

One finds that under almost all circumstances the two decay times are widely different in magnitude. Denoting the larger of them τ_1, then to a very excellent degree of approximation $\tau_1 \gg \tau_2$ and

$$\tau_1 = \frac{(D + \frac{1}{2}B^2)\tau_a + A\tau_b}{AD} \tag{44}$$

$$\tau_2 = \frac{\tau_a \tau_b}{(D + \frac{1}{2}B^2)\tau_a + A\tau_b}. \tag{45}$$

The coefficients in (40) and (41) are given by

$$\theta_1 = (A\tau_1 - \tau_a)/A(\tau_1 - \tau_2) \simeq 1 - \tau_a/A\tau_1, \quad \theta_2 = 1 - \theta_1, \tag{46a}$$

$$\chi_1 = \tau_1/(\tau_1 - \tau_2) \simeq 1 + \tau_2/\tau_1, \quad \chi_2 = 1 - \chi_1. \tag{46b}$$

A circuit whose properties are entirely equivalent to eqs. (32) and (33) is illustrated in fig. 7 where $T_f - T_0 = T_0\theta$ and with

$$C_L = \frac{2nk_B\delta_0}{3\xi \ln(P_0/P_g)}, \quad \xi^{-1} = \tfrac{1}{2}B^2. \tag{47}$$

Two time constants appear in the solution, eqs. (38) to (41), because there are two independent heat reservoirs in the problem. Energy may be stored either in elevating the temperature of the film (represented by C_N) or in heat of desorption (C_L). Energy flowing into the film–gas system is directed through three parallel branches. The current in each path represents, respectively, the heat that goes into warming the film, the addtional kinetic energy of hotter desorbed atoms over colder recondensed ones, and heat of desorption. The net amount of the film desorbed, $\delta_0 - \delta_f = -\delta_0\chi$, is given by the voltage drop across C_L when all thermal impedances, R_{th}, of dimension deg cm^2 s/W are replaced by mass impedances, R_m, of dimension layers cm^2 s/W according to $R_m = (B\delta_0/AT_0)R_{th}$.

In steady state all current into the film–gas system is directed through R_f and the temperature drops across C_L and C_N are equal. The circuits of fig. 7 then reduce to those shown previously in fig. 6.

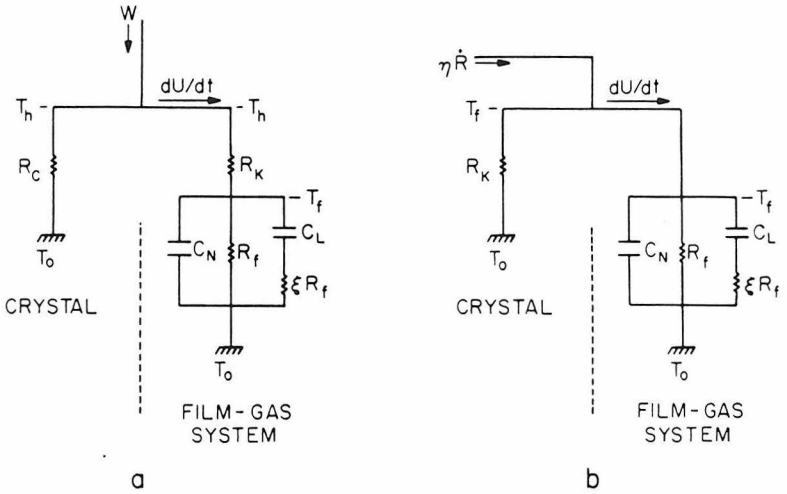

Fig. 7. Equivalent circuits for linearized dynamical equations (32) and (33) of the text. See eq. (47) for definitions of C_L and ξ. (a) Desorption and power sharing geometries. (b) Phonon reflection geometry.

3. Results

The results of the last section yield a very simple behavior for the film thickness, χ, as a function of time during steady heating. Since $\chi_1 \approx 1$ and $\chi_2 \approx 0$, we have

$$\chi \cong \chi_{ss}(1 - e^{-t/\tau_1}). \tag{48}$$

Thus, the film decays to its final thickness with a single time constant τ_1. The temperature, however, has a more complicated behavior because θ_1 is found to vary from nearly zero to nearly one. When $\theta_1 \approx 1$, the temperature follows the film thickness, approaching its final value exponentially with the same time constant, τ_1. However, when $\theta_1 \approx 0$ (and, consequently, $\theta_2 \approx 1$), θ jumps quickly, in time $\tau_2 \ll \tau_1$, to near its final value, and remains nearly constant while the film desorbs. Broadly speaking, $\theta_2 \approx 0$ for thicker films, and $\theta_2 \approx 1$ for thin films. In fact, the value of θ_2 is a result not of the film thickness, but rather of R_f, which, like the film thickness, is controlled by P_g. Very roughly, θ_2 changes from zero to one as P_g goes from about 10^{-1} to 10^{-3} Torr as shown in table 1. The corresponding film thickness depends on temperature, but is typically in the range of one to a few layers above 1 K.

The reason for the rapid temperature jump for thin films (small P_g, large R_f) may be seen in the circuits of fig. 7. R_f and ξR_f present very large impedances (typically, $\xi \sim 0.1$) so neither heat nor mass escapes easily from the film. Virtually all of dU/dt goes, initially, into "charging" C_N. This establishes $T_f - T_0$ quickly with time constant $\tau_2 \to RC_N$ where R is either R_k or $(R_k + R_c)$ as the case may be. The "voltage" across C_L, $\delta_0 - \delta_f$, is initially zero and the capacitor looks like a short. It charges by drawing current through ξR_f in series with $R_f \| R$ resulting in a time constant $\tau_1 \to \xi R_f C_L \gg \tau_2$. In film language, heat is unable to escape through the film–gas interface, so T_f rises quickly (to

Table 1
Coefficient θ_2 in linearized model as a function of initial gas pressure for several temperatures; θ_2 is the fraction of film temperature elevation occurring on a time scale $\tau_2 \ll \tau_1$, where τ_1 is the characteristic time for desorption

P_g (Torr)	θ_2		
	1 K	2 K	3 K
10^{-9}	1.00	1.00	1.00
10^{-7}	1.00	1.00	1.00
10^{-5}	0.97	1.00	1.00
10^{-3}	0.38	0.84	0.94
10^{-1}	0.04	0.10	0.21
1		0.04	0.05

T_h if it is adsorbed on the heater), and then the film desorbs at leisure, the rate being governed by the small value of P_g. As P_g increases and R_f becomes comparable to R, on the other hand, the two capacities are coupled. Desorption keeps the film from warming rapidly, and θ and χ change together. This is the case in which $\theta_1 \approx 1$.

Isothermal desorption at $T_f \approx T_h$ for sufficiently large R_f is not merely a result of linearizing the model. The nonlinear equations (28) and (29) may be integrated numerically and a representative example is presented in fig. 8. One clearly sees that heating and desorption can take place on widely different time scales.

Cole et al. [25] have developed a technique for measuring the temperature of a desorbing film as a function of time by studying the differential behavior of the desorption signal as a function of heater pulse width. Analyzing data of Sinvani et al. [1] for a film less than two layers thick, they show that the film desorbs at an essentially constant temperature close to that of the underlying heater. This observation is in excellent agreement with the model. We predict that the opposite result, namely the film temperature and thickness changing with the time in a coupled manner, should be observed for thicker films. This prediction, like that of isothermal desorption, should be valid even for much larger heat inputs than those required for linearizing the equations, since the most important parameter, R_f, depends only on initial conditions.

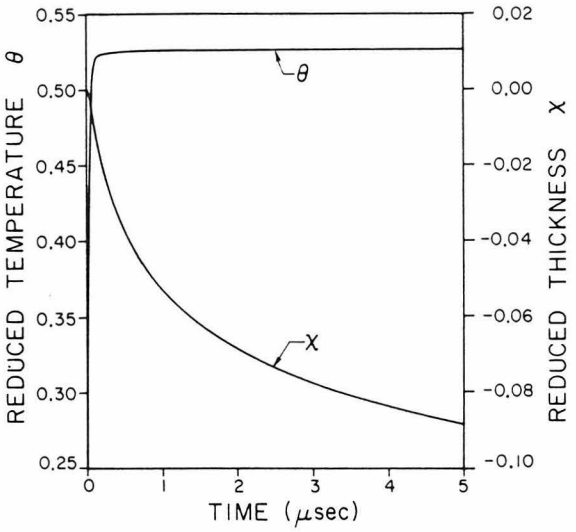

Fig. 8. Numerical integration of eqs. (28) and (29) showing film temperature and thickness as a function of time in desorption geometry of fig. 1 for $T_0 = 3.5$ K, $P_g = 10^{-5}$ Torr, and equivalent heater temperature $T_h = 5.4$ K. Illustrates isothermal desorption under realistic experimental conditions [1].

The model predicts that a heated film will reach steady state with time constant τ_1. Unfortunately, the time constant measurements of Sinvani et al. [1] are made by heating a film, initially at 1–4 K, to a final temperature between 5 and 11 K. The solutions of the linearized equations clearly do not apply to such large temperature changes. In principle, the full nonlinear equations could be integrated to find the relevant times, but there is a severe difficulty in that eq. (11) does not apply above the critical temperature of ^{4}He, 5.2 K. Thus, we are unable to make predictions of time constants which can be compared directly to experimental results. However, an empirical formula is given, which fits the measurements very well,

$$\tau = \tau_0 \, e^{E/k_B T_h}. \tag{49}$$

Here T_h, the calculated heater temperature, is found to be approximately equal to the experimentally determined temperature of the film, the parameter E is found to be approximately equal to $-2\mu/3$ with μ the chemical potential of the film before heating, and τ_0 varies between 10^{-9} and 10^{-10} s. Very crudely, then, the experiments give

$$\tau \approx 1 \text{ ns} \times e^{-2\mu/3k_B T_h}. \tag{50}$$

This empirical form works surprisingly well over a wide range of T_h. If we use it to extrapolate to $T_h \approx T_0$ where our linearized equations are valid, we can compare experiment to our model by comparing the values of τ in eq. (50) with the predictions for τ_1.

For thin films, our calculated values of τ_1, like the values of τ that emerge from eq. (50) depend strongly on the gas pressure, P_g, and only very weakly on temperature at a given P_g. In table 2 we compare $e^{-2\mu/3k_B T_0}$, which is τ in nanoseconds according to eq. (50), to our calculated values of τ_1, over a wide range of pressures at $T_0 = 3$ K. Given the quantitative inaccuracy of the

Table 2
Comparison of $e^{-2\mu/3k_B T_0}$ to the time constants τ_1 predicted by the linearized model, for $T_0 = 3$ K; $e^{-2\mu/3k_B T_0}$ is an extrapolation of the measured desorption time constants of Sinvani et al. [1] expressed in nanoseconds; the experimental data do not extend to pressures above $P_g \approx 10^{-3}$ Torr

P_g (Torr)	$e^{-2\mu/3k_B T_0}$	τ_1 (ns)
10^{-9}	1.8×10^{8}	6.6×10^{8}
10^{-7}	8.4×10^{6}	8.5×10^{6}
10^{-5}	3.9×10^{5}	1.2×10^{5}
10^{-3}	1.8×10^{4}	1.9×10^{3}
10^{-1}	8.4×10^{2}	1.4×10^{2}
10	39	32
180	5.7	9.5×10^{2}

macroscopic model, the approximate nature of (50) and the extrapolation involved, the agreement is remarkable.

The model also permits us to understand the three-layer effect [13–16], discussed in section 1, and to explain why it appears to be present only in experiments done with relatively short heat pulses [5]. The essence of the effect is revealed by, once, again, referring to the circuit of fig. 7b. For times short compared to those necessary to develop the steady state voltage across R_f the capacitors in parallel with it appear as small impedances reducing the net impedance of the film–gas system relative to that of the crystal. As we have already seen, for thin films where R_f is large, C_N charges in a time too short to be detected. Thus, even while C_L charges slowly, the impedance of the film–gas system is governed by $R_f \| \xi R_f$ which is very large. For thicker films where R_f is smaller, however, we saw C_N and C_L develop their voltage with the same time constant τ_1. For times $t \ll \tau_1$ the shorting capacitances C_L and C_N cause the impedance of the film–gas system to appear very small indeed, thereby drawing away almost all of the current $\eta\dot{R}$. In film language, at $t \ll \tau_1$, and when R_f is not too large, a great deal of incident energy is carried away as latent heat, rather than being returned to the crystal, because net desorption is occurring. For longer times or thinner films, that heat is detected instead by the bolometer, and the signal therefore approaches the vacuum result.

More explicitly, in reflection experiments the bolometer intercepts some fraction of the specularly reflected flux, $(1-\eta)\dot{R}$, and also of the heat radiated by the film back into the crystal, $(T_f - T_0)R_k^{-1} = \theta T_0 R_k^{-1}$ (eq. (21b)). When the interface is in vacuum, the entire flux, $\dot{R}$, is returned to the crystal, and the bolometer detects the same fraction of that. Thus,

$$F(t) = 1 - \eta + T_0\theta(t)/R_k\dot{R} \tag{51}$$

is the bolometer signal due to heat leaving the interface at time t after the beginning of the pulse arrives there, divided by the same part of the bolometer signal for the vacuum interface.

The bolometer signal as a function of time depends on $F(t)$ in a very complicated way, since the pulse arrives at different times at different parts of the interface, and the bolometer receives phonons from various parts of the surface at any given time. However, the principal features of the bolometer signal are relatively well defined peaks, each due to specular reflection of a particular mode from a point on the surface, together with reradiated phonons from near the same point [16]. The specular portion of $F(t)$, $1-\eta$, is reflected from that point from time $t = 0$ to $t = t_p$, the pulse width. At $t = t_p$, the film temperature is near the highest value it will reach, so the reradiated portion of $F(t)$ is then at its maximum. Thus, if we evaluate $F(t)$ at $t = t_p$, we should get a result proportional to the maximum height of the bolometer signal for any mode. In other words, $F(t_p)$ is the quantity Guo and Maris [13] define as the reflection coefficient: the height of a peak divided by its value in vacuum.

Using eqs. (36), (38) and (42), we find

$$F(t_p) = 1 - \eta + \eta \frac{R_f}{R_f + R_k} f(t_p). \tag{52}$$

The three layer effect emerges from an examination of eq. (52). It is most easily analyzed for experiments in which

$$\tau_2 \ll t_p \ll \tau_1 \tag{53}$$

This condition is well satisfied in the experiments of Dietsche and Kinder [15], for example. Under these circumstances, we consider two limiting cases:
(1) Very thin films (i.e., much less than three layers). Then P_g is very small and consequently $R_f \gg R_k$. As discussed above, we then have $\theta_1 \approx 0$ and $\theta_2 \approx 1$, so that $f(t_p) \approx 1 - e^{-t_p/\tau_2} \approx 1$ and hence $F(t_p) \approx 1$.
(2) Thicker films (three layers or more). Now P_g is higher, $R_f \approx R_k$, $\theta_1 \approx 1$, $\theta_2 \approx 0$. We have

$$f(t_p) \approx 1 - e^{-t_p/\tau_1} \approx t_p/\tau_1,$$

so that

$$F(t_p) \approx 1 - \eta \left[1 + \frac{R_f}{R_f + R_k} \frac{t_p}{\tau_1} \right].$$

The second term in the brackets is small, so that $F(t_p) \approx 1 - \eta$, barely changing for films of more than three layers.

The predicted reflection coefficient, $F(t_p)$, is compared to the data of Dietsche and Kinder [15] in fig. 9a. The parameter η is obtained by comparing $F = 1 - \eta$ with the bulk value of the reflection coefficient. The agreement between model and experiment is excellent. In fig. 9b, the model is compared to measurements by Guo and Maris [13] at higher temperature. Here the important parameters of the model (i.e., R_f, θ_2, τ_1) behave quite differently, predicting a different form for the experimental results. Nevertheless, the agreement is still quite good.

Power sharing experiments (fig. 3) give results qualitatively similar to reflection experiments (i.e., the three-layer effect) when short pulses like those in the reflection experiments are used. It is now easy to see the reason why. While a film of about three layers is desorbing, it is capable of carrying away, in the form of heat of desorption, nearly as much energy as can enter it via the Kapitza resistance at the film–substrate interface. It thus has the same effect on the signal as bulk liquid does. On the other hand, when power sharing experiments are done with pulses long compared to τ_1 (fig. 4), there is no net desorption. The film reaches steady state and can carry away heat only because desorbing atoms have more kinetic energy than adsorbing ones. Most of the heat returns to the crystal, giving a signal more nearly like the vacuum result.

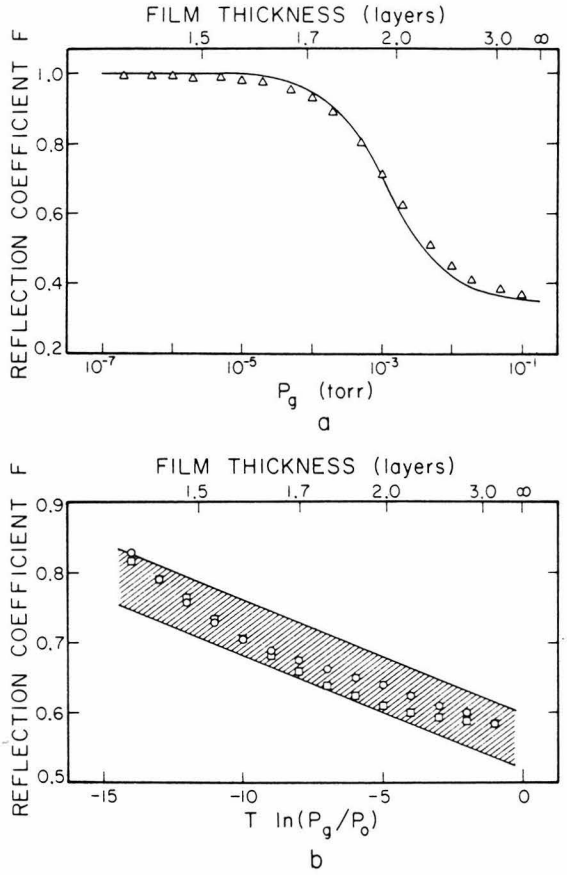

Fig. 9. (a) Comparison of predicted reflection coefficient with data of Dietsche and Kinder [15] at $T = 1.04$ K. Solid line is an empirical fit to their data and triangles represent numerical evaluation of eq. (52) with $\eta = 0.65$ and $t_p = 100$ ns. Film thickness is quoted as atomic layers on silicon. Dietsche and Kinder actually give the area under the transverse mode peak at partial helium saturation divided by that in vacuum. As these peaks are relatively well localized in time we assume the area under them to be proportional to the maximum signal height. (b) Comparison with the data of Guo and Maris [13] again for helium on silicon but in a different temperature and pressure regime. Circules are calculated values for $T = 1.85$ K and squares are calculated for $T = 3.35$ K. $\eta = 0.43$ and $t_p = 100$ ns in both instances. The cross hatched region represents the error bars cited by Guo and Maris.

4. Discussion

Two recent desorption experiments have yielded results which are contrary, not to the predictions of our model, but rather to its assumptions. Taborek [2]

has studied the angular distribution of atoms desorbed from a pulsed heater, and found that it is more sharply peaked in the direction perpendicular to the plane of the film than expected on the basis of a simple $\cos\theta$ distribution. This result contradicts our assumption that $\alpha = 1$, independent of v, and hence that the outgoing flux is equivalent to that from a half space of ideal gas. In addition, Taborek et al. [3] have observed the time of flight spectrum of desorbed atoms due to phonons which propagate through the substrate crystal from a remote heater (as in the reflection geometry, fig. 2). Desorption in this case is caused by a low intensity beam of hot phonons incident at the crystal–film interface. Since the incident energy flux is low, thermal desorption takes place at just above ambient temperature, a result which they observe. In addition, however, they find a second peak in the spectra, at shorter times of flight, which corresponds to atoms at the much higher heater temperature. This result violates our assumption that all phonons incident at the interface are either reflected or thermalized in the film. In fact the interpretation of both of these experiments is that substrate phonons may cause atoms to desorb directly from the film without first being brought into equilibrium by it. Thus, the picture we adopt here, that the desorption rate of an evolving film is equal to that of an equilibrium film of the same temperature and thickness, appears to break down.

These experiments show that our model, regardless of its successes, cannot form a complete account of desorption. In fact it is not intended to do so, but rather to help in separating the effects of predictable macroscopic phenomena from new microscopic phenomena one wishes to study. The model shows that a number of seemingly puzzling results that might have been thought to reflect new underlying principles are actually subtle but predictable consequences of the interplay of energy and mass balance. Thus in evaluating the model we are placed in a somewhat unfamiliar position: we must be disappointed in its successes and skeptical of its failures, since only where it fails are there new discoveries to be made.

In this light, let us review briefly the principal areas in which our treatment has clarified the meaning of experimental results.

(1) Time evolution of the film. The observation that thin films tend to desorb at constant elevated temperature is direct confirmation of one of the model's chief results, namely, that for low gas pressures there are two widely different time constants separately governing the heating and subsequent desorption of the film. The model predicts that the temperature will change at the same rate as the film thickness in thicker films.

(2) The desorption time constant. The empirical observation [1], eq. (49), that desorption time constants have an activated form suggests an underlying microscopic mechanism. Nevertheless, the gross dependence expressed by (49) is in rough agreement with the time constant τ_1 of the model. This appears to mean that a microscopic theory that yields the correct time constants would

have to have accounted correctly for the phenomena that are described using empirical data in the model. Presumably, that would include the Kapitza resistance between the substrate and liquid helium.

(3) Power sharing experiments. The striking difference between short pulse and long pulse power sharing experiments is qualitatively accounted for by the model. The long pulse experiments might alternatively be accounted for by supposing that the signal with an adsorbed film is nearly the same as that with a bare surface because the heater burns the surface dry. The model, however, gives a different explanation: regardless of the final film thickness, the steady state heat transport into the gas depends only on the pre-existing gas pressure, P_g. Heat tends to be returned to the crystal because only a small fraction of it can be carried away as excess kinetic energy of desorbing atoms.

(4) The three-layer effect. We have seen that the model gives an excellent account of the observation that phonon reflection signals saturate at film thicknesses of about three layers. The three-layer effect therefore does not necessarily imply that the helium–solid thermal boundary resistance is film thickness dependent, developing in the first three layers. Rather, the effect arises at low temperatures as a dynamic phenomenon, not simply comparable to the results of dc Kapitza resistance measurements. Nevertheless, the DC Kapitza resistance R_k does play a well-defined role and may in fact be a constant property of the interface, the same for bulk liquid as in the thinnest film.

The quantitative successes of the model are surprising in view of the fact that many film parameters are knowingly represented inaccurately. The values we have used for the film thickness as a function of pressure and temperature, the film heat capacity, entropy, heat of desorption and binding energy are all only crude estimates. Moreover, as we have seen, there are experiments showing that our assumptions $\alpha = 1$ and internal equilibrium in the heated film cannot be wholly correct.

It follows that the phenomena we have accounted for successfully do not depend strongly on any of these factors, all of which express the microscopic nature of the film. The reason the model works well in spite of its apparent quantitative crudity is that its most important parameter, R_f, is proportional to directly measured quantities (T_0, P_g^{-1}) and varies over many orders of magnitude. The phenomena the model describes satisfactorily are those which are governed by the magnitude of R_f.

Interpretation of heat pulse experiments on adsorbed films requires sorting out a number of components which give rise to complications that might obscure the underlying physics. For example, one must understand the behavior of phonons in real, anisotropic crystals, including such effects as focusing [26], and the rules governing reflection at an ideal interface [27]. Then there is the effect of geometric and phase space factors on time of flight desorption signals. This has been discussed by Cole et al. [25]. Finally there are the

consequences of mass and energy balance in the film itself, which have been treated in this paper. We believe our results together with the previous work on these problems will provide a useful framework within which to plan and interpret future research.

Acknowledgements

We are pleased to acknowledge many stimulating discussions with Milton Cole, Moshe Sinvani, Peter Taborek and Flavio Toigo.

Appendix

We provide here details of the computations for the numerical results presented in tables 1 and 2, and figs. 8 and 9.

For all of the numerical results quoted we took as the number density in the film [28] (eq. (5))

$$n = 2 \times 10^{22}\ \mathrm{cm}^{-3}, \tag{A.1}$$

equal to that of bulk liquid at saturated vapor pressure (SVP), and as the conversion from film thickness in ångströms to that in layers

$$\delta_f(\text{layers}) = \delta_f(\text{Å})/3.6. \tag{A.2}$$

The isosteric heat capacity (per unit area) which appears in eq. (14) is assumed to be equal to that of a slice of the bulk liquid at SVP,

$$C_N = 5 \times 10^{-9} c_{SVP} \delta_f\ \mathrm{erg/cm^2 \cdot K}, \tag{A.3}$$

with c_{SVP} in units of erg/g · K and δ_f in layers. In all instances the following gross but smooth approximation which ignores the peaking of the bulk heat capacity due to the λ transition was used (compare ref. [28]):

$$c_{SVP} \approx 1.5 \times 10^6 \quad T^3\ \mathrm{erg/g \cdot K}. \tag{A.4}$$

The data in tables 1 and 2 were computed for these case of a nichrome heater on a sapphire substrate [1–5] with specific values

$$R_c = 17/T^3 \times 10^{-7}\ \mathrm{cm^2\ s\ K/erg}, \tag{A.5a}$$

$$R_k = 16/T^3 \times 10^{-7}\ \mathrm{cm^2\ s\ K/erg}, \tag{A.5b}$$

$$\gamma = 31(\text{layers})^3\ \mathrm{K}. \tag{A.5c}$$

The Kapitza resistance R_k is actually that quoted for HeII on nickel [29]. R_c is computed from the acoustic mismatch theory assuming a similar alloy, constantan, on sapphire [23]. The Van der Waals constant γ (eqs. (2), (11) and

(16)) is that for He on sapphire which is midway between values quoted [30] for representative metals. The latent heat $l_0(T_0)$ (eq. (31)) and the saturated vapor pressure $P_0(T_0)$ were obtained from the NBS tables [31] for the 1958 He temperature scale. The time constants τ_1 and τ_2 were actually computed as roots of the secular equation

$$\tau_a\tau_b s^2 + \left[\left(D + \tfrac{1}{2}B^2\right)\tau_a + A\tau_b\right] s + AD = 0, \tag{A.6a}$$

with coefficients as in eqs. (34) and (35b), and

$$s = -1/\tau. \tag{A.6b}$$

Eqs. (44) and (45) are almost always, however, a sufficiently accurate approximation.

In numerical integration of the nonlinear eqs. (28) and (29) the σ's were computed from the R's of (A.5) via eq. (19). Several additional approximations were made, in particular, the following convenient analytic interpolation for the latent heat and saturated vapor pressure:

$$\frac{l_0(T_f)}{k_B T_f} \approx \frac{11}{T_f}\,\mathrm{K}, \quad P_0(T_f) \approx 10^4\, \mathrm{e}^{-l_0(T_f)/kT_f}\,\mathrm{Torr}. \tag{A.7}$$

Although the example shown in fig. 8 pushes these approximations just slightly above the critical point the qualitative conclusions are independent of this detail. Some care, however, must be exercised in selecting an algorithm for the numerical quadrature. Technically eqs. (28) and (29) are a "stiff" system. Simply stated, this means that widely differing time constants can characterize the growth of the two variables. The equations therefore present special difficulties and the results illustrated in fig. 8 were obtained with the IMSL routine DGEAR [32] which is designed for such problems.

For the comparison with phonon reflection data in fig. 9 values for l_0 and P_0 in the linearized equations were again taken from the NBS tables. The Kapitza resistance [29] and Van der Waals constant [30] appropriate for silicon were used

$$R_k = 20/T^3 \times 10^{-7}\ \mathrm{cm^2\ s\ K/erg}, \tag{A.8a}$$

$$\gamma = 39(\mathrm{layers})^3\ \mathrm{K}. \tag{A.8b}$$

Although several values of the Kapitza resistance between silicon and helium have been quoted [29], to be consistent with our assumptions the one behaving with a $1/T^3$ dependence was adopted. Time constants were again computed as in (A.6a) but with the expression (36b) for D.

References

[1] M. Sinvani, P. Taborek and D. Goodstein, Phys. Rev. Letters 48 (1982) 1259.
[2] P. Taborek, Phys. Rev. Letters 48 (1982) 1737.

[3] P. Taborek, M. Sinvani and D. Goodstein, preprint.
See also P. Taborek, M. Sinvani, M. Weimer and D. Goodstein, Physica 107B + C (1981) 247; G.N. Crisp, R.A. Sherlock and A.F.G. Wyatt, in: Low Temperature Physics, LT14, Vol. 1, Eds. M. Krusius and M. Vuorio (North-Holland, Amsterdam, 1975).
[4] P. Taborek, M. Sinvani, M. Weimer and D. Goodstein, J. Physique C6 (1981) 852, 855.
[5] P. Taborek, M. Sinvani, M. Weimer and D. Goodstein, J. Physique C6 (1981) 825.
[6] J. Frenkel, Kinetic Theory of Liquids (Dover, New York, 1955) p. 19.
[7] R. Gomer, in: Solid State Physics, Vol. 30, Eds. H. Ehrenreich, F. Seitz and D. Turnbull (Academic Press, New York, 1975).
[8] S.C. Ying and B. Bendow, Phys. Rev. B7 (1973) 637.
[9] F.O. Goodman and I. Romero, J. Chem. Phys. 69 (1978) 1086.
[10] Z.W. Gortel, H.J. Kreuzer and S. Spaner, J. Chem. Phys. 72 (1980) 234;
H.J. Kreuzer and P. Summerside, Surface Sci. 111 (1981) 102;
E. Sommer and H.J. Kreuzer, Surface Sci. 119 (1982) L331;
E. Sommer and H.J. Kreuzer, preprint.
[11] M.W. Cole and F. Toigo, Surface Sci. 119 (1982) L346, 490 (E).
[12] There is a vast body of work on the Kapitza resistance. For a recent discussion, see:
A.C. Anderson (ch.1) and A.F.G. Wyatt (ch. 2), in: Non-Equilibrium Superconductivity, Phonons, and Kapitza Boundaries, Ed. K. Gray (Plenum, New York, 1981).
Connections between Kapitza resistance and desorption have been suggested by:
R.C. Johnson and W.A. Little, Phys. Rev. 130 (1963) 596;
G.A. Toombs and L.J. Challis, J. Phys. C (Solid State Phys.) 4 (1971) 1085;
A.R. Long, J. Low Temp. Phys. 17 (1974) 7.
[13] C.J. Guo and H.J. Maris, Phys. Rev. A10 (1974) 960.
[14] A.R. Long, R.A. Sherlock and A.F.G. Wyatt, J. Low Temp. Phys. 15 (1973) 523.
[15] W. Dietsche and H. Kinder, J. Low Temp. Phys. 23 (1975) 27.
[16] P. Taborek and D. Goodstein, Phys. Rev. B22 (1980) 1550.
[17] I.M. Khalatnikov, Introduction to the Theory of Superfluidity (Benjamin, New York, 1965) ch. 23.
[18] D. Goodstein, G. Paternò, F. Scaramuzzi and P. Taborek, in: Non-Equilibrium Superconductivity, Phonons and Kapitza Boundaries, Ed. K. Gray (Plenum, New York, 1981) ch. 21.
[19] T. Ishiguro and T.A. Fjeldly, Phys. Letters 45A (1973) 127.
[20] See A.F.G. Wyatt, in ref. [12].
[21] We are using the surface excess formalism in which no pressure–volume work term appears for the film.
See R. Elgin and D. Goodstein, Phys. Rev. A9 (1974) 2657.
[22] D.O. Edwards, P. Fatouros, G.G. Ihas, P. Mrozinski, S.Y. Shen, F.M. Gasparini and C.P. Tam, Phys. Rev. Letters 34 (1975) 1153.
[23] O. Weis, Z. Angew. Physik 26 (1969) 325;
P. Herth and O. Weis, Z. Angew. Physik 29 (1969) 101;
J.K. Wigmore, Phys. Rev. B5 (1972) 700.
[24] H. Wiechart, J. Phys. C (Solid State Phys.) 9 (1976) 553. Various hydrodynamic models give this result within a factor of order unity (provided $\alpha = 1$).
[25] M.W. Cole, D. Goodstein, M. Sinvani and P. Taborek, in preparation.
[26] H.J. Maris, J. Acoust. Soc. Am. 50 (1970) 812;
B. Taylor, H.J. Maris and C. Elbaum, Phys. Rev. B3 (1971) 1462;
P. Taborek and D. Goodstein, Solid State Commun. 33 (1980) 1191;
A.G. Every, Phys. Rev. B24 (1981) 3456.
[27] P. Taborek and D. Goodstein, J. Phys. C (Solid State Phys.) 12 (1979) 4737.
[28] J. Wilks, The Properties of Liquid and Solid Helium (Clarendon, Oxford, 1967) table A1.
[29] N.S. Snyder, Thermal Conductance at the Interface of a Solid and Helium II, Natl. Bur. Std. Tech. Note 385 (National Bureau of Standards, Washington, DC, 1969) table 1.

[30] E.S. Sabisky and C.H. Anderson, Phys. Rev. A7 (1973) 790.
[31] H. van Dijk, M. Durieux, J.R. Clement and J.K. Logan, J. Res. Natl. Bur. Std. 64A (1960) 4.
[32] The IMSL Library, Vol. 1, 8th ed. (International Mathematical and Statistical Libraries Inc., July 1980).

3. Activated Form of Desorption Time Constants

The linearized model's predictions for the desorption time constant are shown in Fig. 2.10 where they are plotted as a function of pressure for several initial temperatures. To an excellent approximation, τ_1 (nsec) = P_g^{-1}(Torr) at low pressures, independent of temperature, as indicated by the solid line. Expressing this pressure in terms of the equilibrium chemical potential μ, we find

$$\tau_1 = \frac{6\times10^{-12}}{T_o^{2.5}}\, e^{-\mu/T_o} \quad \text{(sec)} \tag{2.54}$$

which is of the form (2.49) for $T_h = T_o$. Comparing (2.54) with the empirical parameterization (2.50) we see that the two differ both in regard to the size of the prefactor and also in the functional dependence on μ in the exponent. In spite of these differences there is, nevertheless, rough agreement in the magnitude of τ_1 predicted by these formulas, as we have already seen in Table 2.

We note in passing that many theories of desorption give results like (2.54), but with $-\mu$ replaced by either a binding energy or a heat of desorption, and with a wide range of magnitudes and interpretations of the prefactor of the exponential (see, in addition to references [6] and [10] quoted in section 2, [Sommer and Kreuzer, Phys. Rev. Lett. **49**, 61 (1982)]).

Figure 2.10. Calculated τ_1 as a function of pressure for T_o = 1 K (circles), 2 K (squares), and 3 K (triangles). Straight line is limiting form for τ_1 at low pressures, τ_1 (nanoseconds) = P_g^{-1} (Torr).

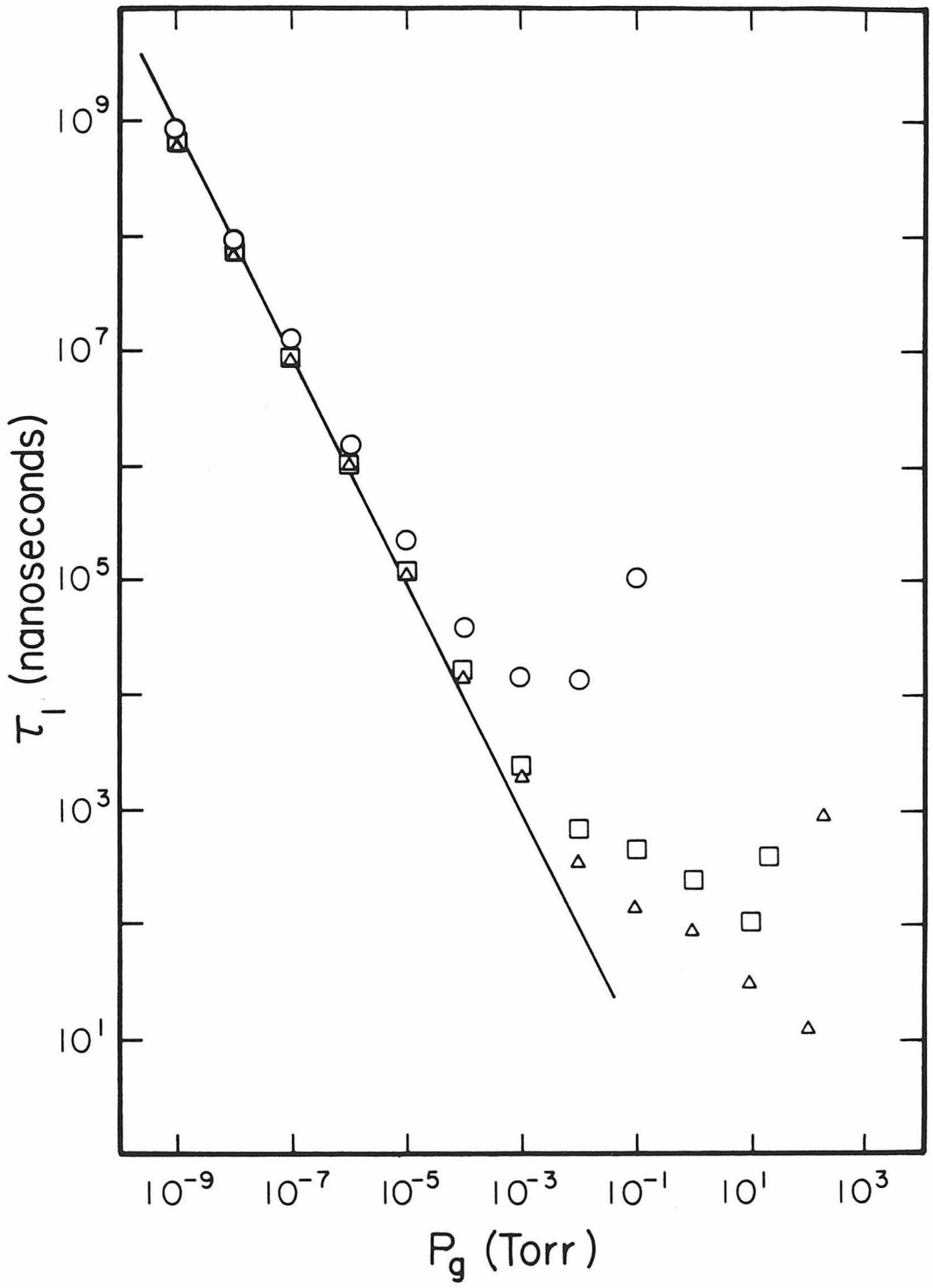

Chapter 3
Mathematical Development of the Model

1. Introduction

The purpose of this chapter is to explore the mathematical structure of the coupled differential equations arising from the continuum model introduced in Chapter 2. The linearized analysis presented there revealed a simple behavior for the system at low ambient pressures corresponding to experimental conditions. We discovered a very rapid approach of the film temperature to that of the heater substrate followed by desorption over a much longer time period. We can understand those results in a qualitative way and, as the numerical integration of Fig. 2.8 suggests, apply that insight to the nonlinear case to develop solutions whose physical meaning is apparent. As we shall see, the techniques and language of singular perturbation theory provide the natural setting for this discussion.

Our goal throughout all of this is to understand the time scales which characterize desorption in realistic situations requiring finite temperature elevations. The experiments, for example, proceed in the following way. A film initially in equilibrium is driven out of equilibrium by a heater pulse of fixed temperature and duration. Varying the duration of this pulse, a time constant, τ, is extracted by monitoring the approach to saturation of the desorption signal (we will see later that the time dependence of the desorption signal does not follow a simple exponential law; this nonexponential behavior is borne out by the experiments to be discussed in Chapter 4). For the same equilibrium conditions, this procedure is repeated for a series of different heater–substrate temperatures, T_s. The time constants so obtained are then assembled into a plot of $ln\tau$ vs. $1/T_s$ which appears linear, and from the slope and intercept of this graph (also known as an Arrhenius plot) an activation energy and prefactor are reckoned. The time constants are then parameterized via the empirical formula

$$\tau = \tau_o e^{E/kT_s} \tag{3.1}$$

with $\tau_o \sim 10^{-9} - 10^{-10}$ sec and $E \sim -(2/3)\mu_o$, where $\mu_o \equiv \mu_f(T_o,\delta_o)$, the equilibrium chemical potential, is a negative quantity.

We want to know whether the time constants of the continuum model can be expected to depend exponentially on the inverse substrate temperature and whether the activation constant, E, can be related in an obvious way to the initial chemical potential of the film. One might think that we have already taken a step toward answering these questions by observing, as we did in (2.54), that the linearized equations yield a desorption time constant of the form

$$\tau_1 = \frac{6\times10^{-12}}{T_o^{2.5}}\ e^{-\mu_o/kT_o}\ \text{(sec)} \tag{3.2}$$

but, unfortunately, this is not what we are really after. The reason is that this formula gives us the value of τ for fixed equilibrium conditions and not its dependence on the steady-state film temperature. In the linear approximation, τ_1 is independent of this temperature in the same way that the time constant for an RC circuit is independent of the voltage which develops across the capacitor. The distinction between (3.2) and what is measured in the experiments then, may be sharpened as follows. Treating τ_1 in the same way as the experimental data, we find for the slope of the Arrhenius plot

$$\frac{d\,ln\tau_1}{d(1/T_s)} \approx -T_o\frac{d\,ln\tau_1}{d(1+\theta_{ss})} = 0\,. \tag{3.3}$$

What (3.2) is actually saying is that, if we measure desorption rates in the linear regime for a succession of different initial temperatures (rather than final temperatures) at fixed chemical potential, then their respective time constants should obey an exponential law with activation energy $-\mu_o$. In order to hold the equilibrium chemical potential fixed while varying T_o, however, both the initial film thickness and equilibrium vapor pressure must be altered. Thus, instead of

providing an answer to the question of how desorption time constants depend on varying steady–state properties for fixed initial conditions, (3.2) tells us, rather, how the time constant for a film negligibly perturbed from equilibrium varies with changing equilibrium circumstances.

Of course it is not hard to imagine how to proceed if (3.3) is to be improved upon. If we simply consider the next order of approximation in an expansion of τ in θ_{ss}, we can already expect a sensible result, for if

$$\tau(\theta_{ss}) = \tau_1 + \tau'\theta_{ss} + O(\theta_{ss}^2) \tag{3.4}$$

then

$$\lim_{\theta_{ss}\to 0} \frac{d\, ln\tau(\theta_{ss})}{d(1+\theta_{ss})} \neq 0 \,. \tag{3.5}$$

The trouble with using (3.2), which is equivalent to setting $\tau(\theta_{ss}) = \tau_1$, is that we have taken the limit the other way around, namely, $d(\lim_{\theta_{ss}\to 0} ln\tau)/d(1+\theta_{ss})$.

What remains puzzling, however, is the following observation. Suppose it is possible, in a higher order of approximation, to express time constants in the form (3.1). We would conclude on the basis of the continuum model that, as a significant number of atoms in the film desorb, the chemical potential of the film should become more negative due to the increased binding energy of those atoms which remain. If the exponent in (3.1) is to be interpreted as an average activation energy for those atoms which desorb, we would then expect to see a value for E which is *greater* than $-\mu_o$ instead of less than $-\mu_o$ as discovered empirically.

2. The Linearized Case Revisited

Once again, we consider the system of linear differential equations resulting from the low–power limit of the thermal model. Instead of solving this system of equations exactly and then approximating those solutions, as we did previously, we seek to develop here an alternative approach that leads naturally and directly to these approximate solutions. Since we cannot hope to solve the nonlinear system of equations exactly in closed analytical form, the virtue of taking another look at how we might re–establish the linearized results lies in the potential promise of a meaningful approximation for the full nonlinear problem.

We begin by rewriting, for reference, equations (2.32) and (2.33) which serve as our starting point:

$$J = \tau_b \frac{d\theta}{dt} - \frac{1}{2}\tau_a B \frac{d\chi}{dt} + D\theta \tag{3.6}$$

$$-\tau_a \frac{d\chi}{dt} = A\chi + B\theta\,. \tag{3.7}$$

Introducing a dimensionless time variable

$$t^* = 3ln(P_o/P_g)t/2nk\delta_o R_f \tag{3.8}$$

and rescaling our dynamical variables to their maximum possible values

$$\tilde{\theta} = \theta/\theta_{ss} \qquad 0 \leq \tilde{\theta} \leq 1 \tag{3.9}$$

$$\tilde{\chi} = \chi/\chi_{ss} \qquad 0 \leq \tilde{\chi} \leq 1 \tag{3.10}$$

these equations may be rewritten, after noting the steady state conditions $\theta_{ss} = J/D$ and $\chi_{ss} = -B/A$, as

$$-\frac{d\tilde{\chi}}{dt^*} = \tilde{\chi} - \tilde{\theta} \tag{3.11}$$

$$AD\frac{\tau_b}{\tau_a}\frac{d\tilde{\theta}}{dt^*} = 1 - \frac{1}{2}\frac{B^2}{D}\frac{d\tilde{\chi}}{dt^*} - \tilde{\theta}\,. \tag{3.12}$$

We have succeeded in reducing, by one, the number of independent parameters originally appearing in the system of equations. The remaining five parameters may be regrouped according to

$$\varepsilon \equiv (R_c+R_k)/R_f = (D\ -\ 1)^{-1} \tag{3.13a}$$

$$\lambda \equiv C_N(T_o)/2nk\ = \tau_b/\tau_a \tag{3.13b}$$

$$\kappa \equiv ln[P_o(T_o)(R_k+R_c)/(\pi m/2kT_o)^{\frac{1}{2}}] = A/3 + ln\varepsilon \tag{3.13c}$$

$$L\ \equiv l(T_o)/kT_o = B\ - A/3 + \tfrac{1}{2} \tag{3.13d}$$

$$\theta_{ss} \equiv [R_fR_c/R_f+R_k+R_c]\ (W/T_o) = J/D \tag{3.13e}$$

where we have confined our attention to the heater–substrate geometry. The heat capacity appearing in the expression for λ is no longer the total heat capacity of the film, but is normalized per layer. All other quantities have their usual meaning. Nowhere among the five dimensionless parameters defined above is there any reference to the initial film thickness, δ_o, or, by extension, the van der Waals force constant, γ. With respect to the nondimensional time, t^*, the theory gives identical predictions for films with the same values of $\varepsilon,\lambda,\kappa,L$ and θ_{ss}, so the initial film thickness serves only to define the overall time scale by which t^* is measured. Expressing everything in terms of scaled variables and the new nondimensional parameters our basic equations become

$$-\frac{d\tilde{\chi}}{dt^*} = \tilde{\chi} - \tilde{\theta} \tag{3.14}$$

$$\frac{3\varepsilon(\kappa-ln\varepsilon)\lambda}{1+\varepsilon}\ \frac{d\tilde{\theta}}{dt^*} = 1 - \tilde{\theta} - \tfrac{1}{2}\ \frac{\varepsilon}{1+\varepsilon}(L-\tfrac{1}{2}+\kappa-ln\varepsilon)^2\ \frac{d\tilde{\chi}}{dt^*} \tag{3.15}$$

and they are to be solved subject to the same homogeneous initial conditions as before, $\tilde{\chi}(0) = 0$ and $\tilde{\theta}(0) = 0$.

We are now interested in finding out what happens in the low pressure (large R_f) regime where ε is small. The significance of our scaling procedure is apparent, for we can now clearly assess the relative importance of each term appearing in the equations, which is a necessary prelude to any qualitative analysis (for a clear and insightful discussion of the role of scaling and dimensional analysis in physical problems we refer the reader to [Lin and Segal]). At first glance it would seem that a straightforward perturbation expansion, in which the solutions are expressed as a power series† in ε and only the lowest term is retained, would provide a sensible approximation.

We cannot naively let ε go to zero for fixed values of κ,λ,L and specified θ_{ss} in (3.15), however, for we are immediately faced with the following difficulty. Equation (3.14) and the scaling (3.9) – (3.10) imply that $d\tilde{\chi}/dt^*$ is of order unity. The coupling term in (3.15) is then of order $\varepsilon ln^2\varepsilon$. If $d\tilde{\theta}/dt^*$ is also of order unity then the left hand side of that equation is order $\varepsilon ln\varepsilon$. For sufficiently small ε both these terms can be ignored and we are left with

$$\frac{d\tilde{\chi}_0}{dt^*} = \tilde{\theta}_0 - \tilde{\chi}_0 \tag{3.16a}$$

$$0 = 1 - \tilde{\theta}_0 \tag{3.17a}$$

(the meaning of the subscript appended to $\tilde{\chi}$ and $\tilde{\theta}$ will become clear shortly). Our two simultaneous differential equations have been reduced to a single differential equation and an algebraic one which are only trivially coupled to each other. The trouble with the system (3.16) and (3.17) is that it is now no longer possible to satisfy the initial condition on $\tilde{\theta}$, $\tilde{\theta}(0) = 0$.

---

† Actually, the appearance of terms like $\varepsilon ln\varepsilon$ and $\varepsilon ln^2\varepsilon$ in (3.15) complicates the notion of any formal series expansion. We may not even have the correct parameter for such an expansion if, in fact, it exists at all. Since we are only interested in the lowest order approximation though, we will continue to do things in the *spirit* of perturbation theory and not worry too much about formalities. The appropriateness of our procedures can always be judged against the exact results in the linearized case and later, when we tackle the nonlinear problem, by recourse to numerical simulation.

This fundamental change in the character of our system of equations (3.14) and (3.15) as $\varepsilon \to 0$ is the telltale sign that we are dealing with a problem in singular perturbation theory; such situations, as a class, are distinguished by the feature that the unperturbed problem (designated by the subscript 0) differs qualitatively from the perturbed one no matter how small the perturbation parameter. In our case, it is the reduction in order of a differential equation whose highest derivative is multiplied by ε that, in the limit as $\varepsilon \to 0$, leaves us with an extra boundary condition. Physically, it is clear what our equations (3.16) and (3.17) mean. The temperature is constant at its steady–state value and the desorption equation gives the rate of evaporation for fixed elevated temperatures. This is not a surprising result in view of our choice of time scale, $t^* = 3\varepsilon(\kappa - ln\varepsilon)t/2nk\delta_o(R_k+R_c)$. As ε approaches zero, it is necessary that t become large if t^* is to remain finite. By this choice of scale, therefore, we are looking at the long time behavior of our original equations. Recall that our exact solutions also showed, to a high degree of accuracy, a steady temperature independent of time for $t >> \tau_2$.

The approximations leading to (3.16) and (3.17) tacitly assumed that $d\tilde{\theta}/dt^*$ was of order unity. This assumption can only be consistent at long times for it is necessary that $\tilde{\theta}$ vary rapidly near $t = 0$ in order to also satisfy the initial condition. We must introduce some other scale for short times if we are to recover the correct behavior in this neighborhood. Defining $t^{**} = t/2nk\delta_o(R_k+R_c)$ $= t^*/3\varepsilon(\kappa-ln\varepsilon)$ we find

$$-\frac{d\tilde{X}}{dt^{**}} = 3\varepsilon(\kappa-ln\varepsilon)(\tilde{X} - \tilde{\Theta}) \tag{3.18}$$

$$\frac{\lambda}{1+\varepsilon}\ \frac{d\tilde{\Theta}}{dt^{**}} = 1 - \tilde{\Theta} - \frac{1}{2}\,\frac{1}{1+\varepsilon}\,\frac{(L-\frac{1}{2}+\kappa-ln\varepsilon)^2}{3(\kappa-ln\varepsilon)}\ \frac{d\tilde{X}}{dt^{**}} \tag{3.19}$$

where $\tilde{X}(t^{**}) = \tilde{\chi}(t^*/3\varepsilon(\kappa-ln\varepsilon))$ and $\tilde{\Theta}(t^{**}) = \tilde{\theta}(t^*/3\varepsilon(\kappa-ln\varepsilon))$. As before, we use (3.18) to argue that the coupling term in (3.19) is of order $\varepsilon ln^2\varepsilon$, since $\tilde{X}$ and $\tilde{\Theta}$

are still of order unity. Then as $\varepsilon \to 0$ we have

$$-\frac{d\tilde{X}_0}{dt^{**}} = 0 \qquad \tilde{X}_0(0) = 0 \tag{3.20a}$$

$$\lambda\frac{d\tilde{\Theta}_0}{dt^{**}} = 1 - \tilde{\Theta}_0 \qquad \tilde{\Theta}_0(0) = 0 \tag{3.21a}$$

Notice that in the region near $t = 0$ we still have two differential equations and it is possible to satisfy both initial conditions. The physical interpretation of (3.20) and (3.21) is straightforward. On the time scale of t^{**} virtually no desorption takes place and all of the energy deposited into the film goes into raising its temperature; again, this is as we expect from our exact analysis for times $t \ll \tau_1$.

In the parlance of singular perturbation theory equations (3.16) and (3.17) are valid in the so–called "outer" region, whereas (3.20) and (3.21) apply in the "inner" region. Since the rapid variation in $\tilde{\Theta}$ near $t = 0$ is forced by the need to satisfy the boundary condition there, this inner region is also called a "boundary layer". The terminology is borrowed from fluid mechanics where many of these ideas were originally developed by Ludwig Prandtl in the study of viscous fluid flow near solid walls [Landau and Lifshitz, *FM*]. It should be emphasized that in contrast to the vivid imagery this parallel conjures up, we are, in fact, discussing here a boundary layer in *time*. (A well motivated and lucid introduction to the ideas of singular perturbation theory may be found in [Lin and Segal] whereas the more extensive and formal treatment of [Bender and Orszag] offers numerous solved examples of boundary layer problems, illustrating the techniques in a variety of circumstances.)

Integrating the inner equations (3.20) – (3.21) subject to the initial conditions we obtain

$$\tilde{X}_0(t^{**}) = 0 \tag{3.20b}$$

$$\tilde{\Theta}_0(t^{**}) = 1 - e^{-t^{**}/\lambda} \tag{3.21b}$$

while the outer equations (3.16) – (3.17) give

$$\tilde{\chi}_0(t^*) = 1 - c_0 e^{-t^*} \tag{3.16b}$$

$$\tilde{\theta}_0(t^*) = 1 \,, \tag{3.17b}$$

where c_0 is an as yet undetermined constant. These two sets of regional solutions represent the behavior of the same functions on two very different time scales. There is a transition regime, at intermediate times, where these two sets of solutions must, in some sense, match. The standard procedure to establish this matching is as follows. We define an intermediate time scale $t^i = t/\rho(\varepsilon)2nk\,\delta_o(R_k+R_c)$ which, as $\varepsilon \to 0$, is long compared to t^{**}, the scale defining the inner region, and short compared to t^*, the scale defining the outer region. Specifically, if we keep t^i fixed and let $\varepsilon \to 0$ with

$$t^* = \rho(\varepsilon)\varepsilon(\kappa - ln\varepsilon)t^i \tag{3.22}$$

$$t^{**} = \rho(\varepsilon)t^i \tag{3.23}$$

then we want a $\rho(\varepsilon)$ such that

$$\lim_{\varepsilon \to 0} t^* = 0 \tag{3.24}$$

and

$$\lim_{\varepsilon \to 0} t^{**} = \infty \,. \tag{3.25}$$

A convenient choice satisfying these criteria is $\rho(\varepsilon) = \varepsilon^{-\frac{1}{2}}$. Then the matching condition consists of setting

$$\lim_{\varepsilon \to 0} \tilde{\theta}_0(t^* = \varepsilon^{\frac{1}{2}}(\kappa - ln\,\varepsilon)t^i) = \lim_{\varepsilon \to 0} \tilde{\Theta}_0(t^{**} = \varepsilon^{-\frac{1}{2}}t^i) \tag{3.26}$$

and

$$\lim_{\varepsilon \to 0} \tilde{\chi}_0(t^* = \varepsilon^{\frac{1}{2}}(\kappa - ln\,\varepsilon)t^i) = \lim_{\varepsilon \to 0} \tilde{X}_0(t^{**} = \varepsilon^{-\frac{1}{2}}t^i) \tag{3.27}$$

for fixed t^i. Following through we find that the matching condition for the temperature variable $\tilde{\theta}_0$ is automatically satisfied, as it must be, since we have no adjustable parameters at our disposal. The condition on $\tilde{\chi}_0$, however, determines c_0 and we find $c_0=1$.

An asymptotic approximation to the true solutions as $\varepsilon \to 0$, uniformly valid over the time interval $0 < t < \infty$ (as denoted by the subscript u), is then given by adding together the inner and outer solutions and subtracting their common limit in the intermediate time regime (the justification for this and the foregoing matching procedures may be found in the aforementioned references). Explicitly, we find

$$\tilde{\theta}_{0,u} = 1-e^{-t/\lambda \cdot 2nk\delta_o(R_k+R_c)} \tag{3.28}$$

$$\tilde{\chi}_{0,u} = 1-e^{-3\varepsilon(\kappa-ln\varepsilon)t/2nk\delta_o(R_k+R_c)} \tag{3.29}$$

In this particular case, $\tilde{\theta}_{0,u}$ is essentially the inner solution (since both the outer solution and intermediate limit for $\tilde{\theta}_0$ are equal to each other), whereas $\tilde{\chi}_{0,u}$ is just the outer solution (as both the inner solution and intermediate limit for $\tilde{\chi}_0$ vanish).

Not surprisingly, (3.28) and (3.29) are of the form

$$\tilde{\theta}_{0,u} = 1-e^{-t/\tau_2} \tag{3.30}$$

$$\tilde{\chi}_{0,u} = 1-e^{-t/\tau_1} \tag{3.31}$$

with $\tau_2/\tau_1 = 3\lambda\varepsilon(\kappa-ln\varepsilon) \ll 1$. This is the behavior we expected based on the exact analysis of Chapter 2. The time constants arrived at here, however, differ slightly from our previous expressions and are, in fact, considerably simpler. In terms of the original notation

$$\tau_1 = \tau_a/A \tag{3.32}$$

$$\tau_2 = \tau_b/D \ . \tag{3.33}$$

Comparing, we see these are just the $R_f \to \infty$ ($\varepsilon \to 0$) limits of (2.44) and (2.45). This change comes about because τ_1 and τ_2 are the roots of the secular equation (2A.6a) arising from the original system of differential equations. Finding these roots in the $\varepsilon \to 0$ limit also requires the techniques of singular perturbation theory and the expressions (3.32) and (3.33) are the result of a zero'th–order analysis of this algebraic problem.

3. Boundary Layer Theory of the Nonlinear Equations

Having established the basic ideas of singular perturbation theory within the context of a familiar and fully workable example in the last section, we now go on the apply these ideas to the more difficult nonlinear problem.

Our starting point is the set of exact nonlinear autonomous equations (2.28) and (2.29). As before, we rescale in time

$$t^* = t/2nk\,\delta_o R_f \tag{3.34a}$$

and introduce a new set of dimensionless parameters

$$\varepsilon = 1/R_f G \tag{3.35a}$$

$$\lambda = C_N(T_o)/2nk \tag{3.35b}$$

$$\kappa = ln[P_o(T_o)/(\pi m/2kT_o)^{\frac{1}{2}} G] \tag{3.35c}$$

$$\kappa - ln\varepsilon = ln(P_o(T_o)/P_g) \tag{3.35d}$$

$$L = l(T_o)/kT_o\,. \tag{3.35e}$$

We recall that G has the units of conductance and point out that the definition of ε adopted here differs by a factor of four, in the low power limit, from the definition given in the previous section. We note further that our choice of time scale, t^*, also differs from that used in the linear case and may be written using (3.35a) as

$$t^* = \varepsilon t C / 2nk\delta_o \,. \tag{3.34b}$$

In addition to these parameters we must also introduce functional relations for the heat capacity, latent heat, and saturated vapor pressure as functions of temperature. As in Chapter 2 we take

$$L = const \tag{3.36a}$$

$$P_o(\theta) = \pi_o e^{-L/(1+\theta)} \tag{3.36b}$$

$$C_N(\theta,\chi) = C_N(T_o)\delta_o(1+\theta)^3(1+\chi) \,. \tag{3.36c}$$

Finally, the input power, Q, may be eliminated in terms of the steady–state temperature through the relation

$$\frac{R_f Q}{T_o} = \theta_{ss} + R_f G[(1+\theta_{ss})^4 - 1] \tag{3.37}$$

which obtains when all time derivatives in the energy equation vanish. Similarly, the mass balance equation allows us to express χ_{ss} in terms of θ_{ss} by setting $d\chi/dt$ to zero.

With the choice of scale (3.34) we are again looking, as $\varepsilon \to 0$, at the large t regime for fixed t^*. Neglecting the terms responsible for coupling the temperature and film thickness changes, as we did in the linear case, the lowest order equations for the outer region become

$$0 = (1+\theta_{ss})^4 - (1+\theta_0)^4 \tag{3.38a}$$

$$\frac{d\chi_0}{dt^*} = 1 - e^{[(\kappa - ln\varepsilon)/(1+\theta_{ss})]\,[(1/(1+\chi_{ss})^3 - 1/(1+\chi_0)^3]} \,. \tag{3.39a}$$

Rescaling to short times via $t^{**} = t^*/\varepsilon$, defining $\Theta = \theta(t^*/\varepsilon), X = \chi(t^*/\varepsilon)$, and neglecting the same coupling terms as before we find, in the inner region,

$$\lambda(1+\Theta_0)^3(1+X_0)\frac{d\Theta_0}{dt^{**}} = (1+\theta_{ss})^4 - (1+\Theta_0)^4 \qquad \Theta_0(0)=0 \tag{3.40a}$$

$$\frac{dX_0}{dt^{**}} = 0 \quad X_0(0)=0 \,. \tag{3.41a}$$

The inner equation for X_0 is trivially solved. The remaining equation for Θ_0 is separable and can be integrated in closed form with the result that

$$[1+\Theta_0(t^{**})]^4 = (1+\theta_{ss})^4 - [(1+\theta_{ss})^4 - 1]e^{-4t^{**}/\lambda} \,. \tag{3.40b}$$

The behavior of θ_0 in the outer region is simply

$$\theta_0 = \theta_{ss} \,. \tag{3.38b}$$

As in the linear case, matching of Θ_0 to θ_0 occurs on a time scale

$$t^i = tG/2nk\,\delta_o\rho(\varepsilon) \tag{3.42a}$$

which satisfies

$$\lim_{\varepsilon\to 0} t^* = \varepsilon\rho(\varepsilon)t^i \to 0 \tag{3.42b}$$

and

$$\lim_{\varepsilon\to 0} t^{**} = \rho(\varepsilon)t^i \to \infty \tag{3.42c}$$

for fixed t^i. Taking $\rho(\varepsilon) = \varepsilon^{-\frac{1}{2}}$ we find, as before, that the matching of inner and outer solutions for the temperature as a function of time occurs automatically. Adding the inner and outer solutions together and subtracting their common part in the intermediate regime we are left with only the inner solution. As a result, our zero'th–order uniform asymptotic approximation to the temperature over the entire time interval, $0 \leq t \leq \infty$, is

$$\theta_{0,u}(t)=(1+\theta_{ss})[1-(1-\frac{1}{(1+\theta_{ss})^4})\,e^{-4tG/C_N(T_o)}]^{1/4} - 1 \tag{3.43}$$

Returning now to the film thickness, it is clear that while $X_0(t^{**}) = 0$, the outer equation (3.39a) is not readily integrable even though $\theta_0 = \theta_{ss}$. The matching

requirement tells us, however, that

$$\lim_{\varepsilon\to 0} \chi_0(t^* = \varepsilon^{\frac{1}{2}} t^i) = \lim_{\varepsilon\to 0} X_0(t^{**} = \varepsilon^{-\frac{1}{2}} t^i) = 0 \tag{3.44}$$

for t^i fixed, which provides an initial condition for (3.39a) in the outer region. Since both X_0 and the intermediate limit vanish, our uniform approximation for χ_0 is the solution to

$$\frac{d\chi_{0,u}}{dt^*} = 1 - e^{[(\kappa - ln\varepsilon)/(1+\theta_{ss})]\,[(1/(1+\chi_{ss})^3 - 1/(1+\chi_{0,u})^3]} \qquad \chi_{0,u}(0) = 0\,. \tag{3.45}$$

Let us pause now to comment on the physical significance of what we have done. Equation (3.43) gives us the temperature as a function of time for a film with the Debye heat capacity (3.36c) after an instantaneous jump in substrate temperature, presuming a Stefan–Boltzmann phonon radiation law and neglecting desorption. On the other hand, (3.45) represents isothermal desorption at the substrate temperature ignoring the small but finite time it takes the film to warm. Changes in film thickness are coupled to changes in temperature through the latent heat term in the energy equation. If the initial evaporation rate is not too large, on the scale of time during which the temperature varies, then we may neglect this term as we have done. An upper bound to the true desorption rate is provided by the isothermal rate (3.45) and we see from this expression that $d\chi_{0,u}/dt^*$ depends not only on ε, but also on θ_{ss}. That is, for a given $\varepsilon \ll 1$, there is θ_{ss} above which the desorption rate is too high for the equations to decouple satisfactorily. Of course, for any given θ_{ss} there is an ε small enough for the decoupling to be valid but this may require pressures which are unattainably low and, furthermore, take us into the physical regime of very low coverage where the idea of a continuous film is no longer tenable. Finally, we remark that for given ε and θ_{ss} the degree of coupling increases as we lower T_o because of the strong temperature dependence of κ through G. Interestingly, the initial desorption rate is independent of the bulk heat of evaporation, L.

4. Desorption in the Isothermal Approximation

Our discussion so far has centered on justifying the idea that desorption is largely isothermal under appropriate conditions. As we have seen, this requires equilibrium pressures and temperature elevations which give rise to initial evaporation rates which, in scaled sense, are "slow." While these results have been obtained within the context of a particular equation of state for the film and specific assumptions about the mechanism of thermal exchange between substrate and film and between film and vapor, they nevertheless appear to be more general. In fact, we might well have come to similar conclusions by a slightly different line of reasoning. Instead of considering a monolayer or submonolayer film to be a distinct medium with its own well–defined phonon modes, thermal boundary resistance and temperature, it might be more reasonable to regard heater and film as a single strongly coupled system possessing a single temperature. The phonon modes will then be those of the composite medium and, presumably, they would resemble the modes of a semi–infinite solid (the substrate) terminated by a planar defect (a monolayer of adsorbate). If the film does not add appreciably to the heat capacity of the bare heater, then we may expect the time required for the film–heater combination to warm to be very similar to that of the heater alone provided no significant fraction of the input energy is carried away by desorption during this process. Such a view bears some resemblance to a description of the sublimation of a loosely bound surface layer from a solid and forces us to inquire directly about isothermal desorption. We turn now to a broader discussion of desorption under such circumstances.

Assuming that quasi–equilibrium is maintained, the fundamental equation for isothermal desorption in the presense of an ambient gas is

$$-\frac{dn(t)}{dt} = \sigma_e(T_s,n)\frac{P_f(T_s,n)}{\sqrt{2\pi mkT_s}} - \sigma_c(T_s,n)\,\frac{P_f(T_o,n_o)}{\sqrt{2\pi mkT_o}}\,. \tag{3.46}$$

$n(t)$ is the number of adsorbed atoms per unit area at any given moment, n_o the

value of $n(t)$ in equilibrium, and $P_f(T_o,n_o)$ the corresponding equilibrium vapor pressure. The vapor pressure of the film at elevated temperatures is related to the instantaneous surface coverage through the equation of state, $P_f(T_s,n)$, where we no longer distinguish between the steady temperature of the substrate, T_s, and the temperature of the film, T_f. (Our notation for surface coverage in the above formula differs from our previous focus on the film thickness, $\delta(t)$, and prior use of the symbol n to denote the bulk liquid density, to emphasize the complete generality of (3.46) and, in particular, its independence from the bulk continuum viewpoint or any other assumptions about the equation of state of the film.)

The evaporation and condensation coefficients are given, as in Chapter 1, by

$$\sigma_e(T_s,n) = <\sigma(\mathbf{p})>_{T_s} \tag{3.47a}$$

$$\sigma_c(T_s,n) = <\sigma(\mathbf{p})>_{T_o} \tag{3.47b}$$

which are averages of the momentum–dependent sticking probability over thermal distributions at temperatures T_s and T_o respectively. These coefficients are written as functions of T_s and n to call attention to their possible dependence on both surface temperature and coverage.

We can simplify matters somewhat if the sticking probability is insensitive to momentum. Then $\sigma_e=\sigma_c=\sigma$ and (3.46) becomes

$$-\frac{dn(t)}{dt} = \sigma(T_s,n)\left[\frac{P_f(T_s,n)}{\sqrt{2\pi mkT_s}} - \frac{P_f(T_o,n_o)}{\sqrt{2\pi mkT_o}}\right]. \tag{3.48}$$

The second term in brackets is a constant for given initial conditions. With respect to the momentum averages (3.47), ignoring their $\mathbf{p}$ dependence is, in practice, tantamount to assuming only that the variation of $\sigma(\mathbf{p})$ is insignificant over a range in momentum characterized by the width of the thermal distributions T_o and T_s. If, furthermore, the sticking coefficient is independent of

coverage then all of the n dependence in (3.48) resides in the vapor–pressure isotherm $P_f(T_s,n)$. It is this last instance that we shall analyze in some detail.

It is clear from (3.48) that in order to infer the desorption rate from measurements of dn/dt one must account for the readsorption term, $\sigma(T_s,n)P_f(T_o,n_o)/\sqrt{2\pi mkT_o}$. If the equilibrium coverage n_o is given, then $n(t)$ is determined through

$$n(t) = n_o + \int_0^t \left[\frac{dn}{dt'}\right] dt' \,. \tag{3.49}$$

Should the complete temperature and coverage dependence of the adsorption isotherms be well–known, then (3.48) and (3.49) provide a way, in principle, of ascertaining $\sigma(T,n)$. Alternatively, if $\sigma(T,n)$ has been found by other means, then (3.48) and (3.49) can be used to map out the isotherm provided n_o and $P_f(T_o,n_o)$ can be measured.

Let us next survey the relationship between the time–dependent surface coverage and the equation of state by examining some instructive examples.

The simplest possibility is that the adsorbed atoms behave like a classical ideal gas in two dimensions. This would be the situation if each particle was bound with energy ε_o to a smooth uniform substrate but could otherwise freely translate in the surface plane without interacting with other adatoms. The equation of state in the Boltzmann approximation is [Dash]

$$P_f(T,n) = \left(\frac{n}{\beta\Lambda}\right) e^{-\beta\varepsilon_o} \tag{3.50}$$

where $\beta \equiv 1/kT$ and $\Lambda \equiv h/(2\pi mkT)^{\frac{1}{2}}$ is the thermal de Broglie wavelength. The isotherms are straight lines in the P_f vs. n plane which pass through the origin and, for reasonable ε_o, have increasing slope with increasing temperature, as illustrated in Fig. 3.1.

Figure 3.1. Isothermal desorption of a two–dimensional classical ideal gas.

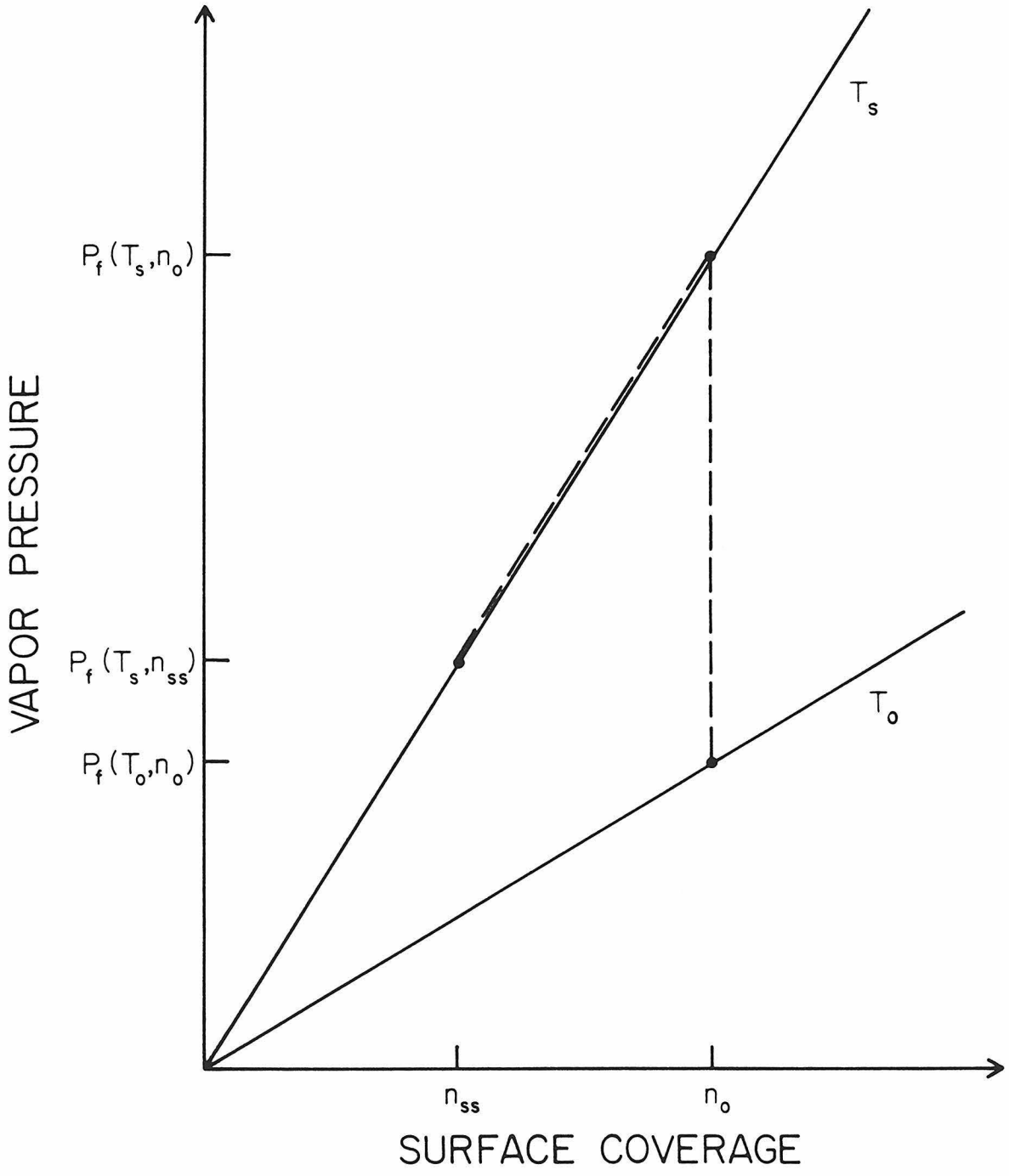

The dashed line in Fig. 3.1 traces for us the film's evolution according to (3.48) assuming that σ is independent of n. When the temperature is suddenly raised the adsorbate departs from its initial point on the equilibrium isotherm to a point at the same coverage on a neighboring isotherm. Thereafter, as more of the film progressively desorbs, the vapor pressure slides down this new isotherm until a steady state is reached when $P_f(T_s,n_{ss})=\sqrt{T_s/T_o}P_f(T_o,n_o)$. We can, in this case, rewrite (3.48) in the form

$$-\frac{dn}{dt} = k_d n - c \tag{3.51}$$

where k_d, the desorption rate constant, is given by $(\sigma/\beta_s h)e^{-\beta_s \varepsilon_o}$ and c is a constant term representing readsorption. Integrating explicitly, one finds

$$n(t)-n_o = (n_{ss}-n_o)(1-e^{-k_d t}) \tag{3.52}$$

with the steady-state coverage, n_{ss}, given by c/k_d which vanishes as β_s approaches zero. The desorption time constant, $\tau=k_d^{-1}$, has the activated form

$$\tau = \left[\frac{h\beta_s}{\sigma}\right] e^{\beta_s \varepsilon_o}. \tag{3.53}$$

In this instance, measuring the time dependence of $n(t)-n_o$ alone serves to completely define τ since $n_{ss}-n_o$ acts only as an overall scale factor. There is no distinction here between the relaxation time to reach steady state and the intrinsic desorption time constant. This simplicity is a consequence of the fact that the vapor pressure, and hence the desorption rate, is strictly linear in the surface coverage.

If we now go on to include the effects of quantum statistics for the particles, we find that the equation of state becomes nonlinear. In the degenerate limit,

$$P_{f\pm} = \pm(e^{\pm n\Lambda^2}-1)\left[\frac{e^{-\beta\varepsilon_o}}{\beta\Lambda^3}\right] \tag{3.54}$$

where the lower (upper) sign refers to Bosons (Fermions) [Dash]. Relative to a Boltzmann gas at the same temperature, these isotherms curve downward with increasing n for Bose statistics, upward with increasing n for Fermi statistics, and they approach (3.50) tangentially at low coverage when $n\Lambda^2<<1$. With (3.48) written as

$$-\frac{dn}{dt} = (\pm)k_d\left[(e^{\pm n\Lambda_s^2}-1)-c^{\pm}\right] \tag{3.55}$$

the coverage as a function of time is

$$n(t)-n_o = \frac{(\pm)}{\Lambda_s^2}\, ln\left[\frac{e^{\pm\Lambda_s^2(n_{ss}-n_o)}}{1+\{e^{\pm\Lambda_s^2(n_{ss}-n_o)}-1\}e^{-(k_d+c^{\pm})\Lambda_s^2 t}}\right] \tag{3.56}$$

where

$$\frac{(k_d+c^{\pm})}{k_d} = e^{\pm\Lambda_s^2 n_{ss}}\,. \tag{3.57}$$

This rather bulky expression concretely illustrates several fundamental points. To begin with, the functional dependence of $n(t)-n_o$ on time is highly convolved. Without knowing *a priori* that this form correctly describes the behavior of the system, there would be no hope of deducing the correct dependences through measurements of $n(t)-n_o$ vs. time alone. (If one could correct for readsorption, then plots of dn/dt vs. n might lead one to hypothesize the proper dependence of (3.55) on coverage.) Furthermore, the decay with time of the term in the denominator of (3.56) is governed by $(k_d+c^{\pm})\Lambda_s^2$, which involves both the rate constant and the readsorption term which depends on initial coverage. We can therefore expect, in general, that if the equation of state is nonlinear then the relaxation time governing (3.48) can no longer be straightforwardly identified with the desorption time constant as was the case in (3.52). Moreover, as we see from (3.56) and (3.57) this relaxation time will, in all likelihood, depend in an essential way on both the initial surface coverage *and* the total amount desorbed

in reaching steady state.

The opposite limit of mobile adsorption is localized adsorption. If there are N_s non–interacting sites of binding energy ε_o on the surface, each of which can accommodate at most a single atom, then the equation of state is

$$P_f = \left[\frac{x}{1-x}\right]\left[\frac{e^{-\beta\varepsilon_o}}{\beta\Lambda^3}\right] \tag{3.58}$$

where $x=N_f/N_s$ is the fraction of occupied sites. This isotherm, which was originally proposed by Langmuir as a model of chemisorption, has the property that the vapor pressure diverges at monolayer completion. Naively inserting (3.58) into (3.48) again yields a nonlinear equation for dn/dt. It is, however, inconsistent with the assumptions upon which (3.58) is based to presume that σ is independent of coverage. Instead, we must take $\sigma\sim(1-x)$ whereupon we obtain results substantially similar to those of the 2–d classical gas.

We have already commented extensively on one model of a film including interactions between the particles, namely the Frenkel–Halsey–Hill isotherm (1.35). Equation (3.45) is, in fact, a heavily disguised version of (3.48) for this equation of state and constant sticking coefficient.

The isotherms of a broad class of real substances physically adsorbed on uniform substrates differ in a fundamental way from anything we have considered so far. As shown schematically in Fig. 3.2, below a certain critical temperature these isotherms exhibit steps in the P_f,n plane and so for substantial ranges in n the vapor pressure is independent of coverage. The plateaus mark regimes of two–dimensional phase coexistence with a condensed phase (e.g., two–dimensional liquid or solid) in equilibrium with a less dense one (e.g., two–dimensional ideal gas). In the region of the first plateau, for example, the attractive forces between adsorbed particles cause extra atoms added to the system to go into forming larger patches of the two–dimensional condensed phase rather than increasing the pressure of the three–dimensional gas above the

Figure 3.2. Isothermal desorption in a regime of two–dimensional phase coexistence.

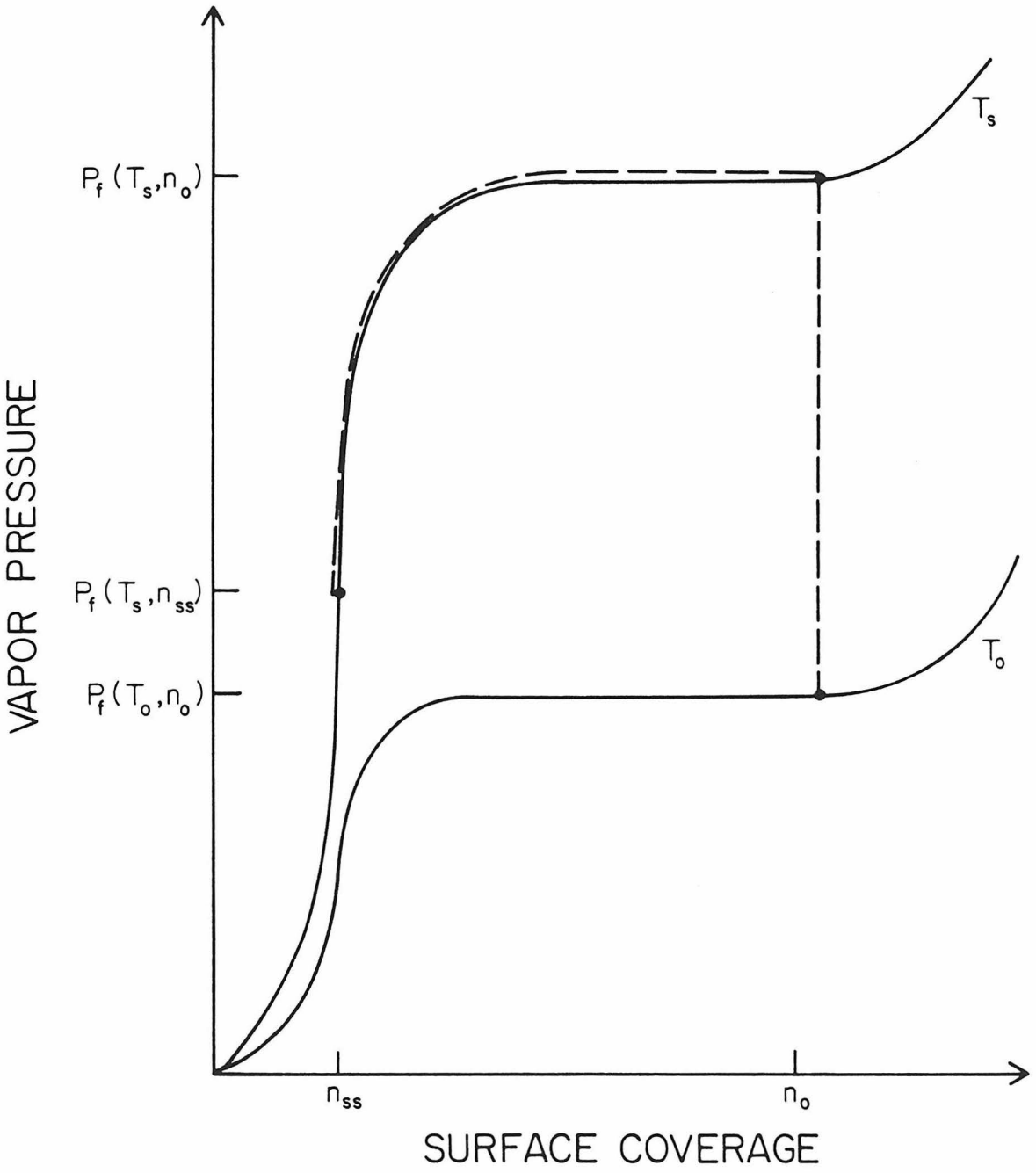

substrate. As these condensed patches grow, the area available to the two–dimensional gas continually declines. When monolayer completion is eventually approached, the vapor pressure rises since it is then no longer possible to maintain the two–phase equilibrium and extra particles must now be promoted to the next, less strongly bound, layer. The whole process then repeats itself in this new layer, and so on.

Isothermal desorption experiments conducted in the two–phase region will show a constant desorption rate independent of coverage, and consequently, the time given by (3.48) for steady state to be reached will be essentially linear in the initial coverage. The possibility of a coverage independent desorption rate for films which grow in a layer–like mode with stepwise isotherms was first pointed out by Venables and Bienfait and subsequently confirmed experimentally by them for the case of Xe adsorbed on graphite [Venables and Bienfait (1976) and Bienfait and Venables (1977)]. Later work by Opila and Gomer revealed similar behavior in the desorption of Xe from W [Opila and Gomer (1981)], and they generalized somewhat the arguments advanced by Venables and Bienfait correctly pointing out the vital roles played by the sticking coefficient and the kinetics of the processes maintaining the two–dimensional phase equilibrium. More recently, this subject has been discussed by Nagai *et al.* [Nagai, Shibanuma and Hashimoto (1984)].

5. Local Linearization of the Rate Equation

A relaxation equation like (3.51), in which the desorption rate is linear in the surface coverage, is said to follow first–order kinetics. A constant desorption rate, as might be evidenced by stepwise isotherms, is termed zero'th order. This nomenclature parallels the classification of chemical reactions where the rate of formation of a substance may often be expressed in terms of a rate constant multiplied by the concentration of reactants raised to integer powers. As examples like (3.55) point out, however, nonlinear isotherms are rarely such simple

functions as integral powers of the surface concentration and therefore, in general, one cannot expect the desorption rate to possess a definite order.

While the rate equations for these nonlinear isotherms may not correspond to a formal order over the whole of their trajectory in the vapor pressure–surface coverage plane, they may be made first order, at least locally, by linearizing at successive coverages, or equivalently, at successive instants of time. In other words, if $n_i=n(t_i)$ is the coverage at a time t_i after the jump in temperature from T_o to T_s but prior to t so that $t>t_i\geqq 0$, and if $n(t)-n_i$ is small, then the vapor pressure can be expanded as

$$P_f(T_s,n) = P_f(T_s,n_i) + \left[\frac{\partial P_f}{\partial n_i}\right]_{T_s}[n(t)-n_i] \tag{3.59}$$

where the partial derivative is with respect to n, evaluated at n_i, and T_s held fixed. Substituting into (3.48) the rate equation becomes

$$-\frac{dn(t)}{dt} = \frac{\Lambda_s\sigma(T_s)}{h}\left[P_f(T_s,n_i)+\left[\frac{\partial P_f}{\partial n_i}\right]_{T_s}[n(t)-n_i]-\left[\frac{T_s}{T_o}\right]^{\frac{1}{2}}P_f(T_o,n_o)\right] \tag{3.60}$$

for σ independent of n. Locally then, (3.60) looks like

$$-\frac{dn(t)}{dt} = k_d^i[n(t)-n_{ss}^i] \tag{3.61}$$

with solution

$$[n(t)-n_i] = [n_{ss}^i-n_i](1-e^{-k_d^i(t-t_i)})\,. \tag{3.62}$$

The local time constant as a function of coverage (or implicitly, time) in (3.62) is given by

$$\tau_{lcf}^{-1}(n_i) \equiv k_d^i = \frac{\Lambda_s\sigma(T_s)}{h}\left[\frac{\partial P_f}{\partial n_i}\right]_{T_s}. \tag{3.63}$$

Similarly, $[n_{ss}^i-n_i]$ represents a local amplitude: the prediction for the steady

state value of $[n(t)-n_i]$ obtained by setting $dn/dt=0$ in (3.60),

$$[n_{ss}^i-n_i] = -\left[\frac{\partial P_f}{\partial n_i}\right]_{T_s}^{-1}\left[P_f(T_s,n_i)-\left[\frac{T_s}{T_o}\right]^{\frac{1}{2}}P_f(T_o,n_o)\right]. \qquad (3.64)$$

In terms of the parameterization (3.62), it is the *slope* of the adsorption isotherm which defines the local time scale governing the approach to steady state. Of course, the true steady state coverage, n_{ss}, differs from n_{ss}^i and both $\tau_{lcl}(n_i)$ and $[n_{ss}^i-n_i]$ are continuously renormalized as $n(t)$ evolves if $(\partial P_f/\partial n_i)_{T_s}$ depends on coverage. A simple geometrical interpretation makes these relationships clear as shown in Fig. 3.3. The situation depicted is an isotherm with positive curvature, $(\partial^2 P_f/\partial n^2)>0$, and the local linearization is shown for the point $n_i(t_i)=n_o(t=0)$; n_{ss}^o is the extrapolated steady state coverage based on the initial slope $(\partial P_f/\partial n_o)_{T_s}$. It is evident from this construction that $(n_{ss}^i-n_i)$ will be less than $(n_{ss}-n_i)$ for isotherms of positive curvature, the linearized estimate of the total amount to be evaporated falling short of the true value. Of course, just the opposite holds for isotherms of negative curvature. In the case of more complex isotherms with sections of both positive and negative as well as vanishing curvature, the behavior will be more complex and limited in extent to regional interpretations. It is also important to mention that stepwise isotherms, in the regime where $(\partial P_f/\partial n)_{T_s}=0$, fall outside the scope of this description for then neither the expansion (3.59) nor the assumed solution (3.62) make sense. This is reflected in the fact that according to (3.63) the local time constant is formally infinite. The correct behavior is, of course, a coverage changing linearly with time and no additional insight is gained by insisting that a rate equation which is globally zero'th order be treated as though it were locally first order.

The local time constant (3.63) and local amplitude (3.64) may both be obtained directly from measurements of $n(t)$. Differentiating the rate equation (3.60) and comparing with the definition (3.63) one finds

Figure 3.3. Isothermal desorption for a system with repulsive interactions between adatoms or displaying strong substrate heterogeneity.

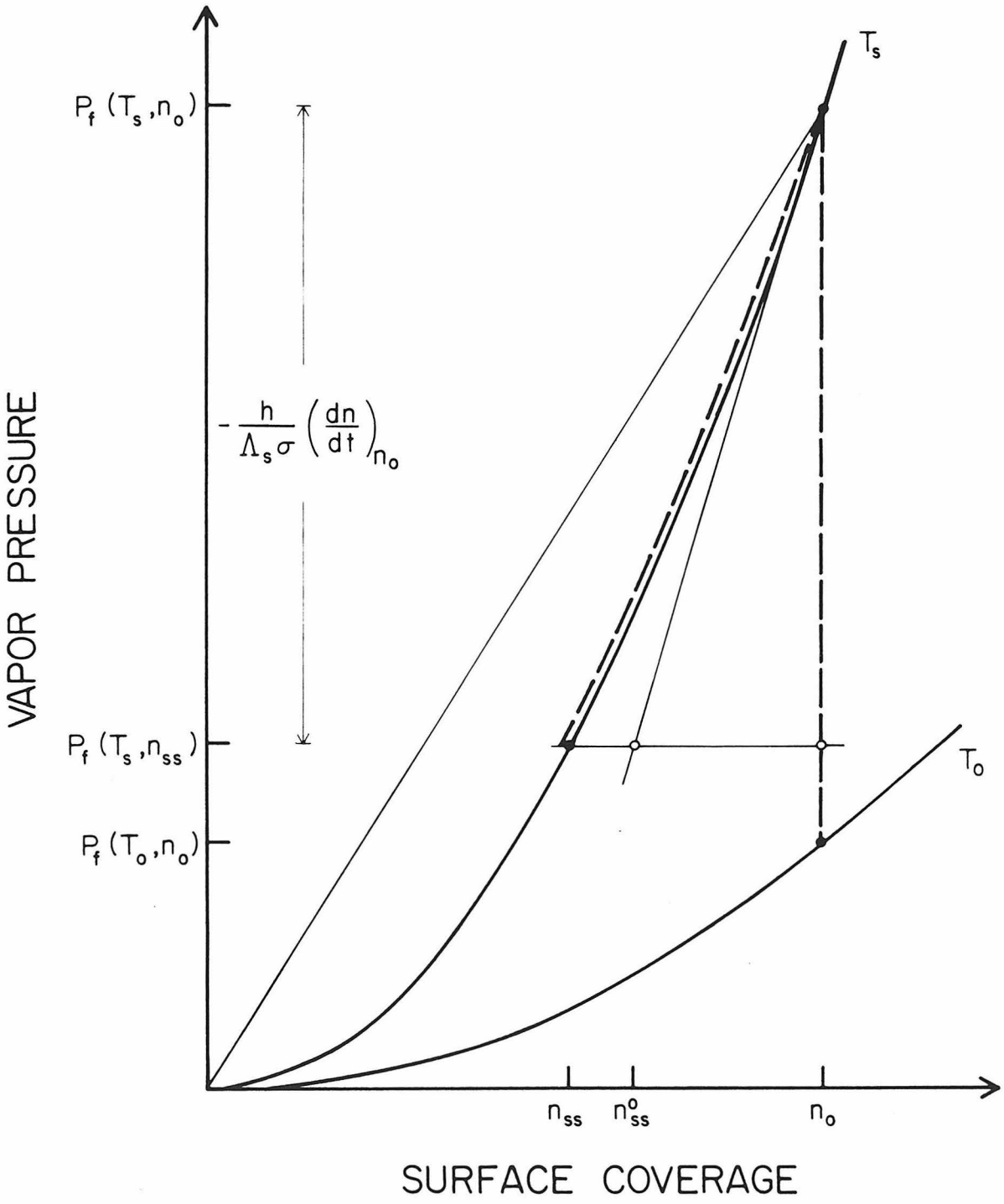

$$\tau_{\rm lcl}^{-1}(t_i) = -\frac{(d^2n/dt_i^2)}{(dn/dt_i)} = -\frac{d}{dt_i}\,ln\left[\frac{dn}{dt_i}\right]. \tag{3.65}$$

This expression determines $\tau_{\rm lcl}^{-1}$ as a function of time, through the instantaneous rate of change in the logarithm of the net desorption rate, and implicitly, through $n_i(t_i)$, as a function of coverage. By the same token, expanding both sides of (3.62) to lowest order in $(t-t_i)$ and using (3.65), (3.64) is given by

$$(n_{ss}^i - n_i) = -\frac{(dn/dt_i)^2}{(d^2n/dt_i^2)}\,. \tag{3.66}$$

We may contrast the behavior of $\tau_{\rm lcl}$ with the quantity which is usually referred to when speaking of a desorption time constant – the mean residence time of a single atom on the surface [Frenkel, de Boer]

$$\frac{n}{\tau} = \sigma(T_s)\,\frac{P_f(T_s,n)}{\sqrt{2\pi mkT_s}}\,. \tag{3.67}$$

This relation equates the adsorption rate in equilibrium at a given temperature and coverage to the rate at which particles leave the surface, as if these particles did so independently of one another with mean lifetime τ. In other words, the desorption rate in (3.67) is written the same way one would the radioactive decay of an ensemble of non–interacting nuclei. Returning to Fig. 3.3, τ^{-1} is proportional to the slope of the *chord* connecting the point $(P_f(T_s,n),n)$ to the origin, and $\tau_{\rm lcl}/\tau$ is just the ratio of the slope of this chord to the actual slope of the isotherm at that point. For truly independent particles, the isotherms are linear and pass through the origin, as indicated in Fig. 3.1, so that τ and $\tau_{\rm lcl}$ are one and the same. For any realistic equation of state including interactions between the adsorbed particles, we see that τ and $\tau_{\rm lcl}$ have somewhat different meanings.

From a general consideration of the statistical mechanics of ideal gases adsorbed on surfaces one can show [Kruyer (1955), de Boer (1956)] that the mean residence time will follow a law like (3.1) in simple instances. Furthermore, one can obtain explicitly formulas for τ_o in terms of the translational, vibrational,

and rotational degrees of freedom available to the adsorbed species. Because it is possible to express the vapor pressure of a film in terms of its chemical potential using the relationship (1.31) for the chemical potential of an ideal gas, τ_{lcl} in (3.63) may also be rewritten in activated form,

$$\tau_{lcl}(n) = \frac{h\Lambda_s^2}{\sigma(T_s)} \left[\frac{\partial \mu_f}{\partial n}\right]_{T_s}^{-1} e^{-\mu_f(T_s,n)/kT_s} . \tag{3.68}$$

Comparing with (3.1) we see that this determines explicitly the coverage and temperature dependence of both the prefactor and exponent for the local time constant. If we set $T_s=T_o$ and $n=n_o$ in (3.68), we then have a closed analytic expression for the time constant, τ_1, of the linearized theory in terms of the equilibrium chemical potential, $\mu_f(T_o,n_o)$, which is valid for any equation of state. This generalizes the results of Chapter 2, and in particular, the numerical relation (2.54), which was derived on the basis of the Frenkel–Halsey–Hill isotherm.

Finally, we note that, if the variation of sticking coefficient with coverage cannot be neglected, the definitions of the local time constant and amplitude must be modified to take this effect into account. Then in place of (3.63) and (3.64) one obtains instead,

$$\tau_{lcl}^{-1}(n_i) = \frac{\Lambda_s \sigma(T_s,n_i)}{h} \left[\frac{\partial P_f}{\partial n_i}\right]_{T_s} + \frac{1}{\sigma}\left[\frac{\partial \sigma}{\partial n_i}\right]_{T_s}\left[\frac{dn}{dt}\right]_{n_i} \tag{3.69}$$

and

$$-(n_{ss}^i - n_i) = \left[\left[\frac{\partial P_f}{\partial n_i}\right]_{T_s}\left[P_f(T_s,n_i) - (T_s/T_o)^{\frac{1}{2}} P_f(T_o,n_o)\right]^{-1} + \frac{1}{\sigma}\left[\frac{\partial \sigma}{\partial n_i}\right]_{T_s}\right]^{-1} \tag{3.70}$$

whereas (3.65) and (3.66) remain unaltered. Naturally, the simple geometrical interpretation in terms of the isotherm (Fig. 3.3) is no longer adequate.

Assembling the various parts before us now we return to the question we posed at the beginning of this chapter: what time scale characterizes the approach to steady state of a film desorbing at finite temperature elevations and how does that time depend on the conditions of the experiment?

It is a well–known property of systems which approach saturation according to an exponential law like (3.52) (such as RC circuits) that the characteristic time constant may be obtained graphically by extrapolating the initial slope of the function to the asymptote representing the steady–state value. The time at which these two lines intersect determines τ. A similar construction for a function obeying a more complicated time evolution but which nevertheless has the same general features – a slope having its maximum value at t=0 and gradually decreasing so that the function turns over to approach a horizontal asymptote – proves to be a useful measure of the desorption time. (Though admittedly crude, this construction comes close to the way experimental data might well be handled. For example, it is not hard to convince oneself that any linear fit to a plot of $ln(1-n(t)/n_{ss})$ vs. time will, for times such that the data do not depart too strongly from a straight line on this logarithmic plot, give a result substantially similar to that of the procedure we have outlined.) A plot of $n_o-n(t)$ vs. t might look something like Fig. 3.4. If the isotherm is one with positive curvature, the initial estimate of steady state, $n_o-n_{ss}^o$, will fall short of the true value, n_o-n_{ss}, as we have already seen. The initial slope of the desorption curve,

$$-\left[\frac{dn}{dt}\right]_{t=0} = \frac{n_o-n_{ss}^o}{\tau_{lcl}(n_o)} \tag{3.71}$$

extrapolated to the actual steady state asymptote defines a time

$$\tau_{exp}(n_o,n_{ss}) = \tau_{lcl}(n_o)\left[\frac{n_o-n_{ss}}{n_o-n_{ss}^o}\right] \tag{3.72}$$

which exceeds $\tau_{lcl}(n_o)$ and depends on both n_o and n_{ss}. This additional dependence on n_{ss} arises because, unlike the exponential solution (3.52), there is no

Figure 3.4. Number desorbed per unit area vs. time for isotherms with positive curvature.

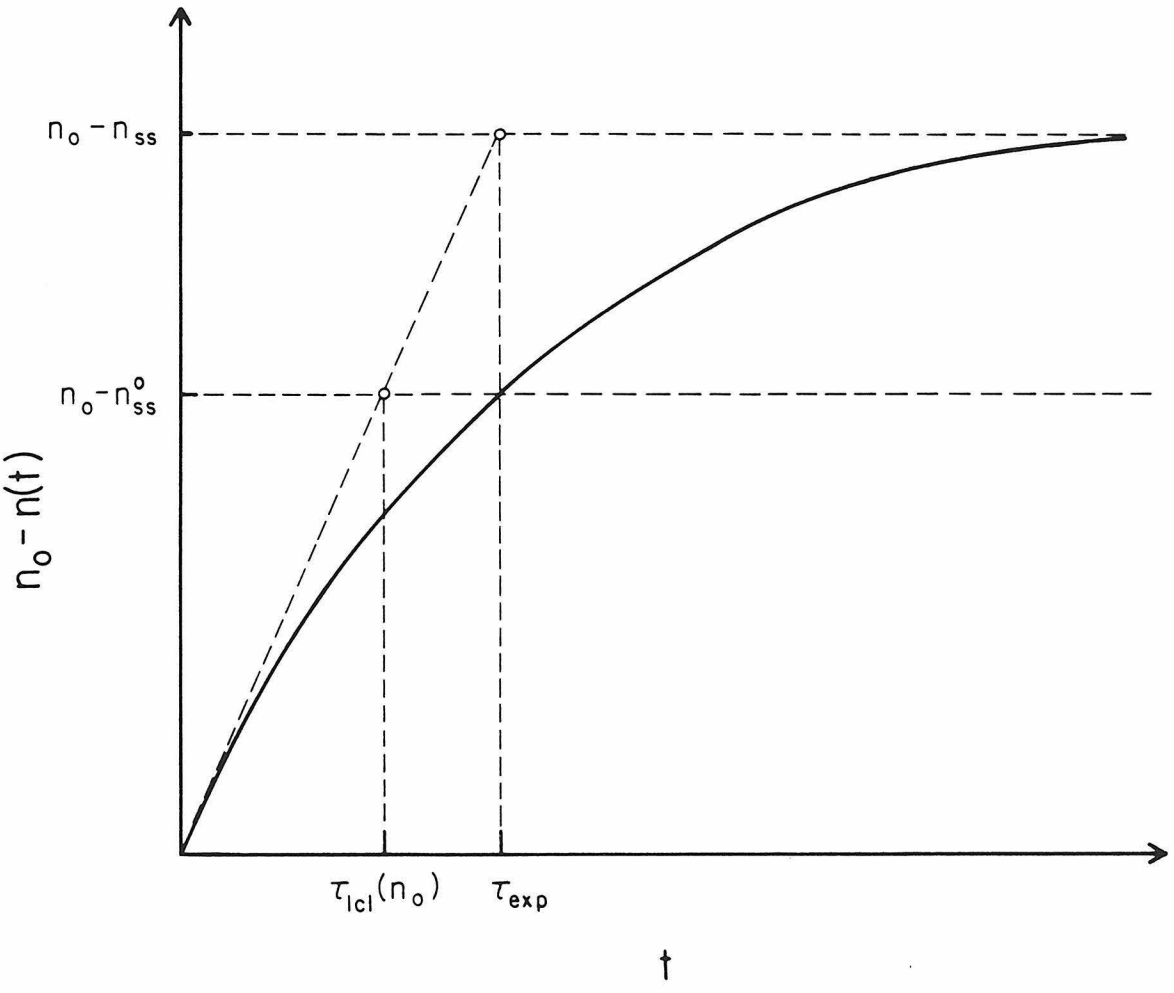

a priori relationship between the local properties of the desorption rate (specifically, those near $t=0$) and the global approach to the true steady state for an isotherm which is nonlinear.

It is important at this point to comment on the physical significance of positive curvature in the equilibrium vapor pressure isotherm as a function of coverage. One clear–cut example of this behavior is the ideal Fermi gas equation, (3.54), but it is not by any means the only instance nor, for our purposes, the most important one. The FHH isotherm must asymptote at high coverage to the bulk vapor pressure $P_o(T)$, and as a result, the curvature of the isotherm at high coverage must be negative. As the number of atoms on the surface is reduced, however, an inflection point is reached at intermediate coverages, and in the one to two layer regime the curvature is distinctly positive (unfortunately, this transition is not apparent in Fig. 1.3 where the vapor pressure has been plotted on a logarithmic, rather than linear, scale effectively softening the essential singularity at low coverage where P/P_o vanishes like e^{-1/n^3}). We have also alluded to this behavior in the knees of stepwise isotherms, and it is reasonable to argue that if repulsive interactions dominate in the adatom–adatom potential, then even for particles obeying Bose statistics the isotherm will likely curve upwards. What appears to be rather general about the FHH isotherm is not the quantitative dependence of $\mu_f(T,n)$ on coverage and temperature, but rather the overall *shape* of the isotherm – a region of positive curvature at low coverage merging through an inflection point to a region of negative curvature at higher coverages. This sigmoidal shape is characteristic of the adsorption isotherms of virtually anything physisorbed on a heterogeneous substrate, i.e., a nonuniform surface with a distribution of sites of different binding energies.

The slope of an Arrhenius plot of τ_{exp} reveals the *total* temperature variation of $ln\tau_{exp}$ with respect to $1/T_s$. We see from (3.72) that this variation consists of essentially two parts: a contribution due to the change in the initial rate of evaporation, $(dn/dt)_{t=0}$, and a contribution from the change in steady state

conditions with temperature so that

$$-T_s^2\frac{d}{dT_s}ln\tau_{exp} = -T_s^2\frac{d}{dT_s}\left[ln\tau_{lcl}(n_o) + ln\left[\frac{n_o-n_{ss}}{n_o-n_{ss}^o}\right]\right] \tag{3.73}$$

A general expression for the first factor in (3.73) is obtained either from (3.63)

$$-T_s^2\frac{d}{dT_s}\,ln\tau_{lcl}(n_o) = T_s^2\left[\frac{\partial^2 P_f}{\partial T_s \partial n_o}\right]\left[\frac{\partial P_f}{\partial n_o}\right]_{T_s}^{-1} - \frac{1}{2}T_s + \frac{T_s^2}{\sigma(T_s)}\frac{d\sigma(T_s)}{dT_s} \tag{3.74a}$$

or by differentiating the logarithm of (3.68),

$$-kT_s^2\frac{d}{dT_s}ln\tau_{lcl}(n_o) = -\mu_f(T_s,n_o) + T_s\left[\frac{\partial\mu_f}{\partial T_s}\right]_{n_o} + \tag{3.74b}$$

$$kT_s^2\left[\frac{\partial^2\mu_f}{\partial T_s\partial n_o}\right]\left[\frac{\partial\mu_f}{\partial n_o}\right]_{T_s}^{-1} + kT_s + \frac{kT_s^2}{\sigma(T_s)}\frac{d\sigma(T_s)}{dT_s}$$

which includes the effect of the variation of both activation energy and prefactor with temperature in the second and subsequent terms. For example, setting aside the change of sticking coefficient with temperature – it would be surprising if this were significant enough to be comparable with other terms over the temperature range of interest – (3.74b) is readily evaluated and gives

$$\varepsilon_o + kT_s \tag{3.75a}$$

for the 2–d Boltzmann and quantum gases,

$$\varepsilon_o + 2kT_s \tag{3.75b}$$

for the Langmuir monolayer and

$$-\Delta V_{ext}(n_o) + l(T_s) - (3/2)kT_s \tag{3.75c}$$

for the FHH isotherm. This last instance is somewhat atypical in that the mixed second partial derivative, $(\partial^2\mu_f/\partial T_s\partial n_o)$, vanishes because μ_f is a sum of separate temperature– and coverage–dependent parts. The latent heat term comes from

$T_s(\partial\mu_f/\partial T_s)$ which also contributes $\mu_l(T_s)-(5/2)kT_s$ cancelling the temperature dependence of $-\mu_f(T_s,n_o)$ and leaving only the potential energy.

Despite the simplicity of the special cases (3.75), the general formulae in (3.74) do not resemble any of the conventionally defined heats of adsorption (the isosteric heat, for example, is defined through

$$q_{st}=kT^2(\partial ln P_f/\partial T)_n=(5/2)kT-\mu_f+T(\partial\mu_f/\partial T)_n\ ).$$

Furthermore, there is no simple relation between (3.74b) and the *equilibrium* value of the chemical potential, $-\mu_f(T_o,n_o)$. All that can be said in general is that $-\mu_f(T_s,n_o)$ will be greater than $-\mu_f(T_o,n_o)$ for T_s exceeding T_o, since $-(\partial\mu_f/\partial T)_n=(\partial S_f/\partial n)_T$ and the partial molar entropy is usually positive.

While it is not possible to deduce a general statement about the behavior of the second factor in (3.73), valid for arbitrary T_s and any equation of state, the following observation is pertinent. For temperature rises small enough for the linearized solutions to be globally valid there is no distinction between n_{ss} and n_{ss}^o, and the ratio $(n_o-n_{ss}/n_o-n_{ss}^o)$ is unity. On the other hand, for an isotherm with positive curvature, as illustrated in Fig. 3.3, this quantity is greater than one for finite temperature jumps, and we conclude that, at least for small enough T_s, it increases with temperature. Therefore,

$$-T_s^2\frac{d}{dT_s}\,ln\left[\frac{n_o-n_{ss}}{n_o-n_{ss}^o}\right]<0\,. \tag{3.76}$$

Comparing with the formulae (3.75) which are positive in the domain of interest to us here, we see that this factor competes with (3.74) since it enters with opposite sign. The apparent slope of the Arrhenius plot is therefore decreased by (3.76). The exact balance between (3.74) and (3.76) will, of course, depend on the details of the equation of state but it is only the curvature of the equilibrium isotherm which determines their relative sign.

6. Numerical Results

Let us now illustrate the ideas we have been discussing with some specific numerical examples. As in chapter 2, we take as a representative equation of state the FHH isotherm and for simplicity assume that the sticking coefficient is constant and equal to one.

We presented a numerical integration of the exact nonlinear equations of the continuum model, (2.28) and (2.29) in Fig. 2.8. That example, with $\varepsilon = 0.8\times10^{-5}$ and $\theta_{ss} = 0.5$, is reproduced in Fig. 3.5 where it is compared with the corresponding approximate solutions obtained via the boundary layer analysis developed in section 3.3. The upper solid line shows the film temperature, $\tilde{\theta}$, and the lower solid line the amount desorbed, $\tilde{\chi}$, (i.e., both θ and χ are scaled to their respective steady state values) for the exact solutions as a function of time. Similarly, the broken curves show an evaluation of the uniform approximation (3.43) for the film temperature and a numerical integration of (3.45) for the film thickness using the same algorithm (DGEAR [IMSL]) as employed for the exact equations. We see that, with such a small value of ε, the approximate solution $\tilde{\chi}_{o,u}$ is indeed a very good one, lying just slightly above the exact result for all times. The discrepancy between the two is most pronounced near $t=0$ where the isothermal approximation fails to take into account the small but finite lag time in warming the film and so always overestimates the amount desorbed. This is illustrated in Fig. 3.6 where the differences $\tilde{\chi}_{0,u} - \tilde{\chi}$ and $\tilde{\theta}_{0,u} - \tilde{\theta}$, relative to steady state, are plotted versus time. For lower pressures, and therefore smaller ε, these differences continue to decrease.

Figures 3.7 and 3.8 show the same sequence under similar conditions except that the pressure has been increased from 10^{-5} to 10^{-3} Torr and, as a consequence, ε is now two orders of magnitude larger than in the previous case (note however that the film thickness has not changed substantially). The approximate solutions still look qualitatively very much like the exact ones, but quantitatively the differences have increased up to the 20% level and extend for longer

Figure 3.5. Comparison of exact and approximate solutions to the continuum model for $\varepsilon = 0.8 \times 10^{-5}$, $\theta_{ss} = 0.5$, $T_o = 3.5$ K and $P_g = 1 \times 10^{-5}$ Torr, $\delta_o = 0.8$ layers. Upper curves: $\tilde{\theta}$ (solid), $\tilde{\theta}_{0,u}$ (dashed). Lower curves: $\tilde{\chi}$ (solid), $\tilde{\chi}_{0,u}$ (broken). Time in units of the global time constant, $\tau_{exp} = 1$ μsec.

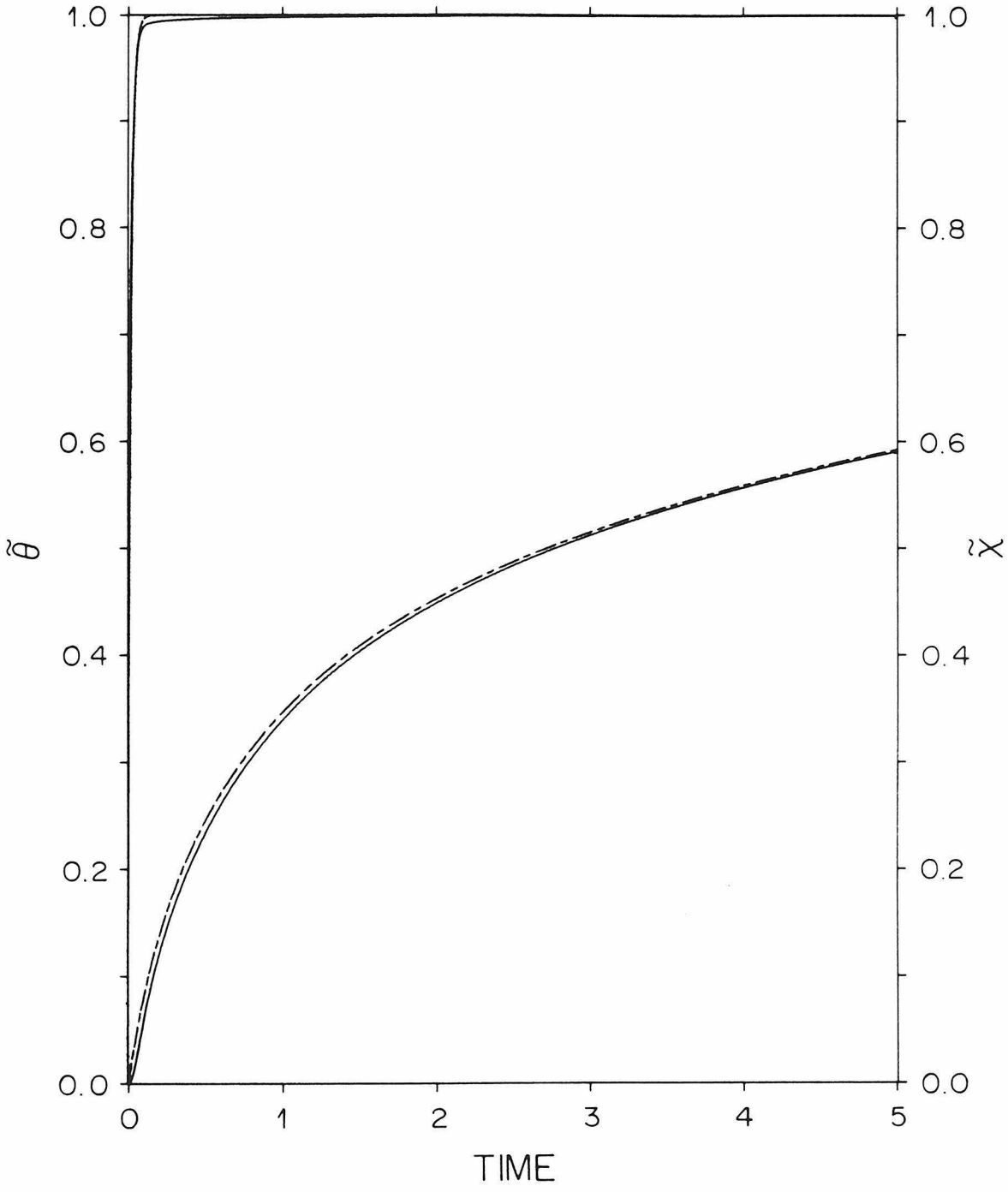

Figure 3.6. Difference vs. time between exact and approximate solutions in Fig. 3.5. Broken curve: $\tilde{\chi}_{0,u} - \tilde{\chi}$. Dashed curve: $\tilde{\theta}_{0,u} - \tilde{\theta}$.

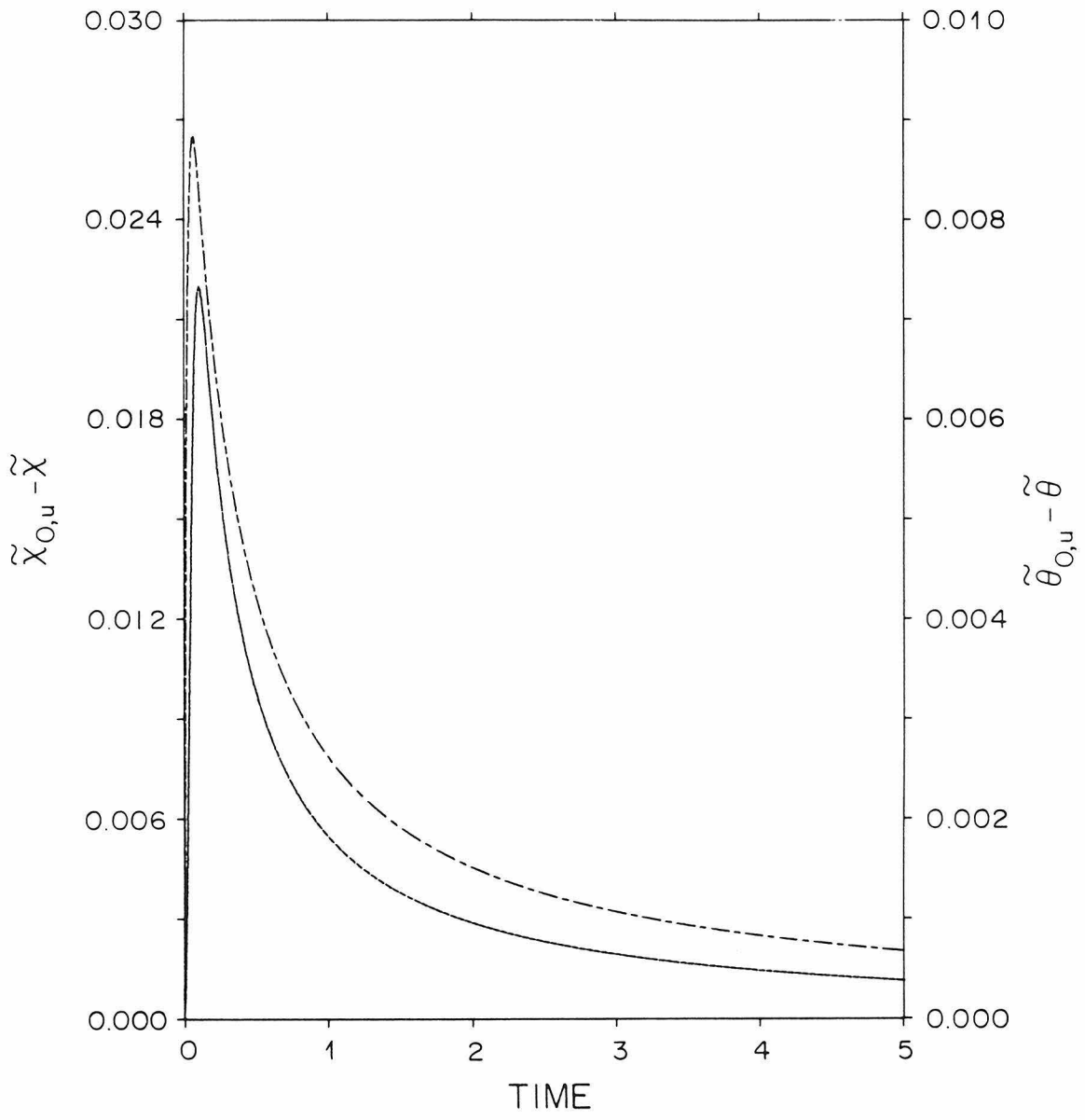

Figure 3.7. Comparison of exact and approximate solutions to the continuum model for $\varepsilon = 0.8 \times 10^{-3}$, $\tilde{\theta}_{ss} = 0.5$, $T_o = 3.5$ K and $P_g = 1 \times 10^{-3}$ Torr, $\delta_o = 0.9$ layers. Upper curves: $\tilde{\theta}$ (solid), $\tilde{\theta}_{0,u}$ (dashed). Lower curves: $\tilde{\chi}$ (solid), $\tilde{\chi}_{0,u}$ (broken). Time in units of the global time constant, $\tau_{exp} = 55$ nsec.

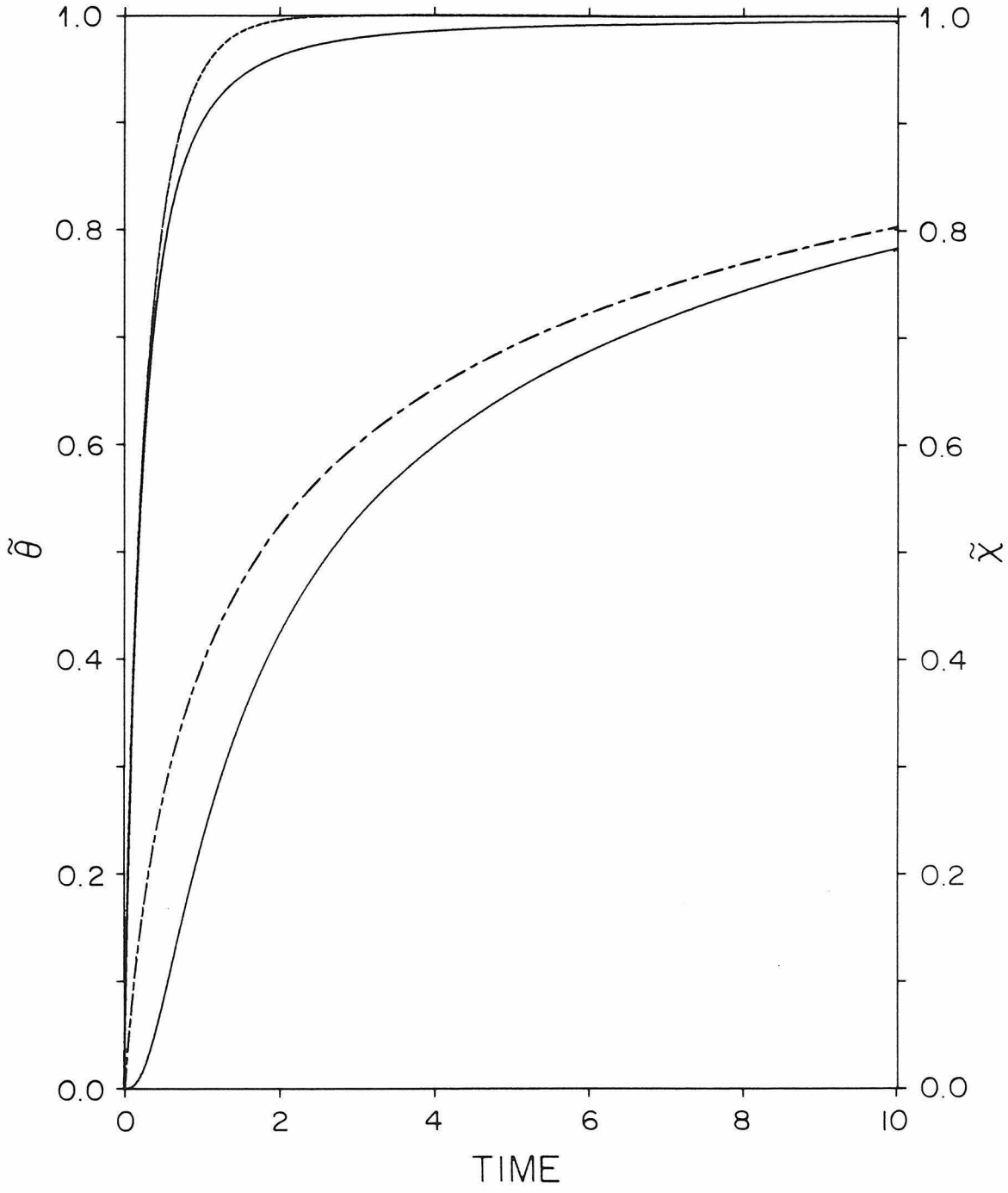

Figure 3.8. Difference vs. time between exact and approximate solutions in Fig. 3.7. Broken curve: $\tilde{\chi}_{0,u} - \tilde{\chi}$. Dashed curve: $\tilde{\theta}_{0,u} - \tilde{\theta}$.

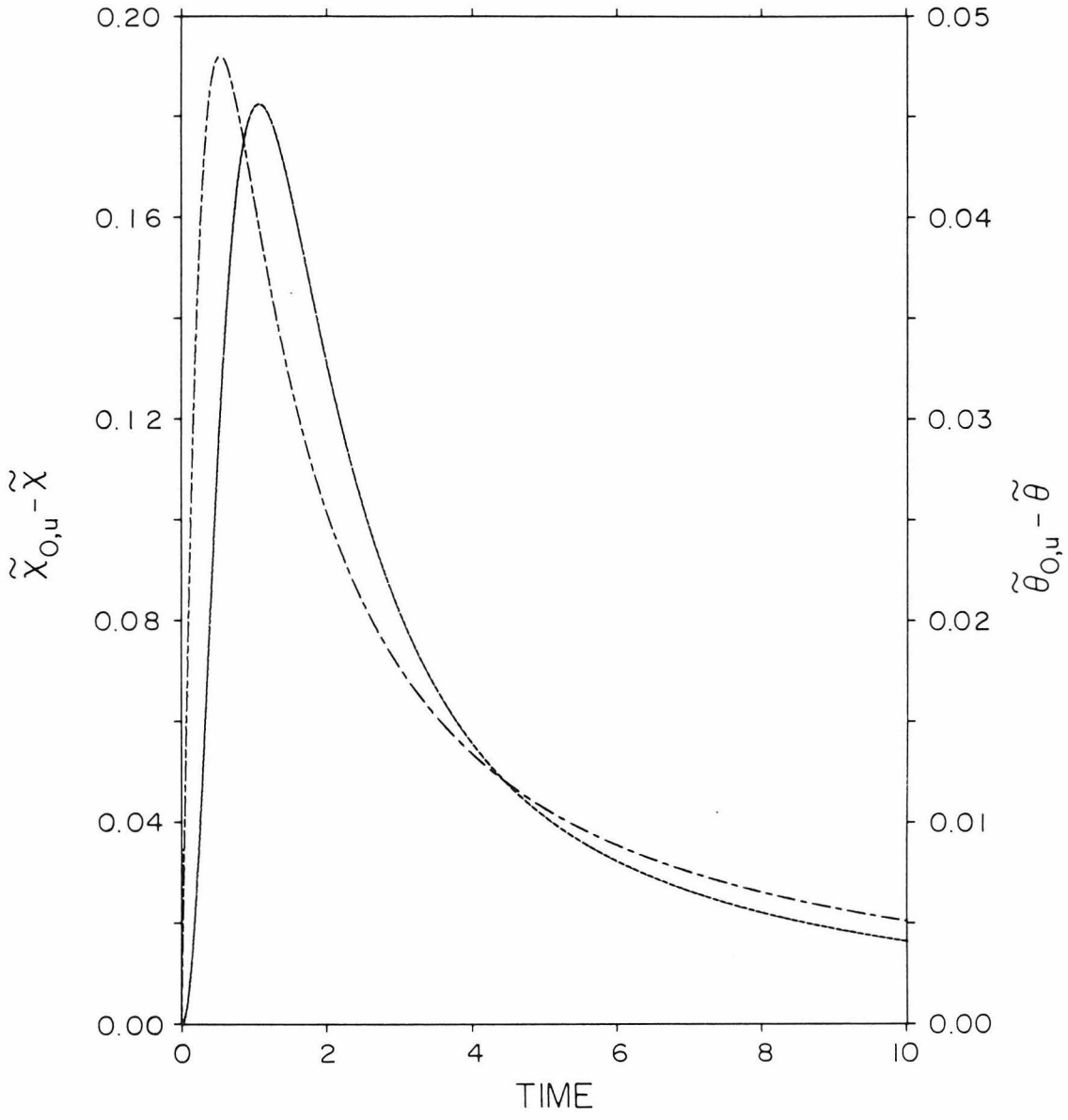

times. As anticipated, we see that the validity of the isothermal approximation procedure begins to come into question for the higher evaporation rates that accompany increased vapor pressure, and just like the linearized solutions at higher pressure, the exact behavior shows strongly coupled evaporation and heating.

Calculations of the global measure of the time to approach steady state, τ_{exp}, are presented in the form of an Arrhenius plot in Fig. 3.9 where the logarithm of this time constant is shown as a function of the dimensionless ratio T_o/T_s. The examples display a succession of realistic equilibrium chemical potentials for a single initial temperature and also show the variations brought about by changes in the equilibrium temperature for a fixed ratio of $-\mu_o/T_o$. The important parameters for each case, including the initial binding energy as a fraction of the equilibrium chemical potential, are listed in Table 3.1.

What is most striking about these plots is that they appear so linear over so many decades for such a variety of initial conditions. At low heater powers, where T_o/T_s is near one, the graphs turn over somewhat and their intercept at $T_o/T_s = 1$ is the time constant τ_1 of the linearized theory under the same equilibrium conditions. At the other extreme, extrapolating the linear portion of these curves, they seem to share a common intercept of roughly 10^{-11} sec at $T_o/T_s = 0$. In terms of the parameterization (3.1), this intercept provides a value for τ_o. The activation energy E, on the other hand, is the slope of these curves as expressed in equation (3.73). Normalizing to the absolute value of the equilibrium chemical potential, this quantity is shown as a function of T_o/T_s in Fig. 3.10 for the same series of curves. We see that, for the higher heater powers, the activation energy lies somewhere between 0.7 and 1.0 in units of $|\mu_o|$, whereas it turns down sharply for less violent departures from equilibrium and intercepts $T_o/T_s = 1$ with a value substantially lower. It is this intercept which represents the nonzero limit discussed in (3.5).

Table 3.1

Relevant parameters for the sequence of examples plotted in each of Figs. 3.9 – 3.13

T_o (K)	$-\mu_o$ (K)	P_g (Torr)	$-\mu_o/T_o$	ε	δ_o (layers)	$\Delta V_{ext}/\mu_o$
3.5	55	5.3×10^{-4}	15.7	4.4×10^{-4}	.87	.87
3.5	70	7.3×10^{-6}	20.0	6.1×10^{-6}	.79	.90
3.5	90	2.4×10^{-8}	25.7	2.0×10^{-8}	.72	.92
2.0	40	1.8×10^{-6}	20.0	1.1×10^{-5}	.97	.85
1.0	20	3.1×10^{-7}	20.0	2.1×10^{-5}	1.33	.66

Figure 3.9. Global time constant as a function of inverse substrate temperature for a variety of initial conditions. Bottom, middle and top solid curves correspond to the first three rows of Table 3.1, respectively. Broken and dashed curves represent rows 4 and 5.

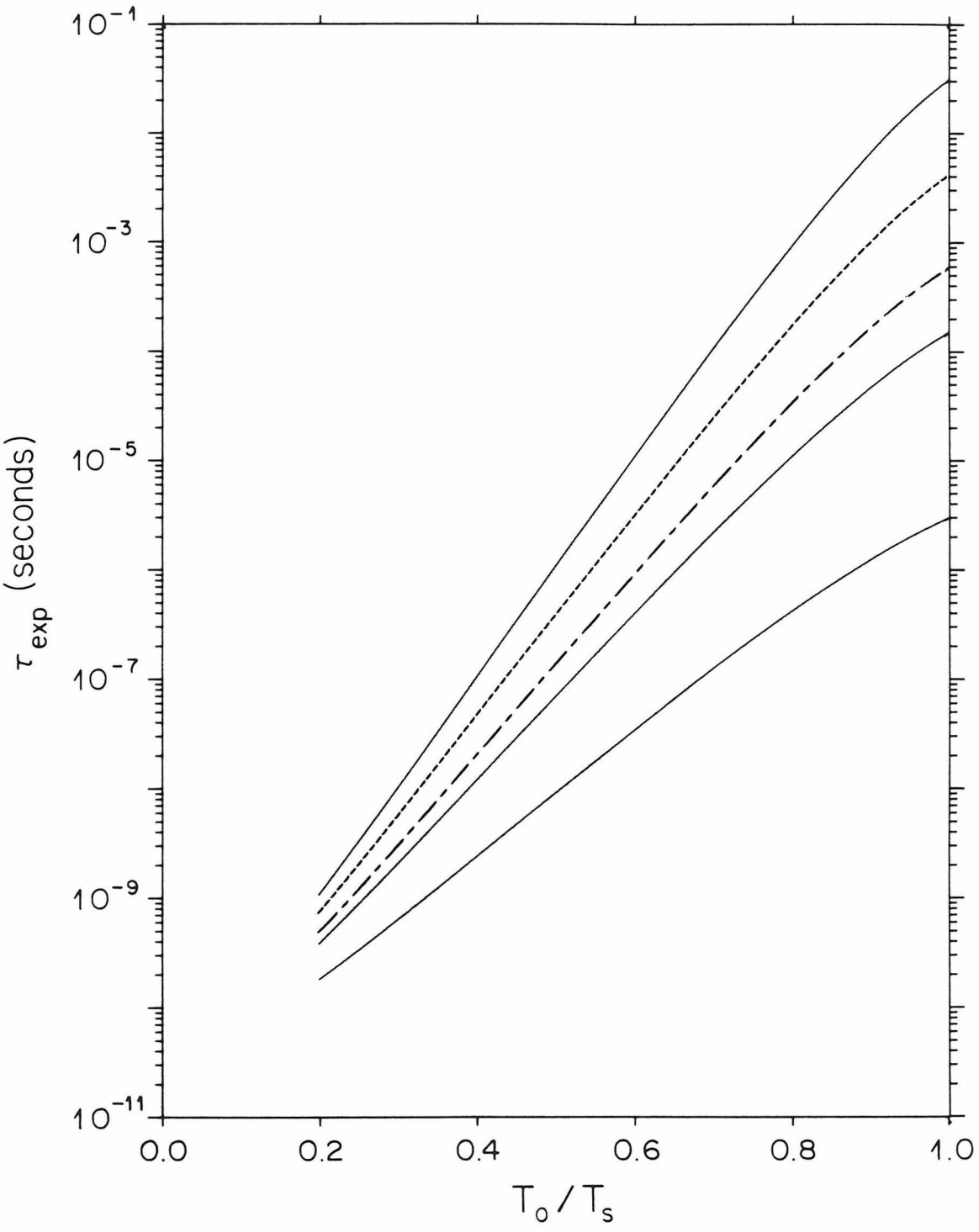

Figure 3.10. Global time constant activation energy in units of the equilibrium chemical potential. Same series of curves as in Fig. 3.9.

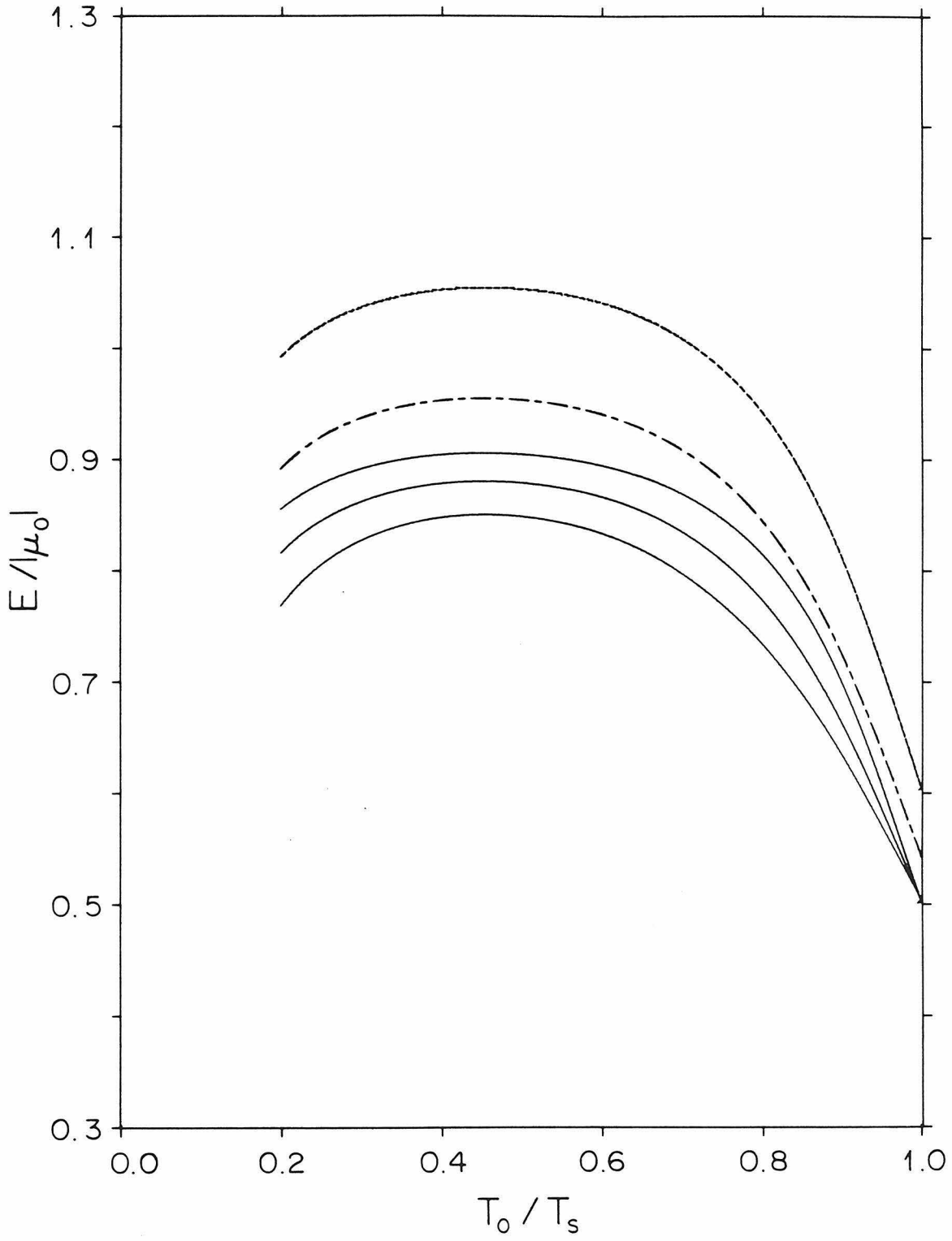

The behavior of the local time constant at the initial coverage, $\tau_{lcl}(n_o)$, also appears to be rather linear over many decades of a semi–logarithmic plot as indicated in Fig. 3.11. These curves, like those for τ_{exp}, also intercept the $T_o/T_s = 1$ axis at τ_1, as they must, for in the equilibrium limit there is no distinction between a local linearization of the rate equation and a global linearization of the coupled equations of motion. As T_o/T_s decreases, however, the curves for $\tau_{lcl}(n_o)$ quickly fall below the corresponding ones for τ_{exp} and this is demonstrated in Fig. 3.12 where the ratio $\tau_{lcl}(n_o)/\tau_{exp}$ is plotted versus T_o/T_s. The results do not seem to depend strongly on initial conditions. From the definition (3.72) we see that $\tau_{lcl}(n_o)/\tau_{exp}$, in fact, equals the local amplitude $n_o - n_{ss}^o$ divided by the steady state difference $n_o - n_{ss}$, and as explained in connection with Fig. 3.4, this quantity is less than one because of the upward curvature of the equilibrium adsorption isotherm. The slope of the local time constant curves (3.74) is shown in units of the equilibrium chemical potential in Fig. 3.13, where it is clear that $E/|\mu_o|$ is approximately one except at higher substrate temperatures.

7. Comparison with Data and Limits to the Analysis

We have in Figs. 3.9 and 3.10 a plausible explanation for the puzzling experimental observations cited at the beginning of this chapter. To a first approximation, the logarithm of the global time constant, $ln\tau_{exp}$, appears linear against $1/T_s$ over a substantial range and this suggests that an activated law like (3.1) is responsible. When the observations are analyzed in this way the energy of activation is found to be correlated with, but less than, $-\mu_o$, the equilibrium chemical potential. We can now understand this result in terms of the inherent nonlinearity of the equation of state for an interacting system, and in particular, the sign of its curvature in the vapor pressure–coverage plane. Because the isotherm is nonlinear there is no single simple time constant but rather a succession of local time constants as a function of time, each related to the slope of

Figure 3.11. Local time constant at equilibrium coverage vs. inverse substrate temperature. Curves as in Fig. 3.9.

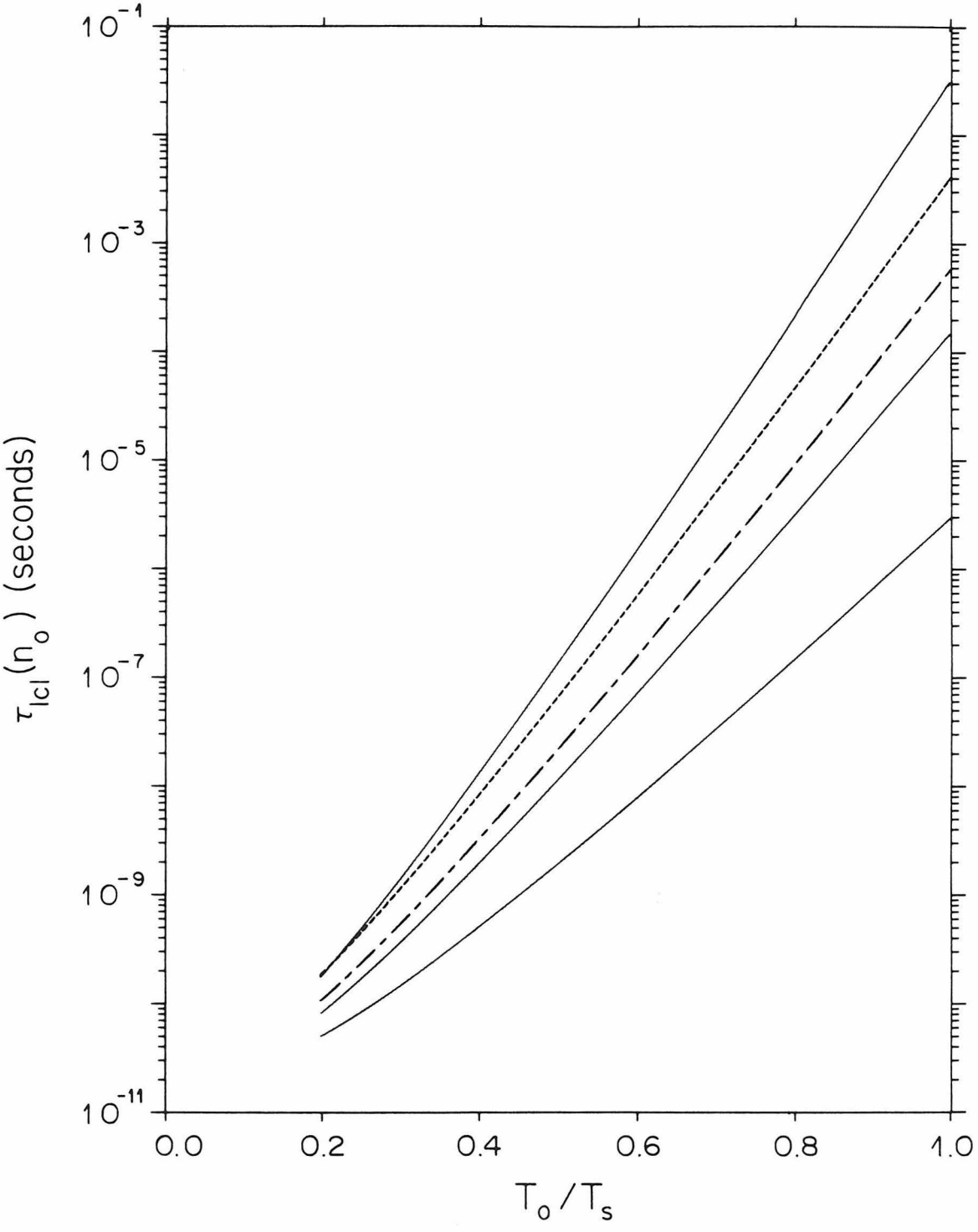

Figure 3.12. Ratio of $\tau_{lcl}(n_o)$ to $\tau_{exp}(n_o)$ or local amplitude at equilibrium coverage relative to amount desorbed in steady state. Curves as in Fig. 3.9 except rows 1 and 3 reversed.

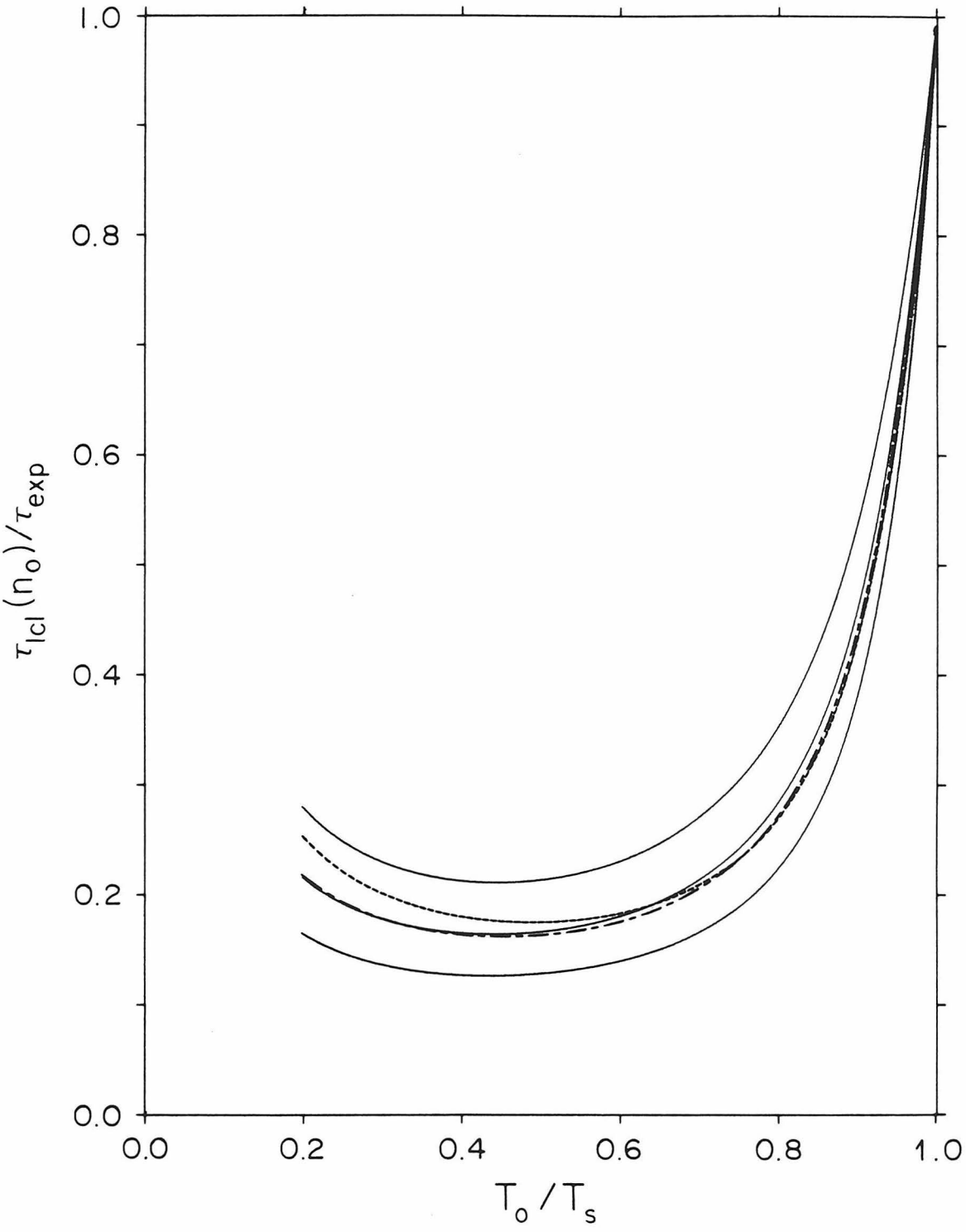

Figure 3.13. Local time constant activation energy in units of the equilibrium chemical potential. Curves as in Fig. 3.9.

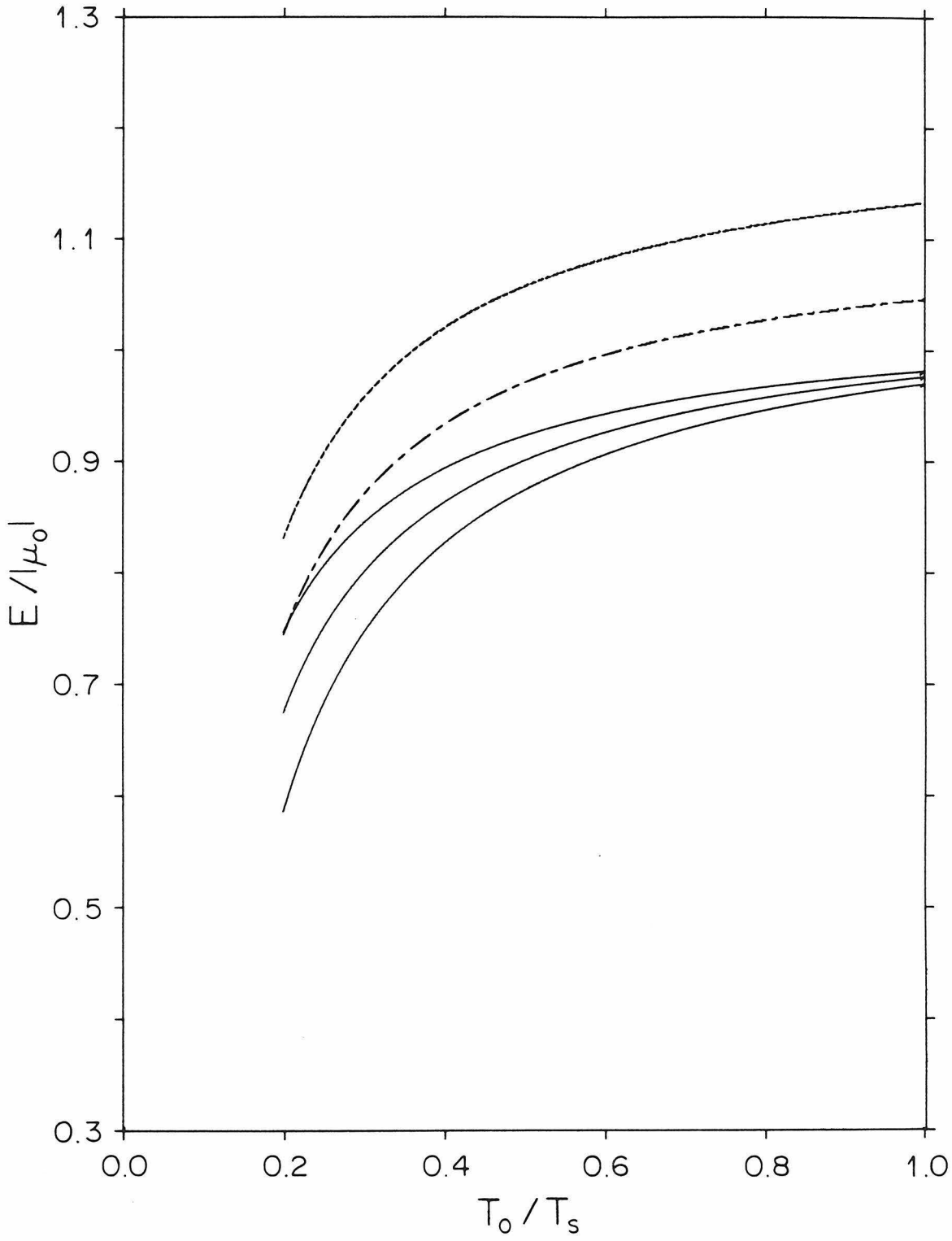

the adsorption isotherm evaluated at the instantaneous coverage. These local time constants may each be written in activated form, (3.68), but bear no direct relation to the overall time characterizing the approach of the system to steady state. Such a time may be defined, however, as the total change in coverage necessary to reach steady state divided by the initial isothermal desorption rate – a quantity which is independent of $n_o - n_{ss}$ only for independent particles obeying first–order kinetics. Changes in this time with desorption temperature, (3.73), then reflect not only the dependence of the local time scale, $\tau_{lcl}(n_o)$, on temperature but also the variations brought about in the global steady state condition. For nonlinear isotherms of positive curvature these two factors compete against one another, (3.76), in determining the apparent activation energy in an Arrhenius parameterization, (3.1), of τ_{exp}. For the FHH model, $E/|\mu_o|$ lies between 0.7 and 1 in the same temperature range as the experimentally quoted value of two–thirds, and τ_o is about 10^{-11} sec versus the observed range of $10^{-9} - 10^{-10}$ sec, in qualitative but not necessarily quantitative agreement with the data.

A more detailed comparison is presented in Fig. 3.14 which shows one set of time constant data from Sinvani *et al.* contrasted with the predictions of the FHH model under similar conditions. The agreement in absolute magnitude is good at the lowest substrate temperatures and remains within a factor of five or so out to the highest temperature point. The slope of the data and model calculations clearly differ, however, being about 0.6 in units of $|\mu_o|$ for the former and about 0.8 for the latter (see the middle solid line of Fig. 3.10). This discrepancy should not be surprising in view of our assumptions: after all, the true equation of state of the film is unknown, the sticking coefficient may not be constant and equal to one as we have supposed, and our definition of the time constant, though appealingly simple, is still somewhat crude.

That the data lie above the calculated curve, that is, that the observed time constants appear to be longer than the model's predictions, could be due to our

Figure 3.14. Continuum model's predictions for the global time constant (solid line) compared with the data of Sinvani *et al.* (squares) for T_o = 3.48 K and $-\mu_o$ = 72 K.

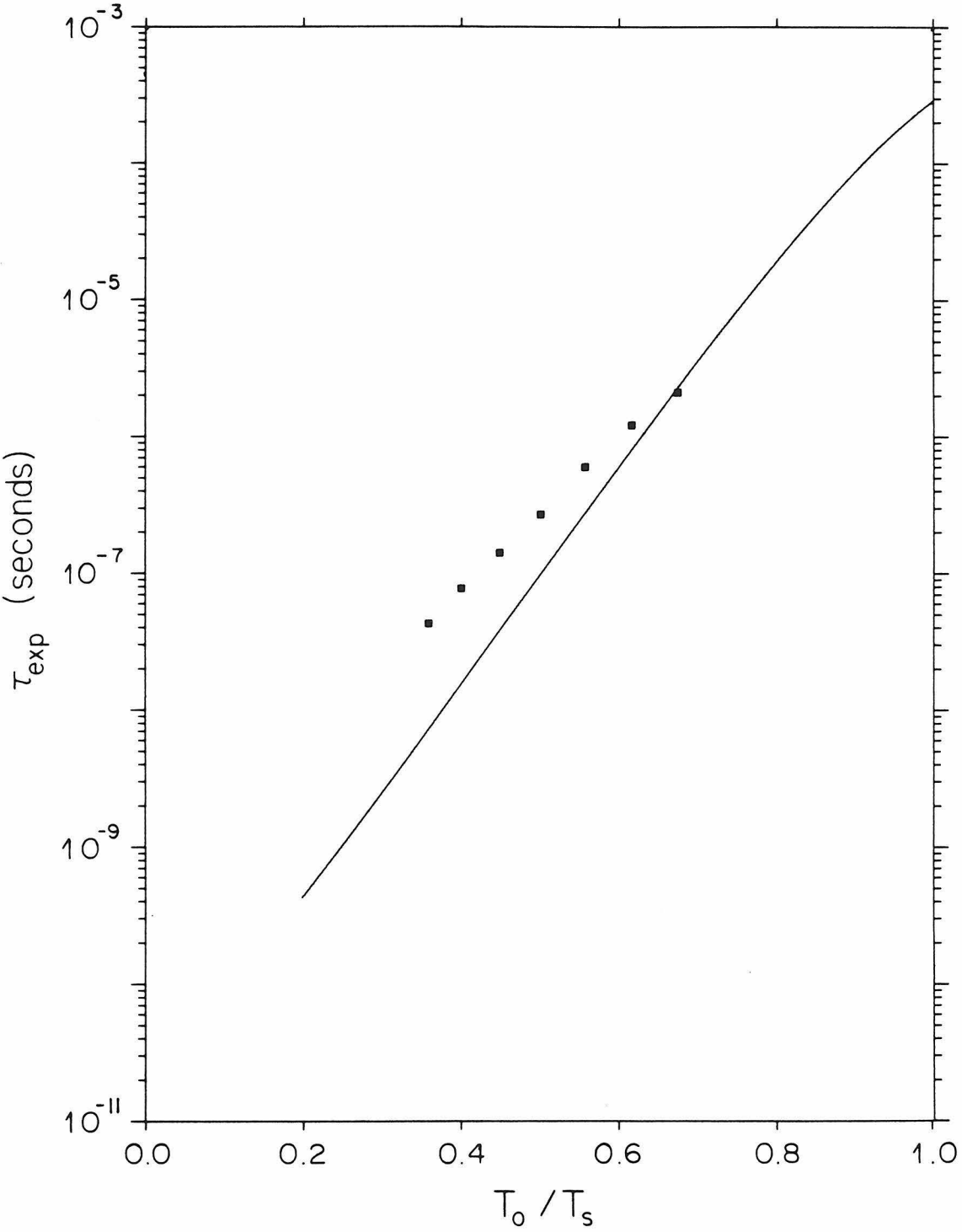

choice of $\sigma=1$ which implies that particles desorb at the maximum rate allowed by detailed balance. For constant σ, (3.48), (3.71) and (3.72) show that $\tau_{exp} \propto 1/\sigma$. Decreasing σ then just shifts the entire τ_{exp} curve uniformly upward. By the same token, the difference in slope might be attributable to a sticking coefficient which is a decreasing function of temperature. One must also bear in mind that, as mentioned at the conclusion of section 3, the isothermal approximation at $t=0$ provides an upper limit to the maximum desorption rate of the exact solutions. The predictions for τ_{exp} based on this approximation may then be too small on account of both a tendency of the boundary layer method to overestimate the maximum slope of the exact desorption curve and the increasing failure of the film to desorb isothermally at higher substrate temperatures, as decoupling becomes more difficult. The likelihood of error in this direction is further reinforced by the capacity of the binding energy to grow without bound in the FHH model which, at high temperature, leads to an underestimate of the change in coverage between equilibrium and steady state.

Alternatively, the substrate temperature assignment in the experiments may be suspect at high heater powers. If it were necessary to shift the experimental points to lower substrate temperatures, they would then be in better accord with the calculated curve. The data also lie in a regime where the number of collisions among desorbing particles as they leave the surface is no longer small, and the significance of this fact with respect to the measurements is not easy to assess. These and other points of experimental detail will be discussed at greater length in the following chapter.

References

Bender, C. M. and Orszag, S. A., *Advanced Mathematical Methods for Scientists and Engineers* (MacGraw Hill, New York, 1978).

Bienfait, M. and Venables, J. A., Surf. Sci. **64**, 425 (1977).

Dash, J. G., *Films on Solid Surfaces* (Academic Press, New York, 1975).

de Boer, J. H., Adv. Catalysis **8,** 85 (1956).

de Boer, J. H., *The Dynamical Character of Adsorption* (Oxford University Press, 1968).

Frenkel, J., *Kinetic Theory of Liquids* (Dover, New York, 1955).

IMSL Library, The, Vol. 1, 8th ed. (International Mathematical and Statistical Libraries Inc., 1980).

Kruyer, S., K. ned. Akad. Wet. **B58,** 73 (1955).

Lin, C. C. and Segal, L. A., *Mathematics Applied to Deterministic Problems in the Natural Sciences* (MacMillan, New York, 1974).

Nagai, K., Shibanuma, T. and Hashimoto, M., Surf. Sci. **145,** L459 (1984).

Opila, R. and Gomer, R., Surf. Sci. **112,** 1 (1981).

Sinvani, M., Taborek, P. and Goodstein, D., Phys. Rev. Lett. **48,** 1259 (1982).

Venables, J. A. and Bienfait, M., Surf. Sci. **61,** 667 (1976).

Chapter 4
The Experiments

1. Introduction

At various places in our exposition we have alluded, as necessary, to one or another aspect of the way in which the desorption time constant experiments are conducted. In the present chapter we elaborate considerably on these issues, describing the important points of experimental technique in detail, and draw attention to those features which, in part, suggested that a new series of measurements be undertaken. The major results of those new experiments are then presented along with a discussion and analysis within the framework of the thermal model.

2. Apparatus and Techniques

It should be kept in mind from the beginning that the experimental methodology used in these investigations has been adapted from previous studies, in this laboratory and others, on thermal phonon propagation in single crystals at low temperature. While our samples were prepared and handled with ordinary care, neither UHV techniques nor the now standard methods of *in situ* surface preparation and analysis were readily compatible with our cryogenic environment. Thus, from the standpoint of modern surface science, our desorption surfaces basically remain uncharacterized.

The experiments are all performed in a cell which is directly immersed in a vapor–pumped helium bath. The cryostat was designed with particular regard to minimizing the overall heat load presented by the running experiment. The equivalent heat leak, determined by monitoring the bath level as a function of time, was found to be under 25 mW and the lowest attainable temperature was 1.10 K. As a practical matter, this design allowed uninterrupted operation of the experiment for upwards of four days between transfers of liquid helium,

depending upon conditions. The temperature of bath and cell were monitored with a Germanium resistance thermometer affixed to the outside of the cell, and this temperature could be controlled by regulating the helium vapor pressure in the dewar via a conventional diaphragm and ballast arrangement. In this way, with a superfluid bath, the temperature could easily be maintained, exclusive of helium transfers, to within ± .002 K over an entire experimental run.

The experimental cell is connected by approximately 1.5 m of 1/4" o.d. thin-wall stainless steel tubing (vacuum isolated from the bath) to a diffusion pumped gas handling system outside the cryostat. Prior to cooling, the entire system (including cell) is evacuated to its base pressure of 3×10^{-7} Torr, and once cold, a controlled quantity of helium gas admitted to the cell forms an adsorbed film on all exposed surfaces. A single disk of Grafoil (0.175 g) in the cell acts as an adsorption ballast so that the amount of helium gas needed is not too small to be handled conveniently. The geometric area of all other free surfaces in the cell is on the order of 10 cm^2, whereas the surface area of the Grafoil, determined from adsorption isotherm measurements, is about 400 times larger.

A schematic representation of the experimental arrangement inside the cell has already been shown in the inset of Fig. 2.1. A single crystal of sapphire, in the shape of a flat cylinder 2-1/4" in diameter and 3/8" thick, forms one face of the vacuum enclosure, and a demountable superfluid leak-tight fitting to the body of the cell (OFHC copper) is made via a pressed indium o-ring seal. The crystal is oriented with its faces parallel to the plane formed by the three- and two-fold symmetry axes of the trigonal sapphire unit cell (the C-X plane) and with its cylindrical axis perpendicular to this plane.

The heater, which serves as the desorption surface, is a 500 Å thick nichrome film vacuum evaporated directly onto the sapphire whose polished faces have a surface roughness under 250 Å. Nichrome, a metallic alloy composed of 61% Ni, 15% Cr and 24% Fe, is chosen not because it is an intrinsically interesting substrate, but rather because its high bulk resistivity (112 $\mu\Omega$ - cm)

and low temperature coefficient of resistance easily permit the patterning of compact heaters of well-defined geometric area which can be impedance matched to the 50 Ω coaxial cable transmitting pulses to them. For example, in the experiments reported here, the heater was a rectangle of length twice its width, with an area of 1.10 mm^2 and a d.c. room temperature resistance of 47.5 Ω. This resistance changed negligibly upon cooling to 4 K.

As we discussed in chapter 2, the heater, when it is at an elevated temperature, radiates a net number of phonons into the crystal, and it is presumed that none of these phonons is scattered back into the heater. In reality, the crystal is not a medium of infinite extent but possesses a far surface in contact with the helium bath. Longitudinal phonons emitted by the heater can reach this surface in about 1 μsec, and transverse phonons take between 1.6 and 1.7 μsec depending on whether they are fast or slow transverse polarized. Roughly half of the phonons incident at this interface are transmitted directly to the helium bath, whereas the remainder are specularly reflected back into the crystal. Even so, no matter how long the heater is pulsed, because of the small solid angle it subtends as viewed from the far surface, and because of the large crystal surface area in direct contact with the bath, almost all these phonons eventually end up coupling to the bath and not going back into the heater. It is this feature of effectively radiating into a "phonon vacuum" at the ambient temperature which allows the heater to be turned on as well as off very rapidly, a fact we tacitly assumed in the derivation of the heat flux term in (2.17). Let us consider the point in more detail now.

A step in the voltage applied across the heater causes a corresponding step in power dissipation at a rate of W watts per unit area. Assuming that this power can only go into raising the temperature, T_h, of the heater or into phonon radiation, then conservation of energy implies

$$W = C_h \frac{dT_h}{dt} + \sigma_c (T_h^4 - T_o^4) \tag{4.1}$$

where C_h is the heat capacity of the heater and σ_c the effective Stephan-Boltzmann constant introduced in (2.17). The specific heat of metals at low temperature is known to have the general form $C=aT+bT^3$, with the electronic and phonon contributions typically comparable in magnitude at a few degrees Kelvin [Ashcroft and Mermin]. This functional dependence does not permit a ready integration of (4.1) (though it should be possible, in principal, via a partial fraction expansion), and furthermore, there does not appear to be any tabulated data on the thermal properties of nichrome at the temperatures of interest to us here. We can still obtain a qualitative feeling for the time dependence of T_h, however, reasoning directly from (4.1) and by appealing to the known properties of related materials.

In steady state the heater reaches a temperature

$$T_s = (W/\sigma_c+T_o^4)^{1/4}\,, \tag{4.2}$$

in terms of which (4.1) may be simply rewritten as

$$C_h\frac{dT_h}{dt} = \sigma_c(T_s^4-T_h^4)\,. \tag{4.3}$$

The rate of change of T_h initially, when $T_h=T_o$, relative to the temperature rise in steady state, T_s-T_o, defines a time scale

$$\tau_h\equiv(T_s-T_o)/(dT_h/dt)_{t=0} = C_h(T_o)(T_s-T_o)/\sigma_c(T_s^4-T_o^4)\,.$$

For $T_s>>T_o$, and using the relation (2.19) between σ_c and the equivalent thermal boundary resistance, R_c, this becomes $R_c(T_s)C_h(T_o)/4$. With time however, as T_h nears T_s, (4.2) may be linearized yielding an exponential behavior for the final approach to T_s with time constant $R_c(T_s)C_h(T_s)$. After the voltage pulse to the heater is switched off instead of (4.3) we have

$$C_h\frac{dT_h}{dt} = -\sigma_c(T_h^4-T_o^4) \tag{4.4}$$

and the initial decay from T_s to T_o now defines a time scale (for $T_o << T_s$) given by $R_c(T_s)C_h(T_s)/4$. Finally, as T_h decreases and approaches the ambient temperature we once again recover exponential behavior, but with a time constant $R_c(T_o)C_h(T_o)$.

A survey of the thermophysical tables [Touloukian and Buyco] reveals that Ni, Cr, as well as various Cr+Fe, Ni+Fe and Ni+Cu alloys all have specific heats around 1×10^{-4} J/gK at 1 K (within a factor of 2 or so) and that, roughly, these values all vary linearly with temperature up to 10K. Based on a bulk density of 8.2 g/cm^3 a 500Å nichrome film has an areal density of 4×10^{-5} g/cm^2. Combining this with the evaluation of R_c in (2.45) we find for the longest of the time constants discussed above, $R_c(T_o)C_h(T_o)$, that

$$\tau_h \sim \frac{7\times10^{-8}}{T_o^2} \text{ sec} . \tag{4.5}$$

Thus, for ambient temperatures around a few degrees Kelvin, a bare heater may be expected to switch on and off from its steady–state temperature, T_s, in a few tens of nanoseconds or less. This is of the same order of magnitude as the time governing the response of the helium film to a step change in substrate temperature, $R_k C_N$. The presence of a helium film adsorbed on the heater will naturally lengthen somewhat its response time as some of the input energy is carried away by those few atoms which desorb quickly, and this in turn will lengthen the time it takes the film to reach a steady temperature. But as we have already seen T_f differs imperceptibly from T_s in the end so that, overall, the only effect of a finite rise and fall time associated with the heater is to broaden slightly the width we would associate with the boundary layer in the time evolution of the film's temperature. What is important is that, under the experimental conditions, this width still remains negligible compared with the time scale characterizing the desorption process itself.

The acoustic mismatch model, in which σ_c and R_c are calculated by considering the reflection and transmission of sound waves at an ideal interface, not only assumes that the crystal substrate is phonon transparent and of infinite extent, but also that the metallic film has the properties of a bulk medium. In particular, it is necessary that the spectrum of phonons created within it by the ohmic heating process correspond, at each instant, to an equilibrium distribution at a definite temperature. For typical speeds of sound in a metallic alloy, $c_l=5\times10^5$ cm/sec and $c_t=2.5\times10^5$ cm/sec, the wavelength of a 2 K longitudinal phonon is 1250 Å and that of a transverse phonon 600 Å. Both of these numbers are comparable to or exceed the thickness of our heater films. At higher temperatures like 10 K these wavelengths are a factor of 5 smaller, and are easily confined within the heater volume, but they then also become comparable to the surface roughness scale at the heater–crystal interface. Thus, at the lower heater temperatures we might expect some deviation from an equilibrium phonon distribution due to the finite heater thickness, whereas at higher temperatures we could reasonably argue that σ_c should become wavelength dependent. Despite these observations, we will nevertheless always assume that under steady conditions the heater possesses a well–defined thermodynamic temperature which is calculable according to (4.2).

Helium atoms desorbed from the heater when it is pulsed are detected as a function of their time of flight by a superconducting–transition bolometer positioned directly overhead. The bolometer is a 2000 Å thick Sn film, vacuum evaporated onto a 1″ square sapphire wafer and photolithographically fashioned into a serpentine extending ~ 0.3 mm on a side and encompassing a total area of ~ 0.1 mm^2. The actual active area of the bolometer is about one–third of this. The bolometer is both suspended above the heater and thermally anchored to the bath by several 1.25 mm thick sapphire spacers placed between the wafer and crystal. The arrangement is held in position by a small dab of relatively stiff Apiezon H vacuum grease (vapor pressure: 2×10^{-9} Torr at 300 K) applied to both

faces of the spacers.

Bulk tin has a superconducting transition temperature in zero magnetic field of $T_c \approx$ 3.7 K. The critical field at absolute zero is $H_c \approx$ 300 gauss. The bolometer may be maintained at its superconducting transition at any temperature below 3.7 K by the simultaneous application of a magnetic field perpendicular to the plane of the film and a small bias current, typically on the order of 1 mA, running through it. The magnetic field is produced by a solenoidal coil of superconducting Nb – Ti wire, in the bath outside the cell, with a field strength of ~ 350 gauss/A. The bias current density determined from the actual bias current and nominal cross section of the bolometer serpentine is only a small fraction (0.25%) of the zero–temperature critical current density for tin, $J_c \approx 2\times10^7$ A/cm^2. This current produces a steady power dissipation in the range of microwatts. The precise operating conditions at a given ambient temperature are determined by varying the magnetic field and bias current in concert until the maximum bolometer sensitivity has been achieved, subject to the requirement that the response be stable at all signal levels.

Briefly, the principle behind bolometric particle detection is straightforward. A film held at the transition between its superconducting and normal states has a high temperature coefficient of resistance α = 1/R dR/dT. Any change in the film's temperature is reflected in a change in resistance which is detected through the action of the bias current as a corresponding voltage drop across the device. This change in temperature is brought about by the variations in an externally incident heat flux due to impinging atoms (the signal we wish to detect) as the bolometer tries to balance the sum of the incoming energy and its steady power dissipation against its losses by phonon radiation into the crystal substrate. In reality, the voltage across the bolometer also depends on the superconducting current coefficient of resistance, $\beta = 1/R dR/di$, because of loading effects due to the finite input impedance of the sensing circuit (in our case a 50 Ω terminated coaxial line). In addition, one must realize that α and β

are functions of the applied field and bias current, as well as of the ambient temperature, resulting in a multidimensional bias–parameter space. Both the bolometer sensitivity and response time at the chosen operating point then arise out of a complex interaction between electrical, thermal and superconductive effects [Maul and Strandberg (1969)].

When biasing our bolometers in the manner described above, previous experiments [Taborek, Sinvani, Weimer and Goodstein (1981)] have shown that their response time to incident phonons must be $\sim$ 20 nsec, which is comparable to the time constants quoted by Maul and Strandberg. These bolometers are used here to detect the relatively slowly varying flux due to a Maxwellian distribution of helium atoms with arrival times spread over many microseconds. We can therefore be confident that, for practical purposes, the bolometer signal faithfully follows the instantaneous incident energy flux.

For a variety of reasons, it would be appealing to know the absolute sensitivity of our devices under their operating conditions. For example, a knowledge of the detected flux in absolute units would allow us to calculate, in principle, the total number of atoms intercepting the bolometer and from this, the number which must have left the desorption surface. As we have already explained, however, it is not an easy matter to predict what this sensitivity will be. Furthermore, a measurement of the thermal and superconductive parameters determining this function is a laborious task in itself, and too cumbersome to perform in conjunction with the desorption experiments. What is needed is a direct, simple, and reliable method of determining the response characteristics for fixed bias parameters and ambient temperature. To address this problem, a somewhat novel variation of techniques originally applied to the absolute determination of phonon fluxes [Horstman and Walter (1973)] was developed and successfully tested in this laboratory [Axan (1984)].

The idea, simply, is as follows. The bolometer is fabricated as previously described, but now an additional, thin, electrically insulating layer covers the

device. A 50 Ω nichrome heater is then evaporated onto this layer so that it just shadows the bolometer underneath. Atoms incident on the multilayer device strike the heater and create phonons which then penetrate the insulating layer to register a signal at the bolometer. Alternatively, a voltage pulse of known power dissipation may be applied directly to the heater and the resulting bolometer response observed. With this test pulse one can read off directly the time constant and absolute sensitivity to thermal energy of the device, and with a knowledge of the sticking coefficient, translate this directly into a corresponding calibration of incident atomic flux. Additionally, the test pulse allows optimization of the bolometer bias parameters under adverse signal conditions (very weak signal or repetition frequencies too short to observe on an oscilloscope) as well as cross normalization of data taken hours apart at the same nominal bias conditions (e.g., compensating for long–term thermal drifts) or even data taken under entirely different operating circumstances. More importantly, it permits a ready determination of the input power levels over which the device responds linearly.

The device we fabricated and tested was linear to within 5% over the typically encountered range of desorption signal strengths and showed a sensitivity of ~ 210 V/W with a time constant of ~ 220 nsec. Surprisingly, neither the speed or sensitivity was appreciably affected by changes in operating temperature once an optimum set of bias conditions was reestablished. These results may be compared with a sensitivity of ~20 V/W, and time constant of 25 nsec, quoted by Maul and Strandberg for a tin film alone, at temperatures near the zero–field critical temperature. Relative to these values, our increase in sensitivity was offset by a corresponding increase in response time which, we believe, was due principally to the heat capacity and thermal resistance of the insulating layer.

It was originally felt that the long response time of the multilayer device made its usefulness in the experiments under consideration questionable and so, weighed with troublesome technical burden of producing a reliable insulating layer, we decided to set aside the calibrated bolometers and to continue working

with our traditional tin films. (Later on, in discussing the signal analysis in detail, we shall discover that much of the information we seek is actually independent of this response time.) The steady–state response of the calibrated bolometer should not differ from that of the simple tin film under similar biasing conditions (even though the transient response certainly does) and because of this we expect that the sensitivity figure reported here for the former can serve as a reasonable estimate of the sensitivity of the devices we actually used. Basically, however, we are constrained, by our inability to satisfactorily determine this number, to measurements of quantities characterizing only the relative time evolution of the signal, such as a time constant. We cannot accurately measure absolute desorption rates, for example, because we do not know how to scale the bolometer signal to $\Delta n(t)$, the actual change of surface coverage with time.

For a rectangular heater pulse of fixed voltage we have two time variables with which to probe the dynamics of an adsorbed film. Varying the pulse duration t_p until the detected signal saturates, we can study the time evolution of the desorption as the film progresses isothermally toward steady state. On the other hand, varying the pulse repetition period t_r while monitoring the desorption signal allows us to study the film's replenishment at the ambient temperature. Roughly speaking, we may think of the first technique as addressing the question, Has the pulse been on long enough for the film to reach steady state? while the second attempts to answer, Has there been enough time between pulses for the film to return to equilibrium?

In the past, these experiments have concentrated on studying the signal as a function of t_r only for t_p long enough to ensure that the film returns to equilibrium between each pulse, and as a function of t_p only for t_r sufficiently long for the desorption signal to have saturated. Here we investigate desorption from films which have not been allowed to return to equilibrium as well, and the replenishment of films which have not been driven all the way towards steady

state, extending our study of the signal's dependence on t_p and t_r throughout this parameter plane.

A block diagram of the electronic instrumentation used in carrying out these experiments, along with the actual bolometer bias circuit, is illustrated in Fig. 4.1. A digital-dial waveform generator is used to set the repetition frequency $\nu_r = 1/t_r$ and provide the repetition trigger for a pulse generator. The pulse generator produces rectangular pulses of 10 V amplitude and 5 nsec rise time with a variable width $t_p \geqq 30$ nsec; it also issues a synchronous reference signal prior to the leading edge of the pulse which in turn is used to trigger the data-acquisition electronics. The pulses are attenuated, as necessary, in 1 db steps and coupled to the heater via 50 Ω transmission lines running down into the cryostat. Similar lines transmit the signal from the bolometer back up to the wideband d.c. amplifiers at room temperature.

The outer conductor of these coaxial cables is connected directly to the outside of the cell, which forms a common for both the heater and bolometer circuits, while each inner conductor is passed through, isolated, to the interior using a glass-to-metal vacuum seal. With this arrangement the heater line appears properly terminated and direct electromagnetic coupling between heater and bolometer lines can be kept to a minimum. The rising (and falling) heater pulse edge then creates an inductive spike of ~ 20 nsec duration in the bolometer circuit (compared with a ringing time of ~ 0.5 μsec encountered in previous experiments) which serves as a fiducial timing mark for the onset of desorption.

The necessary bias current for the bolometer is provided by a voltage source in series with a large resistance. The d.c. offset voltage this produces (capable of saturating the amplifiers) is eliminated using a 100 μF tantalum coupling capacitor which, combined with the 50 Ω input impedance of the preamplifier, forms a high-pass filter with a time constant of 5 msec and a 3 db point at 32 Hz. This allows a.c. signals from the bolometer lasting up to several hundred microseconds to be recovered with minimal distortion. Both the bolometer bias

Figure 4.1. Electronics for the desorption time–constant measurements.

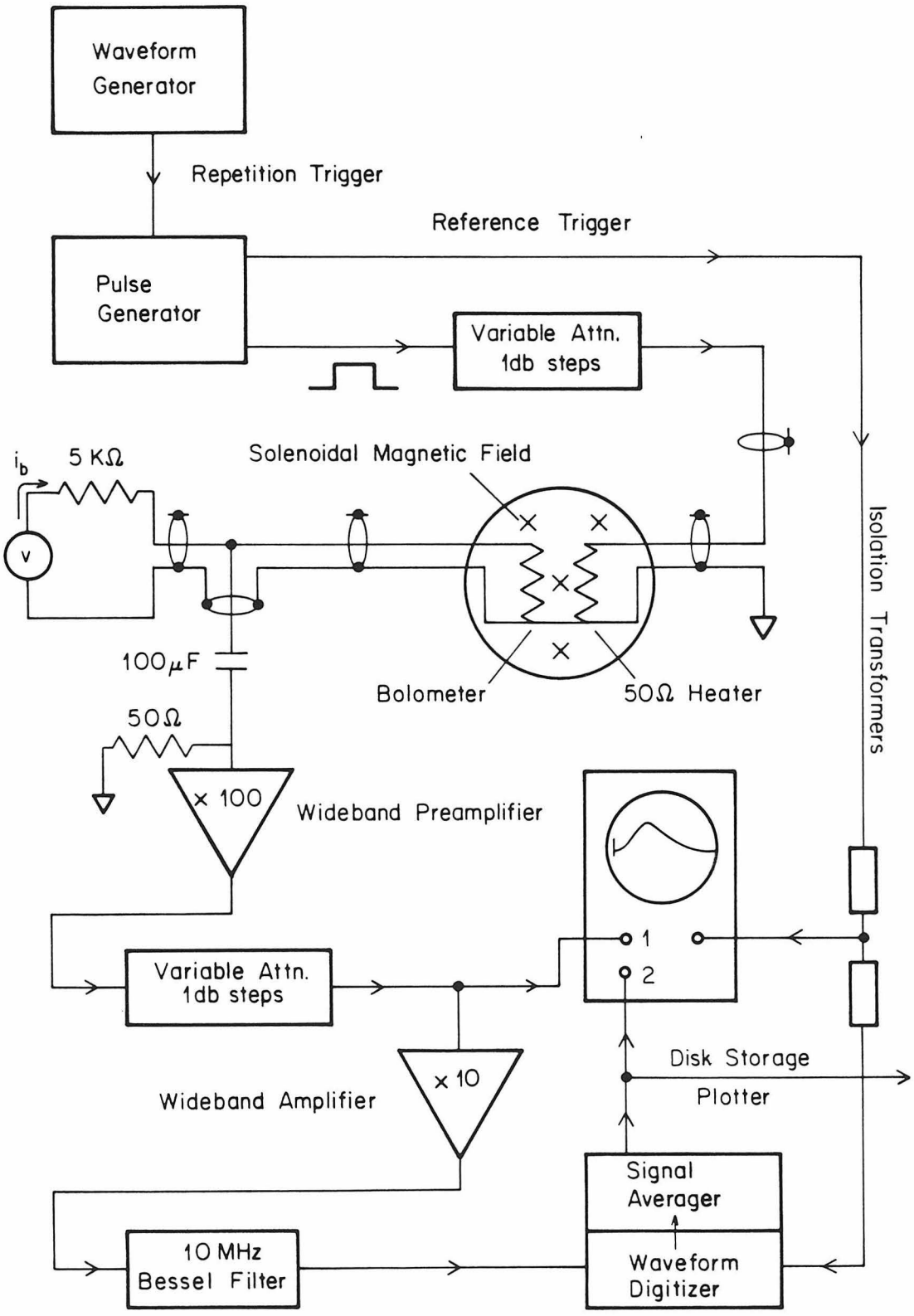

voltage source and the pulse generator are floating and referenced to the ground established at the preamplifier while the cell and its evacuation line are electrically isolated from the remainder of the vacuum system by a Teflon gasket.

The preamplifier has a rise time of 5 nsec (bandwidth dc–70 MHz) and is set for a fixed voltage gain of ×100. Additional gain, when necessary, is provided by a second ×10 wideband amplifier in series with a variable attenuator. The broadband noise observed in this system is dominated by the amplification electronics and is given by ~15 μV rms referred to the preamplifier input. In order to limit this noise, it is desirable to cut down on any unnecessary bandwidth and this is accomplished by means of a low pass filter.

The optimum form of filtering depends of course on those characteristics of the signal which are of importance to us, and among other things, the signal shape (vs. time) contains information we are interested in. In order not to distort this shape, all the significant frequencies in the Fourier decomposition of the signal must lie inside the passband, but the relative phases of these frequency components should also be preserved. Filters which best accomplish this purpose, i.e., those that are maximally flat in phase, are called Bessel filters and can be synthesized from capacitors and inductors [Williams]. They act like a uniform time delay for signals within the passband and relative to RC filters of the same number of poles have a more gentle cut off for those signals outside that band. A 2–pole Bessel filter with a 3 db frequency of 10 MHz and a rise time of 40 nsec (comparable to the rise time of our bolometers) was judged satisfactory for use here.

The instrumentation for signal recovery and signal–to–noise enhancement used in these experiments (a combined waveform digitizer and signal averager) represents a significant advance over that employed previously (a boxcar integrator). All methods of improving the S/N ratio, beyond simple filtering, depend upon the availability of a repetitive signal in order to achieve a further reduction in noise bandwidth (see e.g., [Horowitz and Hill]). As we have already

mentioned above, the maximum repetition frequency ν_r is usually limited by the film's replenishment time, and, as we shall explain in greater detail below, this time is constrained by the conditions of the experiment to lie somewhere between 10 msec and many seconds; consequently, ν_r varies from 100 Hz down to sub–hertz frequencies. If the entire waveform can be sampled at N_s equally spaced intervals with a single repetition, and the results at each point summed with successive triggers, then the number of triggers required to achieve a given improvement I in the S/N ratio goes as I^2. On the other hand, a stepped integrator with a gate width equal to the sampling interval, which is only capable of recovering a single point on the waveform with each trigger, requires at least N_s times as many repetitions of the signal. It is obviously desirable, from the viewpoint of accurately reproducing the signal, that the number of sampled points be as large as possible (typical record lengths have N_s = 1024 or 2048 points) and the waveform digitizer therefore presents an enormous advantage in efficiency. In fact, toward the low end of the repetition–frequency spectrum the task of just recovering a strong signal at all, with minimal or no improvement in S/N, becomes prohibitively time consuming if attempted via boxcar integration.

The digitizer has 8–bit resolution with a quantization level of 2 mV per step. At maximum gain (×1000) this corresponds to 2 μV at the preamplifier input, well below the rms noise value. With sufficient signal averaging this permits an ultimate sensitivity in excess of the nominal 8 bits [Kelly and Horlick (1973); Widrow (1961)] and in practice, resolution equivalent to 10 bits can be achieved. Typical signal strengths originating from the bolometer vary from tens of microvolts (peak) to millivolts (peak) compared with a bipolar full–scale digitizer input of 512 μV at this amplification. Any necessary d.c. offset can be provided by the preamplifier. The digitizer is capable of sampling at rates of up to 100 MHz maximum (sampling interval = 10 nsec), but for the experiments reported here, a rate of 25 MHz (sampling interval = 40 nsec) was employed, resulting in a Nyquist frequency of 12.5 MHz, consistent with our bandwidth–limiting filter. The overall

timing uncertainty of any point on the waveform relative to the onset of the fiducial mark is then about 1 sample interval, or 40 nsec.

The signal averager has a 24–bit deep memory and possesses an extraordinary throughput of 700 × 1 Kbyte samples per second so that we are almost always limited by the repetition frequency and not by the instruction–cycle time for adding two waveforms together. The digitized and averaged signal may be stored on floppy disk and recalled for subsequent viewing and manipulation (baseline subtraction, peak level and position determination, area integration, etc.) as well as plotting.

In order to analyze the bolometer signal and relate it to what is happening at the heater, it is necessary to assume that desorbed atoms travel ballistically from one surface to the other. This means, among other things, that the mean free path in the ambient gas, l_o, must be very long compared with the flight distance, l, so that the fraction of desorbed atoms reaching the detector without colliding with an ambient gas atom,

$$\phi(l) = e^{-l/l_o}, \tag{4.6}$$

[Dushman and Lafferty] is very near unity. The mean free path is evaluated in terms of the pre–existing gas pressure and ambient temperature as

$$l_o\,(\mathrm{mm}) = 2.6 \times 10^{-4} \frac{T_o(K)}{P_g(\mathrm{Torr})}\,. \tag{4.7}$$

P_g can be, and always is, kept low enough in the experiments for the ballistic condition to be fulfilled.

A more vexing problem is posed by the possibility that collisions between the desorbing atoms themselves can seriously perturb the observed flux. Two qualitative lines of argument can be used to help us estimate their number. The first of these, which is easiest to visualize, appeals to the equivalence, arising from detailed balance arguments (Chapter 1), between a desorbing surface with $\alpha = 1$

and an effusive source at the same temperature. The collision frequency in a molecular beam originating from such a source can be calculated [Lubman *et al.* (1982); Troitskii (1962)] and is given by

$$f_c \approx \frac{\rho \sigma \bar{v}}{3} \tag{4.8}$$

where ρ is the local density of the beam, σ the collision cross section, and $\bar{v}$ the mean particle velocity. This result is one–third the corresponding value for a stationary gas of the same density. In practice, (4.8) applies only for distances from the beam source greater than the source diameter, where the motion may be considered unidirectional, whereas in our case the two sizes are comparable. A numerical evaluation of (4.8) must also rely on some estimate of the maximum film vapor pressure obtained from the equation of state (FHH, for example). Furthermore, the molecular beam analogy for calculating the collision frequency only makes sense if the desorbed flux is "quasi–static," i.e., if the desorption times and time of flight are comparable so that, as fast atoms leave the surface and overtake slower ones, they continue to see a steady, well–developed beam ahead of them. This condition is fulfilled when the desorption is slow enough but fails to hold when the desorption times become too short. In that case, (4.8) seriously overestimates the true collision frequency.

A better estimate in this limit is obtained by simplifying an argument of Cowin *et al.* [Cowin, Auerbach, Becker and Wharton (1979); Cole; Cowin (1985)] which views the formation and development of the puff of desorbed atoms as occurring in two steps. Initially, in a time scale given by the desorption time constant τ (which is supposed short compared with the time of flight) a high density particle cloud is produced extending a distance $\bar{v}\tau$ above the surface and containing all the desorbed atoms. Collisions in this cloud are calculated in the same way as for a stationary gas at the same density. After desorption ceases, and velocity spreading ensues, the cloud thins; the collision frequency is then

calculated assuming a density decreasing linearly with time as particles recede from the surface with mean velocity $\bar{v}$. The combined result, from both phases, for the mean number of collisions experienced by a single atom after traveling a time t, is

$$f_c t = \sigma \Delta n (1 + ln(t/\tau)) . \tag{4.9}$$

where Δn is the total number desorbed per unit area. Taking $\sigma \approx 10^{-15}$ cm^2, $t \approx 10$ μsec, and $\tau \approx 0.5-5$ μsec we see that, because the logarithmic term is so slowly varying, the value of $f_c t$ is determined mainly by $\sigma \Delta n$. For monolayer desorption ($\Delta n \approx 10^{15}$/cm^2) this quantity is of order unity. Accordingly, in this formulation, the number of collisions is always significant unless only a small fraction of a monolayer is desorbed.

One of the principal difficulties with the previous experiments [Sinvani *et al.* (1982)] is that this criterion must have been grossly violated because of the rather brutal heating to which the film was subjected. Raising a film from 3.5 K to over 10 K, for example, typically resulted in the desorption of an entire monolayer in less than 50 nsec, and evaluation of (4.9) shows that these atoms must have suffered something like 5 collisions in the course of their trajectory to the bolometer [Cowin (1985)]. How might this affect the results?

The detector cannot measure the total flux of particles leaving the heater surface, but responds only to those arriving in some small solid angle about the surface normal around which it is centered. This segment will only be representative of what is happening to the total flux if the fraction of atoms intercepting the detector, as a function of heater pulse width, remains constant. Cowin has proposed a mechanism [Cowin *et al.* (1979)] whereby the effect of collisions is to produce a forward focusing of the desorption flux so that it is largely concentrated within a narrow cone. If the character or degree of this focusing were to change with pulse duration it could interfere with our measurements and possibly mask the true time evolution of the total desorption flux.

More to the point, however, is the following. We are interested ultimately in deciding whether or not the thermal model gives a satisfactory account of the actual phenomena. The dominant parameter in this theory is P_g, the ambient gas pressure (or its various incarnations, R_f and ε) which is assumed to be undisturbed by the desorption process. It controls the time it takes the film to approach steady state because it is the rate of return of atoms to the film from this gas that determines the steady–state conditions. The requirement of constant P_g is equivalent to assuming that all the desorbed atoms go off in straight trajectories to surfaces at infinity where they then stick (eventually to redesorb on a time scale very much longer than that of the experiment). If the desorbate forms a dense gas with a high collision frequency instead, then some of these atoms are sure to be scattered back towards the heater where they may once again bind. There is then more than one avenue of mass replenishment for the film. Some of those atoms which have already desorbed must be desorbed once again, and the net evaporation rate appears slower than we should otherwise expect; the end result is a longer apparent time constant.

To minimize the effects of these collisions the experiments presented here were conducted at considerably lower pulse power, and to compensate for the attendant loss of flux, a large area heater was employed (the heater used by Sinvani *et al.* was actually 10 times smaller in area than the one described at the beginning of this section – equivalent in size to our bolometers). Restricting our attention to lower substrate temperatures also makes the comparison with theory more straightforward, for if we keep $T_s < 5.2$ K, we need not worry any longer about what happens to our equation of state above the bulk critical temperature of liquid helium.

The ambient pressures which must be maintained in the cell according to (4.7) are too small to measure by conventional means. We must nevertheless know what this pressure is, not just for the sake of evaluating the collision mean free path, but also because we want to be able to correlate our observations on

the desorption time constants with our knowledge about the film's chemical potential, μ_o, which is evaluated in terms of T_o and P_g according to (1.31). Pressures greater than 0.1 mTorr may be measured by a capacitive manometer at the room temperature end of the cell's vacuum line, but these readings must then be corrected for thermomolecular effects [Dushman and Lafferty] to reflect the pressure at $T_o < 4$ K. It was originally hoped that the same Grafoil which serves as an adsorption ballast could be used as an absolute thermodynamic manometer [Taborek and Goodstein (1979)] to directly control and measure the pressure inside the cell. Unfortunately, this proved unsuccessful despite numerous attempts because, we believe, the quantity of gas remaining in the small free volume of our cell was unduly sensitive to very slight departures from equilibrium ($<$ 1 part in 10^5) in the comparatively enormous quantity of gas adsorbed on the Grafoil. At these low pressures, where the mean free paths are orders of magnitude larger than the graphite platelet spacing (0.5 μm), it appears impossible to guarantee (in an operational sense) complete equilibrium between the Grafoil and its vapor, in any finite time.

We believe we are able to ascertain P_g with sufficient accuracy, by an altogether different method, however, involving the pulse repetition period t_r. If this interval is made shorter and shorter for a pulse whose power and duration are sufficient to strip the heater of essentially all adsorbed atoms, we soon reach a point where, as noted above, the film can no longer regain its equilibrium thickness in the time between these pulses. The change shows up as a corresponding decrease in the desorption signal and the repetition interval at which this occurs is called the critical repetition time, t_{rc}; it depends strongly on the ambient pressure in the cell.

To see how this comes about, let us examine the equation analogous to (3.48), governing the rate of increase of surface coverage with time (at ambient temperature T_o) after termination of the heater pulse,

$$\frac{dn}{dt} = \frac{\sigma}{(2\pi mkT_o)^{\frac{1}{2}}} [P_g - P_f(T_o,n)] . \tag{4.10}$$

We first observe that, if the system is far from equilibrium (n very small) at $t=t_p$, just after the substrate has cooled, then $P_f(T_o,n) \rightarrow 0$ (i.e., it is negligible compared with P_g) so that the initial rate of reaccumulation is given by $(dn/dt)_{t=t_p} = \sigma P_g/(2\pi mkT_o)^{\frac{1}{2}}$. If the isotherm is linear, like those of Fig. (3.1), then the subsequent replenishment will be exponential with a time constant

$$\tau_r = \frac{(2\pi mkT_o)^{\frac{1}{2}}}{P_g} \left[\frac{n_o}{\sigma}\right], \tag{4.11}$$

where n_o is the equilibrium coverage, and the reaccumulation rate will decrease steadily from its initial value. Consider now what happens, instead, if the isotherm has positive curvature as depicted in Fig. 3.3, but still passes through the same equilibrium point $P_f(T_o,n_o)=P_g$. Then, relative to the linear isotherm, the reaccumulation rate is always greater for the curved one except at the endpoints $n=0$ and $n=n_o$. (An additional construction on Fig. 3.3 makes this clear. Imagine a horizontal line across the diagram intercepting $P_f(T_o,n_o)$ at $n=0$ and the isotherm in question at $n=n_o$. The vertical distance from this line to a corresponding point on the isotherm below it is proportional to dn/dt at that coverage, according to (4.10), and the linear isotherm lies above the one of positive curvature at all points between $n=0$ and $n=n_o$.) The stronger this curvature is the longer the initial slope, $(dn/dt)_{t=t_p} = (dn/dt)_{n=0}$, persists before turning over towards zero as n approaches n_o. In the case of extreme curvature, the isotherm remains effectively flat (and near zero) over most of the region $0<n<n_o$, rising sharply towards P_g only in the immediate vicinity of n_o, and in this regard resembles the stepwise isotherms of Fig. 3.2 in their plateau to knee transition. Readsorption is constant at the initial rate, in this limit, until the very last moment when it is abruptly cut off. The recovery appears linear in time instead

of exponential, but follows the same asymptotes as those defining the exponential time constant, so that the point at which the break occurs is again (4.11). If we are willing to accept some uncertainty in the experimental determination of τ_r, depending upon just how much curvature characterizes the isotherm, we can use it to effectively determine P_g, identifying $t_{rc}=1/\nu_{rc}\equiv\tau_r$. (This definition blurs the distinction between the time interval during which the pulse is off and the pulse repetition period, but this is of no consequence for the very low duty factors typically encountered in this type of measurement. When the need arises, t_p can always be subtracted from t_r to correct for this omission.)

The idea has been tested at pressures in the mTorr range [Sinvani and Goodstein (1983)], where it is possible to use our capacitive manometer as a standard, and found to give results accurate to 30% if

$$\left[\frac{n_o}{\sigma}\right] \approx 10^{15}\ \text{atoms/cm}^2 = 1\ \text{monolayer}\ . \tag{4.12}$$

The actual pressures we want to determine are many orders of magnitude lower, though, and some considerable extrapolation is therefore involved. But as we have repeatedly emphasized in chapters 2 and 3, the equilibrium coverage is a very insensitive function of the pressure so that, as long as σ does nothing dramatic, we can continue to use (4.12) to a first approximation. Evaluating (4.11) using (4.12) one finds

$$P_g(\text{Torr}) = 6\times10^{-8}\nu_{rc}(\text{Hz})\sqrt{T_o}(\text{K}^{\frac{1}{2}}) \tag{4.13}$$

and consequently, from (1.31), that

$$\frac{\mu_o}{T_o} = ln\left[\frac{6\times10^{-8}\nu_{rc}(\text{Hz})}{156T_o^2(\text{K})}\right]\ . \tag{4.14}$$

A nomograph illustrating the relationship between these quantities is presented in Fig. (4.2) where one can develop some feeling for the relevant orders

Figure 4.2. Equilibrium vapor pressure and chemical potential as functions of the critical repetition frequency.

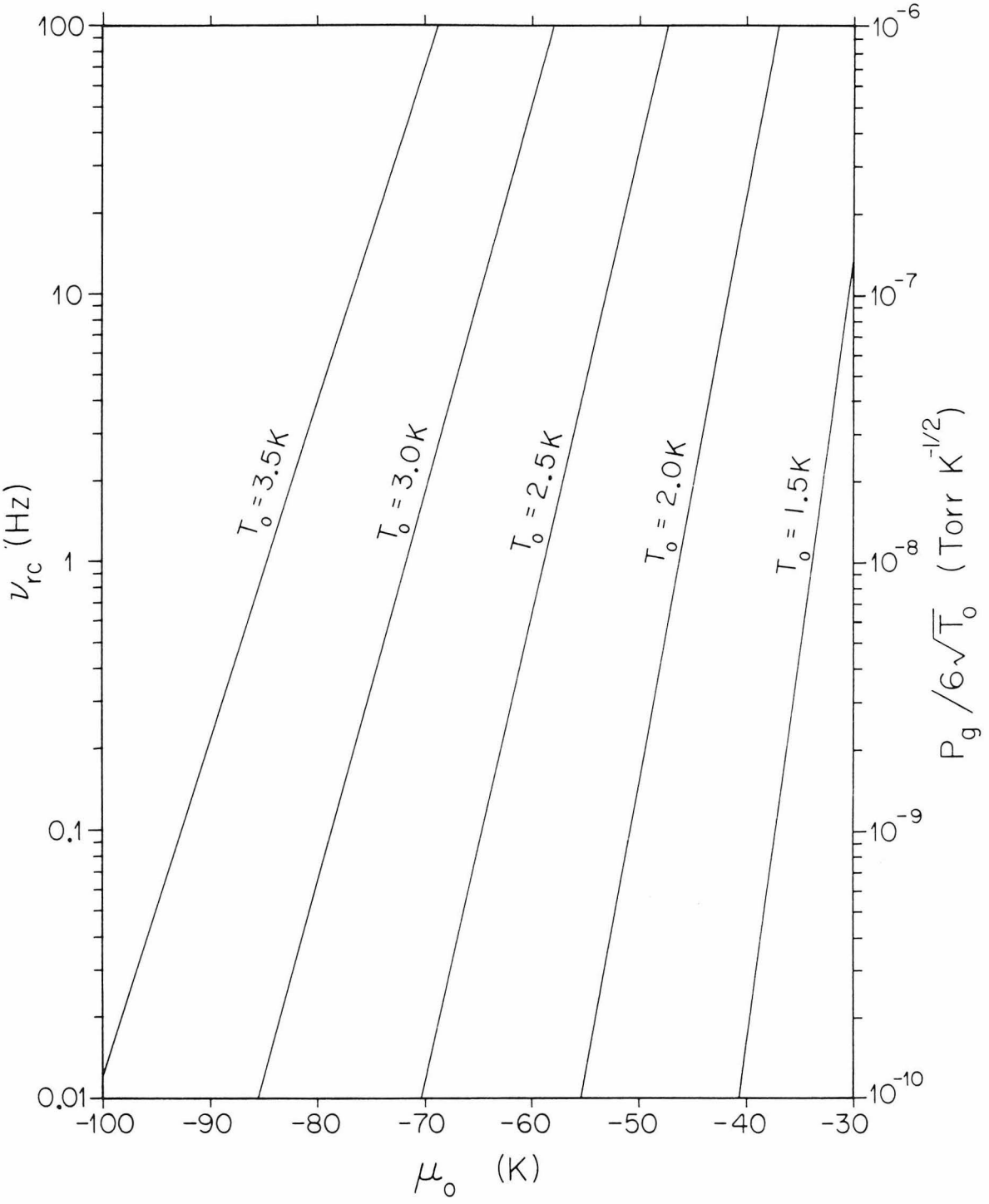

of magnitude. A factor of two uncertainty in ν_{rc} translates directly into a similar uncertainty in P_g, but μ_o is much less sensitive because of the logarithm in (4.14). For example, at T_o =2 K and μ_o = −40 K (a typical ratio), the same uncertainty in ν_{rc} means that $\mu_o/T_o = 20\pm0.7$, a fractional error of only a few percent.

According to (4.13), the maximum repetition frequency which ensures the film's return to equilibrium decreases linearly with pressure limiting the speed with which signals can be recovered when this circumstance is important. Repetition rates are then confined below 100 Hz or so because of the need to satisfy the mean free path requirement, (4.6) and (4.7). At the other end, when the pressure becomes too low, the signals get weaker, recovering them takes proportionately longer, biasing the bolometer itself becomes troublesome and the time it takes the gas in the cell to settle to a steady pressure may be several days; all of these together conspire to severely tax the patience of the experimenter below 0.1 Hz.

A knowledge of the film's chemical potential can serve to place a useful upper limit to the amount adsorbed on the heater even though we do not know the true equation of state for this surface. The reason is as follows. Helium on Grafoil is an adsorption system whose properties, both theoretical and experimental, are well known. The coefficient of the z^{-3} van der Waals adsorption potential is exceptionally large for graphite [Vidali and Cole (1981)] and so we would expect a lower coverage on any other surface at the same chemical potential. A plot of μ_o vs. n_o for He on Grafoil shows a first layer plateau at $-\mu_o$ = 142 K which bends over at about 0.6 layers reaching a new second layer plateau at $-\mu_o$ = 30 K beginning around 1.2 layers. This behavior is only weakly temperature dependent below 4 K. We can therefore be assured that, in the range of accessible chemical potentials in Fig. (4.2), $\delta_o \leqq 1$ monolayer.

3. Signal Analysis

Let us now explain how we interpret the bolometer signal and set down explicitly the formalism we use to recover from it the history of desorption at the heater surface.

Suppose that our desorption source lies in the z = 0 plane with coordinates $\mathbf{r}'=(x',y',0)=(\mathbf{r}'_{\parallel},0)$, that we have a point detector situated at $\mathbf{r}=(x,y,z)=(\mathbf{r}_{\parallel},z)$, and that $f_e(\mathbf{v},t')$ is the distribution function for the number of atoms with velocity $\mathbf{v}$, per unit volume per unit velocity interval, emitted by the surface at time t'. Then the number of atoms per unit time per unit area subsequently intercepting the detector at time t is given by

$$\dot{N}(t) = \int_{-\infty}^{t} dt' \int_{A_s} d^2r' \int_{v_z>0} d^3v f_e(\mathbf{v},t') v_z \delta(t-t'-z/v_z)\delta^2(\mathbf{r}_{\parallel}-\mathbf{r}'_{\parallel}-\mathbf{v}_{\parallel}(t-t')) \quad (4.15)$$

in the absence of any collisions. The δ–functions act as constraints relating the transit time, source–detector separation, and particle velocity when the propagation is ballistic.

The integrations in (4.15) extend over all velocities in the forward direction and encompass the entire source surface area A_s, but apply only for t' prior to t because of casuality. A quick count reveals there are eight independent quantities in the integrand but only six integration variables. This leaves an additional dependence in $\dot{N}(t)$ on the distance between source and detector planes z, which has been suppressed since it is assumed that the bolometer location is fixed (likewise for the boundaries defining A_s). Formally replacing the sum of the distribution function over all velocities by a function of $\mathbf{r}-\mathbf{r}'$, $t-t'$, and t', with units of area$^{-2}\times$time^{-2}, (4.15) may be re–expressed as

$$\dot{N}(t) = \int_{-\infty}^{t} dt' \int_{A_s} d^2r' \dot{N}(\mathbf{r}-\mathbf{r}',t-t';t') \,. \quad (4.16)$$

Appealing to the detailed-balance principle in the form (1.19), the distribution function for desorbed atoms is written as

$$f_e(\mathbf{v},t') = \sigma_s(-\mathbf{v},\beta_s(t'),n(t'))\left[\frac{\beta_s(t')m}{2\pi}\right]^{3/2} e^{-\beta_s(t')mv^2/2}\rho(t')\,, \tag{4.17}$$

where σ_s is the velocity-dependent sticking coefficient for the source surface at its instantaneous temperature and coverage, and $\rho(t')$ is the equivalent density of the bulk gas with which the source would be in equilibrium,

$$\rho(t')=\beta_s(t')P_f(t') = \Lambda_s^{-3}e^{\beta_s(t')\mu_f(t')}\,. \tag{4.18}$$

P_f and μ_f are the vapor pressure and chemical potential of the adsorbed film, respectively, and they are related to the surface coverage n through the equation of state.

If the desorption proceeds isothermally and the sticking coefficient is independent of coverage, or if the desorption is isothermal and the sticking coefficient independent of velocity, then (4.17) splits into a product of distinct velocity- and time-dependent factors. In the former case this means

$$f_e(\mathbf{v},t') = P(\mathbf{v})\rho(t')\,. \tag{4.19}$$

With the velocity distribution so defined, the arrival rate at the detector becomes

$$\dot{N}(t) = \int_{-\infty}^{t} dt' \int_{v'_z>0} d^3v' f_e(\mathbf{v}',t')v'_z \tag{4.20}$$

$$\times \int_{A_s} d^2r' \left[\frac{\displaystyle\int_{v_z>0} d^3v P(\mathbf{v})v_z\delta(t-t'-z/v_z)\delta^2(\mathbf{r}_\parallel-\mathbf{r}'_\parallel-\mathbf{v}_\parallel(t-t'))}{\displaystyle\int_{v'_z>0} d^3v' P(\mathbf{v}')v'_z}\right]$$

showing that $\dot{N}(t)$ can be expressed as a convolution integral

$$\dot{N}(t) = \int_{-\infty}^{t} dt'\dot{n}_{des}(t')\int_{A_s} d^2r' N_o(\mathbf{r}-\mathbf{r}',t-t') \tag{4.21}$$

instead of the more general form (4.16). We recognize this convolution as just the sum of the instantaneous desorption rate per unit area weighted by a Green's function, or propagator, with units of area^{-1} × time^{-1} and defined by

$$N_o(\mathbf{r}-\mathbf{r}',t-t';\beta_s) = \frac{<\sigma_s(-\mathbf{v})\delta(t-t'-z/v_z)\delta^2(\mathbf{r}_\parallel-\mathbf{r}'_\parallel-\mathbf{v}_\parallel(t-t'))>_{\beta_s}}{<\sigma_s(-\mathbf{v})>_{\beta_s}} . \qquad (4.22)$$

The brackets in (4.22) have the same meaning they did in Chapter 1 (averages of the enclosed quantity over an equilibrium flux distribution with temperature β_s) and β_s enters as an additional parameter determining N_o. Physically, the propagator represents the fraction of particles emitted from $\mathbf{r}'$ at time t' that end up at time t in a unit area located at $\mathbf{r}$.

The constraints appearing in (4.22) can be transformed into velocity variables using the elementary identities

$$\delta(t-t'-z/v_z) = (v_z^2/z)\delta(v_z-z/(t-t'))$$

$$\delta^2(\mathbf{r}_\parallel-\mathbf{r}'_\parallel-\mathbf{v}_\parallel(t-t')) = (t-t')^{-2}\delta^2(\mathbf{v}_\parallel-(\mathbf{r}_\parallel-\mathbf{r}'_\parallel)/(t-t'))$$

so that evaluation is straightforward. The result for a velocity-independent sticking coefficient is

$$N_o(\mathbf{r}-\mathbf{r}',t-t';\beta) = \frac{z^2}{(t-t')^5}\frac{(\beta m)^2}{2\pi} e^{-\beta m|\mathbf{r}-\mathbf{r}'|^2/2(t-t')^2}\Theta(t-t') , \qquad (4.23)$$

which includes an explicit factor (the Θ-function in $t-t'$) to enforce causality allowing the upper limit in the dt' integral of (4.21) to be replaced by $+\infty$.

The function (4.23) determines the line shape registered by a particle detector in response to a flash desorption event from a point source. For short time intervals ($t-t'\to 0$) the fraction of particles with sufficient velocity to reach the detector is exponentially small, suppressing any signal. When $t - t'$ increases, however, N_o grows sharply and peaks, reflecting the Maxwellian distribution of velocities in the incident beam. Past this peak, the signal decays at long times

with a polynomial dependence, $(t-t')^{-5}$, as slow particles straggle in. The line shape is, of course, sensitive to the precise geometry of the source, and integrating (4.23) over an infinite plane gives instead

$$\int_{-\infty}^{\infty} d^2r' N_o(\mathbf{r}-\mathbf{r}',t-t';\beta) = \frac{z^2}{(t-t')^3}(\beta m)e^{-\beta m z^2/2(t-t')^2}\Theta(t-t') . \qquad (4.24)$$

The scale factor in the argument of the exponential has changed from $\beta m|\mathbf{r}-\mathbf{r}'|^2$ to $\beta m z^2$, which differ unless the detector happens to be positioned directly above the point in question, and the algebraic fall-off at long times has shifted to a gentler $(t-t')^{-3}$ behavior.

Bolometers are not particle detectors per se, but respond, as we have already mentioned, to the energy flux associated with an incident particle stream. Let us now turn our attention to calculating the signal due to this flux.

We work in what we call the weak-signal approximation where neither the sticking coefficient of the detector σ_d or the binding energy E_b of an extra atom in the film on its surface are disturbed from their equilibrium value. We also suppose the detector's time constant is short enough for it to follow the instantaneous flux, and that its area is small enough for the intercepting beam to be considered spatially uniform. Under these conditions the energy per unit area per unit time deposited at time t is

$$S(t) = \int_{-\infty}^{t} dt' \int_{A_s} d^2r' \int_{v_z>0} d^3v f_e(\mathbf{v},t') v_z \sigma_d(\mathbf{v})(\tfrac{1}{2}mv^2+E_b) \qquad (4.25)$$

$$\times \delta(t-t'-z/v_z)\delta^2(\mathbf{r}_\parallel-\mathbf{r}'_\parallel-\mathbf{v}_\parallel(t-t')) .$$

This formulation includes both sticking and elastic reflection at the bolometer but ignores inelastic scattering (which may be negligible for $kT_o<\frac{1}{2}mv^2<<E_b$). The actual voltage generated is obtained by multiplying $S(t)$ by A_d, the area of the detector in cm^2, and by K, the unknown sensitivity of the bolometer in

V/watt.

Following the same line of reasoning as before with respect to $f_e(\mathbf{v},t')$, (4.25) may also be expressed as a convolution integral,

$$S(t) = \int_{-\infty}^{t} dt' \dot{n}_{des}(t') \int_{A_s} d^2r' S_o(\mathbf{r}-\mathbf{r}',t-t') \tag{4.26}$$

with

$$S_o(\mathbf{r}-\mathbf{r}',t-t';\beta) = <\sigma_s(-\mathbf{v})>_{\beta_s}^{-1} \tag{4.27}$$

$$\times <\sigma_s(-\mathbf{v})\sigma_d(\mathbf{v})(\tfrac{1}{2}m\mathbf{v}^2+E_b)\delta(t-t'-z/v_z)\delta^2(\mathbf{r}_{\|}-\mathbf{r}'_{\|}-\mathbf{v}_{\|}(t-t'))>_{\beta_s} .$$

It comes as no surprise then, that when explicitly evaluated for σ_s and σ_d independent of velocity, (4.27) yields

$$S_o(\mathbf{r}-\mathbf{r}',t-t';\beta) = \sigma_d \left[\tfrac{1}{2}m \frac{|\mathbf{r}-\mathbf{r}'|^2}{(t-t')^2} + E_b \right] N_o(\mathbf{r}-\mathbf{r}',t-t';\beta) \tag{4.28}$$

where N_o is again given by (4.23).

Unfortunately, our story is more complicated than we have pictured for two reasons. First, $f_e(\mathbf{v},t')$ is not just a simple term like (4.19) for all time, even in the isothermal approximation, but is a sum of such terms. Specifically,

$$f_e(\mathbf{v},t') = P(\mathbf{v};\beta_o)\rho_o\Theta(-t') + P(\mathbf{v};\beta_s)\rho(t')[\Theta(t')-\Theta(t'-t_p)] \tag{4.29}$$

$$+ P(\mathbf{v};\beta_o)\rho(t_p,t')\Theta(t'-t_p) .$$

Prior to the onset of the heater pulse at $t'=0$, the distribution function for desorbing atoms is the equilibrium one, with temperature β_o, sticking coefficient $\sigma_s(\beta_o)$ and gas density $\rho_o=\beta_o P_g$. During the interval $0 \leq t' \leq t_p$ for which the heater pulse is on, β_s characterizes the velocity distribution and $\rho(t')$ reflects the diminishing surface coverage at this temperature. Once the pulse has terminated at $t'=t_p$, the velocity distribution regains its former character and

$\rho(t_p,t')$ then reflects the growth in surface coverage at ambient temperature until the film returns to its equilibrium thickness.

The second point concerns the bolometer itself – in equilibrium we see no signal from it, and our analysis must conform with this fact. In equilibrium, atoms originating from the gas and all surrounding surfaces strike the bolometer while an exactly compensating flux leaves the film adsorbed on it (detailed balance) so no net energy gain accrues in the ongoing process of exchange between film and vapor. The device responds only when it senses an excess flux originating from the solid angle subtended by the source. In the spirit of the weak–signal approximation, we assume the bolometer continues to evaporate its own film as it would if undisturbed; the flux which would have been contributed by the source had it remained in equilibrium must therefore be subtracted from both (4.21) and (4.26). When that is done, we obtain for the excess number striking the bolometer

$$\dot{N}(t) = \int_0^{t_p} dt' \int_{A_s} d^2r' [\dot{n}_{des}(t')N_o(\mathbf{r}-\mathbf{r}',t-t';\beta_s) - \dot{n}_{eq}N_o(\mathbf{r}-\mathbf{r}',t-t';\beta_o)] \qquad (4.30)$$

$$+ \int_{t_p}^{\infty} dt' \int_{A_s} d^2r' [\dot{n}_{des}(t_p,t')-\dot{n}_{eq}]N_o(\mathbf{r}-\mathbf{r}',t-t';\beta_o)$$

and for the excess energy,

$$S(t) = \int_0^{t_p} dt' \int_{A_s} d^2r' [\dot{n}_{des}(t')S_o(\mathbf{r}-\mathbf{r}',t-t';\beta_s)-\dot{n}_{eq}S_o(\mathbf{r}-\mathbf{r}',t-t';\beta_o)] \qquad (4.31)$$

$$+ \int_{t_p}^{\infty} dt' \int_{A_s} d^2r' [\dot{n}_{des}(t_p,t')-\dot{n}_{eq}]S_o(\mathbf{r}-\mathbf{r}',t-t';\beta_o)\,.$$

The first thing to notice about (4.30) and (4.31) is that, indeed, no contributions arise from $t'<0$ when the entire system is in equilibrium. Next, the signal has two components – "pulse–on" and "pulse–off" – corresponding to the two

time intervals $0<t'<t_p$ and $t_p<t'<\infty$ (Θ–function in the definition of the propagators cuts off these integrals when t' exceeds t). Each of these components in turn depends on the difference between the instantaneous desorption rate and the equilibrium desorption rate, which is not itself a function of t'. During the pulse–on segment $\dot{n}_{des}(t') \geqq \dot{n}_{eq}$ and the bolometer sees more atoms arriving from the source than usual, with a greater mean velocity, which results in a positive–going signal. For the pulse–off interval, however, $\dot{n}_{des}(t_p,t') \leqq \dot{n}_{eq}$ and the bolometer senses fewer atoms than expected originating from the direction of the source, resulting in a negative–going signal.

The competition between $\dot{n}_{des}$ and $\dot{n}_{eq}$ in the pulse–off integrand looks precisely like the difference between desorption and adsorption driving the *net* rate of change of surface coverage, $\dot{n}(t')$, when σ_s is independent of coverage. The same would be true of the pulse–on integral if we could find some way to circumvent the difference between propagators parameterized by β_s and β_o and if, in addition, σ_s was independent of temperature. The relevant trick is to integrate (4.30) and (4.31) with respect to t. The reason this is helpful is that the propagators are functions only of the difference, $t-t'$. Their time integrals are independent of t' since this argument displaces the origin of those functions but does not alter their shape; as a result, all t' dependence remains with the number emerging from the surface.

To see how it works in detail, we start with (4.23) and find, for $t' \geqq 0$,

$$\int_0^\infty dt N_o(\mathbf{r}-\mathbf{r}',t-t',\beta) = \frac{1}{\pi}\,\frac{z^2}{|\mathbf{r}-\mathbf{r}'|^4}\,. \tag{4.32}$$

This is the fraction of desorbed particles per unit area contributing to the number per unit area which eventually strike the detector. It is a function only of geometry and is independent of β since it does not matter when these particles arrive. A useful check is provided by further integrating (4.32) over an unbounded plane source. The result in this case is 1, as it should be, for if the

source is infinite in extent, the number of atoms per unit area which have left its surface cannot differ, for reasons of symmetry, from the total number per unit area which cross the detector plane.

The total energy per unit area intercepting the detector relies on the corresponding integral of (4.28)

$$\int_0^\infty dt S_o(\mathbf{r}-\mathbf{r}',t-t';\beta) = \sigma_d(2kT+E_b)\int_0^\infty dt N_o(\mathbf{r}-\mathbf{r}',t-t') \,, \tag{4.33}$$

which is the average energy per particle (kinetic plus potential) multiplied by the number that stick. Unlike (4.32), (4.33) depends on the temperature of the source as well as geometry.

Using the fact that (4.32) is independent of temperature to evaluate the time integral of (4.30), we find for the net number excess at the bolometer

$$\int_0^\infty dt\dot{N}(t) = \int_0^{t_p} dt'[\dot{n}_{des}(t')-\dot{n}_{eq}]\,(\int_{A_s} d^2r'\int_0^\infty dt N_o(\mathbf{r}-\mathbf{r}',t-t')) \tag{4.34}$$

$$+\int_{t_p}^\infty dt'[\dot{n}_{des}(t_p,t')-\dot{n}_{eq}](\int_{A_s} d^2r'\int_0^\infty dt N_o(\mathbf{r}-\mathbf{r}',t-t'))\,.$$

Similarly, using (4.33) to evaluate the time integral of (4.31) we find for the net energy excess

(4.35)

$$\int_0^\infty dt S(t) = \sigma_d\int_0^{t_p} dt'[\dot{n}_{des}(t')(2kT_s+E_b)-\dot{n}_{eq}(2kT_o+E_b)](\int_{A_s} d^2r'\int_0^\infty dt N_o(\mathbf{r}-\mathbf{r}',t-t'))$$

$$+\sigma_d\int_{t_p}^\infty dt'[\dot{n}_{des}(t_p,t')-\dot{n}_{eq}](2kT_o+E_b)(\int_{A_s} d^2r'\int_0^\infty dt N_o(\mathbf{r}-\mathbf{r}',t-t'))\,.$$

Both (4.34) and (4.35) have been left as the sum of a pulse–on and pulse–off contribution for reasons which will become clear shortly. For the moment we

observe that, inasmuch as the $\dot{n}_{eq}$ term represents readsorption of the ambient gas by the heater, (4.34) is proportional to $\int_0^\infty dt'\dot{n}(t')$. This integral vanishes because the coverage before the film is disturbed, $n(0)$, is the same as it is at very long times, $n(\infty)$, when the film has had an opportunity to again return to equilibrium; (4.34) is therefore identically zero. What we are really after, however, is

$$\Delta n(t_p) = \int_0^{t_p} dt'[\dot{n}_{des}(t')-\dot{n}_{eq}]\,, \tag{4.36}$$

the change in surface coverage during the pulse–on interval only. How are we to recover this from (4.34) and (4.35)?

The answer lies in distinguishing the influence each of three different time scales has on the observed signal. These time scales are the pulse width itself, the time it takes the film to recover from a pulse of this power and duration, and the time interval accompanying a finite speed of propagation from source to detector. For example, suppose we ask what happens to the propagator at very high temperatures where the particle velocities can become as large as we wish. Then

$$\lim_{\beta\to 0} N_o(\mathbf{r}-\mathbf{r}',t-t';\beta) = \frac{\delta(t-t')}{\pi}\,\frac{z^2}{|\mathbf{r}-\mathbf{r}'|^4} \tag{4.37}$$

and there is no delay between desorption and detection; we have a direct recording in real time of what transpires at the heater surface. The signal is positive on account of the pulse–on component until $t=t_p$ when it abruptly turns negative with the onset of the pulse–off part. We need only integrate with respect to t until $t=t_p$ in (4.34), instead of $t=\infty$, to obtain $\Delta n(t_p)$.

Because (4.34) vanishes, the pulse–on and pulse–off contributions must be equal in magnitude but opposite in sign regardless of how large or small a delay the propagator introduces. They are, however, distributed entirely differently with respect to t under appropriate circumstances as we have just shown.

Consider what happens when the film is driven far from equilibrium by a pulse whose width is comparable to the desorption time constant at temperature T_s. This t_p may vary from tens of nanoseconds to tens or even hundreds of microseconds but the subsequent replenishment at T_o (as gauged by t_r) is spread over tens of milliseconds or longer; the maximum net desorption rate therefore exceeds the maximum net readsorption rate by roughly the ratio of these times. We can argue next, based on the actual source–detector separation z in our apparatus and the range of accessible temperatures T_s and T_o, that the characteristic width of the area–integrated propagator (for example, (4.24)) runs from a few microseconds to several tens of microseconds at most. Relative to the enormous readsorption time this appears "instantaneous" so that, from this point of view, the situation is similar to the one expressed by (4.37). To be more precise, we imagine there is some integration time t_I meeting the following requirements: first, that $t_I - t_p$ is large enough compared with the propagator width for us to include all the effects of the pulse–on contribution; second, that $t_I - t_p$ is still small enough with respect to the replenishment time for the pulse–off contribution to be negligible. Then to a good approximation

$$\int_0^{t_I} d\dot{N}(t) = \int_o^{t_p} dt'[\dot{n}_{des}(t') - \dot{n}_{eq}] \left(\int_{A_s} d^2r' \int_0^{\infty} dt N_o(\mathbf{r}-\mathbf{r}', t-t')\right) \tag{4.38}$$

and

$$\int_0^{t_I} dtS(t) = \sigma_d \int_0^{t_p} dt'[\dot{n}_{des}(t')(2kT_s + E_b) - \dot{n}_{eq}(2kT_o + E_b)]\left(\int_{A_s} d^2r' \int_0^{\infty} dt N_o(\mathbf{r}-\mathbf{r}', t-t')\right). \tag{4.39}$$

Although it would seem we should have no difficulty in always finding an integration time with the necessary properties, we must be cautious about what may occur for either very short pulse widths or near–equilibrium desorption temperatures. For the latter, the replenishment and desorption times become comparable and ultimately, in the fully linearized limit, both processes are

exponential with the same time constant τ_1. This time constant can easily be less than the replenishment time for monolayer desorption (t_{rc}) if the vapor pressure isotherms have positive curvature, but just how much so depends on the details of the equation of state. Alternatively, no matter what the source temperature, if the pulse is sufficiently short then desorption proceeds with a time constant $\tau_{1cl}(T_s, n_o) \leqq \tau_1$ while readsorption still occurs with $\tau_{1cl}(T_o, n_o) = \tau_1$. For (4.32) and (4.39) to remain useful in either case, the propagator width, which decreases with increasing substrate temperature, must be negligible compared with τ_1 so that it is possible to satisfy the condition $t_I - t_p \ll \tau_1$. As a concrete example, suppose the FHH isotherm, for which we found $\tau_1 \sim 1/P_g$, correctly represents the equation of state. Then the restriction on the propagator width implies an additional constraint relating the experimental dimensions, z and A_s, and ambient conditions, P_g and β_o, under which this approximation remains a viable strategy for recovering $\Delta n(t_p)$ at any pulse power and for any pulse duration. Given a more general equation of state, if the equilibrium coverage happens to place us in a region of strongly positive local curvature, such as the knee region of a stepwise isotherm, then τ_1 becomes very short and we may have to rely on other ways of getting at $\Delta n(t_p)$.

So far, we have avoided commenting on the complications introduced by the two temperatures T_s and T_o appearing in the integral of $S(t)$, (4.39). Rearranging things slightly we can write

$$\int_0^{t_I} dt S(t) = \sigma_d[(2kT_s+E_b)\Delta n(t_p)+2k(T_s-T_o)\dot{n}_{eq}t_p]\left[\frac{1}{\pi}\int_{A_s} d^2r' \frac{z^2}{|\mathbf{r}-\mathbf{r}'|^4}\right]. \qquad (4.40)$$

If the detected energy is to be strictly proportional to $\Delta n(t_p)$ it is necessary that

$$\left[\frac{\dot{n}_{eq}t_p}{\Delta n(t_p)}\right]\frac{2k(T_s-T_o)}{(2kT_s+E_b)} << 1 . \qquad (4.41)$$

We would ordinarily expect the first factor to be of order unity or smaller provided the pulse width is not very much longer than the time required by the film to approach steady state. Thus, to be sure to satisfy (4.41), the temperature difference $T_s - T_o$ must be small compared with the binding energy E_b, a condition which can be met only by experiments at both low power and low pressure inasmuch as $E_b \sim O(|\mu_o|)$.

Before leaving this subject, it is well to point out an additional virtue of working with the integrated signal: its value is unaffected by the detector time constant (via conservation of energy), a fact we did not fully appreciate when discarding our calibrated bolometers. So long as the detector time constant remains less than or comparable to the propagation delay time, all of the arguments we have advanced above go through without further modification. The additional information one extracts with a fast enough detector response, but loses if it is too slow, is the line shape of the desorption Green's function $\int_{A_s} d^2r' S_o(\mathbf{r}-\mathbf{r}', t-t'; \beta_s)$. This is directly measured by applying the fundamental theorem of calculus to (4.31) in those instances where $\dot{n}_{des}(t') >> \dot{n}_{eq}$ (for example, for pulse widths short compared with the steady-state time) and where pulse-off effects are negligible, thus deconvolving the Green's function from the desorption history [M. Cole]. One finds

$$\frac{\partial S(t;t_p)}{\partial t_p} = \dot{n}_{des}(t_p) \int_{A_s} d^2r' S_o(\mathbf{r}-\mathbf{r}', t-t_p; \beta_s) \,. \tag{4.42}$$

By taking the difference between two $S(t)$ curves, at $t_p + \Delta t_p$ and t_p, one reconstructs both the instantaneous desorption rate and the sought-after propagator containing the velocity distribution of desorbing atoms.

4. Results and Discussion

The data presented and discussed here summarize the nearly 1,000 waveforms collected during a single experimental run. The aim of the study was to map out, as far as possible, the systematic behavior of the desorption signal as a function of t_p and t_r at low heater powers for a fixed set of ambient conditions, with the hope of understanding and interpreting the details of this behavior within the context of the thermal model.

Of the 1.69 STPcc of helium gas admitted to the cell in total, approximately one–third was added at 77 K while the remainder was bled in at 4.2 K. The cryostat was then slowly cooled to T_o = 2.095 K a full week before any data was collected, ensuring that enough time elapsed for the gas in the cell to distribute itself sufficiently throughout the Grafoil to come to a steady pressure. This pressure was determined by the critical repetition time at maximum heater power as described in Section 2 above. Because of the large area of our source, however, the signal at this power saturated the detector's response and it was necessary to select a special bias point for this measurement alone. The repetition frequency at which the desorption signal first decreased was monitored periodically on an oscilloscope for a saturating pulse width of 150 nsec. It eventually settled at ν_{rc} = 70 Hz and never departed noticeably from there after that. The ambient pressure and chemical potential deduced from (4.13) and (4.14) under these conditions were $P_g = 5.8\times10^{-6}$ Torr and $\mu_o = -40$ K, while the mean free path obtained from (4.7) was l_o = 94 mm. Using this value and taking an upper limit to the flight distance of l = 1.5 mm (which exceeds the nominal source–detector separation of 1.25 mm because of finite heater size), $\phi(l)$, the fraction of desorbed atoms which reached the bolometer without encountering any ambient gas atoms along the way, must have been better than 98.5%.

The pulse power densities used in these experiments span several decades and the substrate temperatures calculated from (4.2) relevant to the data which follow are tabulated in Table 4.1. The ratio T_o/T_s is also presented there along

Table 4.1

Heater temperature T_s calculated as a function of pulse power W, from eq. (4.2).

W_{max} = 2 W/1.10 mm^2

$1/\sigma_c$ = 6800 K^4 mm^2/W

T_o = 2.095 K

W/W_{max} (db)	T_s (K)	T_o/T_s	$\delta(T_o/T_s)$
0	10.549	0.199	.005
−17	4.038	0.519	.012
−20	3.457	0.606	.013
−22	3.140	0.667	.013
−24	2.877	0.728	.013
−25	2.764	0.758	.013
−26	2.663	0.787	.012
−27	2.575	0.814	.011

with the variation in this ratio, $\delta(T_o/T_s)$, due to a 10% change in W/σ_c, illustrating the insensitivity of the result (because of the fourth–root dependence in (4.2)) to uncertainties in our knowledge of the exact material parameters. The effects of 2 mK fluctuations in T_o are negligible by comparison.

Figure 4.3 displays the signal as a function of time for a series of increasing pulse widths at a fixed substrate temperature of 4.04 K. The timing zero coincides with the onset of the heater pulse and the average value of the prepulse baseline has been subtracted from each waveform. These data were collected at the critical repetition frequency but, as will be explicitly shown later, because of the significantly lower input power (–17 db or down by a factor of 50) the film was guaranteed to return to equilibrium between each trigger. Relative to a similar type of experiment at higher substrate temperatures illustrated in Fig. 2.1 (where T_s = 8.2 K, T_o = 3.48 K and $-\mu_o$ = 72 K) these waveforms, which are averages of 1,000 triggers each (and as many as 10,000 in the data which follow) exhibit a marked improvement in signal to noise. Furthermore, the signals in the inset were taken as much as seven hours apart yet they all share the same steep rise with peak heights coincident within 2%, attesting to the long term stability of both the bolometer and the apparatus as a whole.

The qualitative trends in Fig. 4.3 are rather clear. The signal increases with increasing pulse width as atoms continue to leave the hot desorption surface. The inset shows how the signal maximum saturates at this power despite pulse widths longer than the time of flight itself. Very little area is contained in the long–time tails compared with that under the main peak. This observation fostered the notion in the work of Sinvani *et al.* at higher powers that saturation of the signal peak was synonymous with the film's reaching steady state and a quantitative analysis of $\Delta n(t_p)$ vs. t_p was based on characterizing each spectrum by the height of the signal at its maximum, $S_{\max}$. As we have seen in Section 3, a proper analysis requires deconvolving the integral (4.31) and this is achieved by computing areas according to (4.41). The procedure of relying on $S_{\max}(t_p)$ cannot

Figure 4.3. $S(t)$ vs. t, as a function of t_p, for T_s = 4.04 K and ν_r = 70 Hz. Main figure: in ascending order, t_p = 0.10, 0.15, 0.25, 0.35, 0.50, 0.90, and 3.0 μsec. Inset: t_p = 3.0, 20, 35, and 50 μsec. Full–scale signal is 2.52 mV.

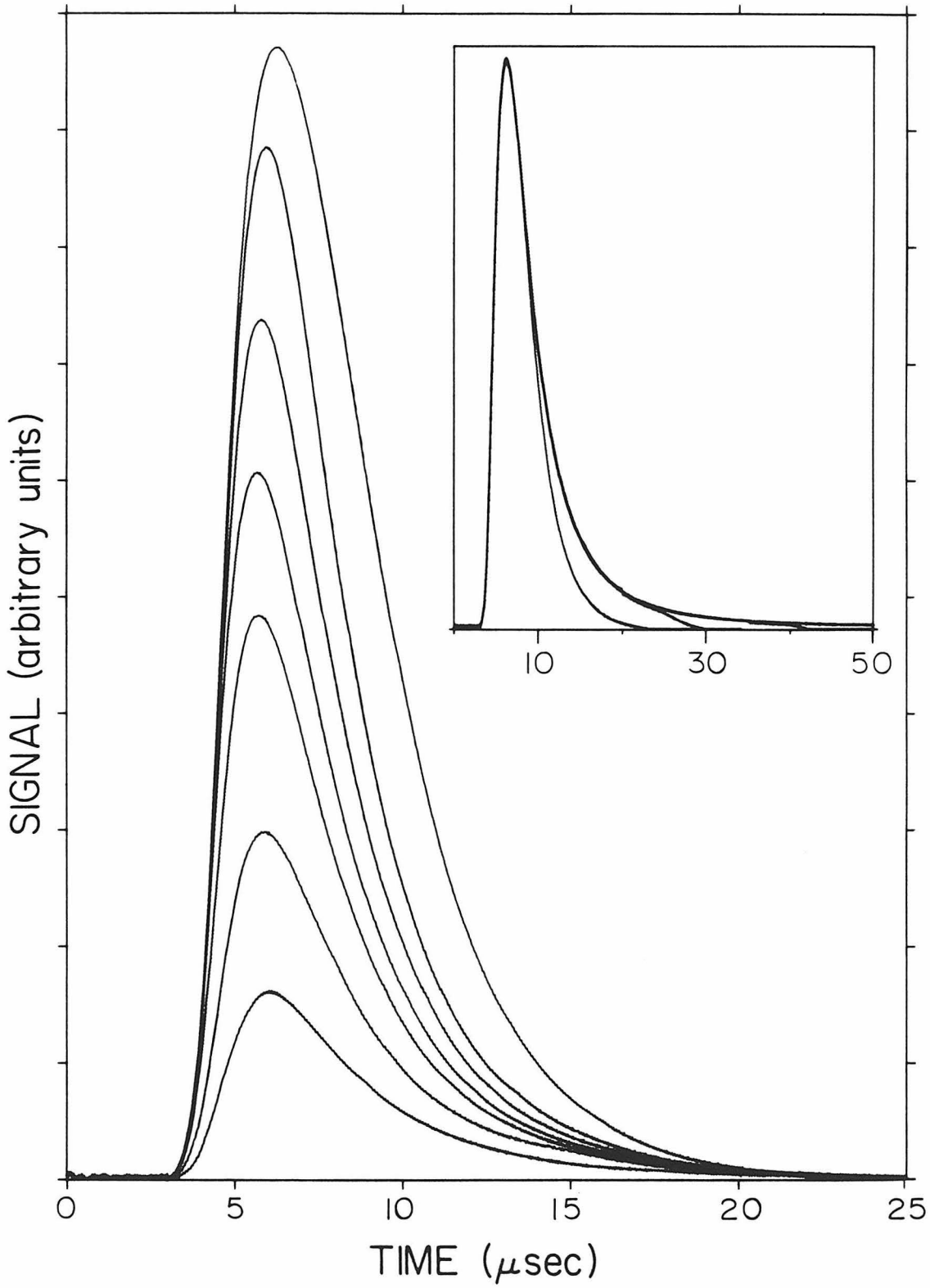

therefore be correct in principle but represents an approximation, albeit a crude one, for well–localized peaks. It depends, in other words, on the desorption time constant being short compared with the time of flight, an assumption which is totally erroneous at still lower powers as demonstrated in the next set of data.

Assembled in Fig. 4.4 is a similar series of signals for T_s = 2.88 K (or –24 db). The spectra in the main figure, in common with those of 4.3, share the same qualitative shape and any differences between the two sets are quantitative issues. For example, the steep initial rise and common shoulder originating from the first particles to reach the detector occurs at slightly later times because of the effect the lower substrate temperature has on their velocity distribution. Moreover, the waveforms here crest distinctly later and are somewhat broader than their counterparts in Fig. 4.3, reflecting changes in the velocity distribution as well as differences in the time evolution of desorption. In fact, full scale in this figure is about one–seventh of what it is in 4.3 on account of the slower desorption rate, and the pulse widths necessary to generate this series are significantly longer than what they are at –17 db, though still all less than the time of flight.

The inset tells a different story. For pulse widths greater than the time of flight the peak height saturates as before but the tails do not. They continue to grow and constitute a substantial portion of the total area under each waveform. This behavior is easily interpreted in terms of the convolution of a time varying desorption rate with a fixed Green's function. If the scale of this variation is long (but not too long) compared with the width of the propagator then by the time t_p becomes comparable to this width all the fast, easily desorbed particles have already contributed to the signal. The broad fall–off in the tails is the result of a much slower (perhaps nearly constant) evaporation rate from a film that has not quite yet reached steady state. If the desorption time scale were to increase further, then the ratio of peak amplitude to tail amplitude would turn in favor of the latter until, in the limit of a truly constant desorption rate, the signal would

Figure 4.4. $S(t)$ vs. t, as a function of t_p, for T_s = 2.88 K and ν_r = 70 Hz. Main figure: t_p = 0.35, 0.70, 1.2, 2.0, 3.0, and 5.0 μsec. Inset: t_p = 5.0, 20, 35, and 50 μsec. Full–scale signal is 350 μV.

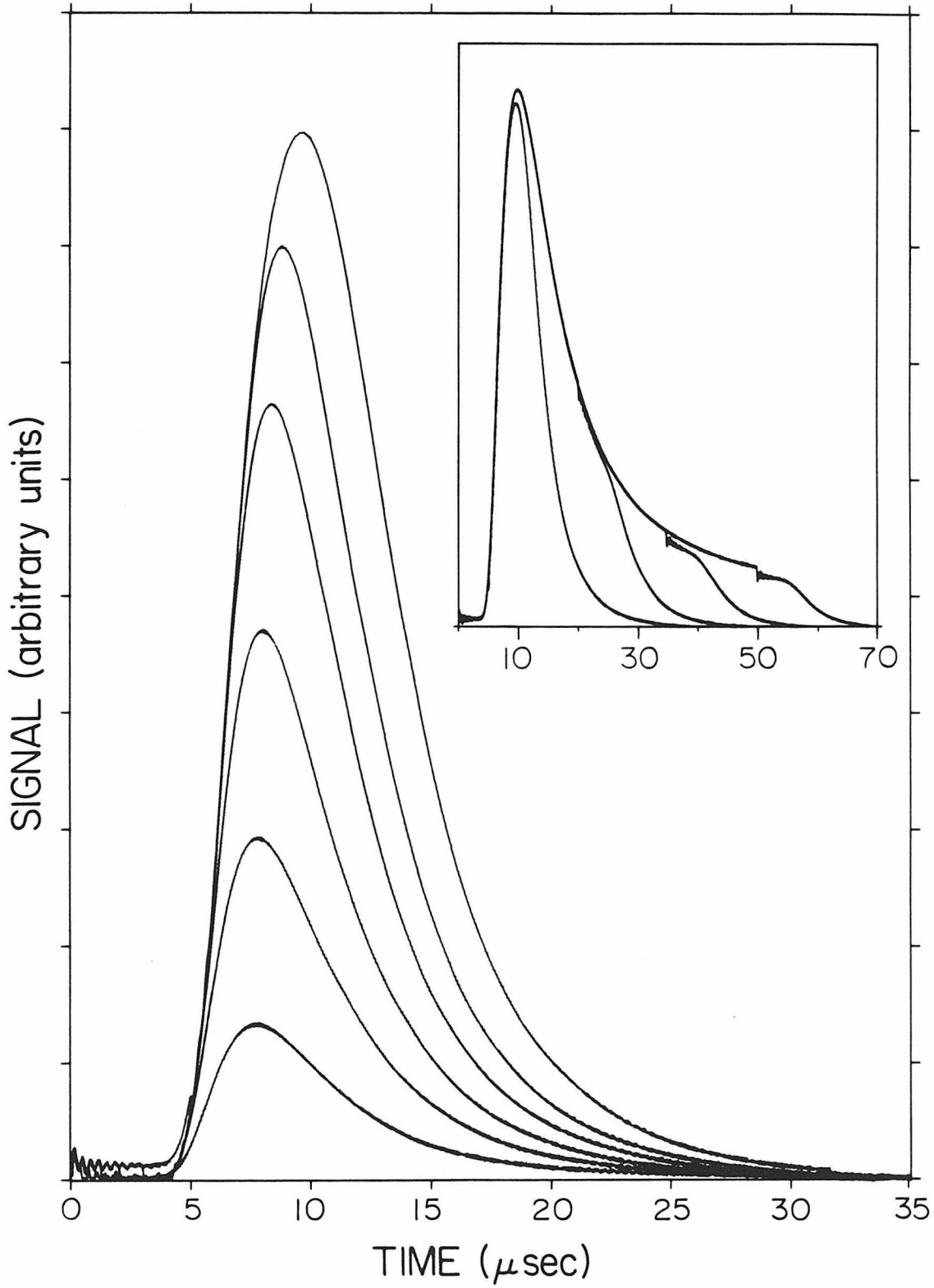

remain fixed at an even plateau except for the abrupt rise, as always, for very short times of flight.

The observant reader will have noticed certain additional features in the spectra presented in the inset to Fig. 4.4 which require further explanation. The first of these points is purely technical and concerns the sharp spike and accompanying offset prominent at 35 and 50 μsec and also just barely noticeable at 20 μsec. There is a small but direct electromagnetic coupling between heater and bolometer in the absence of any gas in the cell that manifests itself as a pedestal of duration t_p whose rise and fall is coincident with the beginning and end of the pulse. This explains the jump in the signal at $t=t_p$ as well as the initial offset of all of the spectra at $t=0$ despite their return to the prepulse baseline at long times. The effect is presumably due to the perturbation produced by the extra "static" magnetic field arising at the bolometer from the nearby sheet of current flowing through the heater, and is masked at higher powers by the strength of the desorption signal. A second question is why the fall-off in the signal after $t=t_p$ has such a peculiar shape and why it is not more similar to the shape exhibited by the waveforms in the main figure. The reason is that there is a finite delay between the time at which the pulse is terminated and the time when this effect is felt at the bolometer. The length of this delay reflects the velocity distribution of the fastest particles and is equal to the duration between $t=0$ and the first onset of signal but, unlike the case of the initial shoulder, it is the slowest particles which govern the form of the subsequent decay.

An appropriate integration time emerges naturally for each of the waveforms in Fig. 4.4 (e.g., t_I=35 μsec would be fine for all of the shorter pulses; t_I=70 μsec for the longer ones) and the signal area versus pulse width, with any pedestal contribution subtracted out, is plotted as the lower set of points in Fig. 4.5. Shown on the same scale for comparison are the results from an identical t_p sequence – excepting the extra point at 100 nsec – at a slightly elevated substrate temperature, T_s = 3.46 K (-20 db), and the same bolometer sensitivity.

Figure 4.5. $\int_0^{t_1} dtS(t)$ vs. t_p for T_s = 3.46 K (squares) and T_s = 2.88 K (circles). Same pulse–width sequence applies in both cases, excepting the first point at t_p = 0.10 μsec which is indicated only for the higher temperature. Full scale is 0.8 $\times 10^{-8}$ V sec in the main figure and 1.2 $\times 10^{-8}$ V sec in the inset.

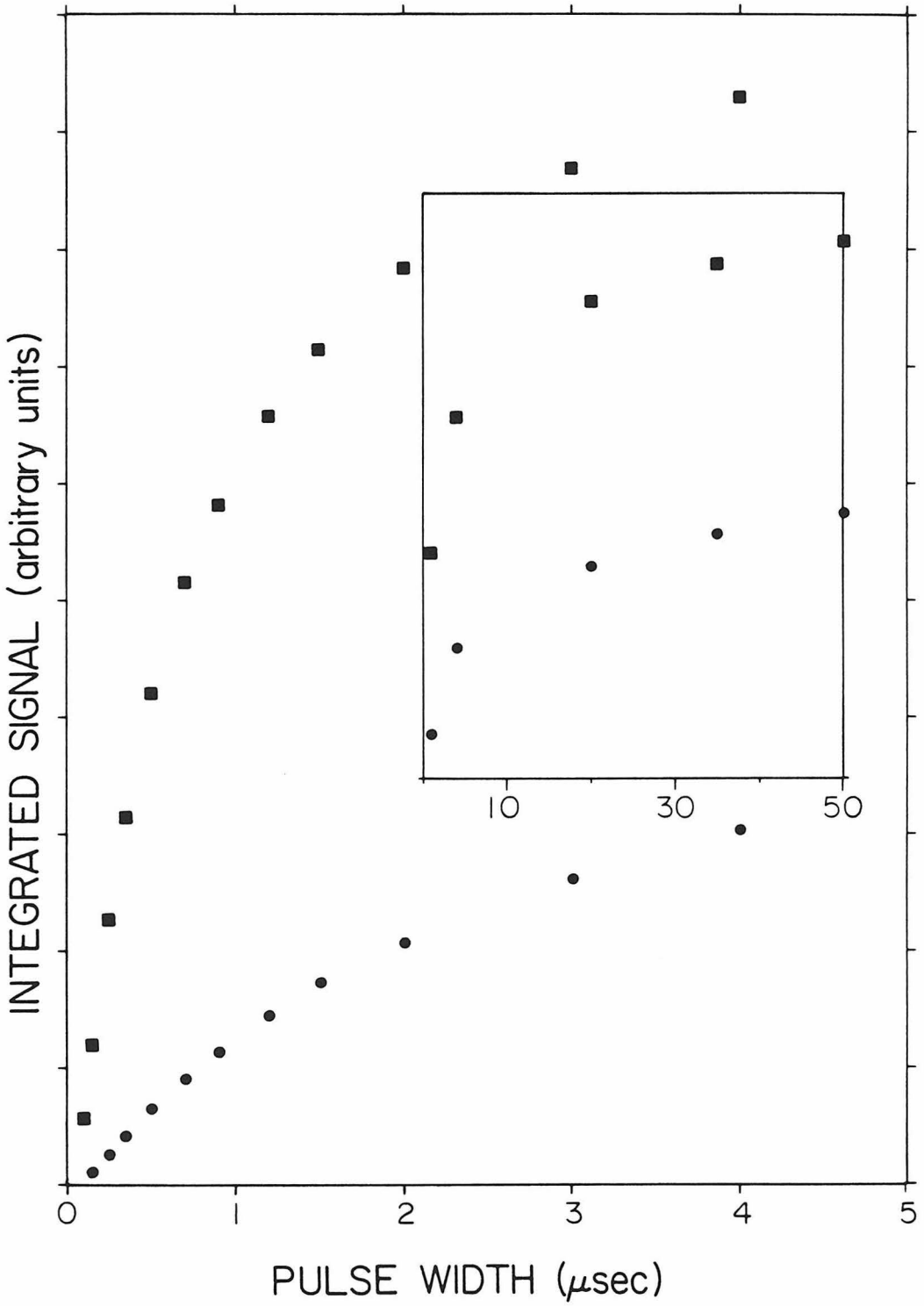

Because of the small difference in substrate temperatures relative to the binding energy ($E_b \sim$ 40 K) we see from (4.40) that the same constant of proportionality relates the respective signal areas to $\Delta n(t_p)$. As plotted, the points therefore accurately reflect differences between the two sets of data in the amount desorbed as a function of time. For example, the desorption rate, which is given by the slope of $\Delta n(t_p)$ vs. t_p, is obviously greater at the higher substrate temperature; at t_p = 500 nsec about six times as much has been desorbed by the film at 3.46 K compared with what happens when it is at 2.88 K. By the time t_p has increased to 50 μsec, however, this ratio has narrowed to 2:1 and the higher power area has pretty well saturated. As we saw in Fig. 4.4 though, this is not true of the −24 db data and its area continues to grow out to pulse widths of over 100 μsec. So despite large variations in the initial desorption rate, the net change in surface coverage at steady state, Δn_{ss}, is less sensitive to substrate temperature.

Practically speaking, it is not an entirely unambiguous matter to decide, at these low power levels, whether or not the film actually has reached a steady state. This is partly due to nuisance concerns associated with long pulses, such as the possibility some energy reaches the detector via direct thermal conduction rather than through desorption, and that the signal never therefore saturates. More to the point is the fact that, in principle, some signal must always originate from the film even when there is no net desorption. This is because atoms leaving the pulsed source are hotter than they would be in equilibrium, contributing an excess energy flux of $2k(T_s - T_o)\dot{n}_{eq}$ in the absence of any excess number flux.

Were we to draw a smooth curve through either set of points in Fig. 4.4, we would immediately notice something interesting, namely that neither curve intercepts the t_p axis at t_p=0, but that each crosses it somewhere between 50 and 100 nsec later! It's not as if we wouldn't see any signal at all for shorter pulses – we in fact do, though it's very small – rather, the extension to short times of a function whose second derivative remains of one sign (the curve we would naturally be lead to draw through the data) is misleading. The true $\Delta n(t_p)$ curve does

not intercept the t_p axis at a finite value with finite slope but presumably joins smoothly to the origin. This distinction is reminiscent of the sort of thing we saw in Chapter 3 contrasting the exact solutions of the thermal model with the zero'th–order boundary layer approximation as illustrated, for example, in Fig. 3.7. If we simply imagine displacing the approximation for the film thickness as a function of time there forward until it overlaps the correct solution then we get something resembling the curve we would use to represent our data. What is missing from our plot in Fig. 4.4 is the behavior of desorption "inside the boundary layer" where the film temperature is still changing rapidly with time. That the 50–100 nsec "lag" we see agrees with our estimate of the combined time it takes for substrate and film to warm lends support to this conjecture.

The logarithm of the rate of change of surface coverage with time (the net desorption rate) is illustrated in Fig. 4.6 for the –20 db example of the previous figure. The values shown are actually averages of the finite difference quotients computed between each pair of points in 4.5, interpolated to the appropriate time with due regard for the unequal spacing in t_p (this is done to facilitate a comparison with the second difference quotients needed to calculate $\tau_{\rm lcl}(t)$). An exponential with a time constant of 508 nsec gives a good fit to first five points but quickly falls below the rest of the data. The upward deflection of the desorption rate from this initial extrapolation means that we have a local time constant increasing with time. As our discussion in Chapter 3 concluded, such a behavior reveals the nonlinearity of the underlying adsorption isotherm, and in particular its positive curvature, when the sticking coefficient is independent of coverage.

Our intuition about $\tau_{\rm lcl}(t)$ is confirmed in the inset to Fig. 4.6 by direct calculation using the finite–difference approximation to (3.65). At short times, $\tau_{\rm lcl}$ is indeed very close to the value given by the exponential fit in the main figure but it increases severalfold thereafter. As the scatter in this plot suggests, it is not easy to reliably compute ratios of first and second derivatives from

Figure 4.6. Finite–difference approximation to the net rate of change of surface coverage with time plotted on a logarithmic scale for T_s = 3.46 K. Straight line is an exponential fit with τ = 0.51 μsec. Inset shows a finite–difference approximation to the local time constant vs. time on a linear scale.

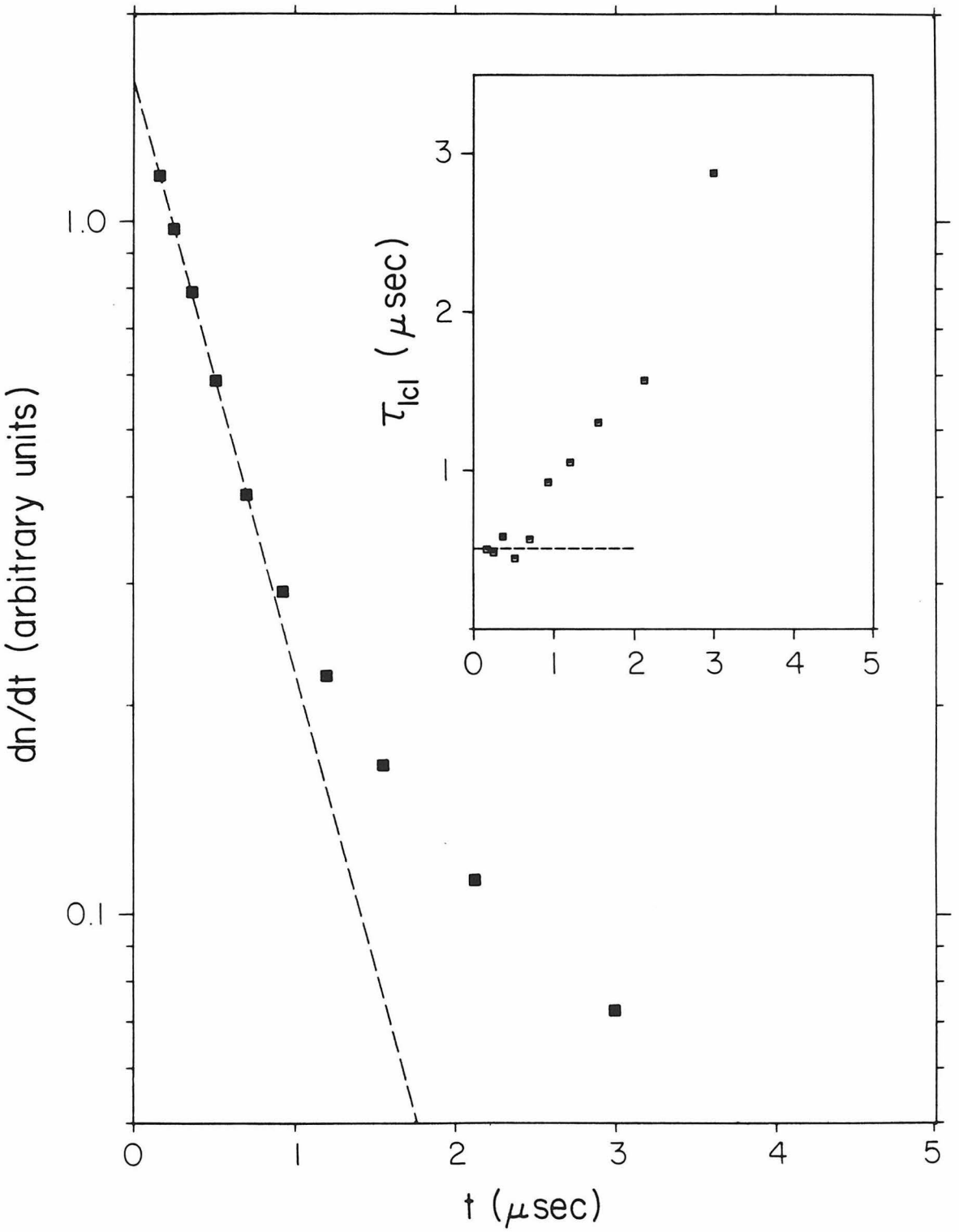

numerical data like ours. Such an effort places severe constraints on the stability and reproducibility of the apparatus, the point spacing relative to the overall curvature of the data, as well as the amount of instrumental uncertainity that can be tolerated. Numerical differentiation in the presence of noise is, in fact, a notoriously unstable process and is still an area of vigorous research activity [Franklin].

It would be appealing to be able to cite these results as functions of the surface coverage rather than time, and to be able to reconstruct the adsorption isotherm (with assumptions about the sticking coefficient) from them. The best we can do, however, is to plot them versus Δn in arbitrary units (using Δn vs. t) which would yield no new information beyond what we have already done. It's been mentioned before, but bears repeating, that to go further requires a knowledge of both the absolute sensitivity K of our detector and the initial surface coverage n_o.

Our results for the global time constant and its dependence on substrate temperature are summarized in Fig. 4.7. The solid squares give τ_{exp} obtained in the low–power experiments addressed here by extrapolating the initial slope of data like that in Fig. 4.4 to the relevant saturation area. Asymmetric error bars reflect conservative estimates of the uncertainty introduced by the difficulties we have alluded to regarding the saturation area, numerical differentiation, and non–isothermal behavior at very short times. The solid line gives the corresponding isothermal prediction of the detail–balance model, with σ=1 and the FHH equation of state, for the same ambient conditions. Alongside these new results appear the data of Sinvani *et al.* (open squares) and the continuum model's expectations (dashed line), reproduced from Fig. 3.14, for generally higher powers and apparently different ambient conditions. What is immediately striking about this plot is not just the fact the two theoretical predictions nearly coincide (the ratios of $-\mu_o/T_o$ are almost the same in both cases: 19.0 and 20.7, respectively), but that the data overlap and seem to lie on a common curve as

Figure 4.7. A comparison of global time constant data and continuum model predictions for T_o = 2.10 K, $-\mu_o$ = 40 K (solid squares and solid line, respectively) with data of Sinvani *et al.* and model predictions for T_o = 3.48 K, $-\mu_o$ = 72 K (open squares and dashed line).

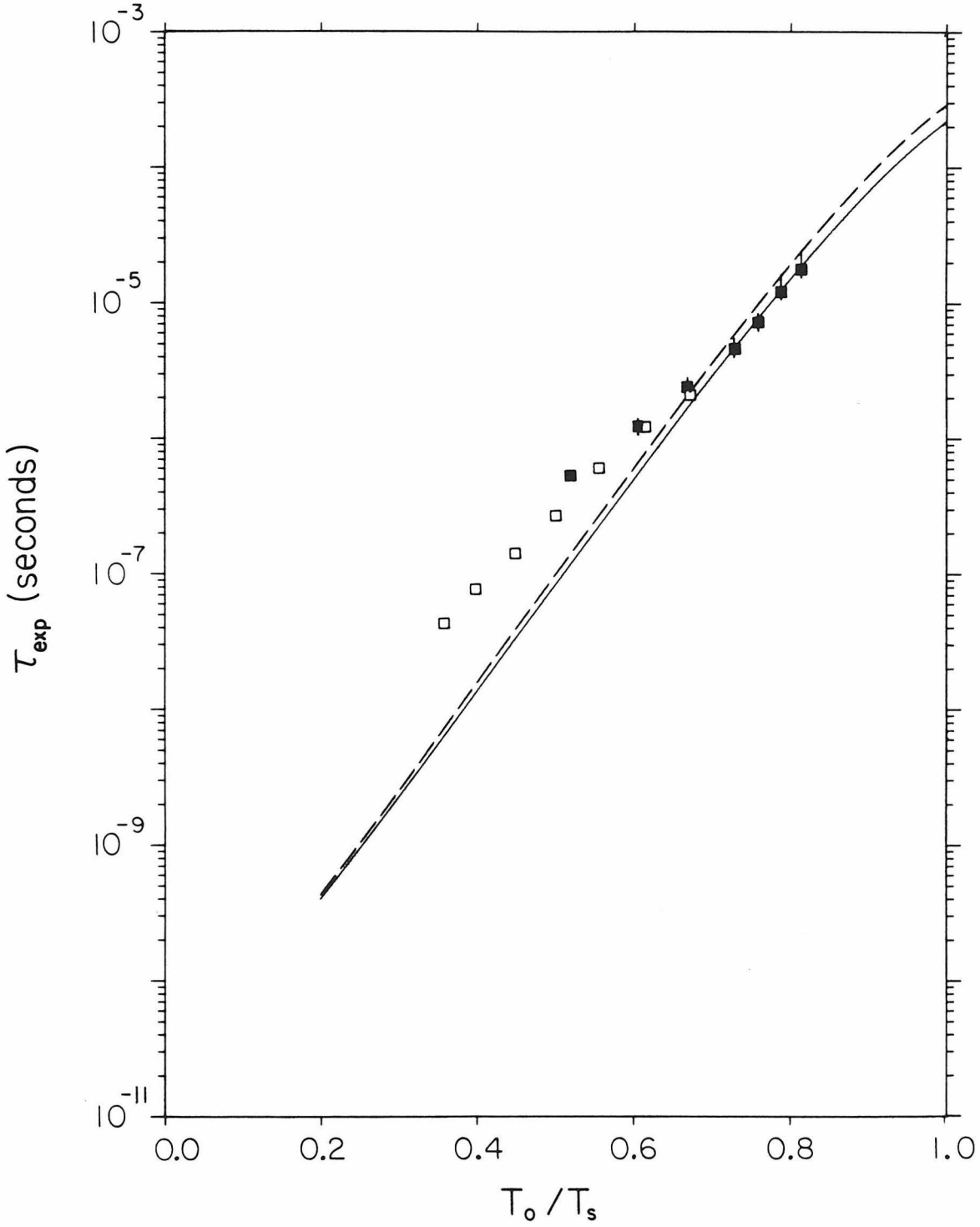

well – and this despite differing methods of analysis for the two sets. Whatever our reservations about the quantitative veracity of the thermal model and all of the approximations we have employed, at the very least this observation is strong evidence that we have chosen the correctly scaled variables with which to describe the desorption process.

A closer examination of the data at very low power shows the agreement with theory to be remarkably good, perhaps better than we have any right to expect given our choice of equation of state. The trend in the data changes as we progress to slightly higher substrate temperatures. In the overlap region, the points all lie markedly above the prediction and share a different slope. One hypothesis to account for this change is that collisions between desorbed atoms are still prominent in the data at intermediate powers (interfering with our ability to properly measure the global time constant), but that these same collisions become negligible at the very lowest substrate temperatures (≤ -24 db). Evidence in support of this contention will be cited shortly.

We present differences of time–of–flight spectra in Fig. 4.8 as a final illustration of what may be learned from the experiments we've been discussing. Our examples are chosen from the series of curves reproduced in part in Fig. 4.4 (an instance where we are confident the transport is ballistic) and serve to demonstrate the deconvolution predicted by (4.42) as well as reconstruct the desorption Green's function for this source temperature. The waveforms for several short pulse widths t_p have been subtracted from ones obtained at $t_p+\Delta t_p$ (where Δt_p varied from 0.10 to 0.30 μsec) and the results normalized to a common peak height before being plotted as a function of $t-t_p$. To the extent these difference spectra computed at disparate absolute times t_p share a common shape versus $t-t_p$ as, qualitatively, it appears they do, then we have confirmed the isothermal assumption on which this decomposition rests (recall, for example, the discussion leading to (4.21)).

Figure 4.8. $\partial S(t;t_p)/\partial t_p$ vs. $t-t_p$ via finite differences for T_s = 2.88 K. Front to back: t_p = 0.15, 0.25, 0.35, 0.70, and 0.90 μsec; Δt_p = 0.10, 0.10, 0.15, 0.20, and 0.30 μsec, respectively.

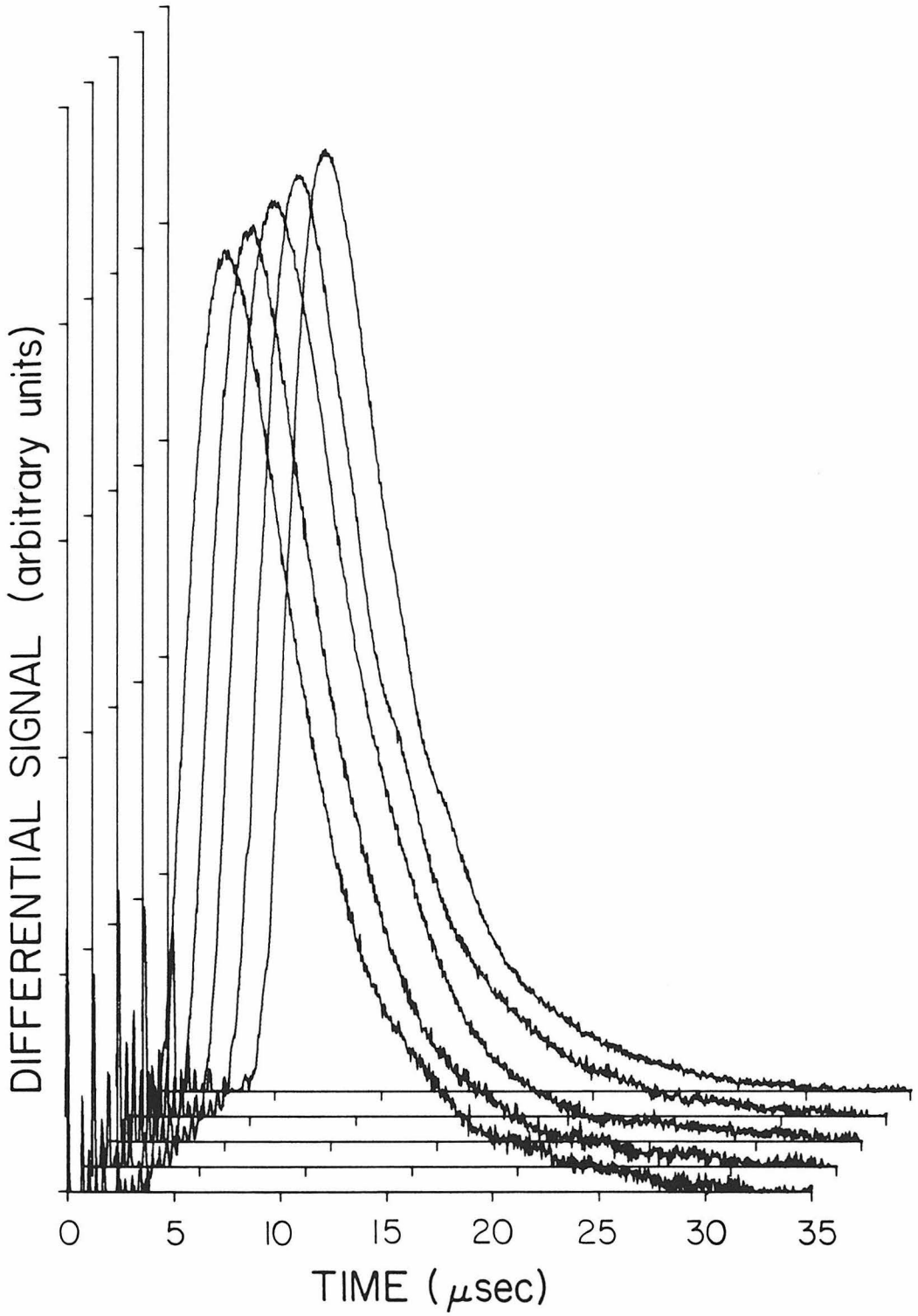

The rather good signal to noise maintained in these comparatively small difference spectra exemplifies the power of our signal recovery electronics. Ideally, these curves could have been normalized to a common area instead of a common peak height but then the effect of small discrepancies in the shape of their tails would be exaggerated, showing up as 10% variations in peak amplitude. The procedure we adopted facilitates a visual comparison of the data. What we have not yet pursued, but might be worthwhile trying, is a detailed fit to the difference curves to see if indeed a single temperature parameter suffices. Among other things, this would require an accurate knowledge of E_b and z and would necessitate computing various moments of the gaussian distribution (e.g., χ^2) to evaluate the integration over a rectangular source area in (4.42). What we might hope to discover from all of this, given we are confident we understand the properties of our detector, is whether the velocity distribution is Maxwellian as we think it should be (might there be an extra velocity dependence in the sticking coefficient?), how sensitive the shape of the desorption Green's function is to small changes in its temperature parameter, and how closely these temperatures agree with our calculations for T_s.

We turn our attention next to the properties of the time–of–flight spectrum as a function of the pulse repetition period. Rather than presenting a sequence of spectra for different t_p with t_r fixed at a value which allows the film's return to equilibrium between pulses, as we have done previously, we now reverse the procedure and show what happens when we vary t_r for a single pulse width which brings the film close to steady state. The results for the 50 μsec heater pulse of Fig. 4.4 are reproduced in Fig. 4.9 to illustrate this type of experiment. It is clear that the total signal decreases with increasing repetition frequency (or decreasing period) but, as a comparison of the first three waveforms at ν_r = 70, 190, and 270 Hz reveals, this decrease is evident only above (or below) a certain threshold. The integrated signal versus t_r for these data, normalized to the value obtained at the critical repetition time (t_{rc} = 14.3 msec), is plotted in Fig. 4.10 (squares)

Figure 4.9. $S(t)$ vs. t, as a function of ν_r, for T_s = 2.88 K and t_p = 50 μsec. In descending order ν_r = 70, 190, 270, 350, 450, 600, and 1000 Hz. Same vertical scale as in Fig. 4.4.

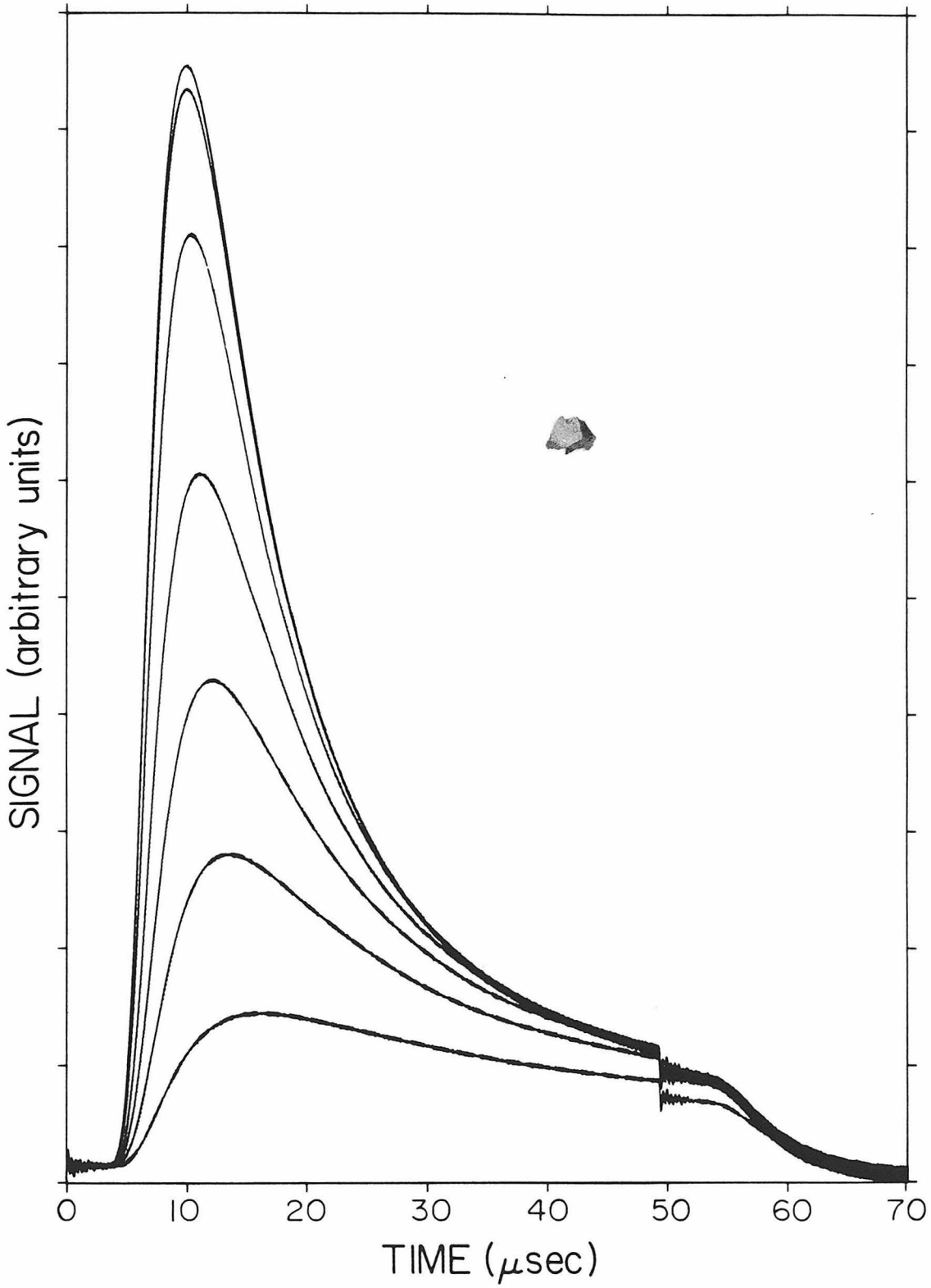

Figure 4.10. $\int_0^{t_l} dtS(t)$ vs. t_r, normalized to $\int_0^{t_l} dtS(t)$ at t_{rc}, for T_s = 2.88 K, t_p = 50 μsec (squares) and T_s = 4.04 K, t_p = 4 μsec (circles).

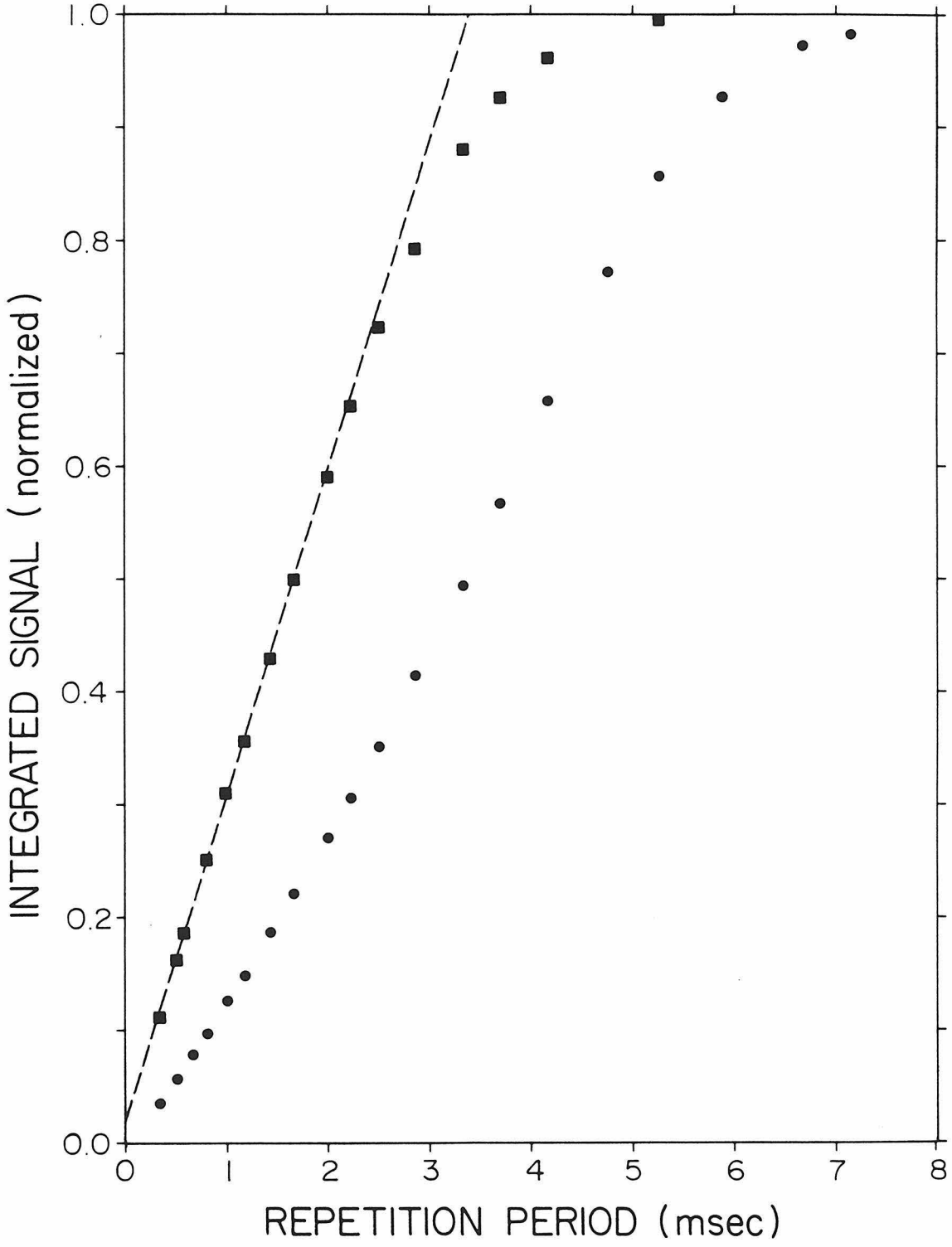

along with similarly computed results for the 4 μsec heater pulse of Fig. 4.3 (circles). Both sets of points, at pulse powers of −24 db and −17 db respectively, show a saturation in the maximum number of atoms desorbed with t_r at repetition times well below t_{rc}, and we interpret this observation as a confirmation of our assertion in the corresponding time constant measurements at ν_r = 70 Hz that the film indeed regains its equilibrium coverage between pulses. This conclusion, while sensible enough intuitively, may nevertheless be unwarranted, in some circumstances, since it is based entirely on noting the lack of further change in what is otherwise a relatively rapid variation of the number desorbed with decreasing repetition frequency. Consider what might happen, for example, if our isotherms were actually step-like and the equilibrium coverage placed us in the middle of a region of 2-d phase coexistence as illustrated in Fig. 3.2. Then complete replenishment after a desorption event like the one shown there could well take longer than any practical repetition interval for the following reason. Readsorption begins in the knee of the equilibrium isotherm and is initially driven by the large difference between the equilibrium vapor pressure and the vapor pressure at ambient temperature and reduced coverage. This rate then decreases rapidly with increasing coverage, reflecting the steep rise of the isotherm, and by the time the plateau which signals the onset of the two-phase region has been reached it has dropped to a comparatively small value. The rate of further readsorption then depends on the difference between vapor pressures at the two ends of the plateau, but this vanishes asymptotically as the region becomes more and more ideally flat. The reaccumulation of a finite coverage at this infinitesimal rate takes essentially forever and so, for any finite repetition period, we end up cycling the system between steady state and the beginning of the two-phase region rather than between steady state and true equilibrium.

The slope of the replenishment curve gives us the instantaneous readsorption rate (when corrected for the normalization factor) and, as we see from the figure, the low temperature data are well approximated by a straight line at

shorter repetition intervals. This constant rate implies that the film vapor pressure is a relatively insensitive function of the amount adsorbed at these lower surface coverages. As the coverage increases we naturally reach a point where the film vapor pressure becomes comparable with the equilibrium pressure; the readsorption rate then drops off from the extrapolation of its initial value and the film eventually approaches its final thickness exponentially with a time constant $\tau_{lcl}\,(T_o, n_o)$. The picture which emerges to substantiate this point of view is just the inverse of the one we have described above, namely, that the isotherm is comparatively flat in the region around n_{ss} but then increases abruptly as we approach equilibrium. The stronger the upward curvature of this isotherm, the longer the time span over which the apparently linear behavior in the replenishment graph persists. It is not entirely clear, on the other hand, what to make of the fact that our linear fit does not pass through the origin as $t_r \to 0$, but intercepts the ordinate axis at around .02 instead. One technical objection is that we have not corrected for the effect of a finite pulse width in these data. Our abscissa really should be $t_r - t_p$ and since t_p = 50 μsec the first two points at t_r = 333 and 500 μsec would be shifted towards the origin 15% and 10% respectively, but this would only tend to increase (slightly) the apparent ordinate intercept. A plausible explanation, consistent with all the pitfalls we have pointed to in our discussion of the signal analysis (especially for long pulses), is that there is some small percentage of the signal area which is not proportional to Δn.

Given the thrust of our explanation for the shape of the replenishment curve versus t_r at low power, our −17 db data now seems puzzling. This curve is S−shaped rather than linear and shows a distinct upswing around t_p = 2−3 msec before bending over again near saturation. We can fit straight lines to the segments at short and intermediate replenishment times and so doing find their slopes to be roughly in the ratio of 2.00/1.25. Such an increase in slope at first appears inconsistent with what we know must be true of any isotherm, namely that the film vapor pressure always grows with the number adsorbed (or at worst,

remains constant). As a consequence, we would expect that the net readsorption rate, which is proportional to the difference between this pressure and the ambient, always decreases with increasing surface coverage (or at worst, remains constant) but that it never increases. All of this is correct, of course, provided the sticking coefficient is *independent* of coverage. Were the sticking coefficient to actually *increase* with the number adsorbed to some maximum value, however, it would then be possible to account for the larger than expected readsorption rate. Furthermore, this suggestion need not be inconsistent with the observed linear dependence at lower power if we simply recognize that the film begins its regrowth, in this case, from an already greater steady–state coverage.

There is another argument which throws a different light on the interpretation of these data, however, and the evidence for it is quantitative rather than merely qualitative. If collisions between desorbed atoms are still significant at −17 db for the greater fractions desorbed at longer repetition intervals, then the reasoning of Cowin *et al.* would dictate that the accompanying upturn in slope we observe results from the dynamical focusing effect of these interactions. Collisions, in other words, sweep more particles into the forward direction (and, therefore, into the solid angle subtended by our detector) than we would expect on the basis of a cosine distribution for the desorption flux. This hypothesis can be tested by calculating the number of atoms per unit area actually striking the bolometer for the maximum integrated signals of Fig. 4.10. We do so using equation (4.40) (ignoring, of course, the $\dot{n}_{eq}$ correction) and our nominal values for the bolometer's sensitivity and active area. It then follows that

$$\Delta n \left[\frac{1}{\pi} \int_{A_s} d^2 r' \, \frac{z^2}{|\mathbf{r}-\mathbf{r}'|^4} \right] = \frac{\int_0^{t_l} dt S(t)}{A_d K \sigma_d (2kT_s + E_b)} \tag{4.43}$$

Estimating $E_b = -\mu_o$ and $\sigma_d = 1$, which places a lower bound on the number intercepting the detector for a given value of its response, the right–hand side of this

expression gives 0.14 ML for the −24 db data (1 ML=1 monolayer or 10^{15}atoms/cm^2) and 0.37 ML at −17 db. A ready analytic quadrature for the integral of the cosine distribution over an extended source ($z=(\mathbf{r}-\mathbf{r}')\cdot\mathbf{n}$) is obtained if we replace our rectangular heater by a circular one of equal area in (4.43). Evaluation yields $1 - z^2/(z^2+\rho_s^2)$ for the fraction of desorbed particles which should intercept the bolometer (ρ_s is the equivalent source radius) and substituting the appropriate dimensions we find 0.18 for this number. As a consequence, the *minimum* change in surface coverage necessary to account for the observed strength of the maximum desorption signal is Δn = 0.8 ML at −24 db and Δn = 2.1 ML at −17 db. Now we know from the adsorption isotherms for helium on graphite that under the conditions of this experiment the equilibrium coverage on that surface would be 1.2 ML and, as we pointed out previously (section 4.2), this places an upper limit to the possible equilibrium coverage on our constantan heater. The only way to reconcile the apparent discrepancy between this limit on n_o and the value of Δn inferred from (4.43) at −17 db is to suppose that the number of desorbed particles reaching the detector is actually greater, by about a factor of two, than predicted assuming a cosine distribution – i.e., the desorption flux is forward focused. This factor agrees (roughly) with the change in slope exhibited by the data in Fig. 4.10, though that may only be coincidental.

We might remain somewhat skeptical of these results in view of our uncertainty regarding the precise sensitivity of the bolometer under the particular operating conditions of this experiment, but a factor of two seems unlikely. The whole argument is made more compelling by quoting the results of another, independent, investigation in which a calibrated bolometer *was* used to study the desorption signal as a function of repetition time. The same sort of S–shaped curve occurred in this case, for a source at 19 K with an area of 0.1 mm^2. Again, the only way to reconcile the observed signal strength (0.1 ML) with monolayer coverage and the predicted intercepting fraction (0.02) was to suppose an additional focusing factor of at least 5. An increasing frequency of collisions with

greater substrate temperature, and consequently higher desorption rates, is consistent with the pictures we have presented for estimating their number. To explain these effects in any other way requires postulating a complex coverage-, temperature-, and velocity-dependence for the sticking coefficient which seems less plausible.

Convinced as we now are that collisions may be safely disregarded at low enough substrate temperatures, let us return to the -24 db example of Fig. 4.9 to comment further on the changes undergone by the time-of-flight spectrum as we vary ν_r. Aside from the overall decrease in signal area with increasing ν_r which we have already pointed out, other features, at first somewhat surprising, are readily apparent. Why, for instance, do these spectra appear to share a common tail whereas in the time-constant experiment of Fig. 4.4 it is the initial shoulder which is similar for all of the curves? The decrease in area (and hence total number desorbed) is concentrated here at short times, exerting its greatest influence on the height and location of the signal maxima. These peaks move toward later times, and are depressed in amplitude relative to their tails, giving the spectra an increasingly squat look. We might have naively expected all of the curves to be identical in shape when rescaled to reflect the relative amounts desorbed. Why is that not the case?

The origin of the differences within this series of waveforms and how they contrast with those of Fig. 4.4 is best visualized in terms of Fig. 4.11 where we have illustrated what happens in both the ideal time-constant and ideal repetition-rate experiments over a segment of the vapor pressure isotherm with positive curvature. At the risk of being repetitive, it is useful to recapitulate the details for each case with particular reference to this diagram. Solid lines trace the system's trajectory while the heater is on and dashed lines do the same when it is subsequently turned off. Starting at the equilibrium coverage n_o a pulse of width t_p will, for example, bring us to the point $n(t_p) = n_1$ on the T_s isotherm before we drop back to the T_o isotherm where reaccumulation of the film begins

Figure 4.11. Desorption at temperature T_s and readsorption at temperature T_o illustrated schematically for different experiments over a positive curvature segment of the vapor pressure isotherms. Refer to text for discussion.

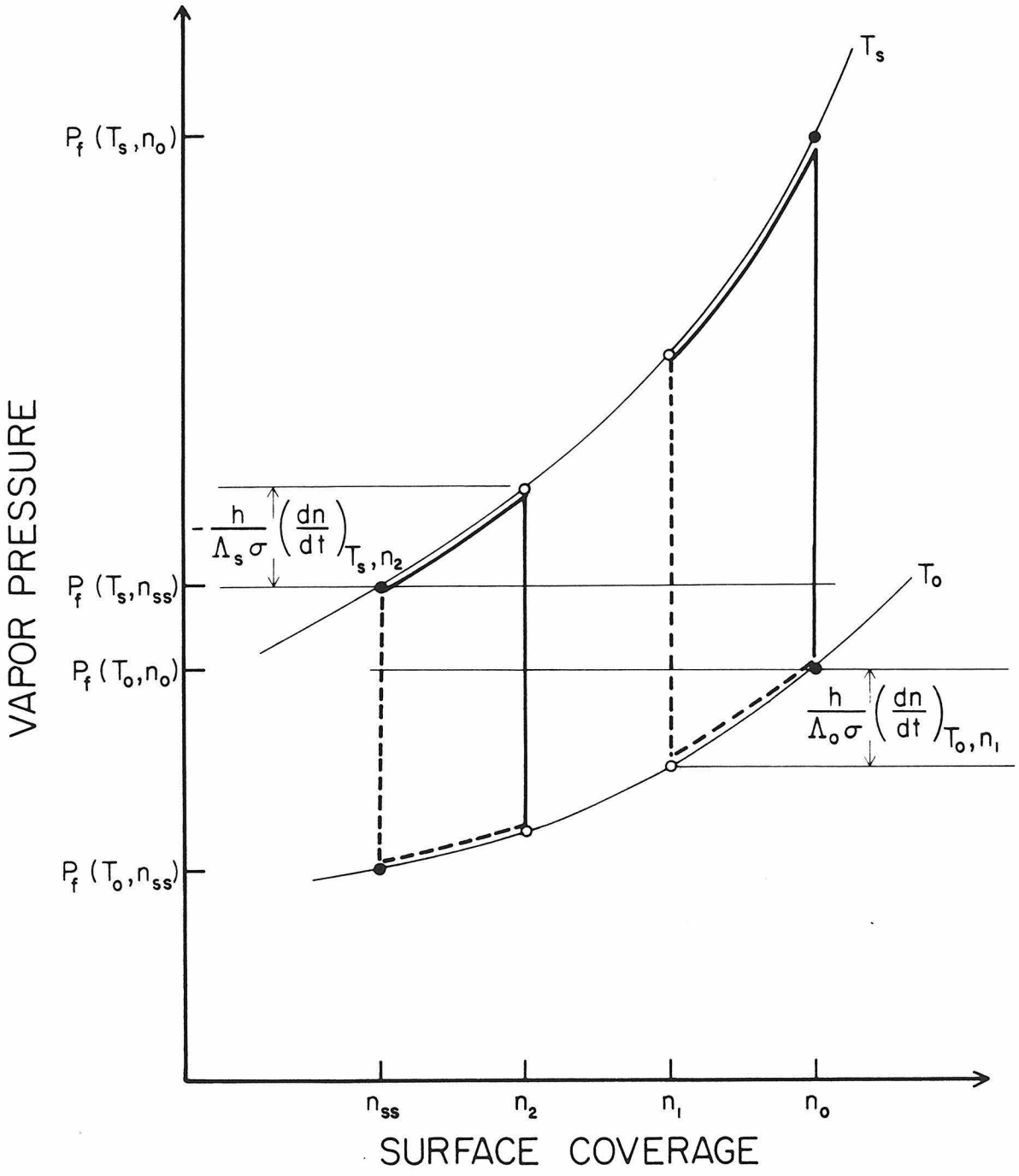

from the same coverage. If enough time elapses to complete the return to equilibrium on the T_o isotherm before the next pulse occurs, the system cycles continuously between n_o and $n(t_p)$. As t_p increases our endpoint slides progressively down the T_o isotherm – to n_2 and so on – eventually halting at the steady–state coverage n_{ss}. Meanwhile, our initial point remains at n_o, provided t_r is longer than the time needed to recover from n_{ss}, and $\Delta n(t_p) = n_o - n(t_p)$ increases until reaching a maximum, $n_o - n_{ss}$. A different cycle is employed to study $\Delta n(t_r)$ on the other hand. First, we select a t_p sufficient to drive the system into steady state (or very close to it) from any point on the T_s isotherm below n_o. Beginning from n_{ss} on the T_o isotherm at the end of this pulse, we then allow only enough time for the film to reach $n(t_r) = n_2$, by restricting t_r, before again driving it back into steady state with the next pulse. Increasing t_r, the initial point for desorption moves further up the T_s isotherm – past n_1 in this case, and eventually all the way up to n_o – while the endpoint remains fixed; $\Delta n(t_r) = n(t_r) - n_{ss}$ likewise increases until reaching a maximum at $n_o - n_{ss}$.

We can get some feeling for how the desorption signal behaves in either of these cases if we return to (4.31) and retain only the pulse–on contribution. To simplify matters, we imagine first that it is possible to evaluate the integral over $\mathbf{r}'$ for the arbitrary source geometry in question and thereby reduce the propagator to a function of $t - t'$ alone with parametric dependences on both β and z. Suppressing the latter in our notation as usual, we define a new Green's Function according to

$$S_o(t-t';\beta) = \int_{A_s} d^2r'\, S_o(\mathbf{r}-\mathbf{r}',t-t';\beta)\,. \tag{4.44}$$

With this substitution, and using the relationship between $\dot{n}(t)$, $\dot{n}_{des}(t)$, and $\dot{n}_{eq}$ given by the equation of motion, the relevant part of (4.31) may be re–expressed as

$$S(t) = \int_0^{t_p} dt' \left[-\dot{n}(t') S_o(t-t';\beta_s) + \dot{n}_{eq}(S_o(t-t';\beta_s) - S_o(t-t';\beta_o)) \right]. \tag{4.45}$$

Whenever the equilibrium desorption rate is small compared to the net rate of change of surface coverage, or the difference in propagators is small compared with the value of the propagator itself (as is likely to be the case when $E_b \gg 2kT$), the first term in (4.45) dominates the observed signal shape. Now when the sticking coefficient is constant, the instantaneous rate of change of surface coverage, as a function of coverage but not of time, may be read off directly from Fig. 4.11. During periods of desorption, this quantity is proportional to the height of the T_s isotherm above the horizontal line at $P_f(T_s,n_{ss})$ (as illustrated for the particular point n_2) and, conversely, during periods of readsorption it is the distance from the T_o isotherm to the horizontal line at $P_f(T_o,n_o)$ that is relevant (as shown for the point n_1). All of the waveforms in the time–constant experiment have a similar initial shape as t_p increases because we obviously trace over the same initial section of the T_s isotherm, implying the same early history for $\dot{n}(t')$ independent of pulse width. Of course, this no longer holds true for the repetition rate experiment where, just as obviously, it is the early history of $\dot{n}(t')$ which varies as we change t_r. How does this distinction affect the signal shape we observe? Suppose, as an example, we compare the signals for two different repetition periods – the t_r which brings us back to n_2 from steady state versus t_{rc}, the critical repetition period, which ensures our return to n_o. To do this we first linearly scale the trajectory from n_2 to n_{ss} so that it gives the same Δn as the trajectory from n_o to n_{ss}, and the two signals then have the same area. This scaling can be visualized as stretching the distance from n_2 to n_{ss} along the horizontal line at $P_f(T_s,n_{ss})$ until it equals the distance from n_o to n_{ss} while at the same time stretching the corresponding segment of the T_s isotherm; the two trajectories can now be compared directly. Because of the positive curvature of the isotherm the actual vapor pressure at n_o, $P_f(T_s,n_o)$, exceeds the scaled value $[(n_o-n_{ss})/(n_2-n_{ss})]P_f(T_s,n_2)$. As a consequence, the initial desorption rate (i.e., the distance to the line at $P_f(T_s,n_{ss})$) in the t_{rc} experiment exceeds that of the scaled t_r experiment. Because the two experiments give the same Δn, however, at

some point in *time* the desorption rate along the t_{rc} trajectory must dip below that of the scaled t_r trajectory (even though this never happens as a function of coverage) since Δn is just the area under the $\dot{n}(t')$ vs. t' curve out to t_p. Therefore, if the isotherm has the structure illustrated, the relative weighting of desorption events favors earlier times relative to later ones with increasing repetition period; were the curvature to be reversed, we would find exactly the opposite result. Put another way, our observation that the signals in fact favor relatively later desorption events with increasing ν_r conforms with our predictions for an isotherm with positive curvature. That this effect is indeed as pronounced as it is in the data is an indication of how strong the nonlinearity in the isotherm may be. A parallel discussion of the desorption rates for a linear isotherm would reveal a signal shape independent of t_r because the segments from n_2 to n_{ss} and from n_o to n_{ss} form corresponding sides of similar triangles and the scaling procedure then makes the trajectories overlap identically.

The behavior of the time-of-flight spectrum as a function of pulse width, at a repetition frequency in excess of the maximum frequency permitting a complete return to equilibrium for a pulse of a given power and arbitrary duration, is illustrated with a representative example in Fig. 4.12. The substrate temperature, vertical scale, and pulse-width sequence are identical with those in Fig. 4.4, so there is a one to one correspondence between the waveforms of each figure: the only difference is that the repetition rate has been changed from 70 to 1000 Hz. Sweeping through t_p, the amplitude of the signal at first increases as previously, though at a noticeably slower rate; it then abruptly reaches a maximum but, unlike before, decreases with ever longer pulse widths after that. This effect is both curious and surprising, and the correct explanation for it, though simple enough in hindsight, took some time to uncover.

The integrated signal versus t_p for the spectra of Figs. 4.4 (open circles) and 4.12 (circles) is presented in Fig. 4.13, along with data at yet higher repetition frequencies (squares, triangles). While the amplitude and shape of the

Figure 4.12. $S(t)$ vs. t, as a function of t_p, for T_s = 2.88 K, ν_r = 1000 Hz. Main figure: left to right, t_p = 0.35, 0.70, 1.2, 2.0, 3.0 and 5.0 μsec. Inset: t_p = 5.0, 20, 35 and 50 μsec. Same vertical scale as in Fig. 4.4.

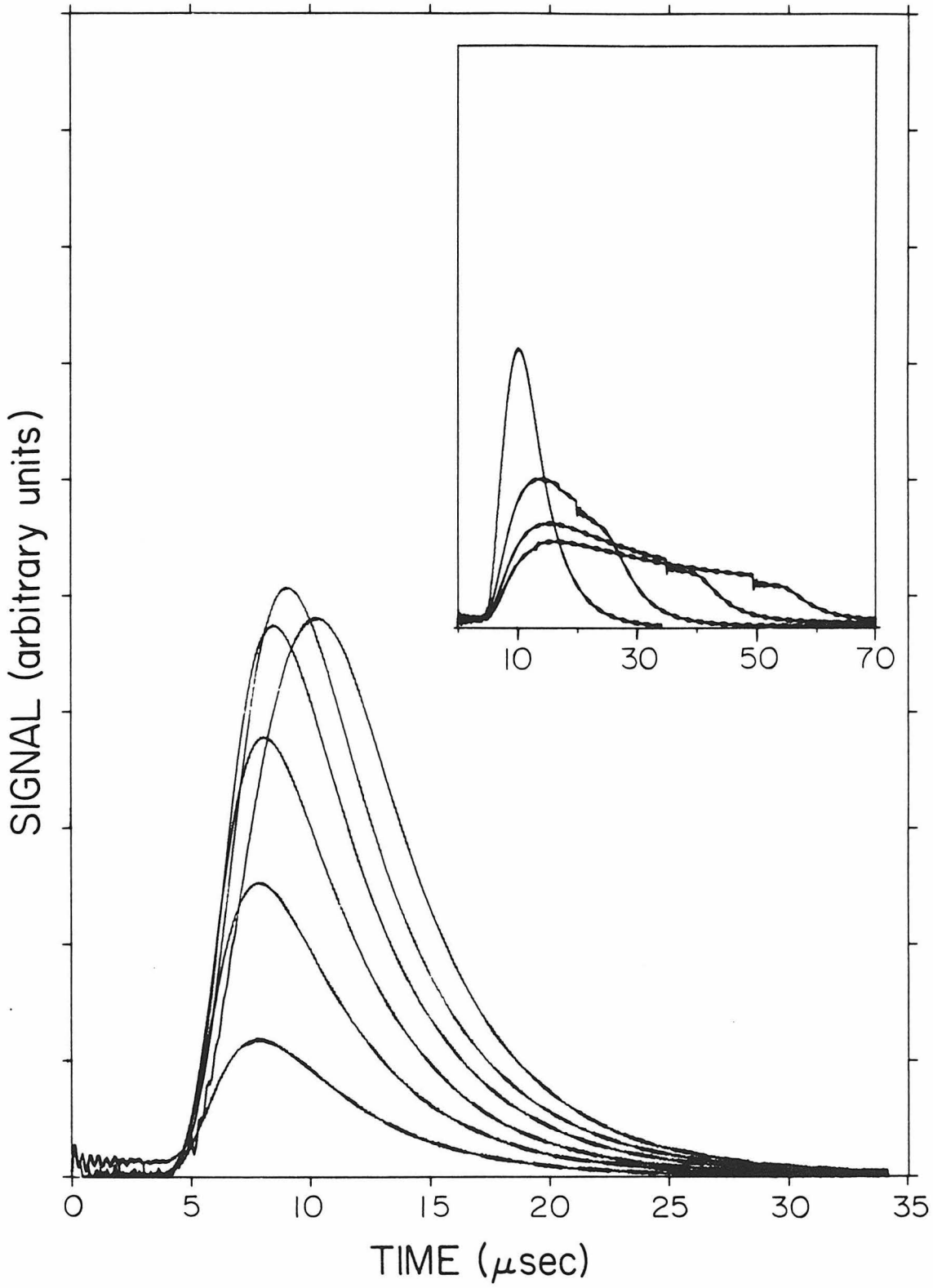

Figure 4.13. $\int_0^{t_1} dt S(t)$ vs. t_p for T_s = 2.88 K and several different repetition frequencies. ν_r = 70 (open circles), 1000 (circles), 2000 (squares), and 4000 Hz (triangles).

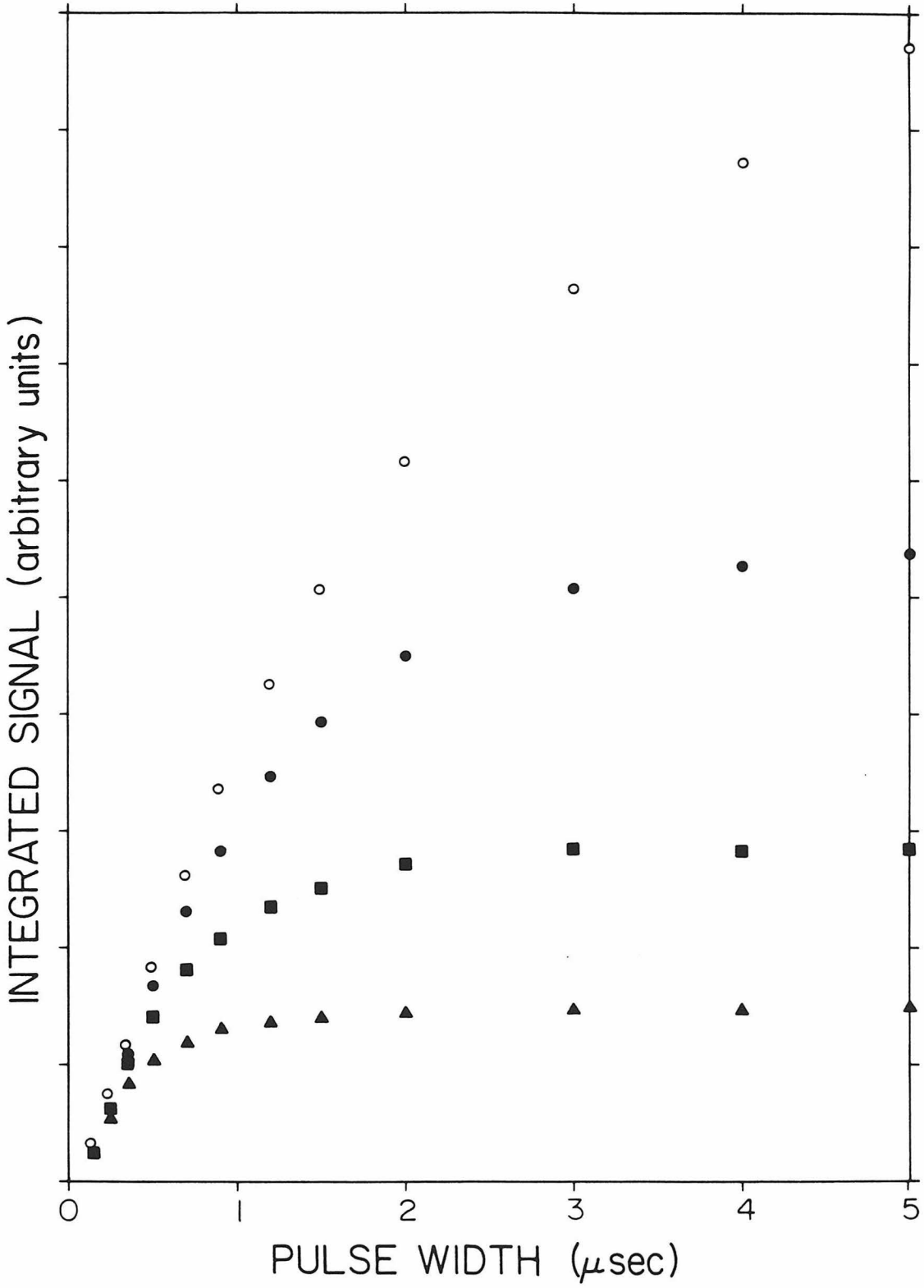

desorption signal as a function of pulse width exhibit unusual features at ν_r = 1000 Hz, the area follows a simple and uniform behavior, growing monotonically with t_p. Compared with the results for the critical repetition frequency though, this area grows more slowly, saturates far sooner (around 5 μsec vs. 100 μsec), and does so at a somewhat lower level. This trend continues with increasing repetition frequency, where the total saturation area continues to decrease and the pulse width at which this value is approached steadily moves to shorter times. For very narrow pulses, the curves appear to share a common envelope, splaying out from the same initial slope; at the other end, the saturation values are in good agreement with the ratios predicted by Fig. 4.10. Taking these data at face value, we could proceed to calculate a global time constant for each of the curves by extrapolating the initial slope to the individual saturation values, identifying the changes in area with changes in the number desorbed. So doing, we would find a time constant that in addition to being dependent upon the pulse power is a function of repetition frequency and is proportional to ν_r^{-1}. Now this conclusion is at odds with what we expected when first setting out to perform these kinds of measurements. The original motivation here was to study the systematics of the time constant under different initial conditions for the film as well as different desorption temperatures. By varying ν_r and restricting the replenishment time, we argued, we are in effect controlling the film thickness at the beginning of the pulse without having to go through the tedious process of changing the ambient gas pressure. Keeping the film artificially thin in this way, we should then be able to test the dependence of the time constant on μ without actually changing the equilibrium conditions. Since the film chemical potential becomes more negative with decreasing coverage we would predict, using (3.1), a time constant *increasing* with ν_r, not decreasing.

There is no real paradox, however, as this argument is altogether specious and presents an object lesson in the pitfalls associated with blindly applying an empirical formula to a situation whose physical underpinnings are not clearly

grasped. First of all, the steady–state condition for a given desorption temperature is set by the pressure of the ambient gas (recall $P_f(T_s,n_{ss}) = (T_s/T_o)^{1/2}P_f(T_o,n_o) \equiv (T_s/T_o)^{1/2}P_g$). This is true no matter where on the T_s isotherm between n_o and n_{ss} we happen to start and there is no fooling the system about this fact. Whereas the *local* time constant surely changes in accordance with variations of the film's chemical potential with coverage as given in (3.68), there is no similarly simple *a priori* prediction for the *global* time constant starting from an intermediate coverage. Although we did confirm successfully, by numerical example in the case of an FHH equation of state, the behavior implied by (3.1) for the variation of the global time constant at equilibrium coverage with *temperature*, this is not really the same thing. In the language of Chapter 3, we are talking about the distinction between how $\tau_{exp}(n_o,n_{ss}(T_s))$ changes with T_s and fixed n_o versus how $\tau_{exp}\,(n_i,n_{ss}(T_s)) = \tau_{lcl}(n_i)(n_i-n_{ss}/n_i-n_{ss}^i)$ changes with n_i at fixed T_s (compare this with (3.72) and Fig. 3.4).

There is a second, more fundamental, objection to the reasoning we used above, though, in that our picture of the experimental boundary conditions was entirely misconstrued. Why? Because for given t_r, but arbitrary t_p, we do not always return to the same spot on the T_s isotherm. Desorption is initiated from a point independent of t_p (e.g., n_2 in Fig. 4.11) only if the pulse width is sufficient to drive the film all the way from that point to steady–state. At shorter pulse widths the effects of t_r and t_p are no longer independent of one another and a self–consistency condition determines the properties of a stable cycle. Then, unlike the case in either the ideal repetition–rate experiment or the ideal time–constant experiment, both beginning and end points of this cycle are sensitive to further changes in one of these parameters. Ultimately, if we think about making t_p very short, the initial point for desorption must move all the way back to equilibrium coverage (i.e., n_o in Fig. 4.11) where it then stays. What is it that determines the self–consistency condition and accounts for this transition?

The key element absent from our discussion that is crucial to a proper interpretation and analysis of the data in Figs. 4.12 and 4.13 is a consideration of the role played by periodicity in these experiments. The signal we observe is the product of steady conditions built up after many cycles – long after any transient effects due to initial conditions or changes in parameters have had an opportunity to die out. This means that, in addition to the usual requirement of continuity in $n(t)$ at $t=t_p$, we must solve the equations of motion for the coverage as a function of time (during both the pulse–on and pulse–off intervals $0 \leqq t \leqq t_p$, $t_p \leqq t \leqq t_r$) subject to the periodic boundary condition $n(t_r) = n(0)$. We cannot possibly hope to do this in general, but a semi–quantitative account of what actually happens can be obtained if we look at the specific example of a linear equation of state where everything can be solved analytically. In that case, the amount desorbed with each pulse, $\Delta n(t_r,t_p) \equiv n(0) - n(t_p)$, is given by

$$\Delta n(t_r,t_p) = \left[\frac{(n_o - n_{ss})(1-e^{-(t_r-t_p)/\tau_o})}{1-e^{-t_p/\tau_s}\, e^{-(t_r-t_p)/\tau_o}}\right](1-e^{-t_p/\tau_s}) \qquad (4.46)$$

while

$$n(0) - n_{ss} = \Delta n(t_r/t_p)/(1-e^{-t_p/\tau_s}) \qquad (4.47)$$

and

$$n(t_p) - n_{ss} = \Delta n(t_r,t_p)/(e^{t_p/\tau_s}-1)\,. \qquad (4.48)$$

The two time constants, τ_s and τ_o (with $\tau_s \ll \tau_o$), represent the effects of desorption at temperature T_s and readsorption at temperature T_o respectively. The situations we have discussed previously correspond to one of two simple limits: either $(t_r - t_p)/\tau_o \gg 1$, in which case

$$\Delta n(t_r,t_p) \rightarrow \Delta n(t_p) = [n_o - n_{ss}](1-e^{-t_p/\tau_s}) \quad \text{and} \quad n(0) \rightarrow n_o$$

(the time–constant experiment), or $t_p/\tau_s \gg 1$, so that

$$\Delta n(t_r,t_p) \rightarrow \Delta n(t_r) = [n_o - n_{ss}](1 - e^{-(t_r - t_p)/\tau_o}) \quad \text{and} \quad n(t_p) \rightarrow n_{ss}$$

(the repetition-rate experiment), where we may approximate $(t_r - t_p)/\tau_o$ by t_r/τ_o for low duty factors. In the first instance, we can think of the amount desorbed as being pulse-width constrained while in the second it is repetition-rate constrained. Now what happens to (4.46) as we sweep through t_p for fixed $t_r \gg t_p$? When t_p/τ_s is much less than one, Δn approaches $[n_o - n_{ss}](t_p/\tau_s)$ for any t_r/τ_o and so appears pulse-width limited. On the other hand, we already know that for $t_p/\tau_s \gg 1$ the amount which can be desorbed is limited by the amount which can reaccumulate between pulses. A graph of Δn vs. t_p will therefore start linearly with a slope independent of t_r but will eventually saturate at a value controlled by the repetition frequency (unless it is also true that $t_r/\tau_o \gg 1$). This is precisely the sort of behavior we see occurring in Fig. 4.13. The turnover in Δn at intermediate pulse widths is just such as to effect a smooth transition between pulse-width constrained and repetition-rate constrained regimes; for this reason, unless t_r/τ_o happens to be much greater than one, $\partial \Delta n(t_p,t_r)/\partial t_p$ is not simply the instantaneous desorption rate, but also reflects changes in the boundary condition at $t = 0$.

The whole situation summarized by (4.46) - (4.48) is analogous to what occurs when we periodically switch a capacitor between two parallel branches of an electrical circuit, one containing a battery of emf $V_o = n_o - n_{ss}$ with series resistance R_o, and the other containing a resistor of value $R_s \ll R_o$. The battery is connected for $t_p \leq t \leq t_r$ and during this interval the capacitor charges with time constant $\tau_o = R_o C$, while for $0 \leq t \leq t_p$ it discharges through R_s with time constant $\tau_s = R_s C$. The voltage across the capacitor at any instant is then given by $V(t) = n(t) - n_{ss}$ and the net charge transferred to or from it during each half cycle of the process is proportional to $\Delta n(t_r,t_p)$ under steady conditions.

What is the nature of the desorption cycle implied by (4.46)-(4.48) and how does its character influence the signal shapes we see in Fig. 4.12? For finite t_r/τ_o,

$n(0)$ starts out at the equilibrium coverage n_o when t_p/τ_s is very small but then decreases with increasing pulse width, finally settling at $n(0)-n_{ss} = [n_o-n_{ss}](1-e^{t_r/\tau_o})$. Simultaneously, $n(t_p)$ decreases from n_o to n_{ss}. When t_r/τ_o is large, $n(0)$ of course stays at n_o but for $t_r/\tau_o \ll 1$ both $n(0)$ and $n(t_p)$ fall precipitously from n_o to n_{ss} at any finite pulse width (i.e., a boundary layer develops in the variation of $n(0)$ and $n(t_p)$ with t_p when t_r/τ_o is small). We can summarize these results by saying that, basically, the whole cycle slides down the T_s and T_o isotherms with increasing pulse width at a rate that is conditioned by the repetition frequency. A heuristic argument as to why this should happen can be made by once again referring to the sketch in Fig. 4.11. Let's forget for the moment the details associated with the linearized case and suppose that $n_o-n_1 = \Delta n(t_{p_1})$ is also equal to $\Delta n(t_r)$, the maximum number which can be read-sorbed between pulses. This is emphasized in the figure by the fact that n_o, n_1, n_2, and n_{ss} are labeled in a way marking off equal Δn increments between them. We then reason crudely as follows. For $t_p \leqq t_{p_1}$ we always trace out cycles starting at n_o because the film is capable of reaccumulating a Δn equal to the amount desorbed in the repetition time allotted. When t_p exceeds t_{p_1}, however, the maximum amount which can be desorbed must be limited by $\Delta n(t_r)$; since the total desorption time has increased, the only way the system can still desorb the same amount as previously is for it to do so at an overall slower rate. This means beginning from a reduced vapor pressure (i.e., sliding down the isotherm) so that, for example, we execute a cycle between n_1 and n_2 maintaining the same Δn. With t_p large enough, the system finally ends up cycling between n_2 and n_{ss}.

The decrease in signal amplitude we observe in Fig. 4.12 therefore has a natural explanation. Its onset marks our emergence from pulse-width constrained desorption into the regime of repetition-rate constrained desorption where the signal area remains fixed. The amplitude of these waveforms must consequently decrease as they become broader in order to preserve their area

and keep the number of atoms desorbed constant. For very short pulse widths, the signal versus time is identical with that in the time–constant experiment (compare Fig. 4.4) whereas for long pulses it looks just like the waveforms in the repetition–rate experiment (compare Fig. 4.9). The linear equation of state model makes an interesting prediction in this regard which runs counter to the actual behavior of the data. Were this model to be correct, then each waveform in Fig. 4.12 would be a miniature of the corresponding one in Fig. 4.4 with a scale factor that depended on the pulse width (and, of course, approached one as t_p went to zero). This assertion follows from the self–similarity property of the exponential functions which are solutions of the linear equations of motion. That is, except for a scaling factor, equal–width segments of the $n(t)$ vs. t curve are identical and, as a consequence, the net desorption rate as a function of time looks the same independent of one's starting point; it is only this initial condition which varies with t_r for fixed t_p. As we have already pointed out in our discussion of Fig. 4.9, however, aside from the decrease in amplitude resulting from the need to preserve area, any further discrepancies between the waveforms of Figs. 4.13 and 4.4 must be attributed to a substantial nonlinearity in the isotherm.

Our understanding of what is occurring in Figs. 4.12 and 4.13 is corroborated by an orthogonal cut through the t_r,t_p plane presented in Fig. 4.14, where we show the integrated signal as a function of repetition time for several different pulse widths. The curves all coalesce for $t_r \to 0$ but show distinct asymptotes as $t_r \to \infty$. The ratio of these asymptotes agrees with the predictions for $\Delta n(t_p)$ at the critical repetition rate from Fig. 4.13. The basic phenomenon here is just the reverse of what is going on there, with the behavior at the left end of the graph repetition–rate limited while the asymptotes at the right end of the graph are pulse–width limited; the desorption cycle remains pinned around n_{ss} for any t_p when t_r is small enough, but then moves steadily up the isotherm with increasing t_r, eventually encompassing n_o.

Figure 4.14. $\int_0^{t_l} dtS(t)$ vs. t_r for T_s = 2.88 K and several different pulse widths. t_p = 50 (circles), 20 (squares), 5 (triangles), and 2 μsec (crosses).

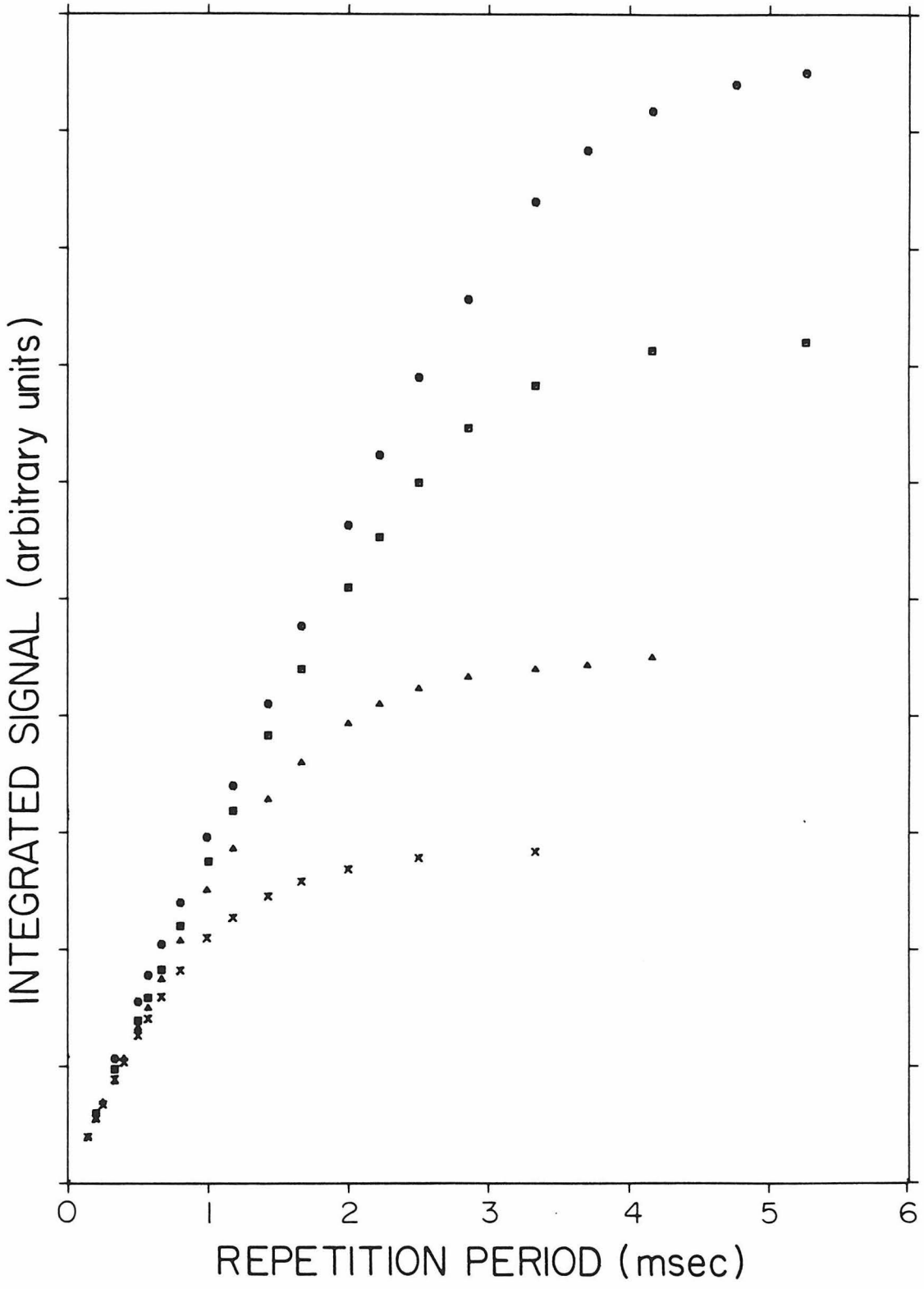

References

Ashcroft, N. W. and Mermin, N. D., *Solid State Physics* (Holt Rinehart and Winston, New York, 1976).

Axan, B., *Absolute Calibration of a Superconducting Transition Bolometer*, Senior Thesis, California Institute of Technology, 1984.

Cole, M. C., private communication.

Cowin, J. P., Phys. Rev. Lett. **54,** 368 (1985).

Cowin, J. P., Auerbach, D. J., Becker, C. and Wharton, L., Surf. Sci. **78,** 545 (1978); Surf. Sci. **84,** 641 (E) (1979).

Dushman, S. and Lafferty, J. M., *Scientific Foundations of Vacuum Technique* (J. Wiley and Sons, Inc., New York, 1962).

Franklin, J. N., private communication.

Horowitz, P. and Hill, W., *The Art of Electronics* (Cambridge University Press, New York, 1980).

Kelly, P. C. and Horlick, G., Anal. Chem. **45,** 518 (1973).

Lubman, D. M., Rettnes, C. T. and Zare, R. N., J. Phys. Chem. **86,** 1129 (1982).

Maul, M. K. and Strandberg, M. W. P., J. Appl. Phys. **40,** 7, 2822 (1969).

Sinvani, M. and Goodstein, D., Surf. Sci. **125,** 291 (1983).

Sinvani, M., Taborek, P. and Goodstein, D., Phys. Rev. Lett. **48,** 1259 (1982).

Taborek, P. and Goodstein, D., Rev. Sci. Instrum. **50,** 227 (1979).

Taborek, P., Sinvani, M., Weimer, M., and Goodstein, D., J. Physique **C6,** 852, 855 (1981).

Touloukian, Y. S. and Buyco, E. H., *Thermophysical Properties of Matter*, Vol. 4 (Plenum, New York, 1970).

Troitskii, V. S., Sov. Phys. JETP **14,** 281 (1962).

Vidali, G. and Cole, M. C., Surf. Sci. **110,** 10 (1981).

Widrow, B., Trans. Amer. Inst. Elect. Engrs. **79,** 555 (1961).

Williams, Arthur B., *Electronic Filter Design Handbook*, (McGraw Hill, New York, 1981).

Summary and Perspective

It should be clear from all of our previous discussions that the meaning of the phrase "desorption time constant" depends on the *context* in which it is used. Of the various time constants we have considered, each has its own domain of applicability and refers to specific experimental circumstances. For example, we have talked about the mean residence time of a single atom on the surface. This is a concept that refers to the dynamic balance between adsorption and desorption in thermal equilibrium and it is this quantity that theorists usually discuss. On the other hand, from the specific circumstances in which our experiments are conducted, we have been led to consider various relaxation times that characterize the approach to a new steady state when the dynamic equilibrium between a film and its vapor is perturbed by a sudden change in the temperature of the film.

For an ideal adsorbate at low coverage, where the equation of state is linear in the surface concentration and the solutions of the rate equations are exponential functions, all of the time constants – the mean residence time, the local relaxation time, and the global relaxation time – are identical. A measurement of relaxation processes therefore bears directly on the question of determining the lifetime of an isolated adatom in a given surface potential. But when the adsorbed particles are capable of interacting with one another and the isotherms become nonlinear, each of these time constants in turn becomes a distinct function of surface coverage and temperature, bearing no simple relationship to the others.

We have provided a geometric interpretation for the various τ's in Chapter 3 where we showed that, for monolayer films, the mean residence time is proportional to the inverse slope of the chord connecting the vapor pressure isotherm to the origin whereas the local relaxation time depends on the inverse slope of the adsorption isotherm itself (Fig. 3.3). It is also possible to express these

quantities in terms of the surface–adatom and adatom–adatom interaction potentials, through the relationship between the vapor pressure and partition function, thereby providing a statistical–mechanical link between macroscopic and microscopic properties of the adsorbate system. Of course, all of this involves only equilibrium concepts – energy levels, counting states, and so on – and so does not yield up any information on the perturbative couplings (between substrate phonons and adsorbed atoms for example) that are responsible for inducing transitions between bound and continuum states. Thus, while our analysis has focused on the distinctive and important consequences arising from a nonlinear equation of state, all of the uniquely kinetic information (as distinct from equilibrium) really resides in the sticking coefficient, which we have *assumed* to be constant and equal to one.

While measurements of such a gross quantity as τ_{exp} are necessarily crude, there is nothing in the results presented here which, in themselves, are inconsistent with our assumptions. When the desorption proceeds slowly enough, and collisions are eliminated, we find that the major features we observe – prefactors, activation energies, dependencies on initial conditions, signal shapes – can all be reconciled with the assumed properties of the sticking coefficient and the equation of state, through detailed balance. This is best summarized by our comparison between data and model predictions in Fig. 4.7 where data taken under ostensibly different initial conditions, when plotted in terms of scaled variables, are shown to lie on a single curve in good agreement with the theory.
If the agreement between data and model had not turned out as satisfactorily as it appears it has, i.e., if the model had demonstrably failed to give a reasonable account of the data, then we would have to look in any or all of three places for an answer as to why:

– Is the behavior of the sticking coefficient different, by orders of magnitude, from what we have supposed?

– Is the equation of state we have used so misleading that the initial desorption rate and steady–state conditions are completely inaccurate?

– Is the quasi–equilibrium hypothesis faulty, i.e., is the desorption essentially non–equilibrium in nature?

Conversely, our success lumps ignorance of each of these three issues together and does not serve to identify offsetting deviations from the conjectured behaviors. In other words, we may just have been lucky and would be hard pressed to assert, solely on the basis of the evidence presented here, that we had shown any or all of these circumstances necessarily pertain.

In retrospect, it seems a more penetrating test of our assumptions would have been obtained had we simultaneously studied the *angular dependence* of the desorption rate. In this way, looking for any deviations from a cosine distribution, we could at least have determined $\sigma(\Theta)$ in relative units. (A similar study of the angular dependence of desorption due to a hot, low–intensity phonon beam incident on a film adsorbed directly on our sapphire crystals has already been conducted by Goodstein *et al.* [Goodstein, Maboudian, Scaramuzzi, Sinvani and Vidali (1985)].) As we mentioned in Chapter 4, it would also have been worthwhile to pin down the *velocity dependence* of σ through a detailed line–shape analysis of collision–free time–of–flight spectra. Both of these determinations would depend on the quasi–equilibrium assumption but they would be independent of the equation of state if the sticking coefficient varied only insignificantly with coverage.

Our central theme has been that, if quasi–equilibrium is maintained, there is an intimate relationship between the structure of an adsorbate (i.e., the equation of state) and kinetics, that link being provided by the dynamical information contained in the sticking coefficient. Kinetic and equilibrium properties are therefore intertwined as long as detailed balance applies. In fact, our contention has been that, in large part, the kinetics may be *dominated* by equilibrium

properties inasmuch as the time scales of the relaxation phenomena are set by quantities such as the film vapor pressures in equilibrium and steady state. These quantities vary over orders of magnitude with changing initial conditions and as a consequence the kinetics may be relatively insensitive to the fine details of substrate–adatom forces which manifest themselves as comparatively small variations in the sticking coefficient.

We have seen that, under appropriate circumstances, isothermal desorption occurs in practical rapid–flash desorption experiments and that this considerably simplifies the interpretation and analysis of the data, allowing a direct connection with the equation of state to be established. The original mystery of the anomalous exponent and prefactor in a Frenkel–Arrhenius parameterization of the rate data has been shown to reflect the underlying curvature of the equilibrium adsorption isotherm. Other aspects of the desorption rate, such as variations in the shape of the detected time–of–flight spectrum in response to different cuts through the repetition–rate, pulse–width parameter plane, have also substantiated this geometrical property.

The true time evolution of the approach to steady state is nonexponential for any realistic isotherm which admits of adatom–adatom interactions or substrate heterogeneity. Our treatment of time constants in this essentially nonlinear problem is similar to the discussion of impedances in circuits containing devices with nonlinear current–voltage characteristics: our local linearization of the rate equation is analogous to the idea of a small–signal impedance. The local time constant contains information about the instantaneous coverage dependence of both the film chemical potential and the sticking coefficient so that a succession of local time constants reflects the continually changing environment in which particles desorb. On the other hand, the global time constant, as we have defined it, represents an amalgam of instantaneous and asymptotic properties.

There are some general limits to the validity of our simple detailed balance/thermodynamic continuum point of view which deserve comment. We have previously alluded to the issue of the bulk critical point in liquid helium and the consequent failure of the FHH isotherm to accurately reflect the film vapor pressure above 5.2 K. It should be clear that this limitation is not fundamental inasmuch as *some* equation of state with the general shape of FHH presumably applies above this temperature. More interesting would be the effect of a 2–d critical point in films which grow in the layer–like mode. Below this critical point one would observe transitions into regions of 2–d phase coexistence, and hence zero–order kinetics, whereas above it the vapor pressure isotherm would be just a smooth curve with an inflection point. Therefore, as the temperature at which isothermal desorption is observed is raised through the critical temperature, the extent in coverage of zero–order kinetics would decrease and eventually disappear above T_c.

More problematic are the limitations imposed by our treatment of the mass–flux term in the equations of motion as that due to a simple Knudsen gas. This is surely appropriate in the low pressure regime where our experiments are conducted (the mean free path is then comparable with the dimensions of our apparatus) but at higher pressure, where we make the transition from simple molecular flow (and ballistic propagation) to sound generation, hydrodynamic effects become important. There are then temperature and pressure gradients in a thin layer of gas within a mean free path of the surface which are created by the desorption flux and these affect the readsorption rate; there is a back action on the desorption from disturbances of the surrounding gas. We, however, have tacitly assumed that this ambient gas remains unperturbed (which is abetted by our notion that most of the desorbed gas atoms encounter cold surfaces where they then stick before redesorbing much more slowly). Therefore, in the usual pressure regime where enough adsorbate condenses to create bulk liquid, our expressions for the mass and energy transfer rates no longer apply and one must

take some account of the motion of the gas as a whole [see e.g., Wiechart and Buchholz (1980), (1983)].

Another area of contention concerns the rapidity and mechanism of thermalization in these films. Helium has a very large heat capacity compared with other materials at low temperature. If the thermal boundary resistance were actually 50–100 times greater than typical helium/solid Kapitza resistances (i.e., if the heat transport were non–anomalous), then we would predict that adsorbed films would take correspondingly longer to warm, which should lead to observable consequences in the desorption flux. Specifically, Weber *et al.* showed that when a LiF crystal was cleaved *in vacuo* at 4 K, the subsequent phonon reflection from the cleaved surface exposed to bulk liquid helium showed very little coupling of solid phonons to the liquid in accord with the mismatch in acoustic impedance between the two media [Weber, Sandmann, Dietsche and Kinder (1978)]. Essentially all of the phonons were reflected at the interface in contrast with what happens in our sapphire crystals, where roughly half are reflected and the rest transmitted to the liquid, despite a similarly large acoustic mismatch. On the basis of our bulk continuum viewpoint we would predict a slower heating rate for helium films adsorbed on these cleaved surfaces. The overall desorption rate may, or may not, then be limited by this fact depending on what has happened to the sticking coefficient. If σ decreases by the same scale factor – not that there is any reason to think it must necessarily do so – then we are back to the same arguments we made before about "isothermal" desorption, but our units of "time" have just become correspondingly longer. Alternatively, if R_k gets large while σ stays near one, we would expect to see coupled heating and evaporation on the basis of our assumptions about how energy flows between film and substrate.

But rapid thermalization may actually be a feature of strong mechanical coupling between a 2–d film and vibrations of the substrate surface. It could thus have little, or nothing at all, to do with Kapitza resistance which relates the

asymptotic temperature and heat–current fields in two continuous media whose collective modes are fully three dimensional. There *is* a relationship between the desorption rate and energy transfer at the gas–solid interface that depends on the coefficient of thermal accommodation, but how this bears on the effective temperature experienced by a film on a partially–covered surface is not clear. Recent theoretical calculations [Gortel and Kreuzer (1985)] show long heating times for mobile, non–interacting helium atoms on a perfectly smooth substrate (i.e., no periodic corrugation) because of weak phonon–adatom coupling, but the assumptions of this model are far removed from the realities of our experiments.

Microscopic theories of desorption kinetics invariably assume non–interacting particles on a perfect surface and then set about calculating the desorption rate, without concurrent readsorption, in terms of the properties of the adatom–surface binding potential and the substrate–phonon/adatom interaction Hamiltonian. These approaches almost never take account of collective properties in the film (a notable exception, and worthwhile attempt in this direction, is the mean field theory of Sommer and Kreuzer for the He–graphite system [Sommer and Kreuzer (1982)]) whereas the thermal model includes these aspects at the outset through the coverage– and temperature–dependent vapor pressure (or film chemical potential), heat capacity, and heat of desorption. To the extent that accurate values for these quantities can be joined with similar knowledge of the sticking coefficient, we can expect to make realistic predictions. Calculating desorption rates in terms of elementary processes (via single phonon absorption or a cascade of single phonon absorption events) and then parameterizing the results in Frenkel–Arrhenius form seems to us to obscure rather than highlight the important physics. It is our opinion that the purposes of both theorist and experimentalist alike would be better served if theories of equilibrium or near–equilibrium desorption explicitly predicted an equation of state and sticking coefficient from first principles. With the further assumption of quasi–equilibrium, the desorption kinetics per se would follow from a

straightforward application of these two quantities in the rate equation and one could then take full account of nonlinearity. Albeit, this prescription puts aside the difficulties inherent in defining a sticking probability in time–varying situations, but then at least the differences between theory and experiment might be narrowed by the development of suitable systems for study on both sides.

When the quasi–equilibrium condition cannot be satisfied, one needs to resort to the full machinery of nonequilibrium statistical mechanics (as in [Gortel, Kreuzer, Teshima and Turski (1981)] and [Kreuzer and Teshima (1981)]), but the range of validity of the detailed–balance approach may, in reality, be greater than theorists appreciate. This is especially likely to be so if their models do not fully reflect all of the ways of sharing energy and causing transitions between the numerous modes of the system; by oversimplifying and neglecting particle–particle interactions, they may be underestimating the rate of internal readjustment among the various energy levels as particles leave the film.

The success of the simple ideas we have used to estimate the net evaporation rate of these films is, in some sense, also our undoing for we have really learned nothing about the details of mechanism which ordinarily stimulate this kind of study. The detailed–balance paradigm does nothing to illuminate mechanism in physisorption (e.g., is the desorption mediated by single–phonon absorption) but, instead, accepts certain properties of the combined substrate/adsorbate system as *given* and goes on from there. All of the fundamental questions remain:

– By what means is energy coupled from substrate to adsorbate and with what efficiency (Kapitza resistance)?

– By what means and with what efficiency are energy and mass coupled from the adsorbate to the gas (sticking probability and accommodation coefficients)?

– Why does the equation of state take the particular form that it does for a given system (energy levels and degrees of freedom in the partition function)?

– What determines the limits of applicability of quasi–equilibrium and detailed balance in any given system (what is the time–dependent distribution of internal states in the film)?

Unfortunately, for all of our effort we are not much closer to having satisfactory answers to any of these questions.

It would be far more instructive if we could study simple adsorbates on well–characterized surfaces whose equation of state is known, and from a combined analysis of adsorption and desorption kinetics extract a sticking coefficient and test the consistency of the detailed–balance assumption. Taborek [Taborek and Senator (1986)] has recently taken a step in this direction using graphite fibers of low thermal mass whose surface is well–understood both thermodynamically and microscopically. The shortcomings there, as in all of our experiments, remain the lack of any determination of absolute rates or of the capacity to measure vapor pressures independently of the repetition–rate manometer. Without a more precise handle on both of these quantities, one cannot hope to sidestep the complications that arise from observing only relaxation times rather than mean residence times in these highly nonlinear systems.

References

Goodstein, D. L., Maboudian, R., Scaramuzzi, F., Sinvani, M. and Vidali, G., Phys. Rev. Lett. **54,** 2034 (1985).

Gortel, Z. W. and Kreuzer, H. J., Phys. Rev. B **31,** 3330 (1985).

Gortel, Z. W., Kreuzer, H. J., Teshima, R. and Turski, L. A., Phys. Rev. B **24,** 4456 (1981).

Kreuzer, H. J. and Teshima, R., Phys. Rev. B **24,** 4470 (1981).

Sommer, E. and Kreuzer, H. J., Phys. Rev. Lett. **49,** 61 (1982).

Sommer, E. and Kreuzer, H. J., Phys. Rev. B **26,** 4094 (1982).

Taborek, P. and Senator, L. J., Phys. Rev. Lett. **56,** 628 (1986).

Weber, J., Sandmann, W., Dietsche, W. and Kinder, H., Phys. Rev. Lett. **40,** 1469 (1978).

Wiechart, H. and Buchholz, F. I., J. Low Temp. Phys. **39,** 623 (1980).

Wiechart, H. and Buchholz, F. I., J. Low Temp. Phys. **51,** 291 (1983).